Identification of
trafficking determinants in novel PNEPs
of the human malaria parasite
Plasmodium falciparum

–DISSERTATION–

with the aim of achieving a doctoral degree
at the faculty of Mathematics, Informatics and Natural Sciences
Department of Biology
Universität Hamburg

submitted by

Alexandra Blancke Soares

Hamburg, 2016

Eidesstattliche Versicherung

Hiermit erkläre ich an Eides statt, dass ich die vorliegende Dissertationsschrift selbst verfasst und keine anderen als die angegebenen Quellen und Hilfsmittel benutzt habe.

Hamburg, den 04.05.2016

Unterschrift

Language certificate

I am a native speaker, have read the present PhD thesis and hereby confirm that it complies with the rules of the English language.

Toronto, April 25, 2016   Tatianna Wong

Summary

The severest form of human malaria is caused by the protozoan parasite *Plasmodium falciparum.* This parasite multiplies within red blood cells which it remodels extensively to ensure its survival and virulence. A major cause of this parasite's perilousness is the virulence factor *Pf*EMP1, which is exported from the parasite and displayed on the red blood cell surface, where it mediates cytoadherence to the endothelium of blood vessels. Besides *Pf*EMP1, the parasite exports a large number of other proteins into its host cell, the function of most of them still being unknown. Most known exported proteins contain a motif called PEXEL that mediates their export into the host cell. However, a growing number of PEXEL-negative exported proteins (PNEPs) is being identified and evidence suggests that these proteins might constitute a significant part of the *P. falciparum* exportome (all exported proteins). The PNEPs that were initially identified all lacked a signal peptide but contained a single transmembrane domain, mediating entry into the secretory pathway and an N-terminus essential for protein export. For PNEPs with other domain organizations, a group of PNEPs only recently identified, the trafficking determinants are unknown.

This work aimed to elucidate the trafficking of these novel PNEPs, including those containing a classical N-terminal signal peptide or those with a signal peptide and a transmembrane domain. In all PNEPs containing only a signal peptide, the N-terminus after the signal peptide (mature N-terminus) was found to mediate export, similar to previously known PNEPs. In contrast, most regions in the PNEPs with a signal peptide and a transmembrane domain were required for export. This suggested a delicate combination of all domains was involved in the export of this so far rarest type of PNEP and that these proteins lacked a clear cut trafficking domain. This indicates common trafficking regions in most but not all of the different types of the presently known PNEPs.

Interestingly, in one of the PNEPs with a signal peptide, called MSRP6, a region in the C-terminus independently of the mature N-terminus also mediated protein export. In addition this region was also necessary and sufficient for the recruitment of MSRP6 to the Maurer's clefts, trafficking organelles within the infected red blood cell. Hence, this domain mediated both export and sorting in the host cell. To identify proteins that interact with this C-terminal part and could potentially explain both the Maurer's cleft localiza-

tion and protein export, proximity-dependent biotin identification (BioID) in combination with quantitative mass spectrometry was performed. In total, of 44 significant hits 33 were exported proteins. In this work, 11 proteins were endogenously tagged with GFP which confirmed a localization at the Maurer's clefts for 10 of them. CoIP experiments then validated 5 proteins as MSRP6 interaction partners, indicative of a novel protein complex at the Maurer's clefts. Together with the trafficking phenotype of MSRP6 these results could suggest that the MSRP6 protein complex, or some components of the complex, are assembled during early trafficking steps and trafficked together until their arrival at the Maurer's clefts. The large fraction of Maurer's clefts proteins identified among the significant hits also indicates that BioID can be a useful tool for proteome analyses in *P. falciparum*.

Zusammenfassung

Plasmodium falciparum, ein einzelliger eukaryotischer Parasit, verursacht die gefährlichste Form der Malaria im Menschen. Der Parasit vermehrt sich in roten Blutkörperchen, die er während seiner Entwickung stark modifiziert um sein Überleben und seine Virulenz zu gewährleisten. Der Virulenzfaktor *Pf*EMP1, der vom Parasiten in die Wirtszelle exportiert und dort auf der Oberfläche der roten Blutkörperchen präsentiert wird, vermittelt Zytoadherenz der infizierten Zelle an das Endothel der Blutgefäße. Dies ist eine der Hauptursachen für die Gefährlichkeit dieses Parasiten. Neben *Pf*EMP1 exportiert der Parasit noch eine große Anzahl von weiteren Proteinen, deren Funktionen häufig unbekannt sind in die Wirtszelle. Die meisten bekannten exportierten Proteine beinhalten ein sogenanntes PEXEL-Motiv, das den Export in die Wirtszelle vermittelt. In den letzten Jahren wurde allerdings eine wachsende Anzahl von PEXEL-negativen exportierten Proteinen (PNEPs) identifiziert, was darauf hindeutet, dass diese Proteine einen signifikanten Teil des Exportoms (alle exportierten Proteine) von *P. falciparum* ausmachen. Die ersten bekannten PNEPs besaßen kein Signalpeptid, sondern beinhalteten eine einzelne Transmembrandomäne, die den Eintritt in den sekretorischen Transportweg vermittelte und einen N-Terminus, der essenziell für den Export war. Der exportvermittelnde Teil in PNEPs mit anderen Domänen-Organisationen, die kürzlich entdeckt wurden, ist bis jetzt unbekannt.

Das Ziel dieser Arbeit war die Untersuchung der Transport-Determinanten dieser neuen PNEPs, die ein klassisches N-terminales Signalpeptid oder ein Signalpeptid und eine Transmembrandomäne beinhalten. In allen PNEPs, die nur ein Signalpeptid besaßen, wurde der nach Abspaltung des Signalpeptids entstehende N-Terminus als exportvermittelnd identifiziert, was der Situation in vorher bekannten PNEPs entspricht. Im Gegensatz dazu wurden fast alle Bereiche in PNEPs mit einem Signalpeptid und einer Transmembrandomäne für den Export benötigt. Dies deutet darauf hin, dass eine fragile Kombination aller Domänen am Export dieser bisher seltensten Art von PNEPs beteiligt war und diese kein scharf umrissenes Exportsignal besitzen. Diese Ergebnisse weisen darauf hin, dass der Export der meisten, allerdings nicht aller zur Zeit bekannten PNEPs, durch ähnliche Bereiche vermittelt wird.

Neben der N-terminalen Exportregion im PNEP MSRP6 wurde interessanterweise noch

eine weitere Region im C-Terminus ermittelt, die unabhängig vom N-Terminus auch Export vermittelte. Zusätzlich war diese Region notwendig und ausreichend um MSRP6 an die Maurer's clefts (Organellen in der Wirtszelle, die für den Transport von vielen Proteinen an die Oberfläche des roten Blutkörperchens wichtig sind) zu rekrutieren. Somit vermittelte diese Domäne sowohl Export als auch die Sortierung in der Wirtszelle. Um Proteine zu identifizieren, die mit diesem C-terminalen Bereich interagieren und möglicherweise die Maurer's clefts Lokalisation und auch den Proteinexport erklären könnten, wurde "proximity-dependent biotin identification" (BioID) in Kombination mit quantitativer Massenspektrometrie eingesetzt. Insgesamt wurden damit 44 signifikante Treffer erzielt, wovon 33 exportierte Protein waren. Für diese Arbeit wurden 11 Proteine endogen mit GFP fusioniert, wodurch eine Maurer's clefts Lokalisation für 10 dieser Proteine bestätigt wurde. Mit Hilfe von CoIP-Experimenten wurden 5 dieser Kandidaten als MSRP6 Interaktionspartner validiert, was auf einen neuen Proteinkomplex an den Maurer's clefts hindeutet. Zusammen mit den Transport-Daten von MSRP6 könnte dies darauf hinweisen, dass der MSRP6-Proteinkomplex, oder Teile davon, in einem frühen Schritt des sekretorischen Weges zusammengefügt und die Komponenten zusammen transportiert werden, bis sie die Maurer's clefts erreichen. Der hohe Anteil an Maurer's clefts Proteinen unter den signifikanten Treffern deutet auch darauf hin, dass BioID ein nützliches Instrument für die Proteomanalyse in *P. falciparum* sein kann.

Contents

List of Figures

List of Tables

Abbreviations

α	*alpha*/anti
μ	micro
crt	gene of the CRT resistance transporter
E. coli	*Escherichia coli*
P.	*Plasmodium*
T.	*Toxoplasma*
aa	amino acids
ACT	artemisinin-based combination therapy
AMA-1	apical membrane antigen-1
APR	apical polar ring
ARL-V	Apicomplexan Related Lineage-5
ATP	adenosine triphosphate
BBB	blood-brain barrier
BioID	proximity-dependent biotin identification
BLASTp	Basic Local Alignment Tool (for proteins)
bp	basepairs
C-	Carboxy-
CIDR	cysteine-rich interdomain region
CM	cerebral malaria
CoIP	co-immunoprecipitation
CRISPR	clustered regularly interspaced short palindromic repeat
CRT	chloroquine resistance transporter
CSA	chondroitin sulphate-A
CSP	circumsporozoite surface antigen
DAPI	4'6-Diamino-2-phenylindol
DBL	Duffy binding-like
DDT	dichlorodiphenyltrichlorethane
dH_2O	distilled water
DHFR	dihydrofolate reductase
DMSO	dimethylsulfoxide
DNA	deoxyribonucleic acid
DTT	dithiothreitol
DVS	dominant vector species
e.g.	exempli gratia/ for example
EBA	erythrocyte binding antigen
ECL	enhanced chemoluminescence
EEF	exo-erythrocyctic from
EPCR	Endothelial Protein C Receptor
ER	endoplasmic reticulum

et al.	et alii
EV	extracellular vesicle
EXP1/2	exported protein 1/2
FDR	false discovery rate
g	grams
GDP	gross domestic product
GFP	green fluorescent protein
GPI	glycosylphophatidylinositol
h	hours
HBsAg	hepatitis B surface antigen
HIV	human immunodeficiency virus
hpi	hours post invasion
HRP	horseradish peroxidase
HSPG	Heparan sulphate proteoglycan
HT	host targeting
ICAM-1	Intercellular Adhesion Molecule 1
IE	infected erythrocyte
IFA	immunofluorescence analysis
IFA	immunofluorescence assay
IMC	inner mebrane complex
IRS	indoor residual spraying
ITN	insecticide-treated bednet
KAHRP	Knob-associated histidine-rich protein
kDa	kilodalton
l	liter
LC-MS	liquid chromatography-mass spectrometry
LLIN	long-lasting insecticide-treated bednet
M	molar
m	milli
MAHRP	membrane associated histidine rich protein
MC	Maurer's cleft
min	minute
MSP-1	merozoite surface protein-1
MSRP	merozoite surface protein 7-related protein
MTOC	microtubule organizing center
mTRAP	merozoite thrombospondin related adhesion protein
n	nano
N-	Amino-
NANP	N-acetylneuraminic acid phosphatase
nm	nanometer
NPP	new permeation pathways
OD	optical density
PBS	phosphate buffered saline
PCR	polymerase chain reaction
PEXEL	*Plasmodium* export element
pH	potentia hydrogenii

PIESP2 .... parasite-infected erythrocyte surface protein 2
PNEP .... PEXEL-negative exported protein
POI .... protein of interest
PPM .... parasite plasma membrane
PTEX .... *Plasmodium falciparum* translocon of exported proteins
PV .... parasitophorous vacuole
PVM .... parasitophorous vacuole membrane
RBC .... red blood cell
REX .... ring exported protein
Rh .... reticulocyte-binding like homolog
RON .... rhoptry neck protein
RTS,S .... purified recombinant circumsporozoite protein vaccine
s .... seconds
SBP .... skeleton binding protein
SERA .... serine-repeat antigen
SP .... signal peptide
SPC .... signal peptidase complex
SPZ .... sporozoites
SRP .... signal recognition particle
STEVOR .... subtelomeric variant open reading frame
TBV .... transmission blocking vaccine
TGN .... trans-golgi network
TM .... transmembrane
TMD .... transmembrane domain
TNF-α .... tumor necrosis factor α
TRAP .... thrombospondin-related anonymous protein
TVN .... tubovesicular network
U .... units
UV .... ultra violet
V .... Volt
v .... volume
WHO .... World Health Organization

1. Introduction

1.1. Malaria

Of over 200 *Plasmodium* species infecting vertebrates only five can cause malaria in humans: *Plasmodium falciparum, P. vivax, P. knowlesi, P. ovale* and *P. malariae.* The protozoan parasites are transmitted by female mosquitoes of the genus *Anopheles,* of which *A. gambiae* is the most relevant vector for humans. Despite significant successes in controlling malaria during the last 10-15 years, the disease is still a major global health issue (World Health Organization, 2015).

1.1.1. Epidemiology

Almost half of the world's population (3.2 billion people) lives in malaria endemic countries and thus at risk of infection. In 2015, 214 million people contracted malaria, of which 438000 died of the disease. Most of the malaria fatalities (~70%) occur in children under the age of five. Both malaria cases and fatalities are concentrated in Africa, constituting 88% and 90%, respectively. The remaining cases and deaths occur predominantly in the South-East Asian region (10% and 7%) and Eastern-Mediterranean region (2-3%). In the central and southern America malaria cases decreased to approximately 0.1% of cases worldwide (World Health Organization, 2015), (figure 1.1).

Of the five human infecting *Plasmodium* species, *P. falciparum* is responsible for the majority of malaria deaths. Although *P. falciparum* is responsible for most of the malaria cases, *P. vivax* shows a wider geographical distribution, spreading further into the northern hemisphere and to higher altitudes. *P. vivax* accounts only for about 1% of malaria cases in Africa, but for 50% of cases in South-East Asia. In total 13.8 million malaria cases (6% of all cases) can be ascribed to *P. vivax.* The wider distribution of *P. vivax* originates from its capacity to complete its development in the mosquito vector at lower temperatures. Additionally, the parasite can produce dormant stages (hypnozoites), which can survive in a patients' liver. Reactivation of hypnozoites causes a new malaria attack and helps the parasite to survive adverse climate conditions unsuitable for the transmission by the mosquito vector (World Health Organization, 2015).
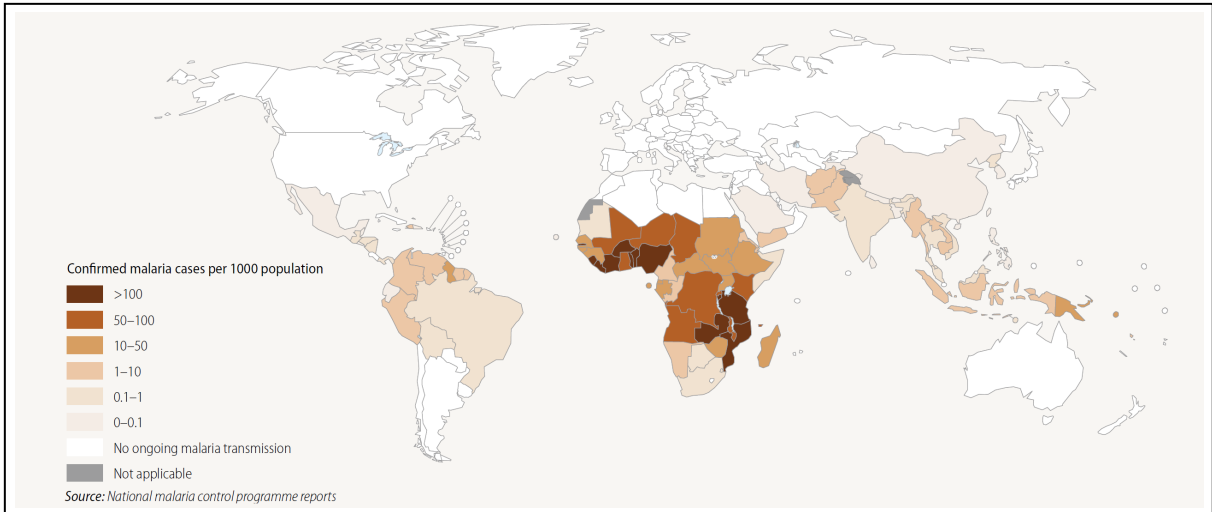
Figure 1.1.: Countries with ongoing transmission of malaria, 2013 Case numbers per 1000 population are represented by different shades of brown

P. ovale malaria predominantly occurs in Africa and the Western Pacific region (Collins and Jeffery, 2005) while the *P. malariae* distribution mostly coincides with that of *P. falciparum* (Collins and Jeffery, 2007). *P. knowlesi* was only recently reported to cause malaria in humans and is restricted to South-East Asia. This parasite is believed to be transmitted by mosquitoes infected by monkeys only and not between humans. Despite the exclusively zoonotic transmission, *P. knowlesi* poses a growing threat in certain regions, e.g. Malaysia, where 81% of the malaria cases were caused by this parasite (World Health Organization, 2015).

Plasmodium distribution is dependent on its vector, the female *Anopheles* mosquito, and its efficiency of malaria transmission. In Africa, the predominant *Anopheles* vectors belong to the *A. gambiae* complex, especially *A. gambiae* and *A. arabiensis*, but other vectors such as *A. funestus* are also important (Sinka et al., 2010). With 19 dominant vector species present, the Asian-Pacific region has a much higher entomological complexity than any other region of the world. *A. dirus* is a highly anthropophilic species complex and the dominant vector in some areas in the Asian-Pacific region (Sinka et al., 2011).

While malaria incidence and mortality have decreased by 37% and 60%, respectively, since the year 2000, declines in malaria cases have slowed down in high-incidence countries (World Health Organization, 2015). The still large number of malaria cases and deaths not only causes suffering to individuals but also has a huge impact on the economy of endemic countries. This is especially evident when comparing the gross domestic product (GDP) of malaria-endemic and malaria-free countries, which is fivefold lower in endemic countries. On the one hand malaria can be a major cause for poverty, the reasons for that ranging from lost work- and schooldays to demographic consequences of the disease. On

the other hand poverty itself is a factor promoting the spread of the disease because of the high costs for malaria treatment and prevention (Sachs and Malaney, 2002).

1.1.2. Clinic

Malaria symptoms can be very diverse and range from mild etiopathologies to death. The severity of symptoms depends on the host itself as well as on the *Plasmodium* species. *P. falciparum* causes falciparum malaria, which represents the most dangerous form of malaria (Bartoloni and Zammarchi, 2012). The incubation period for malaria is dependent on on the duration of the asymptomatic liver stage and the replication rate in the following symptomatic blood phase (Bartoloni and Zammarchi, 2012; Ashley and White, 2014).

A few days before the onset of fever, the hallmark symptom of malaria, prodromal symptoms like malaise, loss of appetite, headache and nausea occur. These symptoms increase and are extended by fever, which is irregular during the first week, and after that may occur periodically on a daily basis (quotidian), every third day (tertian) or in 36 hour intervals (subtertian). Besides flu-like symptoms, other common symptoms include vomiting, diarrhea and respiratory symptoms, which may cause dangerous misdiagnoses (Bartoloni and Zammarchi, 2012). The fever episodes which occur in all malaria types, coincide with the rupture of infected erythrocytes (IEs) and concurrent release of pyrogenic material into the blood stream. Malaria glycosylphophatidylinositols (GPIs) and hemozoin are recognized by toll-like receptors and induce TNF-α production, which is believed to be the major cytokine mediating malaria fever (Schofield et al., 2002; Oakley et al., 2011).

For *P. falciparum* the liver stage lasts for approximately 5 days, and first symptoms appear 9-14 days after infection. *P. falciparum* malaria can cause serious complications summarized in the term severe malaria. Severe malaria can include anemia, metabolic acidosis, multiorgan system involvement and cerebral malaria (CM). Approximately 1% of *P. falciparum* malaria cases result in severe malaria, of which 90% occur in children in sub-Saharan Africa. Clinically, a CM is diagnosed if the patient suffers from unrousable coma in combination with *P. falciparum* parasitemia, although diagnosis is often complicated by co-infections with other pathogens which may cause similar symptoms. In post mortem examinations of cerebral malaria patients sequestration of infected erythrocytes (IEs) in the brain is always evident (Wassmer et al., 2015; Milner et al., 2014). Apart from that, the histopathologic patterns can differ significantly between patients, especially between adults and children, with children presenting endothelial damage and perivascular ring hemorrhages, fibrin-thrombi and monocyte accumulation and more frequent breakdown of the blood-brain barrier (BBB). The primary cause for CM is still under debate, sequestration of IEs and subsequent congestion of blood vessels being one explanation for

CM symptoms (White et al., 2013). Others argue that cytokines play a major role and cause inflammation of endothelial cells and BBB damage (Storm and Craig, 2014). A recent study could show a correlation between the amount of sequestered infected RBCs in the brain and other organs and the severity of CM, demonstrating that sequestration is a major cause for CM (Milner et al., 2015). Besides CM, sequestration of iRBCs in the placenta can cause placental malaria, which leads to fetal growth restriction and therefore low birth weight and lower survival rates (Umbers et al., 2011).

P. vivax and *P. ovale* cause periodic fever attacks. After an incubation period of 12-20 days for *P. ovale* and ~14 days for *P. vivax*, fever attacks lasting 6-10 hours occur every third day (tertian malaria) (Collins and Jeffery, 2005; Bartoloni and Zammarchi, 2012). Usually these parasites cause no severe complications although there is increasing evidence for severe malaria in *P. vivax* infections. This seems to occur despite the rather low parasitemias due to preferential invasion of reticulocytes (Moreno-Perez et al., 2013). Both *P. vivax* and *P. ovale* generate hypnozoites which can lead to malaria relapses months and years after the primary infection (Anstey et al., 2009).

P. malariae has an incubation period of 18-40 days and causes fever attacks every 72 hours (quartan malaria). It only rarely causes severe complications, but blood stages may persist in the host asymtomatically for up to 50 years causing recrudescences (Bartoloni and Zammarchi, 2012). *P. knowlesi* malaria causes a wide spectrum of disease and is clinically similar to either *P. vivax* or *P. falciparum* malaria and complications such as respiratory distress and hyperparasitemia are fairly common (Daneshvar et al., 2009).

1.1.3. Prevention and Treatment

In 1955 the WHO launched the Global Malaria Eradication Programme with the aim to eradicate malaria in most parts of the world, not including African regions where malaria transmission is intense. Through vector control and malaria drugs the disease was eradicated in the United States of America and Western Europe. The emergence of drug resistant parasites and insecticide resistant mosquitoes halted the success of the program and today malaria rates remain high, especially in sub-Saharan Africa and South-East Asia (Greenwood et al., 2008; World Health Organization, 2015). Since the year 2000 several declarations and plans to control or eliminate malaria have been launched, a major one being the United Nations Millennium Declaration. The goal of this declaration was "to have halted by 2015 and begun to reverse the incidence of malaria and other major diseases", such as HIV. Since 2000, malaria cases in 57 countries have been reduced by 75%, thereby achieving one goal of the declaration (World Health Organization, 2015). Future strategies for malaria elimination focus on vector control and drug and vaccine development, and will be discussed below.

1.1.3.1. Vector control

In the past, the most successful vector control measurement in terms of malaria eradication was the use of the insecticide DDT, especially during the years 1943-1972. Its use reduced the population at risk of malaria from 77% in 1900 to about 50% in 1975 (Enayati and Hemingway, 2010). In malaria vector control DDT was predominantly used for indoor residual spraying (IRS), so that significant results could be obtained with small amounts of DDT. In contrast, 70-80% of DDT used worldwide was deployed for pest control in agriculture. After long term effects on human health and ecosystems where discovered most uses of DDT were banned in the 1970s and 1980s. Because DDT is stored in all tissues, especially in fat, it accumulates in the food chain, and DDT and its metabolites can be detected worldwide and probably in all living organisms. Because of its low cost DDT is still used for IRS in some African countries, where a complete ban would cause significantly more malaria infections (Turusov et al., 2002; Pluess et al., 2010; Enayati and Hemingway, 2010). Other insecticides used are organophosphorous insecticides, organochlorines, carbamates and pyrethroids. Resistance against DDT and pyrethroids is common and today limits the usefulness of these insecticides (Turusov et al., 2002).

The use of insecticide-treated bednets (ITNs) and long-lasting ITNs (LLINs) can substantially decrease malaria transmission and was shown to increase child survival in Africa (Greenwood et al., 2008). The use of insecticides however renders this measure also vulnerable to insecticide resistance of the mosquitoes (Turusov et al., 2002). Furthermore, protecting children from malaria infections could leave them more susceptible to severe malaria as adults, because partial immunity, and therefore protection against severe symptoms, cannot be developed during childhood (rebound effect) (Guyatt et al., 1999). To receive the maximum benefit from the use of ITNs, simultaneous reduction of mosquito breeding sites and environmental management in general needs to be achieved (Obala et al., 2015).

In recent years the possibility of releasing gene modified *Anopheles* mosquitoes got into focus. Through the development of novel gene editing techniques (e.g. the CRISPR-Cas9 system) and the gene drive technology it could now be possible to release a small number of mosquitoes resistant to malaria infection. It is predicted that this resistance will then be able to spread through a majority of the mosquito population (Gantz et al., 2015). Other gene drive strategies target the fertility of mosquitoes and could substantially decrease mosquito populations (Hammond et al., 2016). However, the consequences that the gene drive system and release of these mosquitoes could have on the ecosystem are not predictable and are currently under debate (Pennisi, 2015).

1.1.3.2. Drugs

The first anti-malarial compound, quinine, was already discovered in the 17th century. Two legends, that differ between South America and Europe, tell the story of its discovery, which involves a native American or the Spanish Countess of Chinchon, respectively. Before 1820 quinine and the related cinchoa alkaloids quinidine, cinchoine and cinchonidine, were ingested as the pulverized bark of the cinchoa tree mixed into a liquid. Since 1820 the compounds can be extracted from the bark and were subsequently used as the standard treatment for malaria. In the 1920s new synthetic and more effective drugs were released, and chloroquine became the main drug against malaria. Its extensive use led to the development of resistance in the 1950s, which spread across the world from two foci, one in South-East-Asia and one in South America to become common in the 1980s. Since then quinine became more relevant again and today is still used as a drug for malaria management (Achan et al., 2011).

Chloroquine resistance rendered the drug mostly useless against falciparum malaria except for some regions in North Africa, Central America and the Caribbean. Chloroquine and the other quinine derivatives amodiaquine, piperaquine and mefloquine target the formation of hemozoin, a *Plasmodium* specific metabolite of hemoglobin degradation. Resistance against chloroquine is predominantly mediated by the K76T mutation in the *P. facliparum* chloroquine resistance transporter (*Pf*CRT). Mutations in *Pf*CRT also mediate or facilitate resistance against other malaria drugs, e.g. amodiaquine and mefloquine (Müller and Hyde, 2010). After the emergence of chloroquine resistance other drugs such as sulfadoxine-pyrimethamine and atovaquone-proguanil became more important for malaria treatment, but resistance also emerged for many of those (Wongsrichanalai et al., 2002).

Since 2006 the WHO recommends the use of artemisinin-based combination therapies (ACTs) (Wells et al., 2015). In ACTs artemisinin or a derivative, e.g. dihydroartemisinin or artesunate, is combined with a partner drug, e.g. amodiaquine, mefloquine or piperaquine, which is supposed to reduce the risk of resistance development against the highly efficient and fast acting artemisinins (Fairhurst et al., 2012). Artemisinin was discovered by Chinese scientists as a drug for malaria therapy in the 1970s, but it has already been used in traditional Chinese medicine for over 1000 years to treat many diseases (Cui and Su, 2009). Although artemisinins are primarily applied as ACTs, resistance emerged and is now common in the Thailand-Cambodia border region (Dondorp et al., 2009). A mutation in the *Pf*Kelch13 protein (C580Y) is associated with artemisinin resistance and now considered a molecular marker for resistance (Ariey et al., 2014). The biochemical targets and therefore also the resistance mechanisms of artemisinins are not known. A recent study proposed that artemisinin is a potent inhibitor of the *P. fal-*

ciparum phosphatidylinositol-3-kinase (*Pf*PI3K) (Mbengue et al., 2015), while another study suggests that haem activated artemisinin promiscuously targets proteins involved in essential biological processes of the parasite (Wang et al., 2015).

The emerging drug resistances require a constant supply of novel malaria drugs. In recent years several compounds were identified and are currently being tested in clinical trials. Many of these compounds are based on the molecule structure of existing drugs but several new molecules were identified in phenotypic screenings. Nevertheless, the search for new drugs must go on to ensure a continued supply of treatments in the future (Rottmann et al., 2010; Wells et al., 2015).

1.1.3.3. Vaccine development

The complex life cylce of *Plasmodium* makes vaccine development a difficult task. However, this fact also offers multiple potential points of attack for vaccines. Thus, pre-erythocytic, erythrocytic and transmission blocking vaccines are currently under investigation (Moreno and Joyner, 2015). The most advanced and promising vaccine candidate is RTS,S/AS01. It targets the circumsporozoite protein (CSP), which is expressed on the sporozoite surface and by early liver stages. This vaccine targets sporozoite motility and hepatocyte invasion, thus inhibiting efficient invasion (Ouattara and Laurens, 2015). RTS,S/AS01 contains a recombinant antigen consisting of amino acids 207-395 of CSP and the HBsAg (hepatitis B surface antigen), free HbsAg and a specific adjuvant formulation (AS01). The CSP peptide consists of the NANP repeats, which represent the immunodominant B-cell epitope and a C-terminal flanking region (T-cell epitope) (Hoffman et al., 2015). RTS,S/AS01 is the first malaria vaccine tested in a clinical phase 3 trial, and showed an overall efficacy against clinical malaria of 27% in infants and 39% in children aged 5-17 months, when administered in four doses. The WHO recommends large-scale implementation pilots in moderate to high malaria transmission settings in 3-5 sub-Saharan countries to evaluate the consequences of vaccination, including side effects, efficacy and mortality, and feasibility in context of the local health care systems (World Health Organization, 2016).

It has been known for decades that infection with radiation attenuated sporozoites can induce high-grade protection against malaria infection in humans. While early experiments used live mosquitoes to deliver the attenuated sporozoites into the host, it is now possible to induce immunity with intravenous (IV) injection of radiation attenuated, aseptic, purified, cryopreserved *P. falciparum* sporozoites (*Pf*SPZ), developed by the company Sanaria (Seder et al., 2013). The company's aim is to produce an injectable whole *Pf*SPZ vaccine, which is supposed to prevent malaria in non-immune travelers and to eliminate malaria in geographically defined regions. A major obstacle on the road towards a practi-

cable vaccine is the large-scale production of sporozoites, which have to be dissected from mosquito salivary glands.

Erythrocytic vaccines aim to induce immunity against the invasive merozoites and thus to prevent invasion of red blood cells (RBCs). These vaccines either include recombinantly expressed proteins or use a viral vector to deliver the specific DNA. The targets of these vaccines include MSP-1 (merozoite surface protein-1) and AMA-1 (apical membrane antigen-1), which are expressed on the merozoite surface and on the merozoite and sporozoite surface, respectively. None of these vaccines could induce protection against malaria infection in clinical trials, which is in part due to polymorphisms in these antigens (Moreno and Joyner, 2015).

In combination with vaccines that prevent or reduce clinical malaria, transmission blocking vaccines are thought to be a useful agent in the fight against malaria. These vaccines induce the generation of antibodies which inhibit the development of parasites inside the mosquito. Prominent antigens are the pre-fertilization targets Pfs230 and Pfs48/45 and the zygote/ookinete target Pfs25. Up until now only two Pfs25 based vaccines have reached a phase 1 clinical trial, and the ability of transmission blocking vaccines to actually decrease malaria case numbers still needs to be assessed (Nikolaeva et al., 2015).

1.2. *Plasmodium falciparum* biology

Plasmodium falciparum is a protozoan, obligate intracellular parasite belonging to the phylum *Apicomplexa*. *Apicomplexa* are characterized by the presence of the apical complex, specific secretory organelles at the apex of the parasite that are important for cell invasion. Another characteristic of most *Apicomplexans* is a plastid, called apicoplast that was acquired by a common ancestor of the *Apicomplexa* via secondary endosymbiosis of a red alga. While this ancestor was presumably still able to use photosynthesis, this ability was lost in the *Apicomplexans*. Recent findings identify the photosynthetic algae *Chromera* and *Vitrella* as close relatives of *Apicomplexa*, and an organism called Apicomplexan Related Lineage-5 (ARL-V) as the closest known relative. These organisms were found in coral habitats, suggesting that the obligate intracellular lifestyle of *Apicomplexans* might have evolved in corals first (Keeling and Rayner, 2015).

1.2.1. The *P. falciparum* life cycle

Plasmodium parasites reside and develop within different host species and cell types, which require certain adaptions specific for the respective environment. The *Plasmodium* life cycle includes mosquito stages, human liver stages and human blood stages (see figure 1.2).
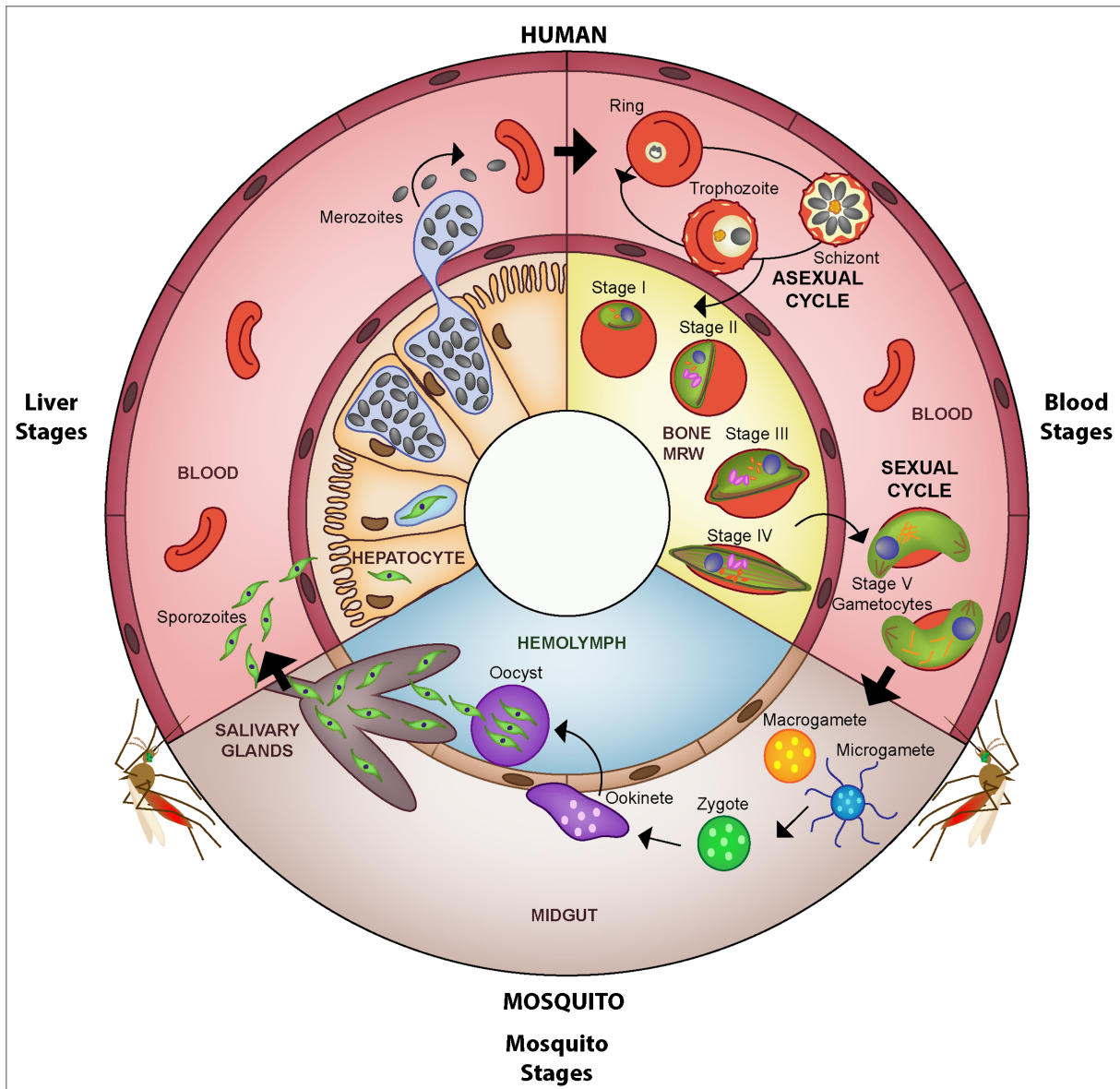
Figure 1.2.: *Plasmodium falciparum* life cycle. Sporozoites are injected into the human host, where they invade liver cells and generate thousands of merozoites that are released into the blood stream. Merozoites invade RBCs and develop through ring, trophozoite and schizont stages and generate new merozoites. A small fraction of parasites develops into male and female gametocytes which can be ingested by mosquitoes where the sexual development takes place. (from Nilsson et al., 2015)

1.2.1.1. Liver stages

The life cycle in humans is initiated with the bite of an infected *Anopheles* mosquito. This leads to the injection of usually several dozens of sporozoites from the salivary gland into the human skin, from where they migrate to dermal blood vessels and lymphatic vessels. Approximately 50% of the sporozoites remain in the skin, where they can develop into exo-erythrocyctic forms (EEFs) and potentially contribute to malaria blood stage infection (Gueirard et al., 2010). Most sporozoites invading lymphatic vessels are phagocytosed or degraded in the lymphnodes, while sporozoites that have reached the bloodstream are transported towards the liver (Amino et al., 2006). In the liver capillaries, the so called sinusoids, sporozoites are sequestered, probably through the interaction of highly sulphated heparan sulphate proteoglycans (HSPGs) extending from stellate cells through fenestrations in endothelial cells and CSP on the surface of sporozoites. Sporozoites then traverse the sinosoid endothelium through endothelial cells or Kupffer cells, to reach the liver parenchyma, where they traverse and invade hepatocytes. Traversal of cells occurs through the formation of a transient vacuole, which is distinct from the parasitophorous vacuole (PV), where replication takes place (Risco-Castillo et al., 2015). Finally, the sporozoite invades a hepatocyte where it develops into a schizont containing many thousand mature merozoites. The interaction between the parasite CSP and thrombospondin-related anonymous protein (TRAP) and the sulphated HSPGs on the hepatocyte surface was shown to be important for hepatocyte infection, while the identity of many other potential receptors is still unknown (Kaushansky and Kappe, 2015). During the invasion process the PV is generated in which the parasite resides during the liver stage, a process that was recently shown to be dependent on the host EphA2 receptor and parasite 6-Cys proteins (Kaushansky et al., 2015). As soon as the sporozoite completes the final invasion, the differentiation into exo-erythrocytic forms is initiated, leading first to the generation of a trophozoite. During this process the sporozoite changes its shape from an elongated into a round form, disassembles the machinery necessary for invasion and modifies the PV membrane (PVM). The PVM protects the parasite from clearance, as host cells infected with PVM surrounded parasites are less susceptible to apoptosis. The liver trophozoite then develops into a schizont, replicating its genome between 10^4 and 10^5 times, generating thousands of merozoites. This goes along with a massive increase in parasite volume and requires the uptake of host cell nutrients. The PVM was shown to contain non-selective solute pores, facilitating small molecules to access the parasite and guarantee the parasites' nutrient supply (Bano et al., 2007; Kaushansky et al., 2015).

At the end of the liver stage the PVM is disintegrated so that the merozoites are free inside the host cell cytoplasm. The release of merozoites into the blood stream occurs via merosomes, host cell membrane derived vesicles containing thousands of merozoites,

which were shown, for the rodent malaria parasite *P. yoelii*, to rupture in the pulmonary microvasculature (Sturm et al., 2006; Baer et al., 2007; Vaughan et al., 2012).

1.2.1.2. Blood stages

Following merosome rupture the merozoites rapidly invade RBCs, a process that usually takes less than 1 minute (Weiss et al., 2015). After an initial attachment to the RBC the merozoite reorients its apical end towards the RBC membrane, followed by the formation of a tight junction. The subsequent release of the rhoptries triggers the active invasion, mediated by the moving junction in combination with an actin-myosin motor, resulting in the formation of a parasitophorous vacuole (PV).

Present evidence suggests that the initial attachment is amongst others mediated by the MSP1 complex, consisting of four proteolytically produced MSP1 fragments and representing a platform for the binding of other merozoite surface proteins (Boyle et al., 2010; Weiss et al., 2016) (also see section 1.2.2.4). MSP1 was shown to bind the RBC membrane protein complex band3/glycophorin A during the initial steps of invasion (Baldwin et al., 2015).

Accompanying the initial attachment, a weak deformation of the RBC membrane can be observed, which increases during reorientation of the merozoite and involves reorganization of the RBC cytoskeleton (Weiss et al., 2015). Two classes of adhesins, the erythrocyte binding antigens (EBAs) and the reticulocyte-binding like homologs (Rhs), released from the micronemes and the rhoptry neck, respectively, mediate irreversible attachment and reorientation of the merozoite (Harvey et al., 2012). These molecules have partially redundant functions, which is why they are referred to as the alternative pathway ligands (Dolan et al., 1990). EBAs and Rhs interact with several known and unknown receptors on the RBC surface and may also be involved in signaling downstream events. Especially the interaction of *Pf*Rh5 with its erythrocyte surface receptor basigin, which occurs in a step downstream of the activity of the other *Pf*Rhs and which also is structurally and functionally different from the other Rhs, probably triggers the release of rhoptry proteins, leading to the formation if the tight junction. (Weiss et al., 2015).

The tight junction is formed after the release of rhoptry neck protein 2 (RON2) and other RON proteins from the rhoptries and subsequent insertion into the RBC membrane and injection into the RBC, respectively. RON2 interacts with AMA1, forming a ring-shaped tight junction, which triggers the release of the rhoptry bulb into the space between RBC membrane and merozoite confined by the tight junction. The released rhoptry proteins and lipids play a role in the formation and modification of the PV. The actions of an actin-myosin motor then pull the tight junction over the merozoite surface, engulfing it with RBC membrane, which is sealed at the end of the process. During this process
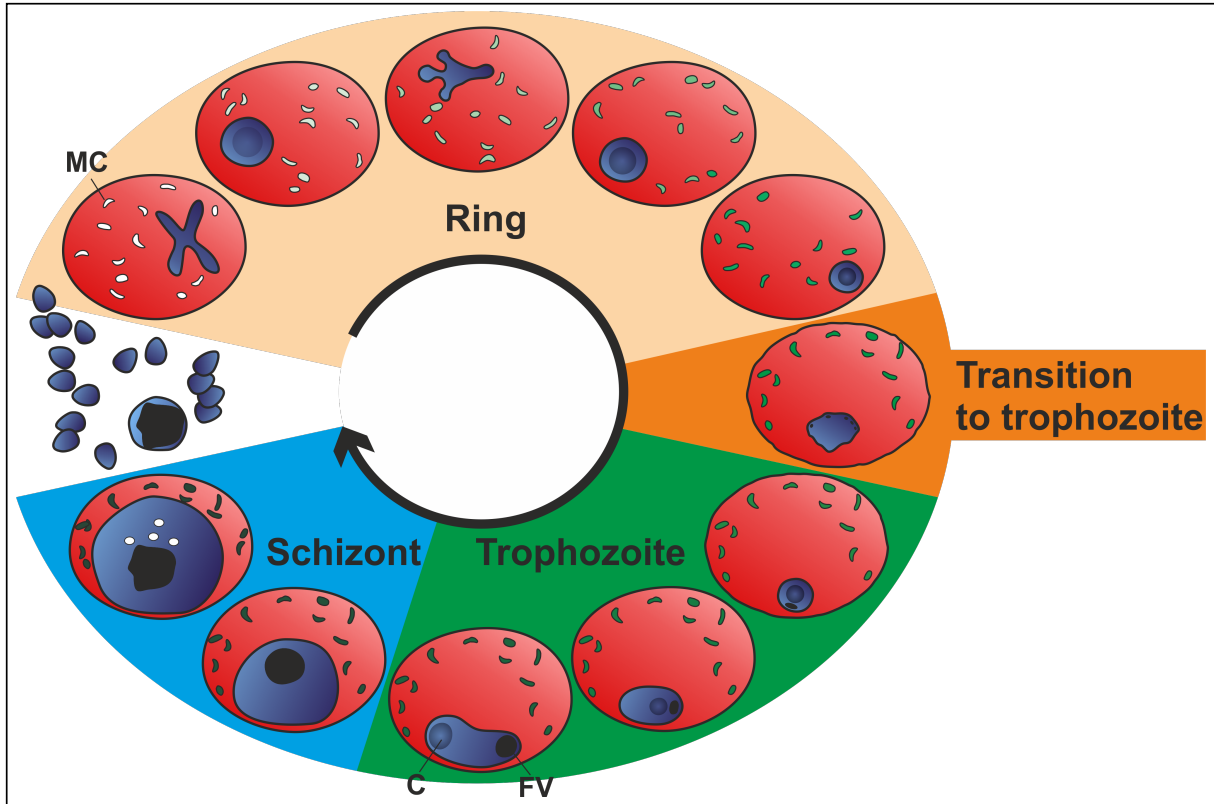
Figure 1.3.: *P. falciparum* **blood stage development.** After invasion the ring stage parasite starts to modify its host cell, e.g. by the introduction of Maurer's clefts. During ring stage development the parasite switches between a round/circular and amoeboid appearance. The anchoring of Maurer's clefts and condensation of the parasite marks the transition to trophozoite stage. The parasite grows in volume and accumulates hemozoin in its food vacuole (FV), often a cavity (C) can be observed. After nuclear division in the schizont stage, merozoites are generated and released into the blood stream (modified from Grüring et al., 2011)

.

most of the merozoite surface protein coat is shed by proteases (Cowman et al., 2012; Weiss et al., 2016).

The freshly invaded parasite, termed ring stage parasite, starts to extensively modify its host cell, which takes approximately 24 hours. After 24 hours the parasite has transitioned into a trophozoite, with the transitioning taking 2-4 hours. During the trophozoite stage the parasite shows a large increase in volume while ingesting a major fraction of the host cell cytosol (Grüring et al., 2011). Throughout the schizont stage, starting 36 hours post invasion, up to 22 daughter parasites are generated. The blood cycle is complete after 48 hours, when the RBC ruptures and new merozoites are released into the blood stream (figure 1.3).

Two to 4 hours after invasion the first exported proteins (see section 1.2.2) can be detected in parasite induced membranous structures in the host cell termed Maurer's clefts (see section 1.2.2.3). These structures play a role in the generation of RBC membrane

modifications termed knobs, which appear at the end of the ring stage and mediate cytoadhesion of infected RBCs to the blood vessel endothelium to protect the parasite from clearance in the spleen (Maier et al., 2009). During ring stage development the parasite switches between a disc shaped and an amoeboid shaped appearance and is motile within the RBC. Similarly, the Maurer's clefts show a very motile behavior (Grüring et al., 2011). The PVM surrounds the parasite during the whole blood stage until just before evasion and an extension of it forms the so called tubovesicular network (TVN), which might function in nutrient uptake (Lauer et al., 1997). Another feature of the PVM together with the parasite plasma membrane (PPM), is the so called cavity, a cup shaped extension of both membranes into the RBC cytosol (Grüring et al., 2011). The function of the cavity is so far not known but it may have a role in lipid storage or as a general surface enlargement (Kruse, 2014).

Starting at 16 hours post invasion haemozoin crystals in separate locations can be observed within the parasite, indicative of the presence of several small food vacuoles. During transitioning into the trophozoite stage the hemozoin crystals accumulate in one food vacuole, which takes up approximately 80% of host cell cytosol (consisting of ~99% hemoglobin) during development. The exact mechanism of host cell cytosol uptake is unknown, but might involve structures called cytostomes that can be observed in electron microscopy. The food vacuole itself is a lysosome-like compartment harboring, amongst others, several proteases for hemoglobin degradation (Klemba et al., 2004). The parasite uses only ~16% of the taken up hemoglobin as a source for amino acids, illustrating that host cell cytosol uptake and hemozoin formation also are a means to generate space for growth inside the RBC (Krugliak et al., 2002).

Following the trophozoite stage, the parasite enters the schizont stage during which the parasite undergoes 3-4 rounds of mitosis resulting in a syncytial schizont containing 16-22 haploid nuclei. *Plasmodium* mitosis differs from the traditional view of mitosis in that the nuclear membrane stays intact during spindle development and chromosome segregation (closed mitosis) and in that nuclear division is asynchronous (Gerald et al., 2011). During a final synchronous round of nuclear division the cytokinesis by budding is initiated. The daughter cells are assembled with the help of a microtubule scaffold, organized by the apical polar ring (APR) which functions as a microtubule organizing center (MTOC). Along the microtubule scaffold the inner membrane complex (IMC) is assembled, which are flattened membrane cisternae underlying the plasma membrane that stabilize the cell morphology and that are also essential for gliding motility and invasion. The apical complex organelles are generated de novo, probably deriving from golgi membranes, and positioned at the apical end of the forming merozoite (Francia and Striepen, 2014). The merozoite plasma membrane is generated by invagination of the mother cell

plasma membrane, probably guided by the basal complex, a cytoskeletal structure at the basal end of the IMC (Kono et al., 2016). Merozoite egress is enabled by the sequential disintegration of the PVM and rupture of the RBC membrane, a process dependent on proteases discharged from the micronemes (Blackman and Carruthers, 2013).

The transmission of the *Plasmodium* parasite depends on the successful generation of the sexual blood stages, which can be taken up by the mosquito vector. Only a fraction of parasites develops into male or female gametocytes. The factors triggering gametocytogenesis are not completely understood. Recent studies implicate infected RBC derived microvesicles and exosome-like vesicles, transferring parasite or host factors, in the initiation of the process, but environmental factors like the host nutritional status or drugs also play a role (Regev-Rudzki et al., 2013; Mantel et al., 2013; Dantzler et al., 2015). Commitment to gametocytogenesis occurs one cycle before the generation of gametocytes (Bruce et al., 1990), with the transcriptional regulator ApiAP-2 playing an essential role in this process (Sinha et al., 2014; Kafsack et al., 2014). Taken together, these studies imply that epigenetic factors could be responding to environmental factors, thus adjusting the decision for gametocytogenesis (Dantzler et al., 2015). The development from a sexually committed ring stage parasite to a mature gamtocyte takes 8-12 days and can be divided into five stages (I-V). Stages I to IV sequester within the host tissue, e.g. in the bone marrow, and only mature stage V gametocytes can be found in the peripheral blood and are ingested by a mosquito during a blood meal (Butterworth et al., 2013).

1.2.1.3. Mosquito stages

When stage V gametocytes are taken up by an *Anopheles* mosquito during a blood meal they are exposed to changes in the environment, which triggers differentiation into male microgametes and female macrogametes. Differentiation can be initiated by a ≥ 5 °C decrease in temperature and the presence of the mosquito metabolite xanthurenic acid (XA). This is followed by a rounding up of gametocytes and egress from the RBC after 10 minutes. During this time male gametocytes undergo three rounds of genome replication and produce 8 motile microgametes, that are attached to a central residual body from which they detach by binding to other RBCs. Upon encountering a female macrogamete the cells fuse and produce the ookinete, which undergoes one meiotic division and after 24 hours migrates through the gut wall and remains underneath the mosquito midgut basal lamina, where it is protected from the host immune system and transforms into an oocyst. During the longest (10-14 days) and only extracellular developmental multiplication stage, the oocyst undergoes several mitotic divisions, generating the sporoblast from which several hundred sporozoites bud and egress the oocyst. Through the hemolymph the sporozoites reach the basal lamina of the salivary glands, where they invade acinar cells

to finally accumulate inside the salivary duct. Here the sporozoites have accomplished complete maturation and thus infectivity (Matuschewski, 2006).

1.2.2. Protein export

Protein export is defined as the trafficking of proteins beyond the PVM. Approximately 5-10% of all *P. falciparum* proteins are predicted to be exported (exportome), illustrating the importance of protein export for the parasite (Spielmann and Gilberger, 2015). For example, cytoadhesion to the endothelium of blood vessels, an important cause for parasite virulence, is mediated by exported proteins and ensures the *in vivo* survival of the parasite (Maier et al., 2009). By blocking the entire protein export, it was demonstrated that it is also essential *in vitro* (Beck et al., 2014). However, the function of most exported proteins is still unknown and their study is impeded by the fact that many of them may only play a role *in vivo* (Maier et al., 2008). Investigating the export mechanism and functions of exported proteins is important for understanding how *P. falciparum* survives in the host cell and how it causes malaria and thus for finding strategies to combat it.

1.2.2.1. Signals and motifs in *P. falciparum* protein export

After entry into the secretory pathway, exported proteins of *Plasmodium* parasites have to cross two membranes, the PPM and the PVM, which necessitates the presence of special sorting signals. Most known exported proteins possess a PEXEL-motif (~450 proteins) (*Plasmodium* export element)/HT-motif (host targeting) with the amino acid consensus sequence RxLxE/Q/D (Marti et al., 2004; Hiller et al., 2004). For being functional the motif has to be localized approximately 20 amino acids downstream of a signal peptide. Interestingly, the signal peptide of PEXEL proteins is often atypical in that it can be recessed up to 80 amino acids from the N-terminus. The functional consequences of this are unknown, but might be related to differences in soluble and membrane proteins, as it was shown that ~90% of soluble proteins contain an atypical signal peptide (SP), but only ~10% of membrane proteins (Deponte et al., 2012). Upon translocation into the endoplasmic reticulum (ER) the SP is removed by the signal peptidase complex (Chang et al., 2008) and the PEXEL motif is cleaved by the protease Plasmepsin V (Boddey et al., 2010; Russo et al., 2010). Plasmepsin V recognizes the arginine and leucine residues and cleaves the motif between position 3 and 4. The new N-terminus xE/Q/D is N-acetylated, although any function of this modification is unclear, and the mature protein is exported into the host cell (Boddey et al., 2009). The downstream region of the mature PEXEL N-terminus (~20 amino acids) was found to contain additional export information which can complement for a mutated xE/Q/D in a reporter construct (Grüring et al.,

2012; Tarr et al., 2013). Earlier reports, stating that the newly exposed N-terminus interacts with phosphatidylinositol 3-phosphate (PI(3)P) on the luminal side of the ER membrane and that it is deciding for export (Bhattacharjee et al., 2012) were recently challenged by showing that PI(3)P is not present in the ER and that there is no interaction with the processed PEXEL motif (Boddey et al., 2016). Non-canonical PEXEL-motifs in *Plasmodium* proteins, e.g. the RxLxxE sequence in the RESA protein family, were also shown to be cleaved by Plasmepsin V and exported to the host cell (Boddey et al., 2013). The major virulence factor of *P. falciparum*, *Pf*EMP1, contains the non-canonical sequence KxLxD which cannot be processed by Plasmepsin V, whereas processing of this motif can occur in other proteins, depending on the surrounding sequence environment (Schulze et al., 2015).

The number of known exported proteins without a PEXEL-motif to date comprises only ~20 proteins (not counting members of protein families) and are referred to as PNEPs (PEXEL-negative exported proteins). 'Classical' PNEPs do not contain a SP and ER entry is mediated by a transmembrane domain (TMD). The export relevant information is located within the first 10-20 amino acids of the N-terminus, however, no consensus sequence could be identified yet, so that export prediction is not possible. Replacement of a PNEP N-terminus with a mature PEXEL N-terminus can rescue the export of a PNEP reporter construct, indicating that PNEPs and PEXEL-proteins share a common export domain and might be exported via the same export pathway (Grüring et al., 2012). Furthermore, for the PNEP REX2 it was shown that, similar to PEXEL-proteins, proteolytic processing of the N-terminus occurs, but the responsible protease and the consequences of the processing for export are unknown. Besides the N-terminus, the TMD also contains export relevant information, as TMDs from non-exported proteins cannot efficiently substitute for a PNEP TMD (Haase et al., 2009; Grüring et al., 2012; Saridaki et al., 2009). Heiber *et al.* and others recently identified several novel PNEPs, some of which contain SPs and no TMD, or both a SP and a TMD, demonstrating that they are structurally more diverse than previously assumed (Külzer et al., 2012; Heiber et al., 2013; Mbengue et al., 2013). The PNEP *Pf*Hsp70-x contains only a SP mediating entry into the secretory pathway, and similar to other PNEPs, the mature N-terminus (8 amino acids) comprises the export signal (Külzer et al., 2012). The mode of export for the other novel PNEPs is currently unknown and their study is part of this work.

Other *Plasmodium* species contain a significantly lower number of PEXEL-proteins, suggesting that PNEPs might represent a larger fraction of exported proteins (Spielmann and Gilberger, 2010; Sargeant et al., 2006). In the rodent malaria parasite *P. yoelii* several members of the *yir* and *pyst* multigene families do not contain a PEXEL-motif but are exported to the host cell. Sequence alignments and secondary structure prediction

resulted in the discovery of a new export signal in *P. yoelii* PNEPs, comprising α-helical properties and conserved amino acid positions at the N-terminus (PYST-proteins) or C-terminus (YIR-proteins), including amino acids in the SP and TMD, respectively. These results imply that, besides sequence requirements, also secondary structure determinants might play a role in protein export (Siau et al., 2014). However, there is currently no data concerning secondary structure features in exported proteins in *Plasmodium* species other than *P. yoelii*.

1.2.2.2. Mechanism of protein export

From the ER to the PV Before exported proteins can reach the host cell, they first follow the classical secretory pathway, leading to the delivery into the PV. This corresponds to the extracellular space in free-living organisms. The ability to secrete proteins into the extracellular space is already present in archeae and bacteria and parts of the molecular machinery are conserved between prokaryotes and eukaryotes. To be secreted, inserted into the plasma membrane or to be localized to the secretory pathway, proteins usually have to be translocated into the ER first. During translation the nascent polypeptide chain can be recognized by the signal recognition particle (SRP) if it contains a SP or a TMD. Binding of the SRP leads to the interaction of the ribosome-nascent chain-SRP complex with the SRP receptor in the ER membrane leading to an interaction between the ribosome and the Sec61 complex. Upon interaction of Sec61 with the ribosome translation continues, resulting in a co-translational translocation into the ER. TMD containing proteins are inserted into the membrane by a lateral release of the polypeptide from the Sec61 pore. Alternatively, proteins can be translocated into the ER post-translationally. This requires newly synthesized proteins to be retained in an unfolded confirmation by cytosolic chaperones. Translocation of these proteins depends on the SP recognition by the ER membrane localized Sec63 complex, which cooperates with Sec61 and the ER luminal chaperone BiP (Rapoport, 2007; Barlowe and Miller, 2013).

The molecular components for co- and post-translational translocation into the ER are conserved in *Plasmodium* parasites, indicating that both modes of ER entry can occur (Tuteja, 2007). Once inside the ER, proteins are post-translationally modified by e.g. GPI anchor addition and disulfide bond formation, and sorted into COPII vesicles, for which the components are conserved in *Plasmodium*. In contrast to other eukaryotes N- and O-linked glycosylation are potentially absent or their extent and significance for *Plasmodium* biology is controversial (Cova et al., 2015; Gowda and Davidson, 1999). The extent to which proteins are specifically recognized and sorted into COPII vesicles is unknown, especially considering the stage specific transcription of *Plasmodium* proteins, non-specific cargo loading (bulk flow) could play a major role in ER exit (Deponte et al.,
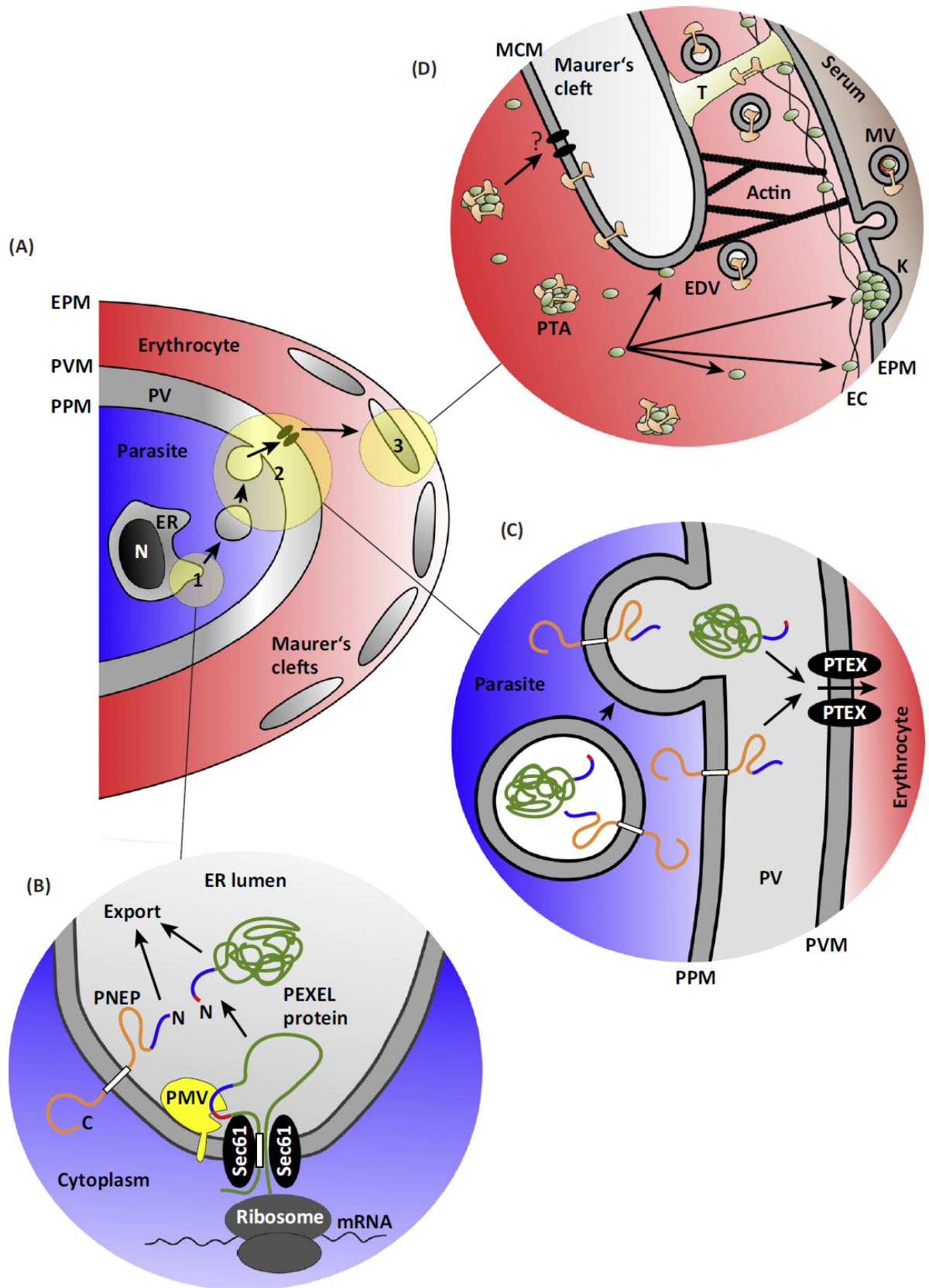
Figure 1.4.: *P. falciparum* protein secretion. (A) Exported proteins are trafficked from the ER to the PV in a vesicular manner. After a translocation step at the PVM proteins reach their final destination inside the host cell. (B) Proteins are translocated into the ER via Sec61. The PEXEL-motif is cleaved co-translationally by Plasmepsin V, which enables export. (C) Vesicular trafficking of soluble and membrane proteins to the PPM, where all proteins are translocated via PTEX. (D) Inside the host cell proteins might be trafficked in protein trafficking aggregates (PTA) that may represent structures termed J-dots. Some proteins localize to Maurer's clefts while others reach the RBC surface, either directly or via transient association with Maurer's clefts. (from Spielmann and Gilberger, 2015)

2012). In ring stage parasites the presence of a single ER exit site was demonstrated, with the number of ER exit sites increasing during blood stage development resulting in one ER exit site for each merozoite (Lee et al., 2008; Struck et al., 2008). The golgi complex in *P. falciparum* is rudimentary and does not exhibit the typical stacked phenotype seen in other eukaryotic cells (Struck et al., 2005). Nevertheless, the golgi might consist of distinct biochemical compartments representing *cis-* and *trans*-golgi (Struck et al., 2008). From the *trans*-golgi proteins are trafficked via vesicles to their final destinations, including the digestive vacuole, apical organelles, mitochondria, apicoplast and PV/PVM (Deponte et al., 2012; Heiny et al., 2014). Important members of the trafficking machinery involved in post-golgi pathways are conserved in *Plasmodium*, including SNARES, clathrin heavy chain and several Rabs. Upon arrival at the parasite periphery vesicles fuse with the PPM and release soluble proteins into the PV lumen and membrane proteins into the plasma membrane (Deponte et al., 2012) (also see figure 1.4 A,B,C).

The branching point at which exported proteins are sorted from proteins destined for other cellular locations, e.g. the PV or PVM, is not known. Exported proteins might already be sorted into designated export vesicles in the ER or golgi and be released into specific export regions inside the PV, or be themselves or via chaperones recognized by components of PTEX (see paragraph 1.2.2.2) or associated proteins inside the PV/PPM (Deponte et al., 2012).

Protein translocation All exported proteins tested so far need to be translocated at the PVM to reach the host cell cytosol (Gehde et al., 2009; Grüring et al., 2012; Heiber et al., 2013). The putative translocon that is responsible for this step was recently identified and named *Plasmodium falciparum* translocon of exported proteins (PTEX). It consists of the putative pore component exported protein 2 (EXP2), heat shock protein 101 (HSP101), PTEX150, PTEX88 and thioredoxin 2 (TRX2) (de Koning-Ward et al., 2009). HSP101 is a ClpB-like AAA+ ATPase essential for PTEX function and might be involved in unfolding of proteins (Beck et al., 2014; Elsworth et al., 2014). TRX2, which is not essential for parasite survival but important for normal growth, is a redox-active thioredoxin family

member and could function in breaking disulfide bonds (de Koning-Ward et al., 2009; Matthews et al., 2013). A PTEX88 knock-out, also shown not to be detrimental *in vitro*, abolished sequestration of infected RBCs in the murine *P. berghei* malaria model (Matz et al., 2015). PTEX150, which is specific for *Plasmodium* species, was shown to be essential for protein export (Elsworth et al., 2014) and also might play a role in regulating PTEX stability (Elsworth et al., 2016). The supposedly pore forming EXP2 is present as a homo-oligomeric protein complex and can complement the *Toxoplasma gondii* GRA17, which might form the nutrient pore in the PVM in this parasite. One explanation for these findings may be, that EXP2 is both a part of the protein translocon and a part of the nutrient pore in *Plasmodium* (Gold et al., 2015). Until recently, no functional data on the proposed translocation activity of EXP2 existed, however, recent results directly link EXP2 and translocation, indicating that EXP2 is indeed part of a translocation entity (Mesén-Ramírez et al., 2016). Blocking the function of HSP101 showed that PTEX is essential for the export of all classes of exported proteins and thus blood stage development (Beck et al., 2014; Elsworth et al., 2014).

PTEX was shown to be a nexus for protein export of all types of proteins, including transmembrane proteins, however these studies do not explain how transmembrane proteins could interact with PTEX (Beck et al., 2014; Elsworth et al., 2014). There is evidence that membrane proteins are released into the PPM following secretion from the golgi and have to be extracted from this membrane to be exported into the host cell (Grüring et al., 2012). Membrane extraction could be mediated by a translocon or chaperone inside the PPM, or by components of PTEX or PTEX associated proteins, or a combination of these options, however, further studies are necessary to test these hypotheses (Spielmann and Gilberger, 2015).

Host cell Following translocation exported proteins need to reach their final destination inside the host cell, e.g. the host cell cytosol, Maurer's clefts or the RBC cytoskeleton or surface. Evidence suggests that soluble proteins as well as membrane proteins are trafficked in a non-vesicular manner, requiring chaperones to maintain the soluble state of membrane proteins (Papakrivos et al., 2005; Grüring et al., 2012). Recently, cholesterol containing protein complexes, containing the co-chaperone Hsp40 and chaperone Hsp70-x, were identified in the host cell and termed J-dots (Külzer et al., 2010, 2012). The integral RBC membrane protein and major *P. falciparum* virulence factor *Pf*EMP1 was shown to be associated with these structures, indicating their involvement in trafficking membrane proteins inside the host cell (Külzer et al., 2010). Several proteins destined for the RBC surface, including *Pf*EMP1 and the knob component KAHRP, transiently localize to Maurer's clefts, where they might be assembled into protein complexes or

otherwise modified, before further trafficking to the RBC surface. Reaching the RBC surface is dependent on Maurer's cleft integrity and probably on the reorganization of host cell actin (Cyrklaff et al., 2011; Kilian et al., 2015; Rug et al., 2014). In contrast, some soluble proteins can directly interact with the host cell cytoskeleton component spectrin underlying the RBC membrane or other parasite proteins localizing at the RBC periphery, thus being recruited to the RBC surface through protein-protein interactions (Parish et al., 2013; Tarr et al., 2014; Oberli et al., 2014). Some proteins even seem to be trafficked beyond the RBC membrane, as several studies reported the presence of erythrocyte-derived extracellular vesicles (EVs) containing Maurer's cleft proteins (also see section 1.2.2.4), (Regev-Rudzki et al., 2013; Mantel et al., 2013), (figure 1.4D).

1.2.2.3. Maurer's clefts: a host cell modification important for protein trafficking

In *P. falciparum* Maurer's clefts were first described by Georg Maurer in 1902, who believed them to be injuries of the RBC caused by parasite attachment (Maurer, 1902). Today, it is known that Maurer's clefts are parasite induced membranous structures inside the RBC cytoplasm. Maurer's clefts can already be detected 2-4 hours post invasion (hpi), their number remaining constant with ~15-20 Maurer's clefts per cell (Grüring et al., 2011). Maurer's cleft morphology ranges from globular to flattened or disk shaped, potentially being stage dependent. In ring stage parasites Maurer's clefts are highly motile (Grüring et al., 2011), with motility resembling Brownian motion (Kilian et al., 2013). During the transition from ring to trophozoite stage Maurer's cleft positions are arrested inside the RBC up to the late schizont stage (2-4 hours before rupture), when their spatial arrangement is partially disassembled (Grüring et al., 2011). After the spatial arresting of Maurer's clefts, tether-like structures connecting Maurer's clefts with the RBC membrane or PVM can be observed by electron microscopy (Hanssen et al., 2008). The only known protein that localizes to these tethers is MAHRP2, which is considered to be essential for parasite survival, as attempts to generate MAHRP2 knock-outs were not successful (Pachlatko et al., 2010). However, no specific function could be assigned to MAHRP2 yet, leaving also the role of the tethers in arresting Maurer's cleft movement in the dark. Interestingly, MAHRP2 is already expressed and localizes to tether-like structures before Maurer's clefts are arrested, indicating that additional processes are necessary for Maurer's cleft attachment (McMillan et al., 2013). It has been proposed, that Maurer's cleft arrest is initially mediated by changes in Maurer's clefts morphology, disturbing unobstructed Brownian motion, in combination with branched actin filaments, which were suggested to influence Maurer's cleft morphology (Cyrklaff et al., 2011; Kilian et al., 2013). The biological function of Maurer's cleft tethering is unknown but was proposed to mark the completion of host cell modifications (Grüring et al., 2011).

Maurer's clefts are considered to be involved in the sorting of exported proteins. Several proteins were transiently detected at Maurer's clefts before their appearance at the RBC membrane, including *Pf*EMP1, STEVOR, PHIST proteins and the knob component KAHRP (McMillan et al., 2013; Mundwiler-Pachlatko and Beck, 2013; Oberli et al., 2014). Genetic ablations of the Maurer's clefts component REX1 resulted in abnormal Maurer's cleft morphology and prevented *Pf*EMP1 display at the RBC membrane, demonstrating that Maurer's clefts play indeed a crucial role in protein trafficking (Spycher et al., 2008; Dixon et al., 2011). Similarly, the knock-out of another Maurer's cleft resident protein, SBP1, abolished *Pf*EMP1 display at the RBC surface (Cooke et al., 2006; Maier et al., 2007). Cyrklaff *et al.* reported branched actin filaments connecting Maurer's clefts with the RBC membrane and knobs, and vesicles in close association with the filaments, indicative of vesicular trafficking (Cyrklaff et al., 2011). This finding is consistent with the observation of budding vesicles from Maurer's clefts in electron microscopy (Hanssen et al., 2008). Furthermore, there is evidence that EVs are derived from Maurer's clefts and released upon rupture of RBCs (Mantel et al., 2013). In combination these studies support the suggested function of Maurer's clefts as organelles involved in protein sorting. However, many open questions remain, e.g. how Maurer's clefts are generated, why they are arrested, and how proteins are sorted into vesicles (Mundwiler-Pachlatko and Beck, 2013).

1.2.2.4. Functions of exported proteins

The functional characterization of proteins in *P. falciparum* is a difficult task, as many tools available in other systems are not applicable in this parasite. In addition homologies to known proteins that could give functional clues are often missing. The functional characterization of exported proteins is especially problematic, as many of those might only have a function *in vivo*. Probably the best characterized exported protein in *P. falciparum* is *Pf*EMP1, the major virulence factor. The *Pf*EMP1 variants are encoded by ~60 *var* genes per genome, of which only one is transcribed at any given time in a parasite, facilitating antigenic switching to ensure immune evasion. *Pf*EMP1 is a membrane protein and in trophozoite and schizont stage parasites is displayed at the RBC surface, concentrated in structures called knobs. The extracellular N-terminal part of the protein contains Duffy binding-like (DBL) and cysteine-rich interdomain region (CIDR) domains, which mediate cytoadhesion via different host surface receptors, e.g. CSA, ICAM-1 and CD36. The different *Pf*EMP1 variants contain individual combinations of DBL and CIDR domains, mediating receptor specificity (Hviid and Jensen, 2015). The C-terminal acidic terminal sequence (ATS) anchors the protein in the knobs and mediates interaction with the RBC cytoskeleton, which was shown to involve proteins of the PHIST family (Oberli

et al., 2014, 2016). KAHRP is the major knob component and essential for the generation of knobs. Upon KAHRP1 knock-out *Pf*EMP1 can still be exported to the RBC membrane, but cytoadhesion is significantly decreased under flow conditions, indicating that knob localization is important for *Pf*EMP1 anchoring to the RBC cytoskeleton (Crabb et al., 1997). Many exported proteins function in *Pf*EMP1 trafficking, cytoadhesion, knob formation and controlling RBC rigidity, demonstrated in a large scale knock-out study by Maier *et al.*, highlighting the importance of *Pf*EMP1 display/cytoadhesion for the parasite (Maier et al., 2008).

Besides the *var* genes, the *P. falciparum* genome encodes several other multigene families encoding exported proteins, including *surfin*, *FIKK* and the members of the 2TM-type supergene family *rifin, stevor* and *Pfmc-2TM* (Boddey and Cowman, 2013). STEVOR proteins were shown to play a role in RBC rosetting, potentially protecting infected RBC from the immune system and enhancing invasion of RBCs (Niang et al., 2014) and in increasing RBC rigidity, thus enhancing sequestration (Sanyal et al., 2012).

To ensure nutrient uptake and osmotic balance in the RBC the parasite induces new permeation pathways (NPPs) in the RBC membrane. The NPPs are facilitated by the plasmodial surface anion channel (PSAC), probably consisting of the proteins CLAG3.1 or CLAG3.2, which are expressed in a mutually exclusive manner and inserted into the RBC membrane upon or shortly after invasion (Desai, 2014).

The *P. falciparum* exportome likely includes more essential proteins, as indicated by the failure of generating knock-outs of these proteins (Maier et al., 2008). Further study of exported proteins is needed to elucidate the functions of these essential proteins and to understand how the parasite thrives in the unique niche of the red blood cell.

1.3. Aim of the thesis

Protein export in *P. falciparum* facilitates the survival of the parasite *in vitro* and is key to parasite virulence in its human host, highlighting the importance of protein export for the parasite. The majority of known exported proteins contains a pentameric amino acid motif termed PEXEL, that mediates protein export. However, the growing number of PEXEL-negative exported proteins (PNEPs) suggests that the parasite has developed additional mechanisms to achieve the export of proteins. The first PNEPs that were identified all had a central transmembrane domain, which is essential for entry into the secretory pathway and additionally contains information important for export. The N-termini of these PNEPs are essential for protein export and are functionally interchangeable with mature PEXEL-protein N-termini. Recently, new types of PNEPs with a different domain organization have been identified, including PNEPs with a classical N-terminal signal

peptide or those with a signal peptide and a transmembrane domain. The aim of this thesis was to identify export and trafficking determinants in these PNEPs, which could help shed light on the mechanisms of protein export and ultimately help to predict further PNEPs of this domain structure to complete the exportome of malaria parasites.

2. Materials and Methods

2.1. Materials

2.1.1. Technical devices

Device	Specifications	Brand/Distributor
Agarose gel chamber	Sub Cell GT basic	Bio-Rad, München
Analytical Balance	870	Kern
Blot device Gel holder cassettes Foam pads Electrode assembly Cooling unit	Mini Protean Tetra Cell System	BioRad, München
Centrifuge	Megafuge 1.0R J2- HS Ultracentifuge Rotor JA-12 Avanti J-26S XP Rotor JA-14	Heraues, Hannover Beckman Coulter, Krefeld
Table centrifuge	Eppendorf 5415 D	Eppendorf, Hamburg
Casting stand Casting plates Casting frames 12-wells combs	Mini Protean	Bio-Rad, München
Cell-Separator	VarioMACS™	Miltenyi Biotech, Bergisch Gladbach
Developer	Curix 60	AGFA-Gevaert, Mortsel/Belgium
Developer cassette	Cronex Quanta III	Dupont, Neu Isenburg

Electrophoresis chamber	Mini Protean 67s	Bio-Rad, München
Electroporator	Gene Pulser X- Cell	Bio-Rad, München
Electroporator	Nucleofector II AAD-1001N	Amaxa Biosystems, Germany
Ice machine	EF 156 easy fit	Scotsmann, Vernon Hills/USA
Bacterial incubator	Thermo function line	Heraeus, Hannover
P. falciparum cell culture incubator	Heratherm IGS400	Thermo Scientific, Langenselbold
Shaking incubator	Max Q4000	Barnstead, Iowa/ USA
Light Microscope	Axio Lab A1	Zeiss, Jena
Fluorescence Microscope	Axioscope 1	Zeiss, Jena
Microscope digital camera	Orca C4742-95	Hamamatsu Phototonics K.K., Japan
Microwave	Micro 750W	Whirlpool, China
Laboratory scale	Atilon	Acculab Sartorius, Göttingen
PCR Mastercycler	epgradient	Eppendorf, Hamburg
Photometer	BioPhotometer plus	Eppendorf, Hamburg
pH-meter	SevenEasy	Mettler-Toledo, Gießen
Pipettes	1-10/200/1000 μl	Gilson, Middleton, USA
Pipettor	Pipetboy acu	IBS, USA
Power supply	EV31	Consort, Belgium
	Power Source 300 V	VWR, Taiwan
Roller mixer	STR6	Stuart
Sterile laminar flow bench	Steril Gard III Advance	Baker, Stanford USA
Thermoblock	Thermomixer compact	Eppendorf, Hamburg
Ultrapure water purification system	Milli Q	Millipore
UV transiluminator	PHEROlum289	Biotec Fischer,Reiskirchen
Vacuum pump	BVC Control	Vacuubrand, Deutschland
Vortexer	Genie 2	Scientific Industries, USA
Waterbath	1083	GFL, Burgwedel

Table 2.1.: Technical Devices

2.1.2. Chemicals

Reagent	Brand/Distributor
Acetic acid	Roth, Karlsruhe
Acrylamide/Bisacrylamide solution (40%)	Roth, Karlsruhe
Agar LB (Lennox)	Roth, Karlsruhe
Agarose	Invitrogen, USA
AlbumaxII	Gibco, Life Technologies, USA
Albumin bovine Fraction V (BSA)	Biomol, Hamburg
Ammonium persulfate (APS)	Applichem, Darmstadt
Ampicillin	Roche, Mannheim
Bacto^{TM} yeast extract	BD, USA
Bacto^{TM} Pepton	
Biotin	Sigma, Steinheim
Blasticidin S	Invitrogen, USA
Bromophenol blue	Roth, Karlsruhe
Coomassie Brilliant Blue G-250	Merck, Darmstadt
calcium chloride ($CaCl_2$)	Sigma, Steinheim
Desoxynucleotides (dNTPs)	Thermo Scientific, Lithuania
Developer solution G150 (Western blot)	Agfa, Leverkusen
4',6-diamidino-2-phenylindole (DAPI)	Roche, Mannheim
Dimethyl sulfoxide (DMSO)	Sigma, USA
Dipotassium phosphate	Merck, Darmstadt
Disodium phosphate	Roth, Karlsruhe
1,4,-dithiothreitol (DTT)	Biomol, Hamburg
Dulbecco's Phosphate Buffered Saline (DPBS)	PAN, Biotech, Aidenbach
Ethanol	Roth, Karlsruhe
Ethidium bromide, EtBr	Sigma, Steinheim
Ethylenediaminetetraacetic acid (EDTA)	Biomol, Hamburg
Ethylene glycol tetraacetic acid (EGTA)	
Fixation solution G334 (Western blot)	Agfa, Leverkusen
Gentamycin	Ratiopharm, Ulm
Giemsa's azure, eosin, methylene blue solution	Merck, Darmstadt
D-Glucose	Merck, Darmstadt
Glycerol	

Glycine	Biomol, Hamburg
(4-(2-Hydoxyethyl)-1-piperazineethanesulfonicacid)(HEPES)	Roche, Mannheim
Hydrochloric acid (HCl)	Merck, Darmstadt
Hypoxanthin	Sigma, Steinheim
Isopropanol	Roth, Karlsruhe
Isopropyl-β-D-thiogalactopyranosid(IPTG)	Roth, Karlsruhe
Lysozym	Fluka Analytical
Magnesium chloride ($MgCl_2$)	Merck, Darmstadt
Manganese(II)chloride ($MnCl_2$)	Merck, Darmstadt
β-Mercaptoethanol	Merck, Darmstadt
Methanol	Roth, Karlsruhe
3-(N-morpholino)propansulfonic acid (MOPS)	Sigma, Steinheim
Milk powder	Roth, Karlsruhe
Percoll	GE Healthcare, Sweden
Phenylmethylsulfonylfluorid (PMSF)	Sigma, Steinheim
Potassium chloride	Merck, Darmstadt
Potassium dihydrogen phosphate	
Protease inhibitor cocktail ("Complete Mini")	Roche, Mannheim
Rubidium chloride	Sigma, Steinheim
RPMI (Roswell Park Memorial Institute)-Medium	Applichem, Darmstadt
Saponin	Sigma, Steinheim
Sodium acetate	Merck, Darmstadt
Sodium chloride	Gerbu, Gaiberg
Sodium bicarbonate	Sigma, Steinheim
Sodium dodecyl sulfate (SDS)	Applichem, Darmstadt
Sodium dihydrogen phosphate	Roth, Karlsruhe
Sodium hydroxide	Merck, Darmstadt
Sorbitol	Sigma, Steinheim
Tetanolysin	Sigma, Steinheim
N, N, N, N-Tetramethylethylenediamin (TEMED)	Merck, Darmstadt
Tris base	Roth, Karlsruhe
Tris-EDTA (TE)	Invitrogen, Karlsruhe

Trichloroacetic acid	Roth, Karlsruhe
Triton X-100	Biomol, Hamburg
Water for molecular biology (Ampuwa)	Fresenius Kabi, Bad Homburg
WR99210 (WR)	Jacobus Pharmaceuticals, Washington (USA)
Yeast extract	Becton Dickinson, Heidelberg

Table 2.2.: Chemicals

2.1.3. Labware & disoposables

Labware and disposables	Specifications	Manufacturer
Chromatography paper		Whatman
Conical falcon tubes	15 ml, 50 ml	
Cryotubes	1.6 ml	Sarstedt, Nümbrecht
Culture bottles	50 mL	
Disposable pipette tips	1-10/20-200/100-1000 µl	
Eppendorf Reaction Tubes	1.5 ml/2 ml	Sarstedt, Nümbrecht/Eppendorf Hamburg
Filter, round	150 mm	Macherey-Nagel, Düren
Filter tips	1-10/20-200/100-1000 µl	Sarstedt, Nümbrecht
Glass cover slips	24x65 mm Thickness 0.13-0.16 mm	R. Langenbrinck, Emmendingen
Glass slides		Engelbrecht, Edermünde
Gloves, latex		Kimtech Science EcoShield™
Gloves, purple nitrile		Kimtech Science
IFA glass slides	10 wells ER-208B-CE24 6.7 mm	Thermo Scientific, USA
Leukosilk tape		BSN medical GmbH
Magnetic columns	CS Columns	Miltenyi Biotech, Bergisch Gladbach
Medical X-Ray screen film blue sensitive	CEA RP NEW	AGFA Health Care NV, Mortsel, Belgium

Nitrocellulose blotting Membrane Protran	Amersham 0.45 µm	GE Healthcare, Deutschland
One way cannula		
One way injection		Braun, Melsungen
Parafilm		Bemis, USA
Pasteur pipette		Brand, Wertheim
PCR Reaction tubes	Multiply-µStrip Pro 8-Strip	
Petri dishes	5 mL/10 ml, 15x60 and 14x90 mm	Sarstedt, Nümbrecht
Plastic pipettes	5/10/25 ml	
Scalpel		Braun, Tuttlingen
Sterile filter	0.22 µm	Sarstedt, Nümbrecht
Transfection cuvettes	0.2 cm	Bio-Rad, München

Table 2.3.: Labware and disposables

2.1.4. Kits

Kit	Manufacturer
NucleoSpin. Plasmid NucleoSpin. Extract II	Macherey-Nagel, Düren
QIAamp DNA Mini Kit QIAGEN Plasmid Midi Kit	Qiagen, Hilden
Western Blot ECL-SuperSignal West Pico	Thermo Scientific, Schwerte
Western Blot ECL-Clarity Detection Kit	Bio-Rad, USA

Table 2.4.: Kits

2.1.5. DNA- and protein-ladders

DNA- or protein-ladder	Manufacturer
GeneRuler^{TM}1000 bp ladder PageRuler^{TM} prestained protein ladder	Thermo Scientific, Schwerte

PageRuler$^{\text{TM}}$ unstained protein ladder

Table 2.5.: DNA- and protein-ladders

2.1.6. Solutions, buffers and media

2.1.6.1. Bacterial culture

10x Luria-Bertani(LB) medium stock solution	10% NaCl
	5% peptone
	10% yeast extract
	in dH$_2$O, autoclaved
LB medium working solution	1% (w/v) NaCl
	0.5% (w/v) peptone
	1 %(w/v) yeast extract
	in dH$_2$O
LB Agar plate solution	1.5% Agar-Agar
	1x LB medium
Ampicillin stock solution	100mg/ml in 70% ethanol
Glycerol freezing solution	50% (v/v) glycerol
	in 1x LB medium

Buffers for competent *E. coli* cells

TFBI buffer	30 mM acetic acid
	50 nM MnCl$_2$
	100 mM RbCl
	10 mM CaCl$_2$
	15% (v/v) glycerol
	pH 5.8 (with 0.2 N Acetic acid)
	ad 500ml H$_2$O
TFBII buffer	10 mM MOPS
	75 mM CaCl$_2$
	10mM RbCl
	15% (v/v) glycerol
	pH 7.0 (with NaOH)
	ad 500ml H$_2$O

2.1.6.2. Solutions and buffers for molecular biology analyses

STET buffer for plasmid preparation

80 g/l saccharose
18.612 g/l EDTA ,pH 8.0
5 g/l TritonX-100
1.211 g/l Tris-Base, pH 8.0
in dH_2O

One-step isothermal DNA assembly buffers

5x isothermal reaction buffer (6ml)

3ml 1 M Tris-HCl pH 7.5
150 µl 2 M $MgCl_2$
60 µl each of 100 mM
dGTP/dATP/dTTP/dCTP
300 µl 1 M DTT
1.5 g PEG-8000
300 µl 100 mM NAD
in dH_2O

Assemby master mixture (1.2 ml)

320 µl 5x isothermal reaction
buffer
0.64 µl 10 U/µl T5 exonuclease
20 µl 2 U/µl Phusion DNA
polymerase
160 µl 40 U/ µl Taq DNA ligase
ad 1.2 ml dH_2O

DNA-gelelectrophoresis

50x TAE-Buffer

2 M Tris base
1 M Pure acetic acid
50 mM EDTA
pH 8.5

6x Loading buffer

40% Glycerol (v/v)
2.5% (w/v) Xylene cyanol

2.5% (w/v) Bromophenol blue

in dH$_2$O

2.1.6.3. Media and solutions for parasite culture and cell biology experiments

P. falciparum in vitro culture

RPMI complete medium	1.587% (w/v) RMPI 1640
	12 mM NaHCO$_3$
	6 mM D-Glucose
	0.5% (v/v) Albumax II
	0.2 mM Hypoxanthine
	0.4 mM Gentamycin
	pH 7.2
	in dH$_2$O
	sterile filtered
10% Giemsa solution	10 ml Giemsa's azure, eosin,
	methylene blue solution
	90 ml dH$_2$O
Synchronization solution	5% (w/v) D-Sorbitol
	in dH$_2$O
	sterile filtered
Transfection buffer (Cytomix)	120 mM KCl
	150 μM CaCl$_2$
	2 mM EGTA
	5 mM MgCl$_2$
	10 mM K$_2$HPO$_4$/KH$_2$PO$_4$
	25 mM HEPES
	pH 7.6
	in dH$_2$O
	sterile filtered
Amaxa transfection buffer	90 mM NaPO$_4$
	5 mM KCl
	0.15 mM CaCl$_2$

	50 mM HEPES
	pH 7.3
	in dH$_2$O
	sterile filtered
Malaria freezing solution (MFS)	4.2% D-sorbitol
	0.9% NaCl
	28% Glycerol
	in dH$_2$O
	sterile filtered
Malaria thawing solution (MTS)	3.5% NaCl
	in dH$_2$O
	sterile filtered
WR99210 stock solution	20 mM WR99210
	in DMSO
WR99210 working solution	1:1000 dilution of stock solution
	in RPMI complete medium
	sterile filtered
Blasticidin S (BSD) working solution	5 mg/ml BSD in RPMI complete medium
	sterile filtered
G418 working solution	50 mg/mL in RPMI complete medium
	sterile filtered
Human red blood cells	sterile concentrate, bloodgroup 0+
	Blood bank Universitätsklinikum Eppendorf (UKE), Hamburg

Solutions for cell biology and biochemical assays

Parasite lysis buffer	4% SDS

	0.5% Triton X-100
	0.5x PBS
	in dH$_2$O
Percoll stock solution	90% (v/v) Percoll
	10% (v/v) 10x PBS
80% Percoll solution	8.9 ml 90% Percoll stock solution
	1.1 ml RPMI compl. medium
	0.8 g Sorbitol
	sterile filtered
60% Percoll solution	6.7 ml Percoll stock solution
	3.3 ml RPMI compl. medium
	0.8 g Sorbitol
	sterile filtered
40% Percoll solution	4.4 ml Percoll stock solution
	5.6 ml RPMI compl. medium
	0.8 g Sorbitol
	sterile filtered
Saponin solution	Saponin 0.03% (w/v)
	in DPBS
RIPA buffer	10 mM Tris/HCl pH 7.5
	150 mM NaCl
	0.1% SDS
	1% Triton X-100
	1 mM PMSF
	2x Protease inhibitor cocktail
Diluting buffer	10 mM Tris/HCl pH 7.5
	150 mM NaCl
	1 mM PMSF
	2x Protease inhibitor cocktail
	in dH$_2$O
DSP (Stock solution)	20 mM in DMSO

Quenching buffer   25 mM Tris-HCl in 1x PBS

2.1.6.4. Buffers and solutions for protein analyses

SDS-Page and Western blot

10x Running buffer   250 mM Tris base
                                                1.92 M Glycine
                                                1% (w/v) SDS
                                                in dH$_2$O

Ammonium persulfate (APS)   10% (w/v) in dH$_2$O

Separating gel buffer   1.5 M Tris-HCl, pH 8.8 in dH$_2$O

Stacking gel buffer   1 M Tris-HCl, pH 6.8 in dH$_2$O

Stacking gel (for two gels, 5%)   0.75 ml stacking gel buffer
                                                4.35 ml dH$_2$O
                                                750 µl Acryl amide (40%)
                                                60 µl SDS (10%)
                                                60 µl APS (10%)
                                                6 µl TEMED

Separating gel (for two gels, 12%)   2.5 ml running gel buffer
                                                4.2 ml dH$_2$O
                                                3 ml Acryl amide (40%)
                                                100 µl SDS (10%)
                                                100 µl APS (10%)
                                                4 µl TEMED

6x SDS sample buffer   375 mM Tris-HCl pH 6.8
                                                12% (w/v) SDS
                                                60% (v/v) Glycerol
                                                0.6 M DTT
                                                0.06% (w/v) Bromophenol blue

10x Western blot transfer buffer   250 mM Tris-Base
                                                1.92 M glycerol
                                                0.1% (w/v) SDS

	in dH$_2$O
1 x Western transfer buffer	10% 10x Western transfer buffer
	20% Methanol
	in dH$_2$O
Blocking solution	5% (w/v) milk powder in 1xPBS

2.1.7. Bacterial and *Plasmodium* strains

P. falciparum strain 3D7	clone of NF54 isolated from an airport malaria patient, near Schipol Airport, Amsterdam, Netherlands
Bacterial strain *E. coli* XL-10 Gold	Tetr Δ(mcrA)183 Δ(mcrCB-hsdSMR-mrr)173 endA1 supE44 thi-1 recA1 gyrA96 relA1 lac Hte [F' proAB lacIqZΔM15 Tn10 (Tetr) Amy Camr]

2.1.8. Enzymes

2.1.8.1. Polymerases

FirePol DNA Polymerase (5 U/µl): Solis Biodyne, Taipei, Taiwan Phusion High-Fidelity
DNA Polymerase (2 U/µl): NEB, Ipswich, USA

2.1.8.2. Restriction enzymes

Restriction enzyme	Restriction site	Manufacturer
AvrII	C^CTAGG	
KpnI	GGATC^C	
MluI	A^CGCGT	
NotI	GC^GGCCGC	
SpeI	A^CTAGT	NEB, Ipswich / USA

XhoI	C^TCGAG
XmaI	C^CCGGG
DpnI	GA^TC (only methylated)
T5 exonuclease	5'–3' exonuclease

Table 2.14.: Restriction enzymes

2.1.8.3. Ligases

T4 DNA-Ligase (3 U/μl): NEB, Ipswich, USA Taq DNA-ligase (40U/μl): NEB, Ipswich, USA

2.1.9. Antibodies

2.1.9.1. Primary antibodies

Antigen	Organism	Dilution		Source
		WB	IFA	
GFP	Mouse	1:1000	1:500	Roche, Mannheim
GFP	Rabbit	1:1000	1:400	Thermo Scientific
SBP1-C	Mouse	1:2000	1:1000	Spielmann lab
MSRP6	Mouse	1:500	1:250	Heiber 2011

Table 2.15.: Primary Antibodies

2.1.9.2. Secondary antibodies

Antigen	Conjugate	Organism	Dilution	Application	Source
Mouse	HRP	Goat	1:3000	WB	Dianova, Hamburg
Rabbit	HRP	Donkey	1:2500	WB	Dianova, Hamburg
Mouse	Alexa-488	Goat	1:2000	IFA	Invitrogen, Karlsruhe
Mouse	Alexa-594	Goat	1:2000	IFA	Invitrogen, Karlsruhe
Rabbit	Alexa-488	Goat	1:2000	IFA	Invitrogen, Karlsruhe
Rabbit	Alexa-594	Goat	1:2000	IFA	Invitrogen, Karlsruhe

Table 2.16.: Secondary Antibodies

2.1.9.3. Antibody coupled beads

Antigen	Conjugate	Organism	Application	Source
GFP	Agarose	Camel	IP	Chromotek, München
Streptavidin	Sepharose		Pulldown	GE Healthcare life sciences

Table 2.17.: Antibody coupled beads

2.1.9.4. Vectors

For cloning of the PNEP trafficking constructs and the BirA*-constructs the pArl1a-vector containing GFP was used (Crabb et al., 2004) and parasites selected using WR99210. The constructs for knock-in cell lines were cloned using the pSLI-PfEHD2xFKBP-GFP vector (Birnbaum, unpublished) and trangenic cell lines selected using WR99210. Genomic integration of constructs was achieved using the G418 selection drug. Co-expression of mCherry containing proteins was achieved by cloning of the respective constructs into pArl2, containing mCherry and a blasticidin-deaminase selection cassette.

2.2. Methods

2.2.1. Microbiological methods

2.2.1.1. Production of competent *E. coli*

To increase plasmid uptake of *E. coli* the rubidium chloride method was applied to decrease the bacterial cell wall stability (Hanahan, 1983). 20 ml of LB medium was inoculated with the *E. coli* XL-10 Gold strain from a glycerol stock and incubated overnight at 37°C with vigorous shaking. 10 ml of this culture was then transferred to a 1 L Erlenmeyer flask with 200 ml LB-medium and incubated at 37°C with vigorous shaking up to an OD_{600} of 0.5-0.6. After harvesting of the bacteria by centrifugation at 2400 x g at 4°C the pellet was re-suspended in 60 ml TFBI buffer and incubated on ice for 10 min. After another centrifugation step (2,400 x g at 4°C) the pellet was suspended in 8 ml TFBII and aliquoted (100 µl) into 1.5 ml reaction tubes and stored at -80°C.

2.2.1.2. Transformation of chemo-competent *E. coli*

The chemo-competent *E. coli* (100 µl) were thawed on ice and plasmid DNA (0.5 µl of a plasmid preparation or 5-10 µl ligation) was added and the mix incubated on ice for 30 min. After a heat-shock of 42°C for 45 seconds the mix was immediately placed on ice again for 2 min. 20-100 µl of the bacteria were then plated on LB-agar plates containing

Ampicillin. The plates were incubated at 37 °C overnight and stored at 4 °C until further use.

2.2.1.3. Overnight culture of *E. coli* for subsequent plasmid DNA preparation

For plasmid mini preparations 2 ml of LB medium in a 2 ml reaction tube were inoculated with bacteria from an agar plate or glycerol stock and incubated overnight at 37 °C with vigorous shaking. For plasmid midi preparations 150 ml LB medium in an Erlenmeyer flask were inoculated and incubated overnight at 37 °C with vigorous shaking.

2.2.1.4. Freezing of *E. coli*

For long term storage of *E. coli*, 500 µl overnight culture were mixed with 500 µl of glycerol in a 1.5 ml reaction tube and stored at -80 °C.

2.2.2. Molecular biological methods

2.2.2.1. Polymerase chain reaction (PCR)

PCRs (Saiki et al., 1988) were either performed for the specific amplification and subsequent cloning of DNA fragments (preparational PCR), or for analytical purposes, which include colony PCRs and integration checks (analytical PCR). Preparative PCRs were usually performed using the Phusion polymerase, analytical PCRs using the FirePol polymerase. Information for primer sequences for the amplification of *P. falciparum* genes was obtained from PlasmoDB. A list of primers can be found in the Appendix section A. Typical PCR-reactions for preparative and analytical PCRs are listed in table 2.18. The typical temperature profile is shown in table 2.19. PCR products were analyzed using agarose gelelectrophoresis.

Reagents	Volume
Preparative PCR	
5x Phusion buffer	10 µl
dNTPs (2.5 mM)	5 µl
Primer F (10 µM)	4 µl
Primer R (10 µM)	4 µl
Template DNA (1-200 ng/µl	0.5 µl
Phusion polymerase	0.3 µl
dH$_2$O	ad 50 µl

Analytical PCR

10x FirePol buffer	1 µl
MgCl$_2$ (25 mM)	0.6 µl
dNTPs(2.5 mM)	1 µl
Primer F (10 µM)	2 µl
Primer R (10 µM)	2 µl
Template gDNA/bacterial colony	0.5 µl/NA
FirePol polymerase	0.1 µl
dH$_2$O	ad 10 µl

Table 2.18.: PCR reactions

Phase		Temparature	Time
Denaturation		95 °C	4 min
25-30 Cycles	Denaturation	95 °C	30 sec
	Primer annealing	48-70 °C	30 sec
	Elongation	64-72 °C	X min
Storage(optional)		4 °C	∞

Table 2.19.: PCR temperature profile. (X) depends on the length of the PCR-product. Usually 1 minute per 1000 bp

2.2.2.2. PCR-product purification

To purify PCR-products and digested vector DNA for subsequent ligation the NucleoSpin Gel and PCR Clean-up kit was used according to the manufacturer's protocol. PCR-products and vector DNA were eluted with 30 µl dH$_2$O.

2.2.2.3. DNA restriction digest

PCR-products and vectors were submitted to preparative restriction digest to generate "sticky ends" for subsequent ligation. Depending on the vector that was used, specific restriction enzymes were incubated with the vector and PCR-product, respectively. DpnI was used in most preparative digests of PCR products to deplete methylated template DNA. A typical restriction digest is shown in table 2.20. Analytical restriction digests of mini and midi DNA preparations were used to test the correct insertion of the insert and to

exclude recombination events during ligation or bacterial passage. Analytical restriction digests were usually performed in a 10 µl volume, using 1.5 µl plasmid DNA and 0.3 µl of each enzyme. Preparative digests were incubated at 37 °C for 2-3 hours, analytical digests for 30-90 minutes.

Reagents	Volume
10x NEB CutSmart buffer	5 µl
Enzyme I	1.5 µl
Enzyme II	1.5 µl
DpnI (only for PCR-products)	1 µl
DNA (plasmid/PCR)	4 µl/whole volume
dH$_2$O	ad 50 µl

Table 2.20.: Preparative DNA digest

2.2.2.4. DNA ligation

Digested vector DNA and PCR-products were ligated to produce a plasmid, that can be transformed into *E. coli* to be multiplied on LB-agar plates. A typical ligation reaction is shown in table 2.21. Ligation reactions were incubated for 30-60 minutes at room temperature (RT) or overnight at 16 °C.

Reagents	Volume
10x T4 ligase buffer	1 µl
T4 ligase	1 µl
vector DNA	0.5 µl
PCR-product	7.5 µl

Table 2.21.: DNA ligation

2.2.2.5. One-step isothermal DNA assembly

The one-step isothermal DNA assembly (Gibson et al., 2009) is an alternative ligation method for the ligation of up to 6 inserts into a vector. In this work it was used for the generation of all knock-in constructs and some of the episomal expression constructs. For this protocol the PCR-product was only DpnI digested, for which no PCR purification

was necessary, as the enzyme is also active in the Phusion buffer. For this protocol PCR products need to have an overlap of 15-35 bp with the vector sequence. A typical reaction is shown in table 2.22. After 60 minutes of incubation at 50 °C, 5-10 µl of the assembly mix were transformed into *E. coli.*

Reagents	Volume
Assembly master mixture	7.5 µl
vector DNA	1 µl
PCR-product	1 µl
dH$_2$O	ad 10 µl

Table 2.22.: One-step isothermal DNA assembly

2.2.2.6. Colony PCR-screen

The DNA ligation protocol used in this work results in a mix of plasmids containing the original insert and the new insert. To identify bacterial colonies containing the plasmid with the correct (new) insert, the colonies were screened using PCR. For this purpose, primers binding the new insert and the vector DNA were used, so that a PCR product was only generated when the plasmid containing the new insert was present within a colony. The PCR reaction resembled that of an analytical PCR (see section 2.2.2.1). A small amount of bacteria from 10-50 colonies was separately transferred to each PCR-reaction using sterile pipet tips. PCR products were analyzed using agarose gel electrophoresis.

2.2.2.7. Plasmid preparation

Plasmids were either purified with the Nucleo Spin Plasmid Kit for small scale purification (2 ml of overnight culture), or with the QIAfilter Plasmid Midi Kit for medium scale purification (150 ml of overnight culture) according to the manufacturers protocols.

2.2.2.8. Agarose gel electrophoresis

DNA molecules are negatively charged due to their phosphate backbone and can thus be separated in an electric field as they move towards the anode according to their size. In this work usually 1% agarose gels were used. For this purpose agarose was dissolved in 1x TAE buffer by boiling. After cooling down, ethidiumbromide was added to a final concentration of 1 µg/ml, the solution transferred to a gel tray and a comb inserted to generate pockets for DNA loading. Once the gel was hardened it was transferred to the electrophoresis chamber containing 1x TAE buffer. The DNA was mixed with 6x DNA

loading buffer and loaded into the pockets. A voltage of 100 V was applied for 15-30 minutes and DNA bands analyzed under UV light in comparison to a DNA ladder.

2.2.2.9. Isolation of genomic DNA from *P. falciparum*

Genomic DNA from transgenic and wildtype *P. falciparum* was isolated to confirm the correct integration of knock-in constructs into the parasite genome. For this purpose 5 ml of parasite culture was harvested and centrifuged at 1800 x g for 3 minutes. Genomic DNA from the pellet was purified using the QIAamp DNA Mini Kit according to the manufacturers protocol. DNA was eluted with 200 µl dH$_2$O.

2.2.3. Biochemical methods

2.2.3.1. Discontinuous SDS-PAGE

Proteins were separated using discontinuous SDS-PAGE (Laemmli, 1970). The separation of proteins within the polyacrylamid gels, according to their molecular weight, occurs via voltage application. The influence of the proteins internal charge is hereby neutralized by the attachment of the negatively charged SDS, so that the proteins receive a negative net charge. The DTT, contained in the SDS-sample buffer, leads to the reduction of disulfide bonds, so that the proteins are present in an unfolded confirmation. In this work, 12% polyacrylamide separating gels were used. After 5-10 minutes of heat denaturation (85 ℃) protein samples were loaded into the gel pockets, next to a prestained protein marker containing dye labeled proteins of defined sizes. A voltage of 100-150 V was applied for 60-90 minutes and the gels containing the separated proteins submitted to Western blot analysis.

2.2.3.2. Western blotting

For the identification and analysis of specific proteins, the proteins were separated by SDS-PAGE were transferred to nitrocellulose membranes by the wet transfer method. For this purpose the polyacrylamide gel was layered on a nitrocellulose membrane and sandwiched between 6 Whatman filter papers and 2 sponges. The sandwich was transferred to a tank blotting chamber filled with blotting buffer, with the nitrocellulose facing the anode and the polyacrylamide gel facing the cathode. A voltage of 100 V was applied for 1 hour, or 15 V overnight, at 4℃.

2.2.3.3. Immunodetection of proteins

After the transfer of proteins to a nitrocellulose membrane, proteins can be visualized by immunodetection. First, the membrane was blocked with 5% milkpowder in 1xPBS for 1 hour at RT to block unspecific antibody binding. Then, the membrane was incubated with the primary antibody, diluted in 5% milkpowder in 1xPBS for 1-2 hours at RT or overnight at 4 °C. After 5 washing steps (5 minutes each) with 1x PBS the secondary antibody diluted in 5% milkpowder in 1xPBS was applied for 1 hour at RT. After 5 more washing steps (5 minutes each) the membrane was transferred to a transparent film and the enhanced chemiluminescence (ECL) substrate pipetted onto the membrane. The membrane was covered with another transparent film and chemiluminescence detected using a blue sensitive medical x-ray screen with exposure times ranging from 1 second to 1 hour.

2.2.3.4. Pulldown of biotinylated proteins for subsequent mass spectrometry analysis (BioID)

For the pulldown only reaction tubes from the company Eppendorf, and falcon tubes from the company Falcon were used, as they were shown to be more compatible with mass spectrometry analysis. All buffers were prepared using Ampuwa dH$_2$O and all steps were performed on ice. The described experiments were performed as duplicates.

Harvested trophozoite and schizont stage parasites (see section 2.2.4.7 and 2.2.4.8) from 100-200 ml of parasite culture were washed with DBPS twice and lysed in 1 ml lysisbuffer (50 mM Tris-HCl pH7.5, 500 mM NaCl, 1% TritonX-100, + freshly added 1 mM DTT, 2x protase inhibitor cocktail, 1 mM PMSF). Until further usage lysates were frozen at -80 °C. After thawing the lysates were frozen at -80 °C and thawed again for a more efficient protein extraction. After 10 minutes of centrifugation at 20000 x g the supernatants were transferred to 2 ml reaction tubes (Eppendorf) and diluted with 1 ml 50mM Tris-HCl pH 7.5. 50 µl of Streptavidin-sepharose, equilibrated with 50mM Tris-HCl pH 7.5, were transferred to the diluted supernatants and incubated overnight at 4 °C with gentle overhead mixing. Then, the sepharose was pelleted by centrifugation at 1600 x g for 1 minute at 4 °C. The sepharose pellet was washed 2 times with lysisbuffer, 1 time with dH$_2$O (Ampuwa), 2 times with 50mM Tris-HCl pH 7.5 and three times with 100 mM TEAB. After the last washing step the sepharose was re-suspended in 50 µl 100 mM TEAB and shipped on ice for mass spectrometry analyis. The mass spectrometry analysis was performed by Wieteke Hoeijmakers (Radboud Institute, Nijmegen, Netherlands) using dimethyl labeling for quantification (Boersema et al., 2009).

2.2.3.5. Co-Immunoprecipitation (CoIP)

CoIP was used to analyze the potential interaction candidates of MSRP6. All steps were performed on ice. 2 times 20-40 ml of parasite culture were harvested by centrifugation at 2000 x g for 5 minutes (no break) and subsequently schizonts and trophozoites were purified with a Percoll gradient (see section 2.2.4.6). The purified parasites were washed twice with DPBS (centrifugation steps at 10000 x g) and re-suspended in 250 µl RIPA buffer (+2x protease inhibitor and 10 mM PMSF). The lysates were frozen at -80 °C and thawed twice for better protein extraction. Then, the lysates were centrifuged at 20000 x g at 4 °C and the supernatants diluted with 750 µl dilution buffer (+2x protease inhibitor cocktail) each. The diluted supernatants were pooled in a 2 ml reaction tube and 50 µl transferred to a tube containing 17 µl 4x SDS-sample buffer for subsequent Western blot analysis (Input fraction). 20 µl GFP-agarose beads (equilibrated in dilution buffer) were transferred to the diluted supernatants and incubated for 1-2 hours at 4 °C with gentle overhead mixing. The agarose beads were pelleted by 2 minutes of centrifugation at 2500 x g. 50 µl of the supernatant were transferred to a tube containing 17 µl 4x SDS-sample buffer for subsequent Western blot analysis (Supernatant fraction). The beads were washed 5 times with dilution buffer (centrifugation steps at 2500 x g). 50 µl of the supernatant of the last washing step were transferred to a tube containing 17 µl 4x SDS-sample buffer for subsequent Western blot analysis (final wash fraction). The agarose pellet was incubated with 30 µl of 4x SDS sample buffer at 85 °C for 10 minutes to elute proteins bound to the agarose beads. The beads were pelleted by centrifugation at 20000 x g for 1 minute and the supernatant (eluate fraction) used for subsequent analysis. 5 µl of the input, supernatant and final wash step and 10 µl of the eluate were loaded on the polyacrylamidgel for SDS-PAGE and subsequent Western blot analysis.

2.2.4. *P. falciparum* cell biological methods

2.2.4.1. *P. falciparum* cell culture

P. falciparum blood stages were cultured in 15x60 mm and 14x90 mm petri dishes at 37 °C in a low oxygen atmosphere (5% CO_2, 1% O_2, 94% N_2). 15x60 mm petri dishes usually contained 6 ml and 14x90 mm petri dishes 12 ml of RPMI complete medium and red blood cells to a hematocrit of 5%. Transgenic parasites were selected by the addition of 10 nM WR99210, 1.5 µg/ml blasticidin or 0.3 mg/ml G418 (for knock-in cell lines). The parasites were usually cultured with a parasitemia of 0.2-5% and RPMI complete medium was changed every 24-48 hours, depending on the parasitemia. Parasites were diluted at a parasitemia of 2-10%.

2.2.4.2. *P. falciparum* freezing and thawing

For long term storage of parasites cryo-stabilates were produced and stored in liquid nitrogen. 5-10 ml of parasite culture, containing 1-5% ring stages, were pelleted by 3 minutes centrifugation at 1800 x g. The pellets were re-suspended in 1 ml parasite freezing solution and transferred to cryo tubes and immediately frozen in liquid nitrogen.

For thawing of parasites, the frozen cryo tubes were thawed at 37 ℃, the parasite suspension transferred to a sterile 1.5 ml reaction tube and centrifuged for 1 minute at 2000 x g. The supernatant was discarded and parasites carefully re-suspended in 1 ml parasite thawing solution, centrifuged for 1 minute at 2000 x g, re-suspended in 1 ml RPMI complete medium, centrifuged again and the pellet transferred to a 15x60 mm petri dish containing 6 ml RPMI complete medium and 200 μl red blood cells. The selection drug was added after 16-24 hours and medium changed every 24 hours for 5 days.

2.2.4.3. Blood smears and Giemsa staining

To generate Giemsa stained blood smears for the assessment of the parasitemia in a parasite culture 0.5 μl of infected red blood cells were transferred to a glass slide. The drop containing the infected red blood cells was smeared using another glass slide to obtain a single layer of red blood cells. After drying, the parasites were fixed in methanol for 10-20 seconds and then stained with Giemsa staining solution for 10-60 minutes. After washing off the staining solution with water and drying of the glass slides the smears were analyzed using an optical light microscope.

2.2.4.4. Parasite synchronization

In order to obtain parasite cultures with synchronized parasite stages, 5-10 ml of parasite culture was pelleted by centrifugation for 3 minutes at 1800 x g. The pellet was re-suspended in 3 ml 5% D-sorbitol in dH_2O and incubated for 15 minutes at 37 ℃. After 3 minutes centrifugation at 1800 x g, the parasites were washed with 6 ml RPMI complete medium and then transferred to a petri dish containing RPMI complete medium.

2.2.4.5. Transfection of *P. falciparum*

Transfection using the BioRad system 100 μg plasmid DNA was precipitated using 1/10 volume of 3 M sodium actetate and 3 volumes of ethanol. The precipitated DNA was pelleted by centrifugation for 5 minutes at 20000 x g. The DNA pellet was washed with 70% ethanol, centrifuged again and the pellet air dried. The pellet was dissolved in 15 μl TE-buffer and 385 μl of cytomix was added. In the meantime, 5-10 ml of parasite culture containing 5-10% ring stage parasites was pelleted by 3 minutes centrifugation

at 1800 x g. The pellet was mixed with the cytomix/DNA solution and transferred to an electroporation cuvette (2 mm, BioRad). The electroporation was performed using the Gene Pulser Xcell (350 V, 950 µF, ∞Ω). After electroporation the parasites were immediately transferred to a 15x60 mm or 14x90 mm petri dish containing RPMI complete medium and 5% hematocrit. After 6 hours the medium was changed and the selection drug added. During the following 5 days the medium was changed every 24 hours.

Transfection using the Amaxa system 50 µg plasmid DNA was precipitated using 1/10 volume of 3 M sodium actetate and 3 volumes of ethanol. The precipitated DNA was pelleted by centrifugation for 5 minutes at 20000 x g. The DNA pellet was washed with 70% ethanol, centrifuged again and the pellet air dried. The pellet was dissolved in 10 µl TE-buffer and 90 µl of Amaxa transfection solution was added. In the meantime late schizont stage parasites were harvested by overlaying 4 ml of 60% Percoll solution with 8 ml of parasite suspension and subsequent centrifugation for 6 minutes at 2500 x g. The schizont layer was transferred to a new 15 ml tube and washed with RPMI complete medium. Then, the schizont pellet was transferred to a 1.5 ml reaction tube and re-suspended in the DNA solution. The suspension was transferred to an electroporation cuvette (2 mm, BioRad). The electroporation was performed using the Nucleofector II AAD-1001N (program U-033). Immediately after electroporation the parasites were transferred to a 1.5 ml reaction tube containing 250 µl red blood cells and an equal amount of RPMI complete medium. The tube was incubated at 37 ℃ with rigorous shaking for 30-60 minutes. Then, the parasites were transferred to a 15x60 mm petri dish containing 6 ml RPMI complete medium. After 12-16 hours the medium was changed and the selection drug added. During the following 5 days the medium was changed every 24 hours.

2.2.4.6. Percoll gradient

In this work the Percoll gradient was used to separate trophozoites and schizonts from uninfected red blood cells and ring stage parasites for subsequent Western blot analysis and CoIPs. In a 2 ml reaction tube, 500 µl of 40% Percoll solution was overlayed by 500 µl of 60% Percoll solution and 500 µl of 80% Percoll solution. 10-20 ml of parasite culture were pelleted by centrifugation at 1800 x g for 3 minutes. The pellet was layered on the Percoll gradient and the reaction tube centrifuged for 5 minutes at 20000 x g. The layer containing the trophozoites and schizonts was transferred into a 1.5 ml reaction tube and washed with DPBS twice. The resulting pellet containing trophozoites and schizonts was used for further analysis.

2.2.4.7. Biotin labeling of parasite proteins (BioID)

Biotin labeling of proteins was achieved using parasite cell lines expressing BirA* fusion proteins (Roux et al., 2012). For subsequent mass spectrometry analysis large amounts of parasite culture had to be harvested. For this purpose parasites were grown in 50 ml cell culture flasks (Sarstedt). Before harvesting the parasites were cultured in the presence of 20 mM biotin for 24-48 hours. The cells were harvested at a parasitemia of 5-10%, preferably mostly trophozoites and schizonts. The medium was changed every 24 hours. For Western blot analysis of parasite lysates the parasites were cultured in 14x90 mm petri dishes.

2.2.4.8. Large scale magnetic purification of trophozoits and schizonts (BioID)

50-100 ml of parasite culture was pelleted by centrifugation for 5 minutes at 2000 x g (no break). The pellet was re-suspended in approximately 20 ml of RPMI complete medium. A column containing ferromagnetic fibers (CS, Miltenyi) was placed into the VarioMACS magnetic stand (Miltenyi) and washed with ~50 ml RPMI complete medium. Afterward, the parasite suspension was added to the column and was allowed to slowly flow through the column. Due to their high amount of hemozoin trophozoites and schizonts were captured by the ferromagnetic fibers. The column was washed with ~50 ml RPMI complete medium to remove all unbound cells. Then, the column was removed from the magnetic stand and bound parasites eluted with ~25 ml RPMI complete medium. The parasite suspension, now containing only trophozoites and schizonts was centrifuged for 5 minutes at 2000 x g. The pellet was transferred to a 1.5 ml reaction tube and submitted to further processing (see section 2.2.3.4).

2.2.5. Microscopy

2.2.5.1. Live cell and fluorescence microscopy

Live cell imaging and fluorescence microscopy of IFAs was performed using a Zeiss Axioscope M1, equipped with a 100x oil objective (NA 1.4) and a 63x oil objective (NA 1.4). Pictures were acquired using a Hamamatsu Orca C4742-95 camera and the Zeiss Axiovision software (version 4.7).

500 μl of parasite culture were transferred to a 1.5 ml reaction tube. DAPI was added to a final concentration of 1 μg/ml and incubated for 10 minutes at RT. The parasites were pelleted by centrifugation for ~10-20 seconds at 9000 x g and washed with RPMI complete medium once. The pellet was re-suspended in one pellet volume of RPMI complete medium, 5 μl transferred on to a glass slide and covered with a coverslip. The

cells were imaged immediately. This microscope was also used for IFA imaging. The acquired images were processed using GIMP 2.8.

2.2.5.2. Immunofluorescence analysis (IFA)

500 µl of parasite culture was transferred to a 1.5 ml reaction tube and pelleted by centrifugation for ~10-20 seconds at 9000 x g. The pellet was washed with DPBS once and then re-suspended in 1 ml DPBS. Approximately 10 µl of parasite suspension was transferred to each well of a 10-well glass slide and air-dried. The parasites were fixed in acetone for 30 minutes, after which the slides could be stored until further usage. All subsequent steps were performed in a humid chamber. For antibody labeling of parasite proteins, first the cells were re-hydrated with 20 µl DPBS per well for 15 minutes. Then unspecific binding sites were blocked with 3% BSA in PBS for 30-60 minutes. The primary antibodies were diluted in 3% BSA in PBS, 20 µl administered per well and incubated for 1 hour at RT or overnight at 4 °C. After 5 washing steps with DPBS the cells were incubated with the secondary antibodies, diluted in 3% BSA in PBS, containing 1 µg/ml DAPI, for 1 hour at RT. After 5 washing steps with DPBS, a few drops of DAKO fluorescent mounting medium were added to the glass slide and covered with a cover slip. The cover slip was fixated using nail polish. After a few hours the IFAs could be imaged by fluorescence microscopy.

2.2.6. Software and online tools

Software/online tool	Version	Application
GIMP	2.8	Image processing
Inkscape	0.48.4	Figure compilation
Aviovision	4.7	Image acquisition
ApE	2.0.49	DNA sequence editor
Clustal Omega		Sequence alignments
BLAST, blastp suite		Identification of protein homologs
Jpred	3	Secondary structure prediction
PlasmoDB	28	retrieval of *P. falciparum* sequences
ImageJ	Fiji 1.50c	Plot intensity profiles

3. Results

3.1. Export requirements for novel PNEPs

Heiber *et al.* identified several novel PNEPs that besides conventional PNEPs with a single central TMD also included PNEPs of novel domain composition. These "unusual" PNEPs contained a TMD and an additional SP or only a SP. The export of known PNEPs with a central TMD is mediated by the N-terminal part in combination with a PNEP-specific TMD, while the export requirements for "unusual" PNEPs were not addressed (Heiber et al., 2013). This part of the thesis aims to identify the export mediating regions in these "unusual" PNEPs.

3.1.1. Export requirements for PNEPs with a SP and a TMD

3.1.1.1. PF08_0004

PF08_0004 deletion constructs PF08_0004 contains a SP and a TMD and as a GFP fusion protein localizes to the Maurer's clefts with additional staining of the parasite periphery, potentially caused by the GFP tag that could partially interfere with efficient trafficking (Heiber et al., 2013). To narrow down the part of the protein necessary for protein export it was divided into 4 parts. The contribution of these parts in export was assessed by individually deleting or replacing them in an episomally expressed (under the *crt*-promoter) modified PF08_0004 construct fused to GFP. Parts 1-3 covered the entire region N-terminal of the TMD and were individually deleted. Part 4 covered the entire C-terminus and was replaced with a myc epitope tag (see figure 3.1, A). Each part consisted of 16-25 amino acids (aa), the SP comprising 25 aa and the TMD 23 aa. The 7 aa just N-terminal of the TMD were not modified as they contain positively charged lysines, shown to be important for correct membrane topology of TMDs (von Heijne, 1992). Figure 3.1 B shows representative fluorescence images of the cell lines expressing the different deletion constructs. Deletion of part 1 (PF08_0004Δ1-GFP), part 3 (PF08_0004Δ3-GFP) and replacement of part 4 with a myc-tag (PF08_0004Δ4myc-GFP) had the most deleterious effect on protein export, with the fusion protein almost exclusively localizing to the parasite periphery. PF08_0004Δ2-GFP and PF08_0004Δ3-GFP both showed a

weak punctate fluorescence signal in the host cell with a prominent signal in the parasite periphery, suggesting low levels of export. The level of fluorescence in the host cell was higher for PF08_0004Δ2-GFP compared to PF08_0004Δ3-GFP and this was the best exported version of the modified PF08_0004 proteins, although export was still low.

To exclude effects on protein export induced by the complete deletion of protein parts, the sequence of part 1 and 3, whose deletions resulted in the strongest export decrease, was replaced with a randomly scrambled version of this region. The resulting constructs PF08_0004d1scr-GFP and PF08_0004d3scr-GFP have a similar phenotype as their counterparts with the corresponding deletions. In summary these results show that all the domains are necessary for the efficient export of PF08_0004.

In other known PNEPs the N-terminus is necessary or sufficient for protein export (Külzer et al., 2012; Grüring et al., 2012; Heiber et al., 2013). To test whether this was also the case for PF08_0004, a minimal construct was generated, containing the SP, part 1 and a small fraction of part 2 to assess a possible capacity to drive export independent of the TMD. This construct localized to the PV and in structures resembling the TVN, demonstrating that the N-terminus is not sufficient to mediate export.
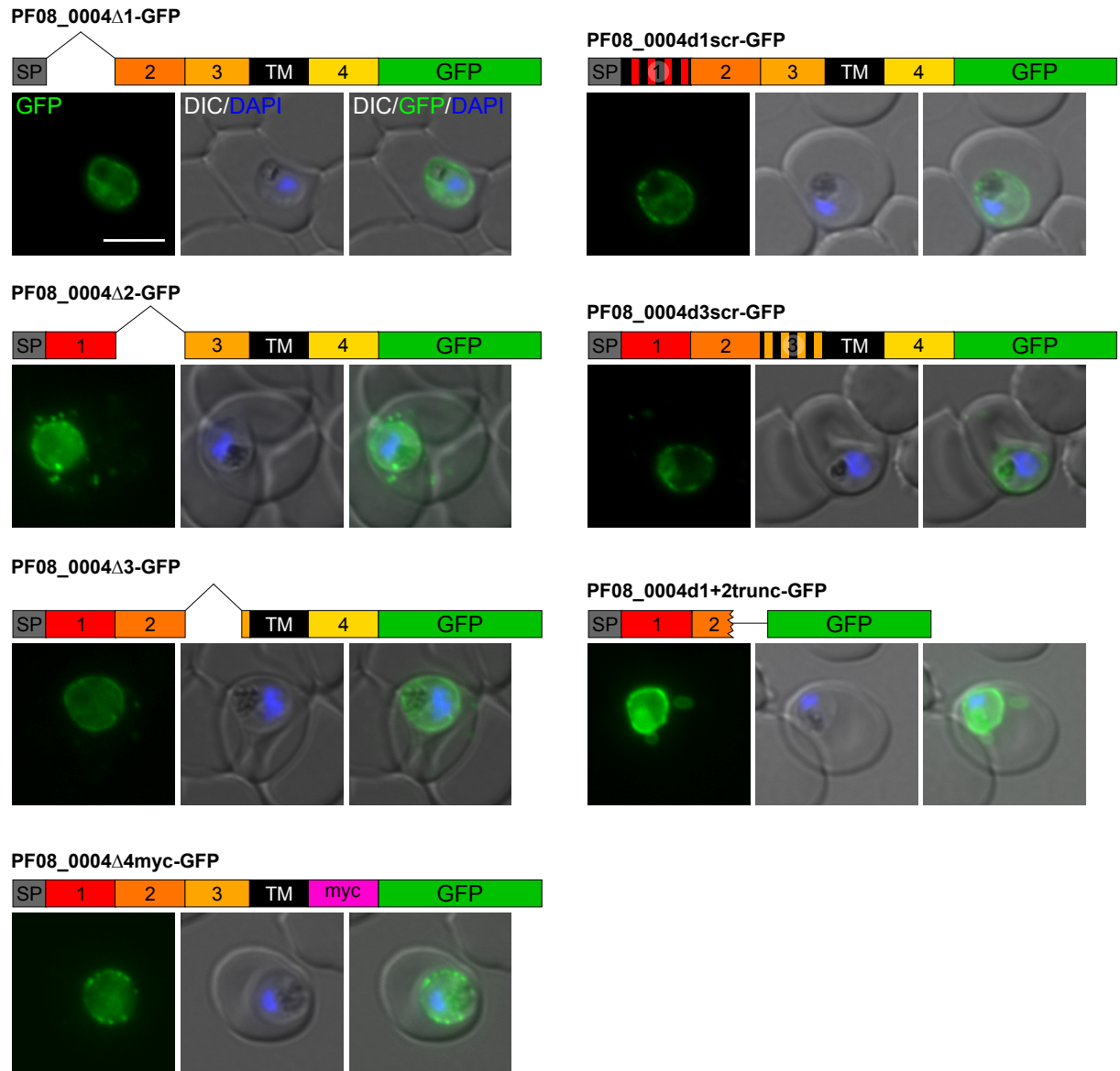
Figure 3.1.: Deletion constructs of PF08_0004. A Schematic showing the subdivision of PF08_0004 into 4 parts (not to scale). (SP) signal peptide, (TM) transmembrane region. **B** Live cell images of 3d7 parasites expressing GFP-fusion constructs under the *crt*-promoter. Nuclei were stained with DAPI. Construct schematics and names are shown above the respective images. Scrambled parts are represented by a striped pattern. (scr) scrambled (DIC) differential interference contrast. Scale bar: 5 μm.

The PF08_0004 SP and TMD PF08_0004 seemed to be strongly affected in export by all deletions tested and therefore behaved differently to the previously analyzed PNEPs. In other PNEPs the type of TMD affects export with only PNEP TMDs permitting export (Haase et al., 2009; Grüring et al., 2012; Saridaki et al., 2009). To test if PF08_0004 resembled the other PNEPs in this respect, it was tested whether a PNEP TMD could replace its TMD. For this the TMD of the PNEP REX2 was chosen and inserted into PF08_0004 to replace the original TMD (PF08_0004-Rex2TM-GFP) (figure 3.2). The resulting construct was not exported and localized to the parasite periphery. One possibility for the entirely different behavior of PF08_0004 to other PNEPs may be an altered membrane topology compared to the conventional PNEPs. Using the TMHMM Server v. 2.0 the localization and orientation of the TMDs in the different constructs was predicted (figure 3.3). For the topology prediction the sequences were used without the SP (if present) and without GFP, as depicted in the schematics. In PF08_0004 the N-terminus is predicted to be inside (the parasite cytoplasm) while for REX2 it is predicted to be outside. This is in accordance with the "positive inside rule", saying that the domain with the net positive charge flanking a TMD faces the cytoplasm (von Heijne, 1992). Surprisingly, when the flanking regions were replaced with amino acids flanking the REX2 TMD (PF08_0004Rex2TM+Rex2flanks) the predicted topology did not change, although the probability value of the prediction decreased (figure 3.3). The corresponding GFP-fusion construct (PF08_0004 Rex2 TM+Rex2 flanks-GFP) showed a punctate localization in the host cell and staining in the parasite periphery, indicating that the REX2 flanking regions could at least partially rescue the export of PF08_0004-Rex2TM-GFP (figure 3.2). Completely removing the TMD flanking amino acids (PF08_0004 Rex2TM+no flanks-GFP) resulted in a mostly perinuclear localization of the construct, typical for the ER (figure 3.2). This was probably not due to an altered topology, as the construct was predicted to have the same topology as PF08_0004 (figure 3.3).

Next, the PF08_0004 TMD was replaced with the TMD of the non-exported protein mTRAP (PF08_0004-mTRAP TM-GFP), which resulted in a staining in the parasite periphery, similar to PF08_0004-Rex2TM-GFP. Replacement of the C-terminal half of the TMD with the original TMD sequence (PF08_0004-mTRAP TM-N-GFP) could partially rescue the export (figure 3.2), indicating that the C-terminal part of the TMD could contribute to export.

PFL0065w is another PNEP identified by Heiber *et al.*, which contains a SP and a TMD. Because of the similar structure it was reasoned that the PFL0065w TMD of this protein might better correspond to the TMD of PF08_0004 and was used to replace the PF08_0004 TMD. The resulting construct, expressed as a GFP fusion (PF08_0004-PFL0065wTM-GFP), showed no export but staining at the parasite periphery (figure
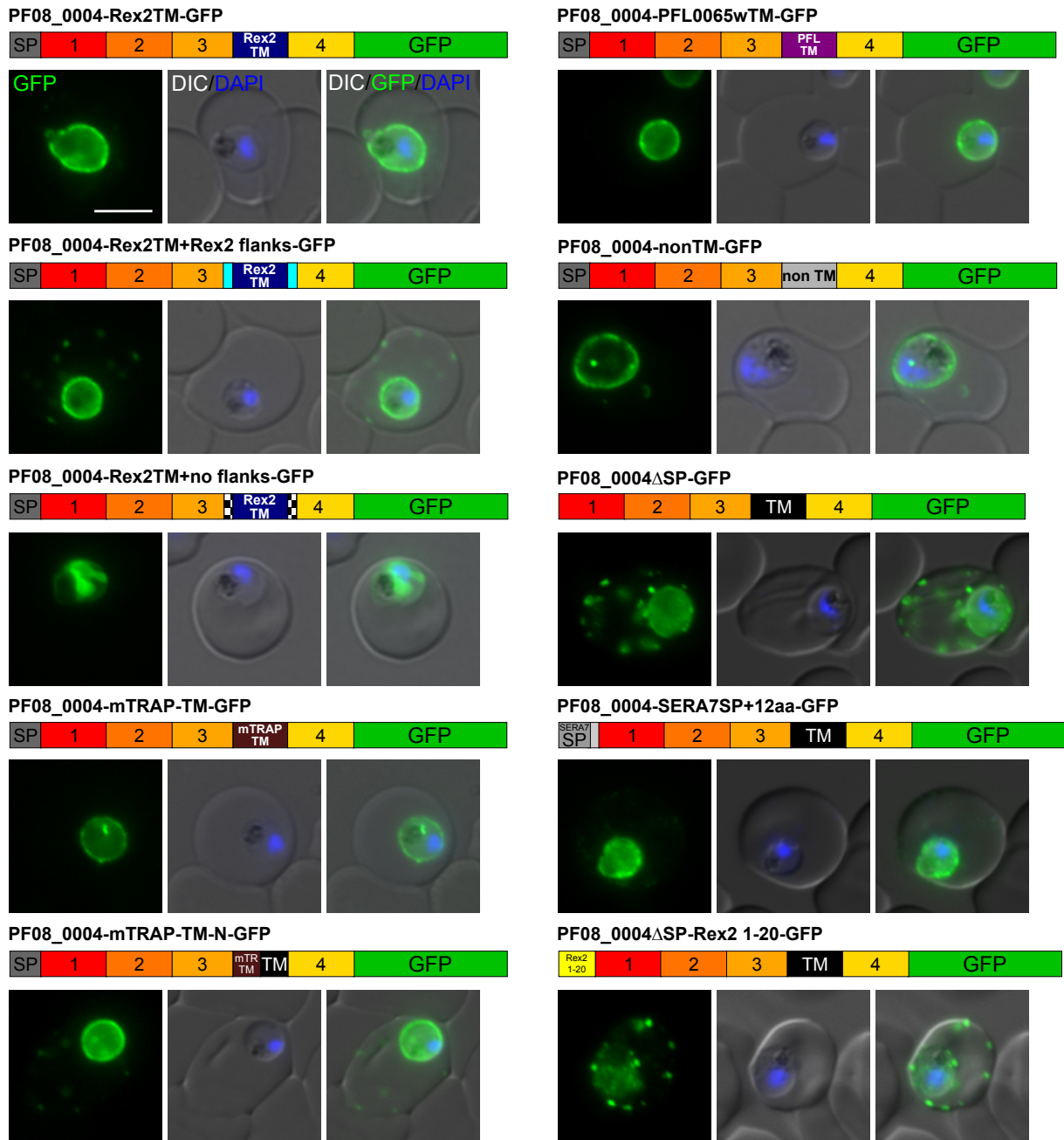
PF08_0004-Rex2TM-GFP

PF08_0004-PFL0065wTM-GFP

PF08_0004-Rex2TM+Rex2 flanks-GFP

PF08_0004-nonTM-GFP

PF08_0004-Rex2TM+no flanks-GFP

PF08_0004ΔSP-GFP

PF08_0004-mTRAP-TM-GFP

PF08_0004-SERA7SP+12aa-GFP

PF08_0004-mTRAP-TM-N-GFP

PF08_0004ΔSP-Rex2 1-20-GFP

Figure 3.2.: The role of the SP and TMD in the export of PF08_0004. Live cell images of 3d7 parasites expressing GFP-fusion constructs under the *crt*-promoter. Nuclei were stained with DAPI. Construct schematics and names are shown above the respective images. (SP) signal peptide, (TM) transmembrane region, (DIC) differential interference contrast. Scale bar: 5 µm.
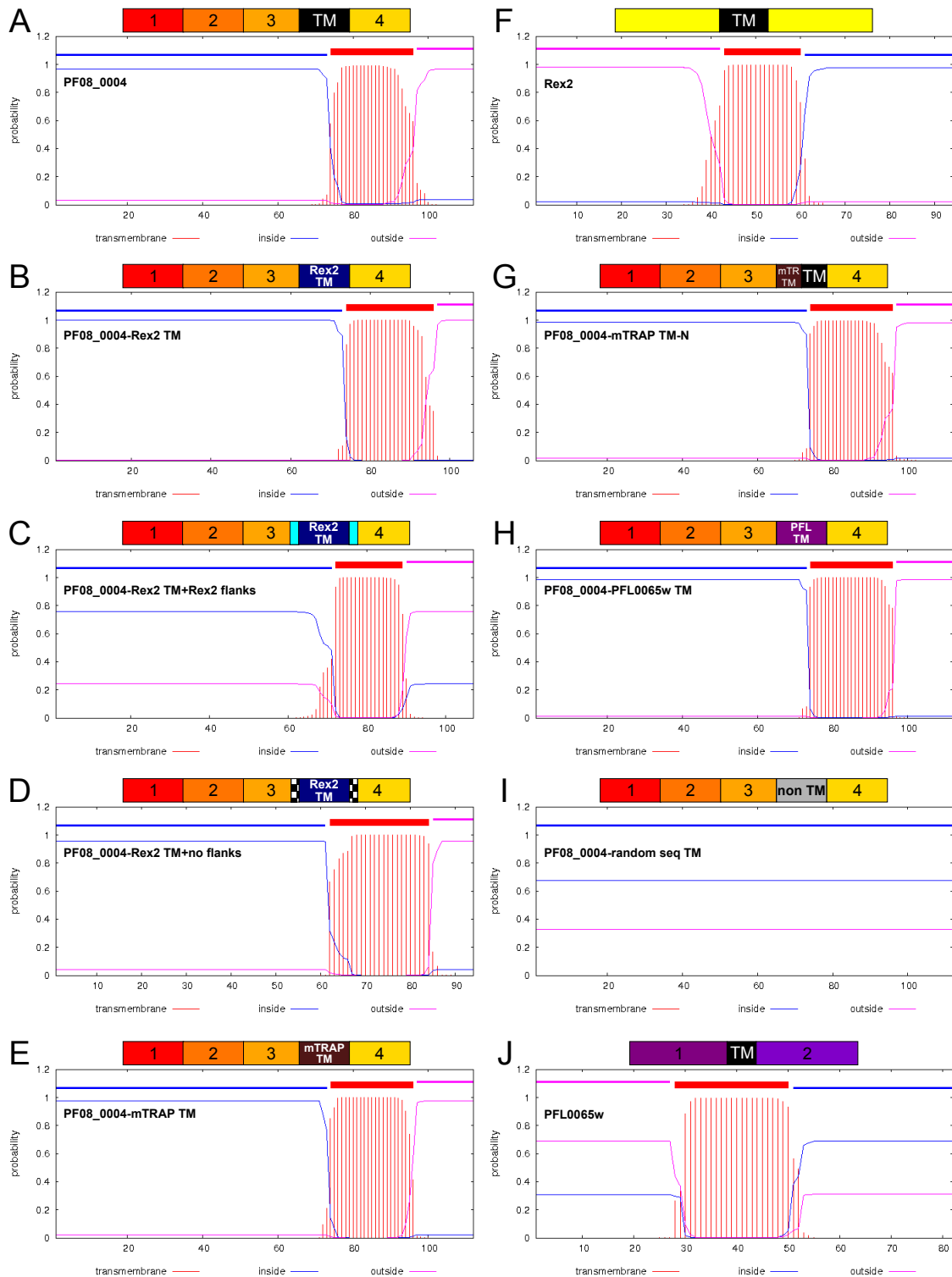
Figure 3.3.: Predicted TMDs in PF08_0004, REX2 and PFL0065w constructs. Membrane topology predictions generated by the TMHMM Server v. 2.0 are shown for PF08_0004, REX2, PFL0065w and derived constructs **(A-J)**. Sequences used for the predictions do not include the SPs and GFP. Red bars show the TMD probability, the horizontal red bar represents the TMD. The blue line shows the probability for a part of the protein to face the outside (initially the ER lumen), the purple line for facing the cytoplasm. (SP) signal peptide, (TM) transmembrane region.
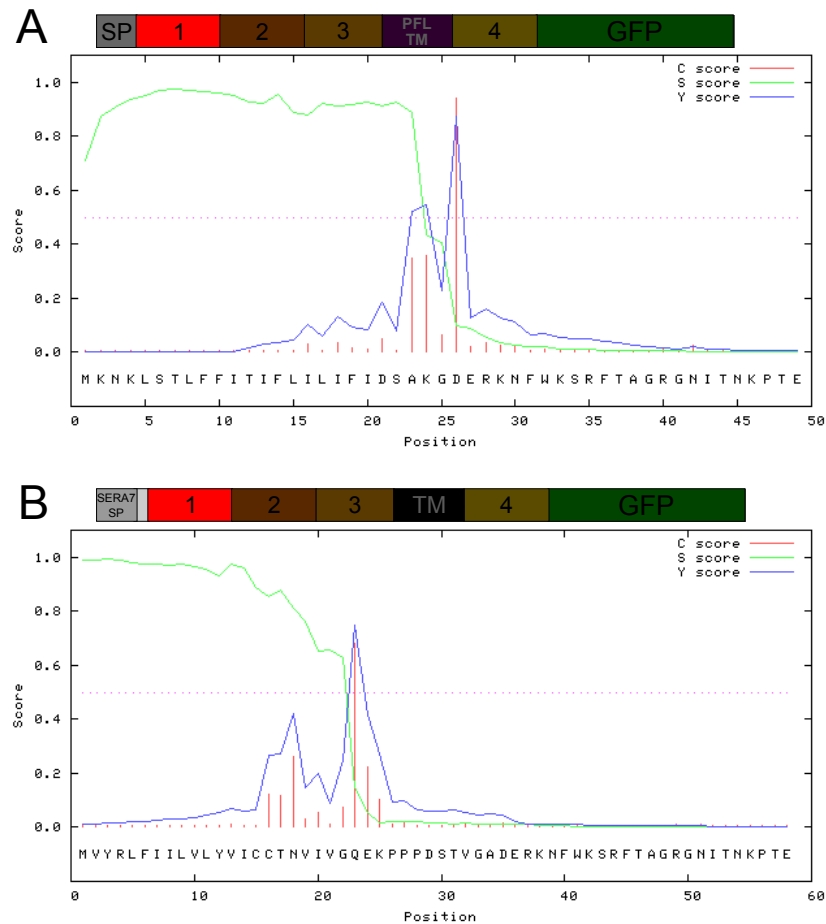
Figure 3.4.: PF08_0004 signal peptide cleavage site prediction. Signal peptide cleavage predictions generated by the SignalP 3.0 Server (Bendtsen et al., 2004) are shown for **A** PF08_0004 and **B** PF08_0004SERA7SP+12aa. Only the SPs and part 1 were used as a sequence input for better representation, in the schematics the rest of the protein is depicted in darker shades. The blue lines and red bars represent the cleavage probability/position, the green line shows the SP probability. Amino acids are shown in single letter code. (SP) signal peptide, (TM) transmembrane region

3.2). Similar to the other constructs with TMD replacements the predicted membrane topology resembled that of PF08_0004 (figure 3.3). Taken together these data indicate that also the TMD of PF08_0004 plays a crucial role in export of this PNEP and that in contrast to other PNEPs this function cannot be replaced by a TMD of a PNEP and also not by that of a non-exported protein. Only the additional replacement of the flanking regions of the REX2 PNEP TMD restored some export.

In the "classical" PNEP REX2 the TMD is necessary for entry into the secretory pathway (Haase et al., 2009). To investigate the influence of the PF08_0004 TMD for this process the TMD was replaced with a random amino acid sequence obtained by scrambling amino acids 301-321 of mTRAP. The resulting construct had no predicted TMD (figure 3.3, PF08_0004-nonTM) and localized to the parasite periphery and structures probably resembling the TVN, showing that the SP is sufficient for recruitment into the secretory pathway (see figure 3.2, PF08_0004-randomseqTM-GFP), but that such a construct is not exported. Surprisingly, a construct without a SP but with a TMD (PF08_0004ΔSP-GFP) was efficiently exported and showed a punctate pattern in the host cell, suggesting that the TMD alone is also sufficient for secretory pathway recruitment and that the SP is not necessary for export. Hence, this resembled the situation in conventional PNEPs without a classical N-terminal SP.

To further investigate the role of the SP it was replaced with the PV-residents' SERA7 SP, accidentally including the 12 aa downstream of the SP (PF08_0004 SERA7 SP+12aa-GFP). This construct showed almost no export and localized predominantly to the parasite periphery (see figure 3.2). A prediction of the SP cleavage sites in PF08_0004 and PF08_0004 SERA7 SP+12aa using the SignalP 3.0 server (Bendtsen et al., 2004) shows that the first 6 aa of mature N-terminus of PF08_0004 SERA7 SP+12aa are QEKPPP, in contrast to DERKNF of PF08_0004 (see figure 3.4). It was shown, that a stretch of prolines can block the export of an otherwise exported protein (Ullrich, 2016), which could be an explanation for the observed phenotype, rather than a dependence on the PF08_0004 SP. The first 20 aa of REX2 can mediate export of a reporter construct (Grüring et al., 2012), and replacement of the PF08_0004 SP with those resulted in efficient export of the construct (see figure 3.2, PF08_0004ΔSP-Rex2 1-20-GFP). These results indicate some influence of the mature N-terminus on export, similar to other PNEPs.

In summary, these results show that almost every change to the PF08_0004 sequence leads to loss of export, including even the exchange of the TMD for another PNEP TMD. The exception is the SP that was found to be dispensable for export. So, in contrast to the other PNEPs investigated so far, the export region could not be narrowed down to a single part of the protein.

3.1.1.2. **PFL0065w**

As the results for PF08_0004 were inconclusive and the export mediating part of the protein could not be clearly identified (see section 3.1.1.1), a second PNEP of the same domain organization was chosen for further investigation of PNEPs with a SP and a TMD. For this, PFL0065w was chosen, which is exported to the Maurer's clefts with additional staining in the parasite periphery, probably due to the fusion of GFP (Heiber et al., 2013). PFL0065w consists of 106 aa and was divided into 2 parts, localizing N- and C-terminally of the TMD and with a length of 23 or 20 aa, respectively. The TMD includes 23 aa, with 6 aa flanking the TMD N-terminally and 10 aa C-terminally (figure 3.5 A). Those amino acids were not modified to ensure the correct membrane topology. Membrane topology prediction indicated that the C-terminus faces the cytoplasm, similar to REX2 (figure 3.3, PFL0065w).

First, two constructs were generated where either part 1 or part 2 was replaced by a scrambled sequence of the corresponding region. This resulted in a complete export block and localization of the constructs in the parasite periphery (figure 3.5 B, PFL0065w N-scrambled-GFP and PFL0065w C-scrambled-GFP). To test, whether at least parts of these regions are dispensable for export, part 1 and 2 were further divided into two smaller parts each and scrambled individually. PFL0065w N1-scrambled GFP shows a weak export signal, suggesting that the very N-terminus is less important for export than the other parts of the protein. Both PFL0065w N2-scrambled-GFP and PFL0065w C1-scrambled-GFP showed no or almost no export, and a very weak export signal was detected for PFL0065w C2-scrambled-GFP (figure 3.5 B).

Again, very little change seems to be tolerated without causing a severe export phenotype in this protein. Overall, the results suggest that parts of the protein closer to the TMD are more important for export than the peripheral parts, again implying a role for the TMD in export. Contrary to PF08_0004, where deletion of part 1 abolished export (see section 3.1.1.1), the N-terminus of PFL0065w seems to be least essential for export. However, the differences in export levels were only minimal, so that the conclusions that can be drawn from these experiments must be considered with caution.
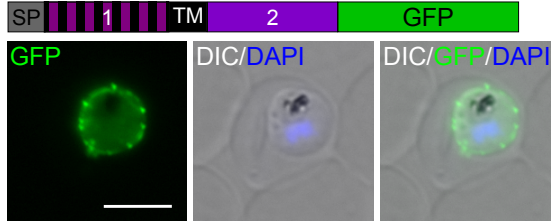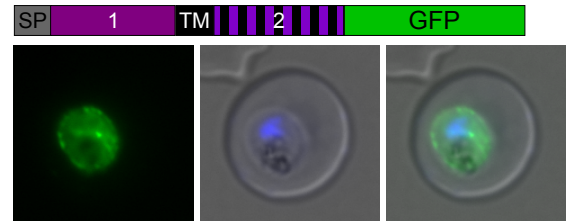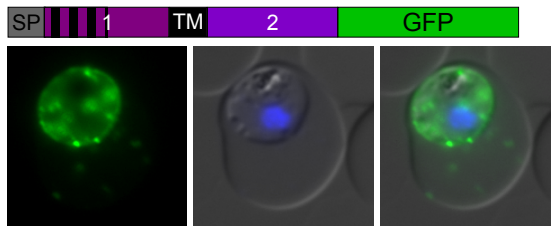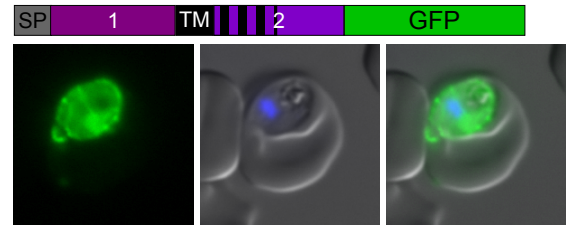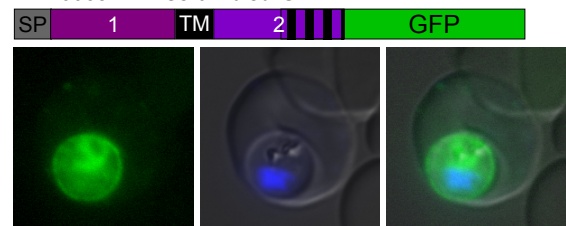
A **PFL0065w-GFP**

B **PFL0065w N-scrambled-GFP**

PFL0065w C-scrambled-GFP

PFL0065w N1-scrambled-GFP

PFL0065w C1-scrambled-GFP

PFL0065w N2-scrambled-GFP

PFL0065w C2-scrambled-GFP

Figure 3.5.: Domains influencing the export of PFL0065w. A Schematic showing the subdivision of PFL0065w into 2 parts (not to scale). (SP) signal peptide, (TM) transmembrane region. **B** Live cell images of 3d7 parasites expressing GFP-fusion constructs under the *crt*-promoter. Nuclei were stained with DAPI. Construct schematics and names are shown above the respective images. Scrambled parts are represented by a striped pattern. (scr) scrambled, (DIC) differential interference contrast. Scale bar: 5 μm.

3.1.2. Export requirements for PNEPs with a SP but no TMD

3.1.2.1. PF08_0005 and PFB0115w

PF08_0005 PF08_0005 is a PNEP with an N-terminal SP (figure 3.6 A). The PF08_0005 GFP fusion protein was exported to the host cell where it showed a cytosolic localization (Heiber et al., 2013). To identify the regions involved in its export it was initially divided into 3 parts of 120-125 aa each, that covered its entire sequence except for the SP. These parts were individually deleted and the constructs expressed as GFP fusion proteins in the parasite (figure 3.6 B).

The deletions of parts 2 and 3 had no effect on protein export (figure 3.6 B, PF08_0005Δ2-GFP and PF08_0005Δ3-GFP). No fluorescence was observed with the construct harboring the deletion of part 1, suggesting that this protein was unstable. It was therefore
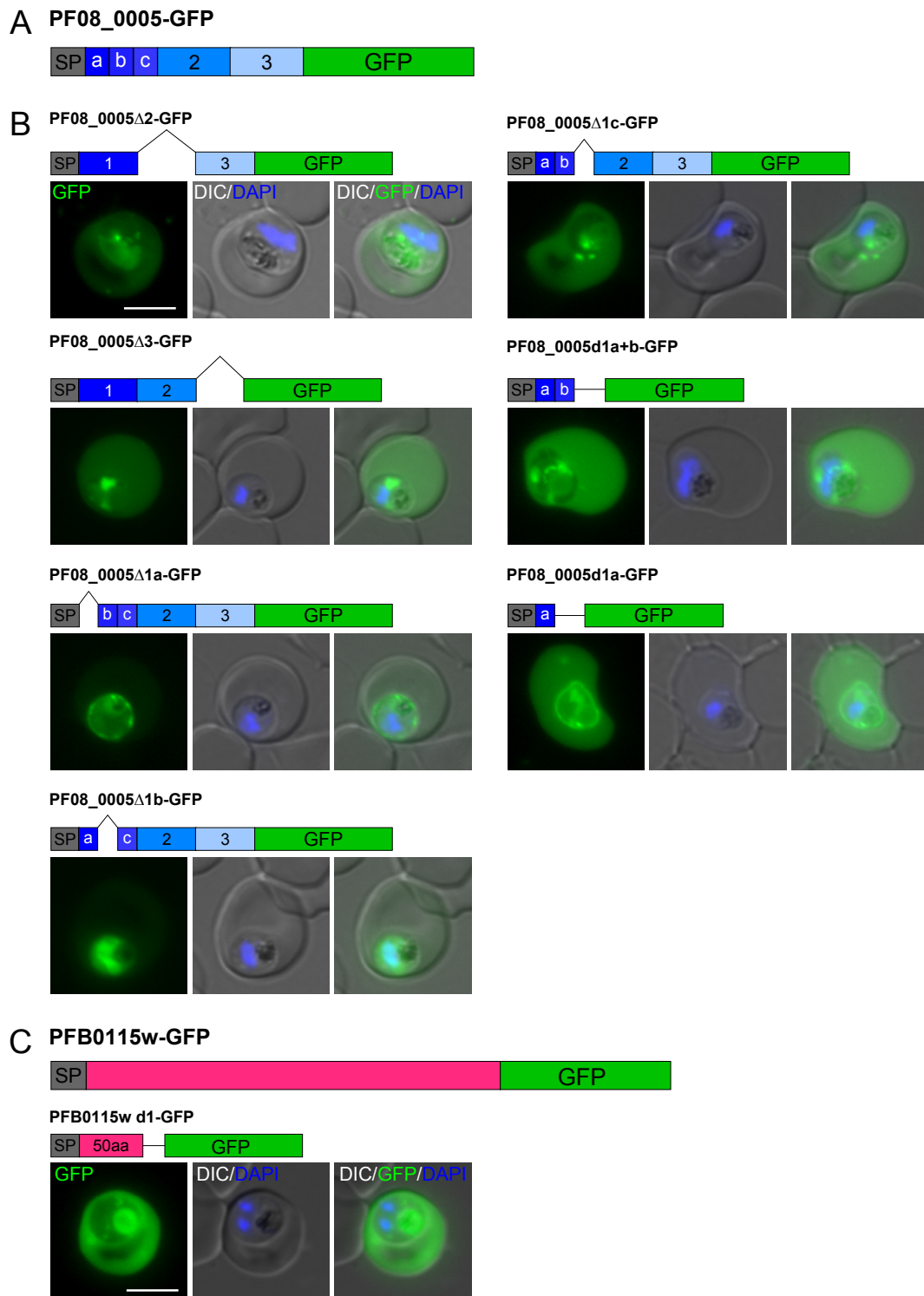
Figure 3.6.: Export requirements for PF08_0005 and PFB0115w. A Schematic showing the subdivision of PF08_0005 into 5 parts. Parts a,b and c are subdivisions of part 1 (not to scale). (SP) signal peptide **B** Live cell images of 3d7 parasites expressing GFP-fusion constructs under the *crt*-promoter. Nuclei were stained with DAPI. Construct schematics and names are shown above the respective images. **C** Schematics and live cell images of parasites expressing a PFB0115w GFP-fusion construct. (DIC) differential interference contrast. Scale bar: 5 μm.

next divided into 3 sub-parts named a (25 aa), b (50 aa) and c (45 aa) (figure 3.6 A). For the division into the three parts a secondary structure prediction using the Jpred 3 server (Cole et al., 2008) was performed and the sequence divided with regard not to destruct secondary structure elements. The construct with the deletion of part 1 c was fully exported (figure 3.6 B, PF08_0005Δc-GFP). In contrast, the deletions of parts 1 a and b resulted in a severely reduced export, with the fusion proteins localizing to the parasite periphery or the perinuclear region, respectively (figure 3.6 B, PF08_0005Δa-GFP and PF08_0005Δb-GFP). These results indicate, that the export mediating region in PF08_0005 is localized within parts 1 a and b.

To test whether parts 1 a and b are sufficient to mediate export, they were expressed as a minimal construct, containing the SP and parts 1 a and b fused to GFP, separated by a short linker sequence to minimize the influence of GFP on the export of the construct. PF08_0005d1a+b-GFP was efficiently exported to the host cell, demonstrating that this part of the protein is not only necessary but also sufficient to drive export (of GFP) (figure 3.6 B, PF08_0005d1a+b-GFP). A minimal construct containing only the SP and part 1 a was generated to further narrow down the export region in PF08_0005 (PF08_0005d1a-GFP). The resulting cell line showed strong fluorescence in the host cell with additional staining in the parasite periphery (figure 3.6 B, PF08_0005d1a-GFP), indicating that part 1 a is sufficient to drive export, but might require further amino acids from part b, or a greater distance from GFP, to induce full export. Some redundancy between region a and b might also explain the weak export signal seen for constructs PF08_0005Δa-GFP and PF08_0005Δb-GFP.

In summary, these results show that the C-terminal part of PF08_0005 is dispensable for protein export, and that similar to other known PNEPs the N-terminus contains the export region.

PFB0115w   PFB0115w was identified coincidentally in a screen for essential proteins and found to be a novel PNEP exported to the host cell, where it is localized at the RBC membrane (Reichard, 2015). A truncated version of this protein (414 aa) was shown to be still exported and localizing to the RBC membrane (Reichard, 2015). Similar to PF08_0005 it contains only a SP (figure 3.6 C, PFB0015w-GFP). To find out if the N-terminus of this protein is sufficient for export, a minimal construct with the SP and the following 50 aa was expressed as a GFP fusion protein (PFB0115w-50aa-GFP). This construct was efficiently exported and showed a RBC cytosolic localization (figure 3.6 C, PFB0115w-d1-GFP), demonstrating that the N-terminus of this PNEP is also sufficient for protein export. Additionally, these results indicate that the region of the protein mediating RBC membrane localization is contained between amino acids 77 and 414.

3.1.2.2. **MSRP6**

Similar to PF08_0005 and PFB0115w, MSRP6 is a soluble PNEP with a SP. As a GFP
fusion protein it localizes to the Maurer's clefts (Heiber et al., 2013). Previous work found
conflicting results on the export of this PNEP and the export mediating region could not
be clearly identified (Flemming, 2011; Schoeler, 2012). MSRP6 had been divided into 3
parts, with part 1 comprising only the first 30 aa, part 2 and 3 270 aa each (figure 3.7
A). Constructs containing deletions of these regions were expressed as GFP fusions. The
previous results (Flemming, 2011; Schoeler, 2012) are summarized in figure 3.7 B. It was
demonstrated, that the deletion of part 1 or part 2 did not have an effect on protein export
or localization (figure 3.7 B, MSRP6Δ1-GFP and MSRP6Δ2-GFP). In contrast deletion
of part 3 abolished Maurer's cleft localization but surprisingly this construct was still
exported (figure 3.7 B, MSRP6Δ3-GFP). Hence, no region seemed essential for export but
unexpectedly a minimal construct containing the SP and part 1 was not exported (figure
3.7 B, MSRP6 d1-GFP). Expression of the deletion constructs in a MSRP6 knock-out
background showed the same results, excluding interaction with the endogenous MSRP6
protein. Maurer's cleft localization could be restored by the reintroduction of the C-
terminal half of part 3 (parts 3 c and d, referred to as "cd" below), indicating that cd
mediates interaction with Maurer' cleft components (Flemming, 2011; Schoeler, 2012). In
summary these results lead to the puzzling conclusion, that none of the deleted parts alone
is essential for export, and that the N-terminus alone is also not sufficient. Additionally,
part cd was identified as a Maurer's cleft interaction domain.

This part of the thesis aimed to resolve these inconclusive results and elucidate the
export requirements for MSRP6. As the N-termini of the other two PNEPs investigated in
this study could alone mediate export of GFP, it was reasoned that the MSRP6 N-terminus
might also have an export driving capacity, despite of the previous results. To test this,
a GFP-fusion construct was generated, containing the SP, part 1 and an additional 71 aa
of part 2, as part 1 alone could not mediate export. Indeed, this construct was efficiently
exported to the RBC (figure 3.7 C, MSRP6 d1+2trunc-GFP), demonstrating that an
extended N-terminus of MSRP6 is sufficient to drive protein export.

In conventional TMD PNEPs, e.g. REX2 or MAHRP1, the first 20 aa can mediate
export of a reporter construct (mTRAP-R), consisting of the mTRAP sequence with a
REX2 TMD fused to GFP (Grüring et al., 2012). To test whether this property is shared
by soluble PNEPs, the N-terminus of MSRP6 was assessed for this ability. To this end,
aa 23-47 (first 25 aa after the SP) were fused to the mTRAP-R and expressed in 3d7
parasites. This construct was efficiently exported and localized to punctate structures in
the RBC (figure 3.7 C, MSRP6 aa23-47 mTRAP-R-GFP). These results show, that 25 aa
of the mature MSRP6 N-terminus are sufficient to mediate export of a reporter construct.
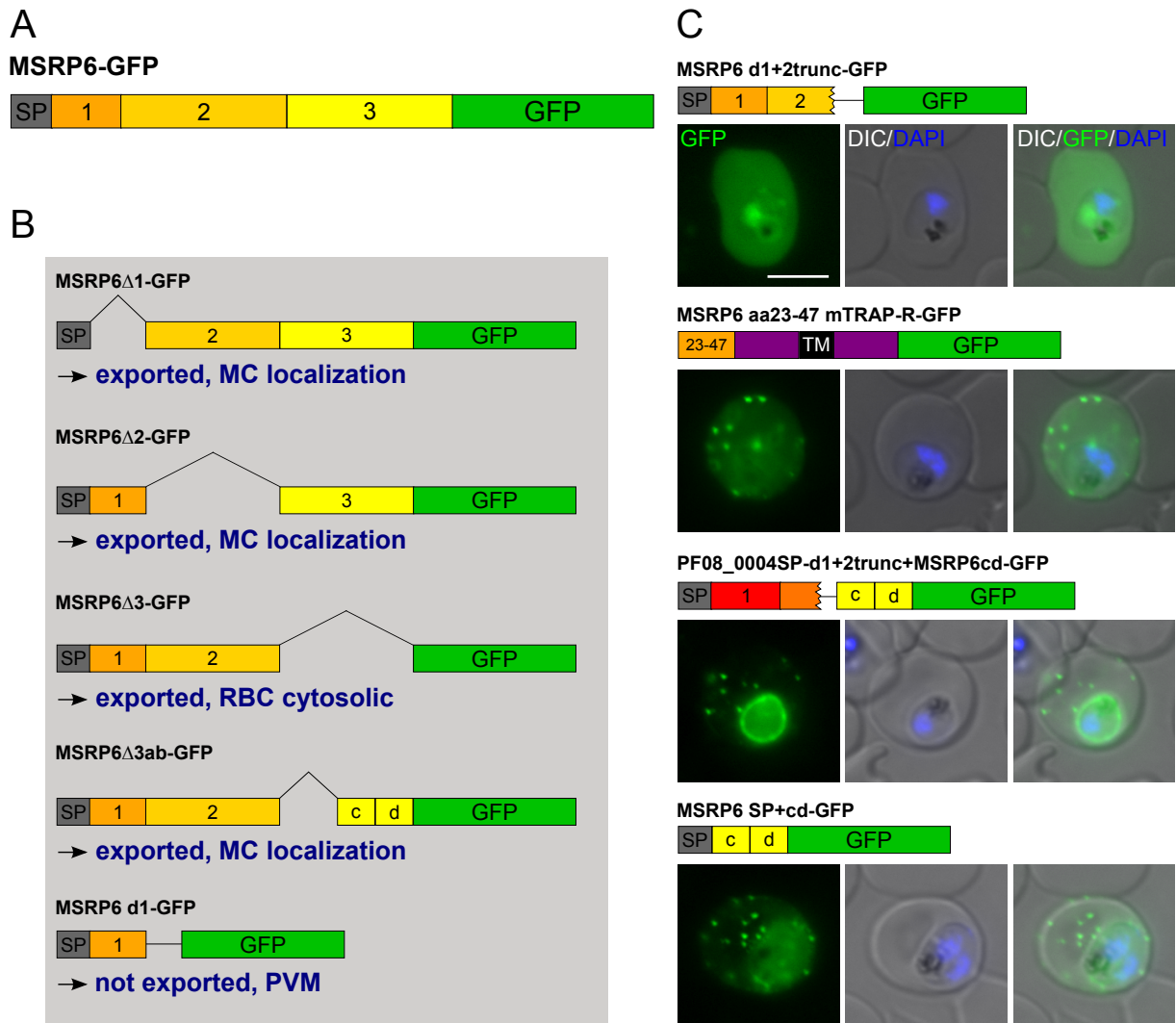
Figure 3.7.: Export requirements for the PNEP MSRP6. A Schematic showing the subdivision of MSRP6 into 3 parts (not to scale). (SP) signal peptide. **B** Schematics showing the previously generated MSRP6 deletion constructs and phenotypes obtained when expressed as GFP-fusions in 3d7 parasites (MC) Maurer's clefts (experiments performed by Flemming, 2011; Schoeler, 2012). **C** Live cell images of 3d7 parasites expressing GFP-fusion constructs under the *crt*-promoter that were generated in this thesis. Nuclei were stained with DAPI. Construct schematics and names are shown above the respective images. Scrambled parts are represented by a striped pattern. (scr) scrambled, (DIC) differential interference contrast. Scale bar: 5 μm.

Previous results indicated, that the N-terminus is dispensable for the export of MSRP6 (figure 3.7 B, MSRP6Δ1-GFP and MSRP6Δ2-GFP). However, the results here show that the N-terminus, if sufficiently long, can mediate protein export, typical for soluble PNEPs (see section 3.1.2). As however all deletion constructs of MSRP6 were still exported, this implies the presence of a second region mediating export in MSRP6. Since cd can mediate Maurer's cleft localization it was suspected that it might also be responsible for the observed export phenotypes of the MSRP6 deletion constructs, for instance by mediating interaction to another exported protein leading to a piggyback export. To test this hypothesis cd was fused to a non-exported protein construct described in section 3.1.1.1, which localized to the parasite periphery and hence ensures recruitment into the secretory pathway (figure 3.1 B, PF08_0004d1+2trunc-GFP). Indeed, the resulting GFP-fusion protein was partially exported to the host cell, localizing to punctate structures, with additional staining in the parasite periphery (figure 3.7 B, PF08_0004SP-d1+2trunc+MSRP6cd-GFP). To test if cd alone could also mediate export, it was fused to the MSRP6 SP to mediate entry into the secretory pathway without additional sequences, and expressed as a GFP-fusion protein. Surprisingly, this construct was exported to the host cell even more efficiently than the construct containing the PF08_0004 N-terminus (figure 3.7 B, MSRP6 SP+cd), demonstrating that cd possesses the capacity to mediate export independent of the N-terminal export domain.

In summary, these results show that both the N-terminus and the cd region in the C-terminus of MSRP6 can independently mediate export. In addition to the export capacity of cd, this region of the protein also mediated Maurer's cleft interaction (Flemming, 2011; Schoeler, 2012).

3.2. Identification and characterization of MSRP6 interaction partners

A short region in the C-terminus of MSRP6 (part cd) was shown to mediate both export and Maurer's cleft interaction, independent of the N-terminal export region (see section 3.1.2.2). These results imply that both functions might be connected and point to one or more MSRP6 interaction partners located at the Maurer's clefts, causing the Mauer's cleft localization of the otherwise soluble MSRP6. An interaction of MSRP6 cd with such interaction partners during the progression through the intracellular secretory pathway might result in a "co-export" of MSRP6 cd by a piggyback mechanism. To test this hypothesis and to find the protein causing Maurer's cleft localization of MSRP6, potential cd interaction partners were identified using proximity-dependent biotin identification (BioID).

## 3.2.1. Identification of MSRP6 interaction partners using BioID

BioID uses the promiscuous biotin ligase BirA* fused to the protein of interest so that it can tag proteins in close proximity, usually interaction partners, with biotin. This can be done in living cells under physiological conditions. The biotinylated proteins can subsequently be purified using streptavidin beads and identified via mass spectrometry (Roux et al., 2012).

In this work BioID was used to identify interaction partners of the cd region of MSRP6. For this purpose, a construct containing a truncated version of the soluble PEXEL protein REX3 (70 aa), the cd region of MSRP6, BirA* and GFP was generated and expressed in 3d7 parasites (figure 3.8 A, Rex3trunc+cd-BirA*-GFP). The 70 aa of REX3 (REX3trunc) were included to facilitate efficient export of the fusion protein, and GFP for detection of the protein. Rex3trunc+cd-BirA*-GFP was exported and localized to the Maurer's clefts (figure 3.8). To distinguish cd specific interaction partners from proteins binding to the backbone of the construct and from unspecifically biotinylated (soluble) exported proteins, a cell line containing a similar construct lacking part cd was generated (figure 3.8 A, Rex3trunc-BirA*-GFP) which localized to the RBC cytosol. As a control for unspecific biotinylation of Mauer's clefts proteins a truncated version of the transmembrane Maurer's cleft protein STEVOR (the first 260 aa), fused to GFP and BirA* was used, which localized to the Maurer's clefts (figure 3.8 A, Stevortrunc-GFP-BirA*).

3.2.1.1. Western blot analysis reveals successful biotinylation of the BioID constructs

The cell lines expressing the BirA* fusion constructs were incubated with biotin to start the biotinylation and grown for 24-48 hours. Whole cell lysates of trophozoite and schizont stage parasites were then generated and submitted to Western blot analysis (figure 3.7 B). The Western blot was probed with GFP antibodies and streptavidin, respectively, to detect the GFP fusion proteins and biotinylated proteins. Anti-GFP detected bands for all constructs at the expected sizes (calculated molecular weights for Rex3trunc-BirA*-GFP: 73 kDa, Rex3trunc+cd-BirA*-GFP: 91 kDa, Stevortrunc-GFP-BirA*: 92 kDa) and were not

Figure 3.8. *(following page)*: **Validation of BioID constructs. A** Live cell images of 3d7 parasites expressing BirA*-GFP fusion proteins under the *crt*-promoter. Construct schematics and names are shown above the respective images. Nuclei were stained with DAPI. (SP) signal peptide, (DIC) differential interference contrast. Scale bar: 5 μm. **B** Western blot analysis of cell lines expressing the different BirA*-GFP-fusion constructs. Cells were incubated with biotin to enable biotinylation by BirA*. Western blots were probed with GFP-antibodies to detect the expressed constructs and streptavidin to detect biotinylated proteins. 3d7 lysates were used as a control. (kDa) kilodaltons.
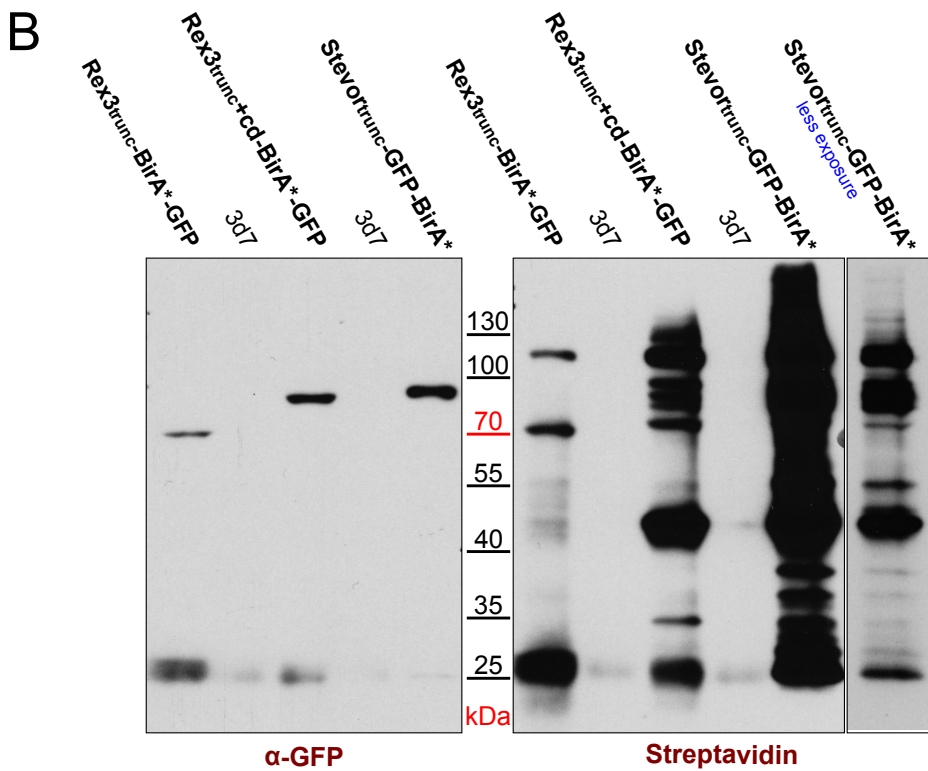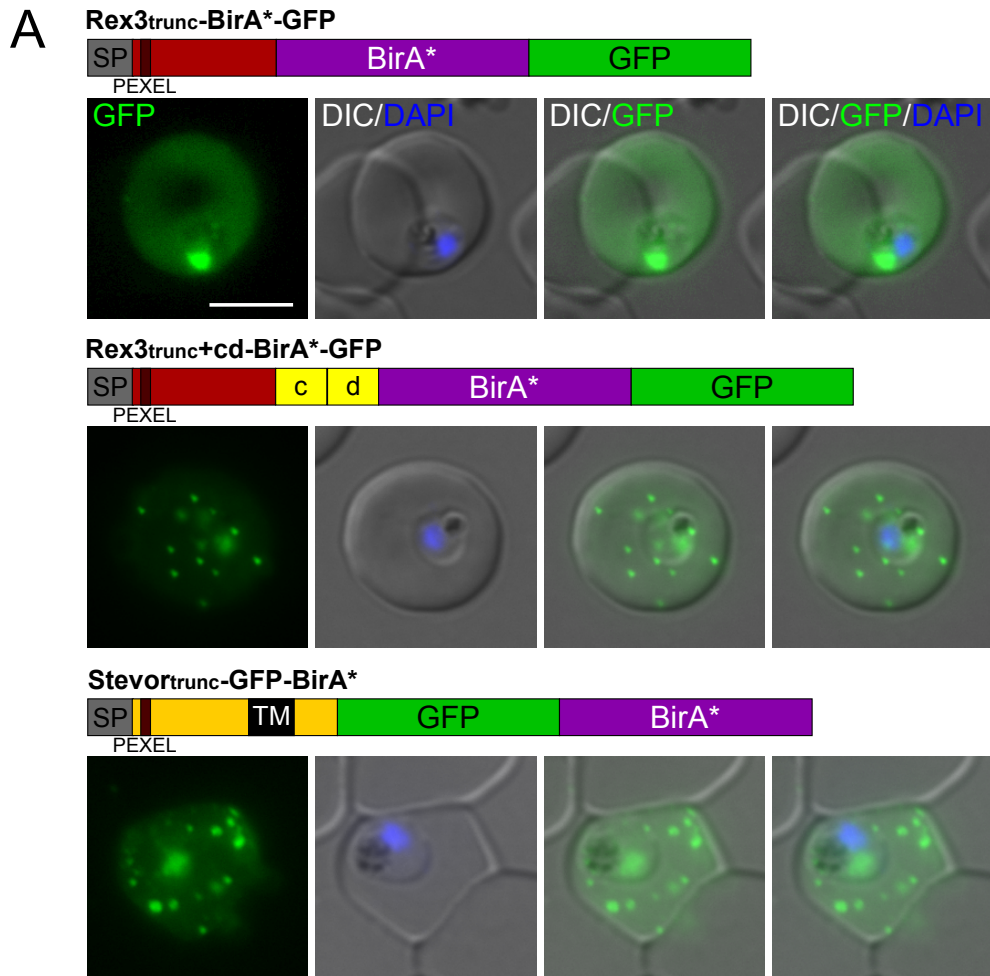
detected in wildtype 3d7 parasites. An additional band between 25 kDa and 35 kDa was present in several lanes, including the 3d7 controls and could represent an unspecific signal caused by hemoglobin dimers, which have an expected size of 32 kDa. With streptavidin a distinctive pattern of bands was observed for each cell line. Overall the number of bands and the signal intensity was highest for Stevortrunc-GFP-BirA* and least prominent for Rex3trunc-BirA*-GFP, which correlated with the intensity of the respective GFP band and might be caused by different protein concentrations in the lysates or different expression levels of the respective constructs. A band with the same size as the respective GFP-fusion construct was detected in Rex3trunc-BirA*-GFP and might represent self-biotinylation, a known property of BiA*. Due to the larger number of bands in the respective area of the blot, this was less obvious in Stevortrunc-GFP-BirA* and Rex3trunc+cd-BirA*-GFP. Both in Stevortrunc-GFP-BirA* and Rex3trunc+cd-BirA*-GFP a prominent band with a size between 40 kDa and 55 kDa was detected, and a similar pattern of bands between 70 kDa and 130 kDa (figure 3.8 B), indicating that the two Maurer's clefts localized constructs biotinylated a partially similar set of proteins.

These results show that all constructs were expressed with the correct size and possessed the capability to biotinylate proteins. It is however not possible to draw conclusions about the identity of biotinylated proteins or specificity of biotinylation from these blots, as a quantitative analysis of the bands would be difficult and was not performed.

3.2.1.2. Mass spectrometry identification of biotinylated proteins

The identification of cd specific interaction partners required a comparative analysis of the biotinylated proteins in the three cell lines outlined above. For this purpose the biotinylated proteins from these cell lines were purified and analyzed via quantitative liquid chromatography-mass spectrometry (LC-MS) (the quantitative LC-MS was carried out by Wieteke Hoeijmakers, Bartfai lab). Two independent experiments were performed (biological replicas), each in a duplicate (technical replicas). The results are depicted as plots, with enrichment of biotinylated proteins in one cell line over the other cell line plotted as the respective log2-ratios in each duplicate. Plots are shown for both biological replicas (figures 3.9 and 3.10).

The enrichment of biotinylated proteins in Rex3trunc+cd-BirA*-GFP (referred to as Rex3cd) over Rex3trunc-BirA*-GFP (referred to as Rex3) is shown in figure 3.9. In experiment 1, 14 proteins were identified that were enriched in Rex3cd over Rex3 with a false discovery rate (FDR) below 0.1, and 4 proteins that were enriched in Rex3 over cd (figure 3.9 A). In experiment 2, 25 proteins were enriched in Rex3cd over Rex3 with a FDR below 0.1, and 5 proteins enriched in Rex3 over Rex3cd. In total 27 different proteins were enriched in Rex3cd over Rex3, including both experiments. 26 of these
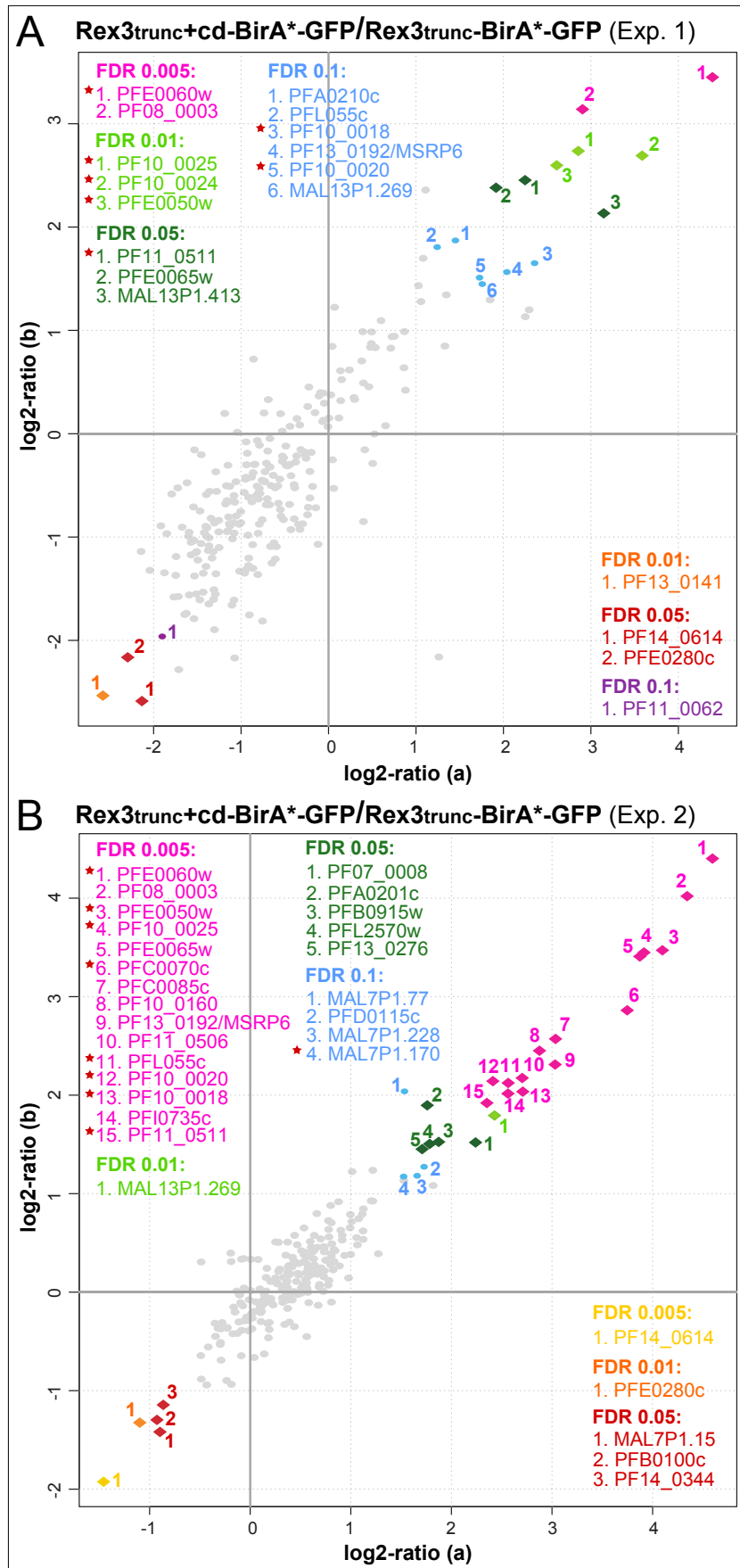
A **Rex3trunc+cd-BirA*-GFP/Rex3trunc-BirA*-GFP** (Exp. 1)

FDR 0.005:
★1. PFE0060w
★2. PF08_0003

FDR 0.01:
★1. PF10_0025
★2. PF10_0024
★3. PFE0050w

FDR 0.05:
★1. PF11_0511
2. PFE0065w
3. MAL13P1.413

FDR 0.1:
1. PFA0210c
2. PFL055c
★3. PF10_0018
4. PF13_0192/MSRP6
★5. PF10_0020
6. MAL13P1.269

FDR 0.01:
1. PF13_0141

FDR 0.05:
1. PF14_0614
2. PFE0280c

FDR 0.1:
1. PF11_0062

B **Rex3trunc+cd-BirA*-GFP/Rex3trunc-BirA*-GFP** (Exp. 2)

FDR 0.005:
★1. PFE0060w
2. PF08_0003
★3. PFE0050w
★4. PF10_0025
5. PFE0065w
★6. PFC0070c
7. PFC0085c
8. PF10_0160
9. PF13_0192/MSRP6
10. PF11_0506
★11. PFL055c
★12. PF10_0020
★13. PF10_0018
14. PFI0735c
★15. PF11_0511

FDR 0.01:
1. MAL13P1.269

FDR 0.05:
1. PF07_0008
2. PFA0201c
3. PFB0915w
4. PFL2570w
5. PF13_0276

FDR 0.1:
1. MAL7P1.77
2. PFD0115c
3. MAL7P1.228
4. MAL7P1.170

FDR 0.005:
1. PF14_0614

FDR 0.01:
1. PFE0280c

FDR 0.05:
1. MAL7P1.15
2. PFB0100c
3. PF14_0344

Figure 3.9.: Biotinylated proteins enrichend in Rex3cd over Rex3. A Plotted are
the log2 ratios obtained from duplicates representing the enrichment of biotinylated proteins in
Rex3cd over Rex3 in experiment 1. Hits with a false discovery rate below (FDR) 0.1 are plotted
as colored diamonds with numbers corresponding to the respective protein names. The colors
represent different FDRs ranging from 0.001 to 0.1. Red asterisks mark candidates chosen for
further analysis. **B** Experiment 2 (biological replica). (FDR) false discovery rate.

Candidate	Rex3cd over Rex3				Rex3cd over Stevor			
	Experiment 1		*Experiment 2*		*Experiment 1*		*Experiment 2*	
	A	B	A	B	A	B	A	B
PFE0060w	4.39	3.45	4.59	4.40	1.62	2.02	2.39	2.47
PFE0050w	2.61	2.60	4.10	3.47	0.57	0.99	2.23	2.05
MAL7P1.170	0.54	0.83	1.52	1.17	1.49	1.96	2.33	2.29
PF11_0511	2.25	2.45	2.35	1.92	0.54	2.03	1.96	1.30
PF10_0025	2.86	2.74	3.91	3.45	0.79	0.24	1.56	1.68
PF10_0024	3.59	2.69	4.00	ND	1.13	1.46	2.37	ND
PFC0070c	3.08	ND	3.75	2.86	1.13	ND	2.38	1.74
PFL0055c	1.24	1.81	2.56	2.12	0.82	0.80	1.09	1.15
PFI0086w*	2.29	1.20	ND	2.12	0.25	0.48	ND	0.90
PF10_0018**	2.36	1.65	2.71	2.04	0.65	0.21	1.16	1.04
PF10_0020**	1.73	1.51	2.41	2.14	0.02	0.31	0.42	0.72

Table 3.1.: Log2 enrichment ratios for MSRP6 interaction candidates. This table
shows the log2 ratios obtained from the quantitative MS analysis for the selected candidates
enriched in Rex3cd over Rex3 and Rex3cd over Stevor. (*) Not significantly enriched in any
experiment. (**) Significantly enriched only in Rex3cd over Rex3.

proteins are annotated or reported to be exported (PlasmoDB). Of the 14 enriched pro-
teins in experiment 1 (Rex3cd over Rex3), 12 were reproduced in experiment 2, with the
other two proteins being only detected in in one of the duplicates in experiment 2, but
with high log2 ratios (4.0 and 4.59), suggesting that they also may be valid candidates.
Of the 15 candidates with a FDR of 0.005 in experiment 2 (Rex3cd over Rex3), 5 were
not significantly enriched in experiment 1 (i.e. FDR not below 0.1). However, the log2
ratios for both duplicates are between 1.0 and 3.0 for 4 of these proteins, and at 3.08 in
one duplicate for the other candidate (see appendix, section B). This suggested specific
enrichment of proteins in the Rex3cd over the Rex3 control. In contrast, only one protein
was reproducibly enriched in Rex3 over Rex3cd with a FDR below 0.1. Together these
results show that the biotinylation of Rex3cd over Rex3 specific proteins is highly repro-
ducible in independent experiments. The fact that almost all of the proteins significantly
enriched in Rex3cd over Rex3 are exported proteins is further evidence for the specificity
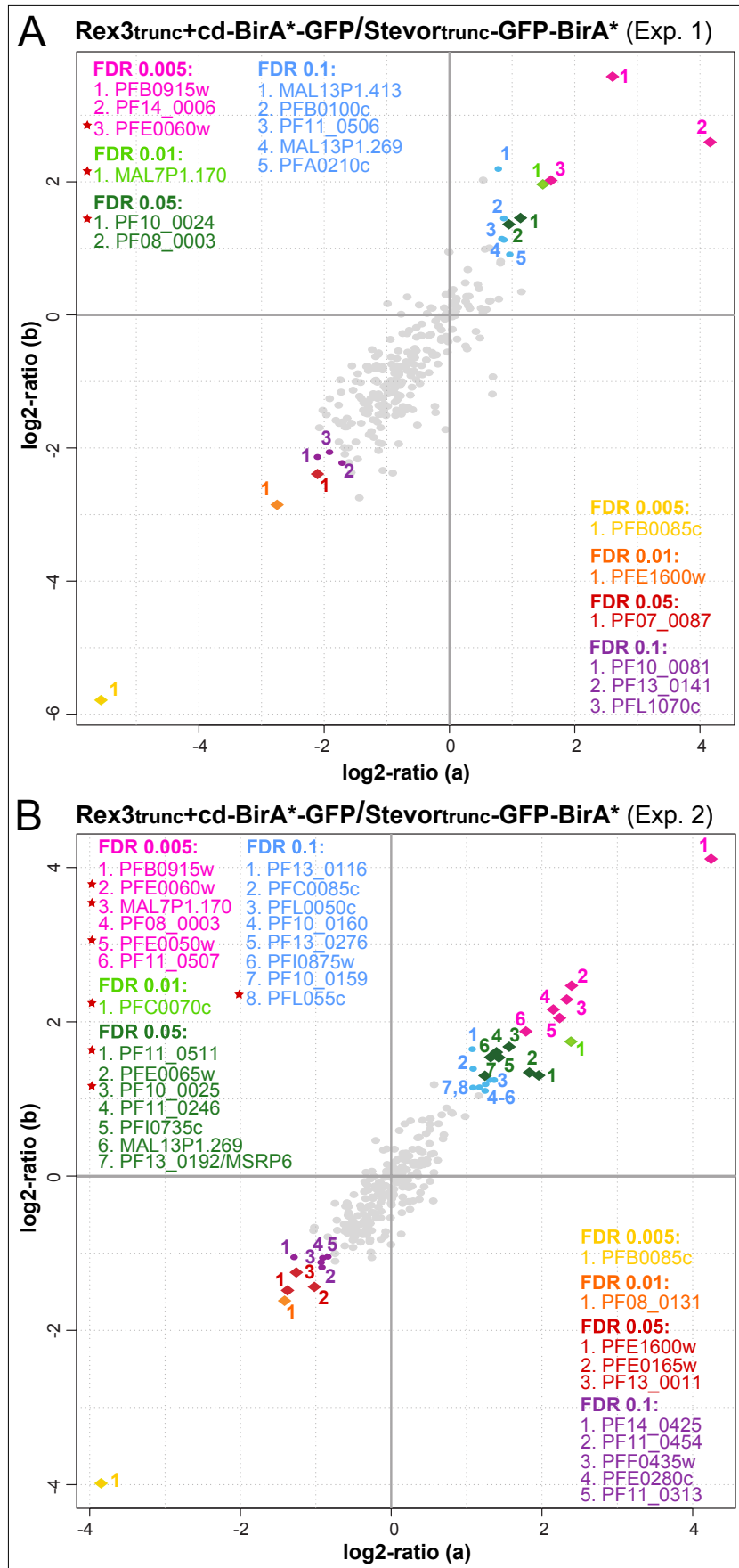of the results.

A **Rex3**trunc**+cd-BirA*-GFP/Stevor**trunc**-GFP-BirA*** (Exp. 1)

FDR 0.005:
1. PFB0915w
2. PF14_0006
★ 3. PFE0060w
FDR 0.01:
★ 1. MAL7P1.170
FDR 0.05:
★ 1. PF10_0024
2. PF08_0003

FDR 0.1:
1. MAL13P1.413
2. PFB0100c
3. PF11_0506
4. MAL13P1.269
5. PFA0210c

FDR 0.005:
1. PFB0085c

FDR 0.01:
1. PFE1600w

FDR 0.05:
1. PF07_0087

FDR 0.1:
1. PF10_0081
2. PF13_0141
3. PFL1070c

B **Rex3**trunc**+cd-BirA*-GFP/Stevor**trunc**-GFP-BirA*** (Exp. 2)

FDR 0.005:
1. PFB0915w
★ 2. PFE0060w
★ 3. MAL7P1.170
4. PF08_0003
★ 5. PFE0050w
6. PF11_0507
FDR 0.01:
★ 1. PFC0070c
FDR 0.05:
★ 1. PF11_0511
2. PFE0065w
★ 3. PF10_0025
4. PF11_0246
5. PFI0735c
6. MAL13P1.269
7. PF13_0192/MSRP6

FDR 0.1:
1. PF13_0116
2. PFC0085c
3. PFL0050c
4. PF10_0160
5. PF13_0276
6. PFI0875w
7. PF10_0159
★ 8. PFL055c

FDR 0.005:
1. PFB0085c

FDR 0.01:
1. PF08_0131

FDR 0.05:
1. PFE1600w
2. PFE0165w
3. PF13_0011

FDR 0.1:
1. PF14_0425
2. PF11_0454
3. PFF0435w
4. PFE0280c
5. PF11_0313

Figure 3.10.: Biotinylated proteins enrichend in Rex3cd over Stevor. A Plotted are the log2 ratios obtained from duplicates representing the enrichment of biotinylated proteins in Rex3cd over Rex3 in experiment 1. Hits with a false discovery rate below (FDR) 0.1 are plotted as colored diamonds with numbers corresponding to the respective protein names. The colors represent different FDRs ranging from 0.001 to 0.1. Red asterisks mark candidates chosen for further analysis. **B** Experiment 2 (biological replica). (FDR) false discovery rate.

Next, Rex3trunc+cd-BirA*-GFP (referred to as Rex3cd) was compared to Stevortrunc-GFP-BirA* (referred to as Stevor) in an attempt to distinguish proteins interacting with cd from general Maurer's clefts proteins. In experiment 1, 11 candidates were found to be significantly enriched in Rex3 over Stevor (FDR≤0.1), and 6 proteins enriched in Stevor over Rex3cd (figure 3.10). Experiment 2 identified 22 proteins enriched in Rex3cd over Stevor and 10 proteins enriched in Stevor over Rex3cd. In total 28 significantly enriched candidates (Rex3cd over Stevor) were identified, of which 27 are annotated or reported to be exported (PlasmoDB). Five of these candidates were significantly enriched in both experiments. Of the 8 candidates with a FDR of 0.1 in experiment 2 all showed log2 ratios between -1.19 and 0.94 in experiment 1, indicating that these are not specific for Rex3cd. The 6 candidates with a FDR≤0.05 in experiment 1 were either significant in experiment 2 or had log2 ratios of 1.86 and 2.37 in one of the duplicates, respectively, suggesting that they may represent specific hits. For candidates with a FDR≥0.1 in experiment 1 or FDR≥0.05 in experiment 2 the respective log2 ratios from the other experiment are more diverse, indicating that these hits might not be relevant. In summary, these results demonstrate that biotinylation was specific for exported proteins and that the most significant hits were reproduced in the two independent experiments.

Of the 35 significantly enriched (Rex3cd over Rex3 plus Rex3 over Stevor) hits identified in total, 19 were significantly enriched in both Rex3cd over Rex3 and Rex3cd over Stevor, which then would fulfill the criteria for Maurer's clefts proteins in close proximity to or specifically interacting with cd. PFE0060w was the most striking candidate, being present in the 0.005 FDR category in all experiments. In total, 11 candidates were chosen for further characterization (table 3.1). This selection included 7 candidates from the 19 candidates significantly enriched in Rex3cd over Rex3 and over Stevor in at least one of the replicas. Three candidates were only significantly enriched in either Rex3cd over Rex3 or Rex3cd over Stevor, and one candidate showed no significant enrichment in any of the experiments, but had high log2 ratios in at least one technical replica in Rex3cd over Rex3 in both experiments and was chosen before a detailed quantitative analysis of both biological replicas was available (table 3.1). The properties of the chosen candidates are summarized in table 3.3.

Candidate	Annotation (PlasmoDB)	PEXEL	SP	TMD	Transcription Profile	Peak Transcription (RPKM)
PF10_0018	alpha/beta hydrolase, putative	yes	yes	no		155
PF10_0020	alpha/beta hydrolase, putative	yes	yes	no		886
PF10_0024	Plasmodium exp. protein (hyp2), unknown function	yes*	yes	3		30
PF10_0025	PF70 protein (PF70), PTP5	yes	yes	no		2301
PFL0055c	RESA-like protein w. PHIST and DnaJ domains	yes	yes	no		79
PFC0070c	Plasmodium exp. protein, unknown function	yes	yes	1		65
PFE0050w	Plasmodium exp. protein, unknown function	yes	yes	no		1722
PFE0060w	parasite-infected erythrocyte surface protein (PIESP2)	yes	yes	2		839
MAL7P1.170	Plasmodium exp.protein, unknown function	no	yes	no		4244
PF11_0511	Plasmodium exp. protein, unknown function	yes	yes	no		938
PFI0086w	Plasmodium exp., unknown function	yes	yes	no	no data available	NA

Table 3.3.: Potential MSRP6 cd interaction partners chosen for further analysis. This table lists potential interaction partners of part cd of MSRP6. Listed are gene IDs, PlasmoDB annotations, the presence of a PEXEL-motif, SP and TMD, transcription profiles and peak transcription values (based on Le Roch et al., 2003). The asterisk (*) indicates an unconventional PEXEL-motif downstream of a TMD. (SP) signal peptide, (TMD) transmembrane domains, (RPKM) reads per kilobase per million mapped reads.

3.2.2. Characterization of potential MSRP6 interaction partners

Of the 11 potential MSRP6 interaction partners (tables 3.1 and 3.3) chosen for further analysis (see section 3.2.1.2) 10 had PEXEL-motifs, and 3 proteins contained one or more TMDs. To analyze the subcellular localization of these proteins and test the interaction with MSRP6 via co-immunoprecipitation (CoIP) all of the selected candidates were endogenously tagged with FKBP and GFP. FKBP was included into the tag to facilitate a potential further analysis by knock-sideways. The correct integration into the genome was confirmed by diagnostic PCRs for all candidates (figure 3.11). All proteins were localized and an interaction analysis using CoIP was carried out for 5 of them. The results are outlined in sections 3.2.2.1, 3.2.2.2 and 3.2.2.3.

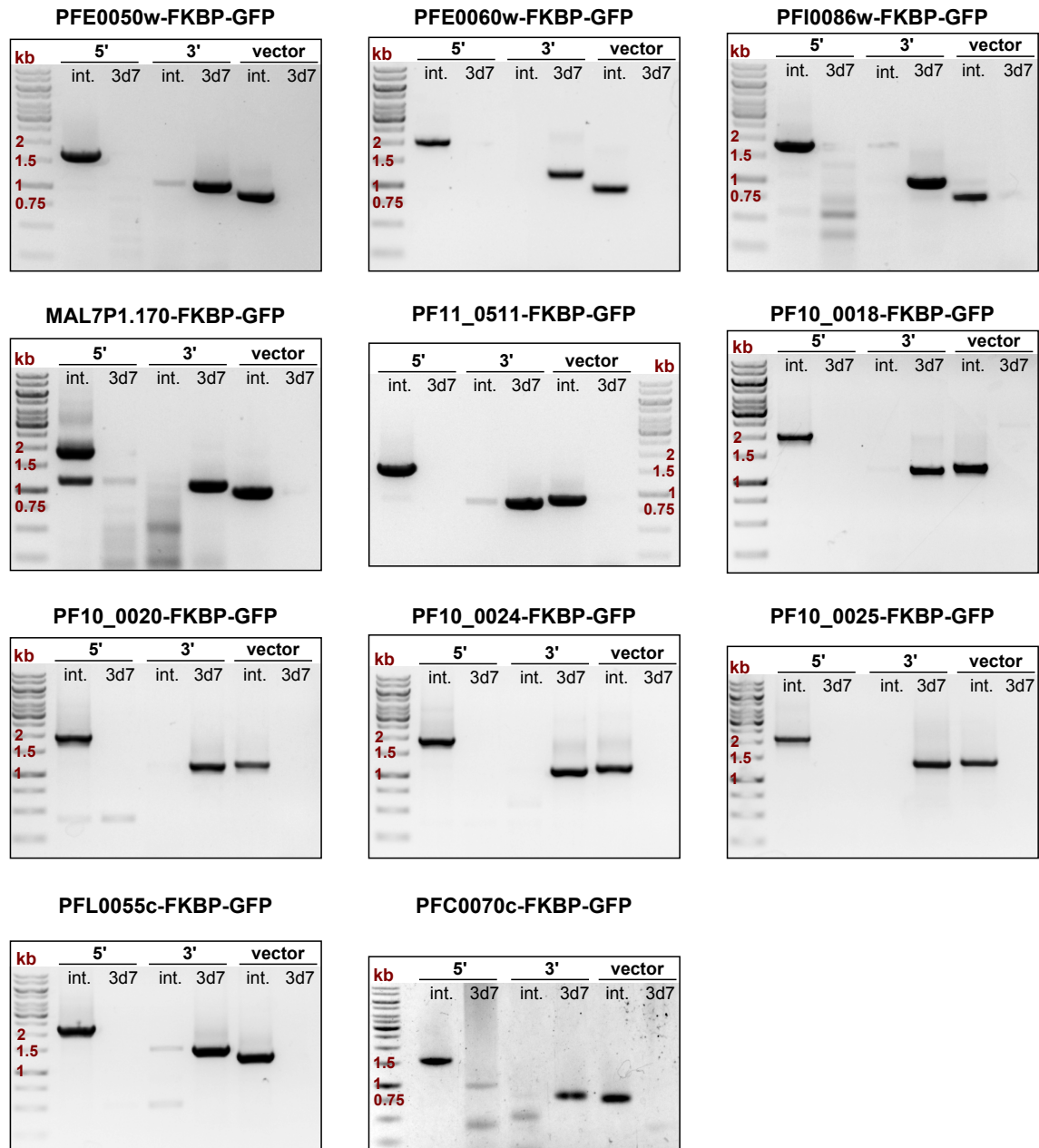**Figure 3.11.: Diagnostic PCRs for integration cell lines.** Color inverted gels are shown of the diagnostic PCRs performed on genomic DNA purified from the respective integration cell lines. 3d7 genomic DNA was used as a control. Primers used for diagnostic PCRs and expected band sizes are listed in the Appendix section A and table A.2, respectively. (int.) integrant genomic DNA, (kb) kilobases

3.2.2.1. Transmembrane Proteins

PF10_0024 PF10_0024 is a protein of 469 aa and contains an N-terminal SP followed by a TMD. The C-terminus contains two further TMDs, separated from one another by only 5 amino acids. A PEXEL-motif (RLLAE) was identified downstream of the first TMD, the functionality being unknown however, as PEXEL-motifs usually occur approximately 20 amino acids downstream of a SP (figure 3.12 A). A BLASTp search identified two *P. falciparum* proteins as paralogs, PF10_0023 and PF10_0025. PF10_0025 is one of the other potential MSRP6 interaction partners and is described in section 3.2.2.2. Additionally, BLASTp identified homology to the VID27 superfamily, a family of fungal and plant proteins with mostly unknown functions. mRNA transcripts for PF10_0024 could only be detected in merozoites and early ring stages, and the overall transcription level is very low (Le Roch et al., 2003) (table 3.3). Both the function and localization of PF10_0024 are unknown.

In live ring stage 3d7 parasites the PF10_0024-FKBP-GFP fusion protein localized to punctate structures within the RBC, with some fluorescence also present within the parasite. In later stages GFP fluorescence was mostly cytosolic within the parasite with additional prominent fluorescence inside the food vacuole (figure 3.12 B). The fluorescence intensity was very low in all stages and could only be detected using a 63x (NA 1.4) objective that permits more light-transmission than the usually used 100x (NA1.4) objective.

To further specify the subcellular localization of PF10_0024, immunofluorescence assays (IFA) were performed (figure 3.12 C). The PF10_0024-FKBP-GFP fusion protein was predominantly detected within the parasite, with additional foci inside the RBC, which partially co-localized with MSRP6 (figure 3.12 C).

In summary, PF10_0024 is a very lowly expressed protein, exported to the host cell where it shows a punctate localization in ring stages. There was only a partial co-localization with MSRP6, possibly because MSRP6, in contrast to PF10_0024, is exclusively expressed in later stages. These results indicate that PF10_0024 is not a likely interaction partner of MSRP6 and may also be found in structures in the host cell that do not represent Maurer's clefts.

Figure 3.12.: Subcellular localization of PF10_0024-FKBP-GFP. A Schematic showing the protein features of PF10_0024 fused to 2xFKBP and GFP. (SP) signal peptide (TM) transmembrane region. **B** Live cell images of 3d7 parasites expressing PF10_0024-FKBP-GFP from the endogenous locus. Shown are ring stage parasites and trophozoite stage parasite. Nuclei were stained with DAPI. (troph) trophozoite, (DIC) differential interference contrast. Scale bar: 5 μm. **C** IFA of acetone-fixed 3d7 parasites expressing PF10_0024-FKBP-GFP from the endogenous locus. Cells were stained with GFP-antibodies (green channel) and MSRP6-antibodies (red channel). Nuclei were stained with DAPI. Scale bar: 5 μm.

PFC0070c PFC0070c is a protein of 243 aa and contains an N-terminal SP followed by a PEXEL-motif and a TMD domain in the C-terminal part of the protein (figure 3.13 A). No homologs could be identified in a BLASTp search. mRNA transcripts were reported in all blood stages, although the overall transcription level were low (Le Roch et al., 2003), (table 3.3). Both the function and localization of this protein are currently unknown.

When endogenously expressed in 3d7 parasites, PFC0070c-FKBP-GFP showed a cytosolic localization in the parasite and additional foci within the parasite, their number depending on the developmental stage (figure 3.13 B). In trophozoites/early schizonts 2-4 bright foci could be detected, while in late schizonts bright foci were still present but additional foci with weaker fluorescence were detectable. No fluorescence was detected in the host cell in any of the investigated blood stages, indicating that PFC0070c is not exported and likely is not an MSRP6 interaction partner. It should however be noted that (if this protein is not essential for parasite survival) a GFP tag close to the C-terminal proximal TMD may interfere with the export of this protein, as was previously reported for another exported TMD protein (Heiber et al., 2013).

A

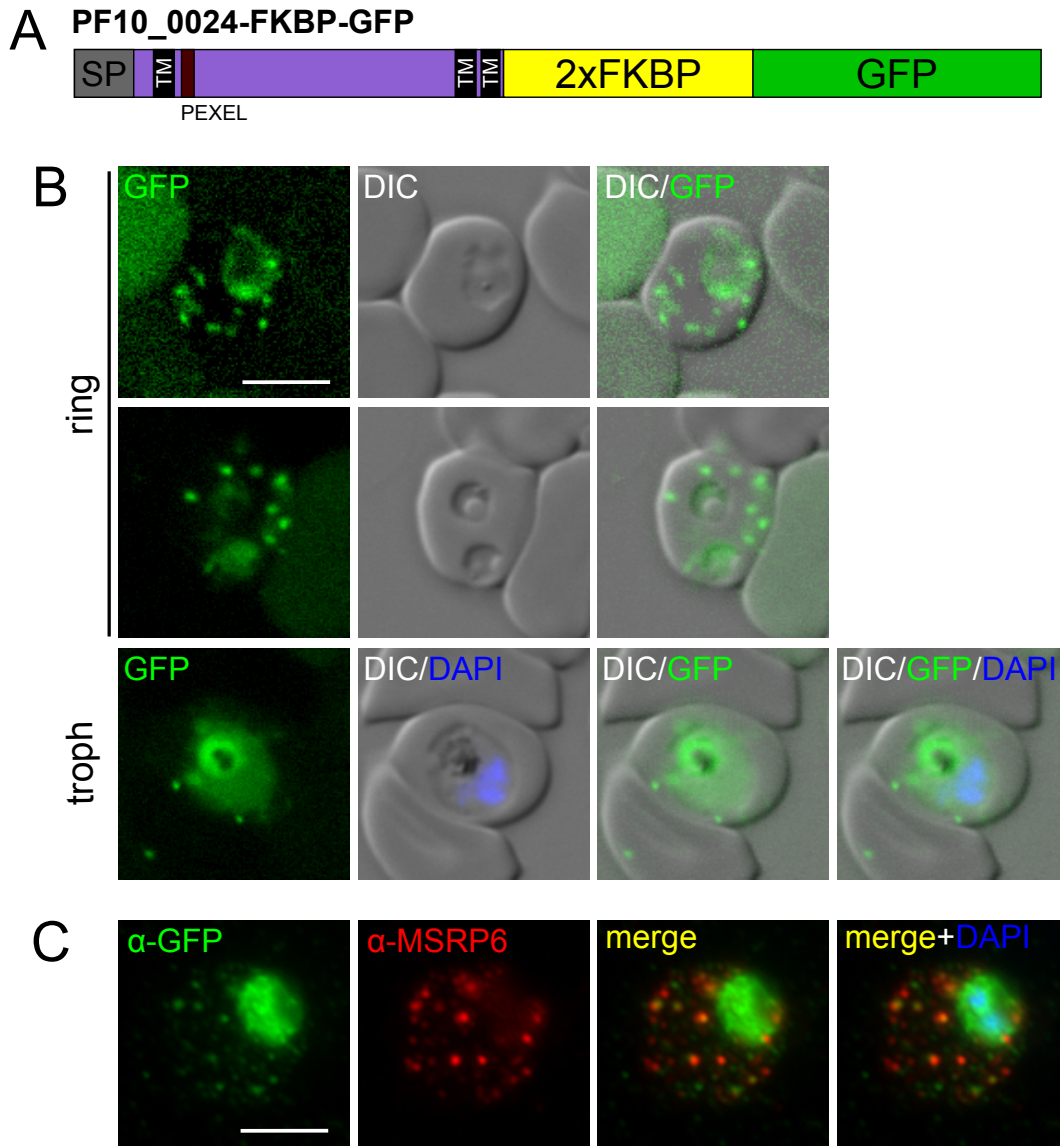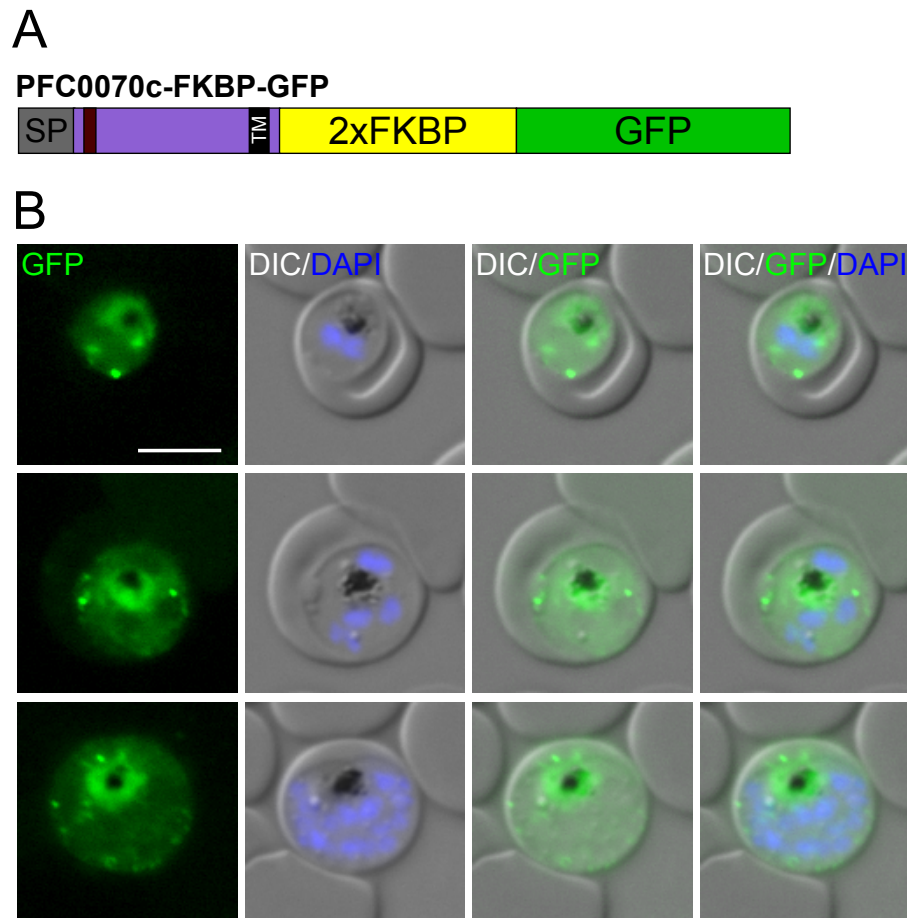**PFC0070c-FKBP-GFP**

| SP | | | TM | 2xFKBP | GFP |

B

Figure 3.13.: Subcellular localization of PFC0070c-FKBP-GFP. A Schematic showing the protein features of PFC0070c fused to 2xFKBP and GFP. (SP) signal peptide (TM) transmembrane region. **B** Live cell images of 3d7 parasites expressing PFC0070c-FKBP-GFP from the endogenous locus. Shown are trophozoite/early schizont and schizont stages. Nuclei were stained with DAPI. (DIC) differential interference contrast. Scale bar: 5 µm.

PFE0060w PFE0060w is a protein of 408 aa and contains a SP followed by a PEXEL-motif and 2 TMDs at the C-terminus (figure 3.14 A). There are no known homologs, except for an ortholog in *P. reichenowi*. The mRNA transcription shows a peak in the early trophozoite stage, with total transcripion levels being comparably high (Le Roch et al., 2003), (table 3.3). PFE0060w was first identified as a RBC surface protein and subsequently named parasite-infected erythrocyte surface protein 2 (PIESP2) (Florens et al., 2004). Another study, aimed to identify novel Maurer's cleft proteins, found PFE0060w to be localized at the Maurer's clefts (Vincensini et al., 2005). The function of this protein is unknown, however, a knockout of PFE0060w had no effect on *Pf*EMP1 trafficking or RBC rigidity, and only a slight decrease in RBC adhesion to CSA under physiological flow conditions was observed (Maier et al., 2008).

Endogenously expressed PFE0060w-FKBP-GFP showed a punctate localization in ring, trophozoite and schizont stages (figure 3.14 B). The localization of PFE0060w was further

Figure 3.14.: Subcellular localization of PFE0060w-FKBP-GFP. A Schematic showing the protein features of PFE0060w fused to 2xFKBP and GFP. (SP) signal peptide (TM) transmembrane region. **B** Live cell images of 3d7 parasites expressing PFE0060w-FKBP-GFP from the endogenous locus. Shown are ring, trophozoite and schizont stage parasites. Nuclei were stained with DAPI. (troph) trophozoite, (DIC) differential interference contrast. Scale bar: 5 μm. **C** IFA of acetone-fixed 3d7 parasites expressing PFE0060w-FKBP-GFP from the endogenous locus. Cells were stained with GFP-antibodies (green channel) and SBP1-antibodies (red channel) or GFP-antibodies (green channel) and MSRP6-antibodies (red channel), respectively. Nuclei were stained with DAPI. Scale bar: 5 μm.

analyzed by IFA, were it co-localized with the Maurer's cleft resident protein SBP1 and MSRP6 (figure 3.14 C), demonstrating that PFE0060w is a Maurer's clefts protein and that this protein may potentially interact with MSRP6 (see section 3.2.2.3).

3.2.2.2. Soluble proteins

PF10_0018   PF10_0018 is a protein of 921 aa and contains an N-terminal SP and a PEXEL-motif (figure 3.15 A). mRNA transcripts were reported in merozoites and ring stages, with a peak transcription value of 155 reads per kilobase per million mapped reads (RPKM) in early ring stages (Le Roch et al., 2003), indicating that protein expression is comparably low (table 3.3). PF10_0018 belongs to the alpha/beta hydrolase superfamily, whose members include e.g. proteases and lipases. Several homologs were identified in *P. falciparum* (OrthoMCL DB), including PF10_0020, which is described below. Homologs also include putative lysophospholipases in several *Plasmodium* species and *Toxoplasma gondii* (PlasmoDB, BLASTp).

The PF10_0018-FKBP-GFP fusion protein localized to the parasite cytoplasm and food vacuole, additionally a punctate staining was observed inside the RBC. The protein was only detected in trophozoite and schizont stage parasites, and fluorescence levels were very low (figure 3.15 B). IFA showed that PF10_0018-FKBP-GFP partially co-localized with both, SBP1 and MSRP6, indicative of a Maurer's cleft localization of PF10_0018 (figure 3.15 C).

A PF10_0018-FKBP-GFP

| SP | | PEXEL | 2xFKBP | GFP |

B

troph

| GFP | DIC/DAPI | DIC/GFP | DIC/GFP/DAPI |

schizont

C

| α-GFP | α-SBP1 | merge | merge+DAPI |

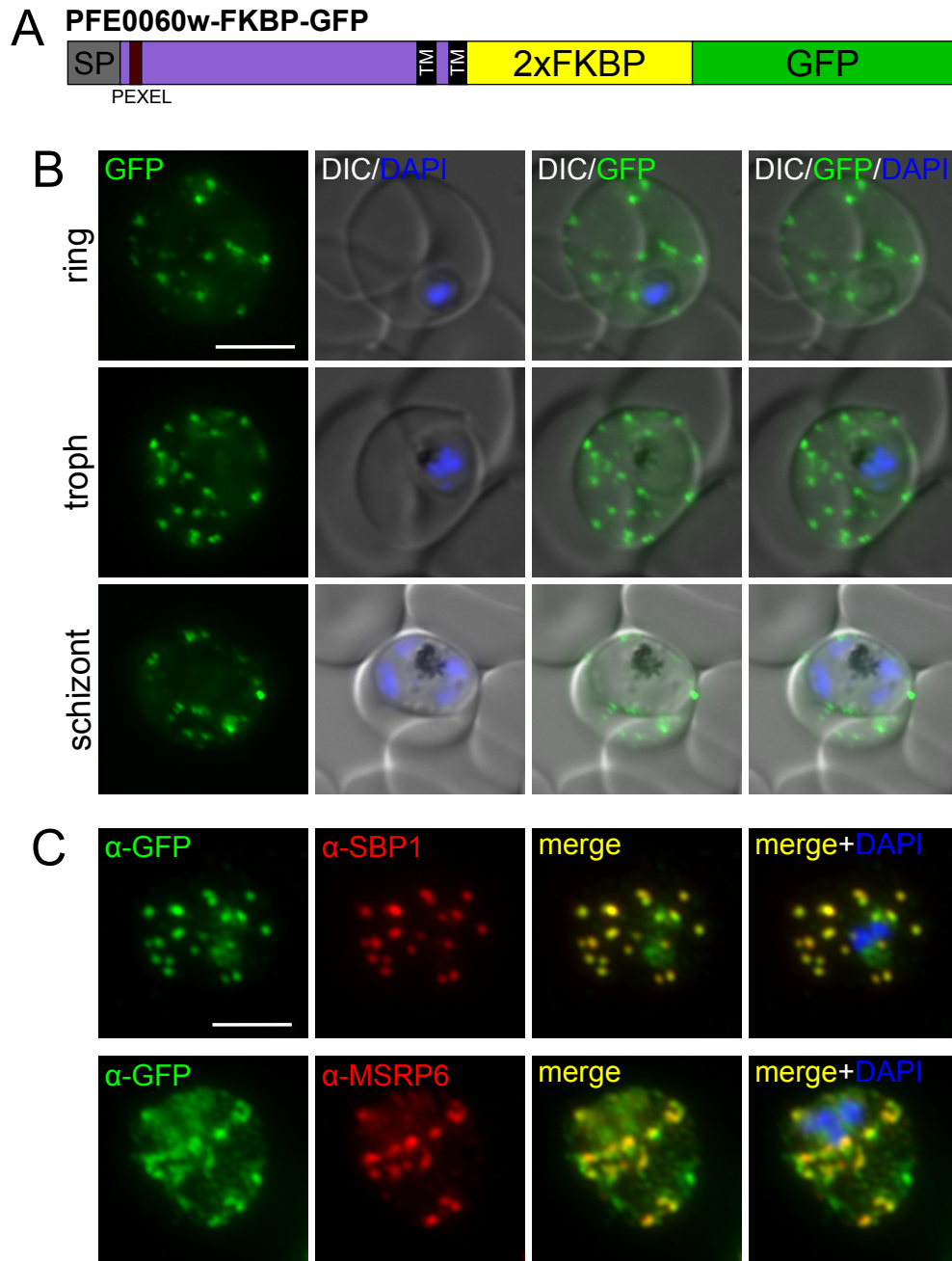| α-GFP | α-MSRP6 | merge | merge+DAPI |

Figure 3.15.: Subcellular localization of PF10_0018-FKBP-GFP. A Schematic showing the protein features of PF10_0018 fused to 2xFKBP and GFP. (SP) signal peptide. **B** Live cell images of 3d7 parasites expressing PF10_0018-FKBP-GFP from the endogenous locus. Shown are trophozoite and schizont stage parasites. Nuclei were stained with DAPI. (troph) trophozoite, (DIC) differential interference contrast. Scale bar: 5 μm. **C** IFA of acetone-fixed 3d7 parasites expressing PF10_0018-FKBP-GFP from the endogenous locus. Cells were stained with GFP-antibodies (green channel) and SBP1-antibodies (red channel) or GFP-antibodies (green channel) and MSRP6-antibodies (red channel), respectively. Nuclei were stained with DAPI. Scale bar: 5 μm.

PF10_0020 PF10_0020 is a protein of 763 aa and contains a potential SP and a PEXEL-motif. SP prediction was performed using the SignalP 3.0 and 4.1 servers, with the SignalP 3.0 prediction score not reaching the SP cutoff value, and SignalP 4.1 predicting no SP at all. PF10_0020 was reported to be transcribed in trophozoite stages, with a peak transcription in early schizonts (886 RPKM) (Le Roch et al., 2003), (table 3.3). PF10_0020 is a homolog of PF10_0018, also belonging to the alpha/beta hydrolase superfamily and showing homology to lysophospholipases of *Plasmodium* (BLASTp).

The PF10_0020-FKBP-GFP fusion protein showed a prominent staining of the parasite cytoplasm, food vacuole and filament-like structures and foci within the parasite, more abundant in late schizont stages (figure 3.16 B). Additionally, a faint punctate staining in the RBC was observed. Total fluorescence was very low, non-detectable in ring stage parasites and increasing during the progression to schizont stages. Similar to PF10_0018 a partial co-localization with SBP1 and MSRP6 was detected in IFAs, indicating that a fraction of PF10_0020 localized to Maurer's clefts.
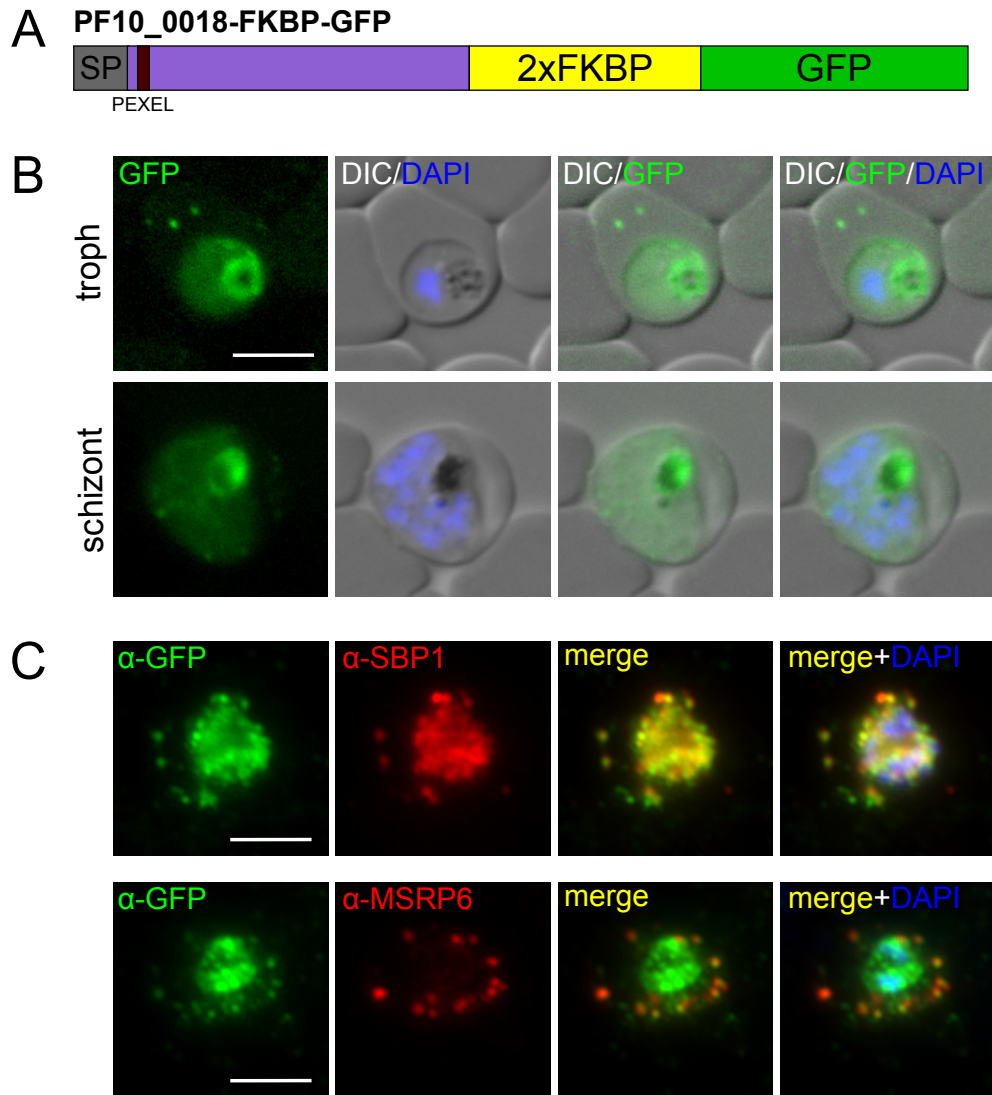
Figure 3.16.: Subcellular localization of PF10_0020-FKBP-GFP. A Schematic showing the protein features of PF10_0020 fused to 2xFKBP and GFP. (SP) signal peptide. **B** Live cell images of 3d7 parasites expressing PF10_0020-FKBP-GFP from the endogenous locus. Shown are trophozoite/early schizont and schizont stage parasites. Nuclei were stained with DAPI. (troph) trophozoite, (DIC) differential interference contrast. Scale bar: 5 μm. **C** IFA of acetone-fixed 3d7 parasites expressing PF10_0020-FKBP-GFP from the endogenous locus. Cells were stained with GFP-antibodies (green channel) and SBP1-antibodies (red channel) or GFP-antibodies (green channel) and MSRP6-antibodies (red channel), respectively. Nuclei were stained with DAPI. Scale bar: 5 μm.

PF10_0025 PF10_0025 is a protein of 631 aa and contains a a recessed SP and a PEXEL-motif (figure 3.17 A). It was reported to be transcribed in all blood stages, with a peak transcription in merozoites (2301 RPKM). The average transcription levels were comparably high (Le Roch et al., 2003), (table 3.3). PF10_0025 is homologous to PF10_0024 and PF10_0023. A BLASTp search identified homology to *Ehrlichia* tandem repeats, found in an immunodominant outer membrane protein of the obligate intracellular human pathogen *Ehrlichia chaffeensis*, gram-negative bacteria infecting monocytes.

PF10_0025-FKBP-GFP expressed from the endogenous locus in 3d7 parasites was detected in trophozoite and schizont stages, ring stage fluorescence was almost undetectable. The fusion protein localized predominantly to punctate structures inside the RBC, with some additional fluorescence detectable in the parasite cytoplasm and food vacuole. The subcellular localization was similar in trophozoite and schizont stages (figure 3.17 B). IFA analysis showed a co-localization of PF10_0025-FKBP-GFP with SBP1 and MSRP6 (figure 3.17 C). Together, these results indicate that PF10_0025 is a Maurer's cleft protein, expressed predominantly in trophozoite and schizont stage parasites.
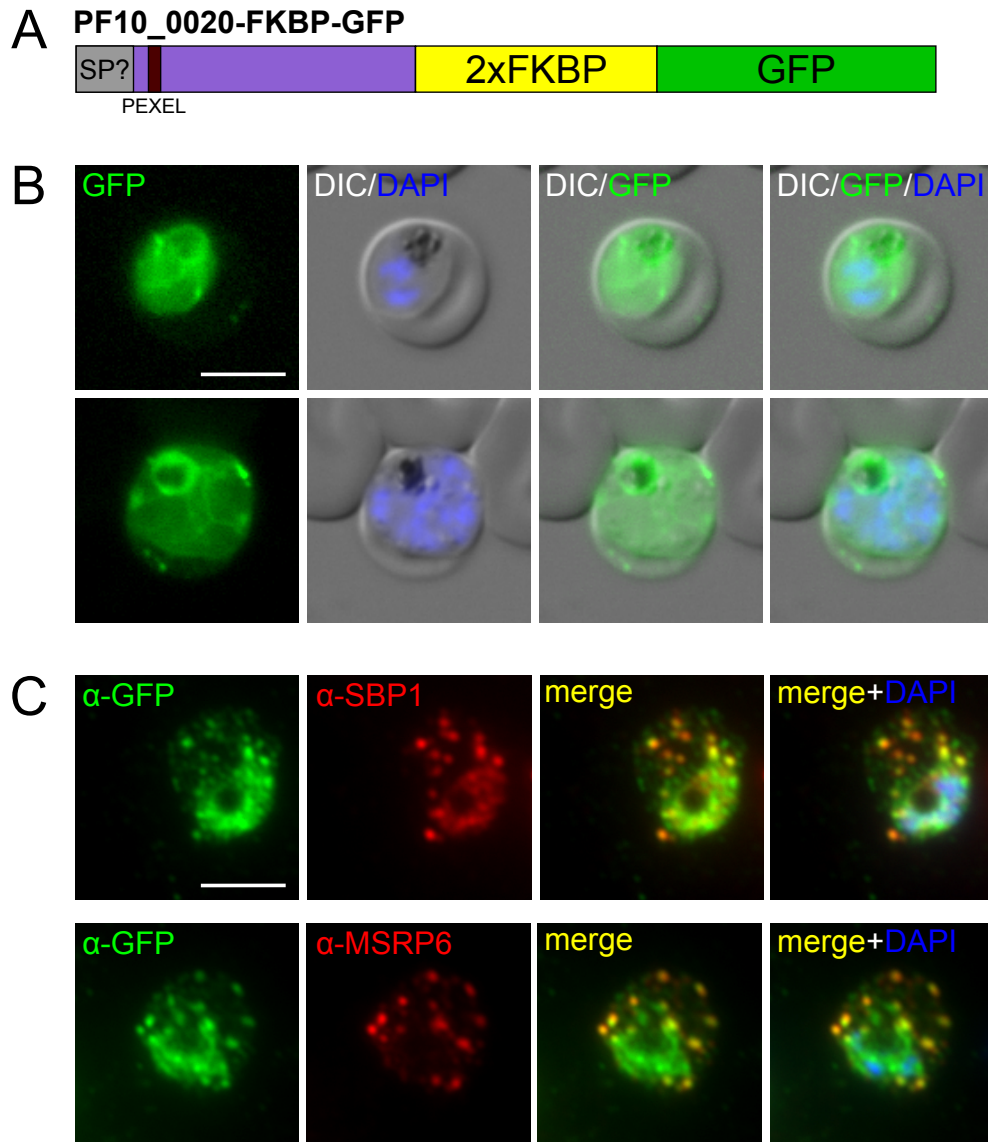
Figure 3.17.: Subcellular localization of PF10_0025-FKBP-GFP. A Schematic showing the protein features of PF10_0025 fused to 2xFKBP and GFP. (SP) signal peptide. **B** Live cell images of 3d7 parasites expressing PF10_0025-FKBP-GFP from the endogenous locus. Shown are trophozoite and schizont stage parasites. Nuclei were stained with DAPI. (troph) trophozoite, (DIC) differential interference contrast. Scale bar: 5 µm. **C** IFA of acetone-fixed 3d7 parasites expressing PF10_0025-FKBP-GFP from the endogenous locus. Cells were stained with GFP-antibodies (green channel) and SBP1-antibodies (red channel) or GFP-antibodies (green channel) and MSRP6-antibodies (red channel), respectively. Nuclei were stained with DAPI. Scale bar: 5 µm.

PFL0055c PFL0055c is a protein of 900 aa and contains a recessed SP and a PEXEL-motif (figure 3.18 A). The transcription was reported to peak in late ring stages and is comparably low (Le Roch et al., 2003), (table 3.3). PFL0055c is annotated as a RESA-like protein with PHIST and DnaJ domains and contains a PRESAN domain in the N-terminal part, a DnaJ domain with Hsp70 interaction sites, and a DnaJ-X domain in the C-terminal part of the protein (PlasmoDB). Kilili *et al.* also identified a MESA erythrocyte cytoskeleton-binding (MEC) domain within the N-terminal part of PFL0055c (Kilili and LaCount, 2011). PRESAN domains were reported to mediate interaction with the RBC cytoskeleton (Tarr et al., 2014). DnaJ domain containing proteins act as chaperones and can interact with Hsp70 heat shock proteins and stimulate their ATPase activity (Cheetham and Caplan, 1998). The exact function of DnaJ-X domains is not known.

In early trophozoites PFL0055c-FKBP-GFP expressed from the endogenous locus localized predominantly to the RBC periphery, with an additional bright focus inside the parasite, reminiscent of a golgi localization (figure 3.2.2.2 B, early troph). In trophozoites the intra-parasitic fluorescence was lost, and the protein showed a punctate staining inside the RBC in addition to the RBC peripheral staining (figure 3.18 B, troph). In schizont stage parasites the RBC peripheral staining was lost and the fusion protein predominantly localized to punctate structures within the RBC (figure 3.18 B, schizont). Often, one or more fluorescent foci were observed near the food vacuole (figure 3.18 B). In ring stage parasites no fluorescence was detectable. The results indicate a stage specific localization of PFL0055c, including the RBC periphery, a structure within the parasite cytoplasm and foci inside the RBC, reminiscent of Maurer's clefts.

A

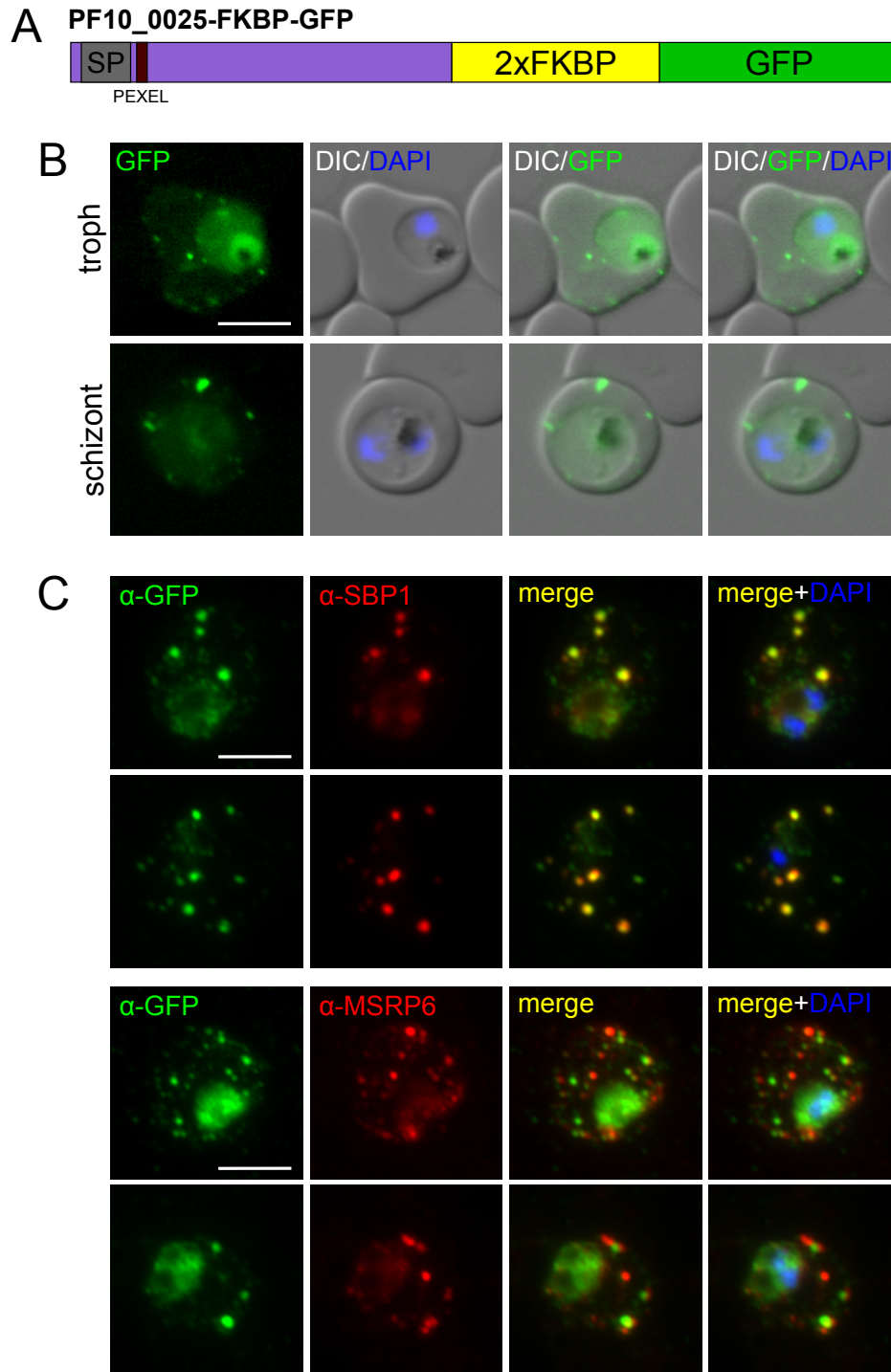**PFL0055c-FKBP-GFP**

| SP | | 2xFKBP | GFP |

PEXEL

B

Figure 3.18.: Subcellular localization of PFL0055c-FKBP-GFP. A Schematic showing the protein features of PFL0055c fused to 2xFKBP and GFP. (SP) signal peptide. **B** Live cell images of 3d7 parasites expressing PFL0055c-FKBP-GFP from the endogenous locus. Shown are trophozoite/early schizont and schizont stage parasites. Nuclei were stained with DAPI. (troph) trophozoite, (DIC) differential interference contrast. Scale bar: 5 μm.

PFE0050w   PFE0050w is a protein of 260 aa and contains a recessed SP and a PEXEL-motif (figure 3.19 A). The highest transcription levels were reported from early ring to late trophozoite stages with a peak in early trophozoites(Le Roch et al., 2003), (table 3.3). Similar to PFE0060w, this protein was identified in a MS based screen for RBC surface proteins, but was not independently localized (Florens et al., 2004). Other than that, no further information on PFE0050w is available and no homologies (except for an ortholog in *P. reichenowi*) to known proteins could be identified (BLASTp, PlasmoDB).

PFE0050w-FKBP-GFP, expressed from the endogenous locus, could be detected in all stages, with the fusion protein localizing to punctate structures within the RBC (figure 3.19 B). In some cells the foci had a heterogeneous distribution of fluorescence, with one bright focus surrounded by a more diffuse fluorescence (figure 3.19 B, third panel, arrowheads). Despite detection in the proteome of supposed surface proteins (Florens et al., 2004), no RBC surface localization was detected for this cell line. IFA showed a co-localization with SBP1, demonstrating that PFE0050w localizes to the Maurer's clefts (figure 3.20 A). PFE0050w also co-localized with MSRP6, in some cells however, PFE0050w showed additional staining surrounding or adjacent to the MSRP6 foci (figure 3.20 B), reminiscent of the diffuse staining in live parasites (figure 3.19 B, third panel, arrowheads). This phenotype was only observed in a small fraction of cells in the MSRP6 IFAs and not observed in the SBP1 IFAs, indicating that the phenotype might be stage specific (as SBP1 is predominantly expressed in earlier stages) or that it could be an artifact.

Together these results show that PFE0050w localizes to the Maurer's clefts in all investigated blood stages and that it co-localizes with MSRP6.
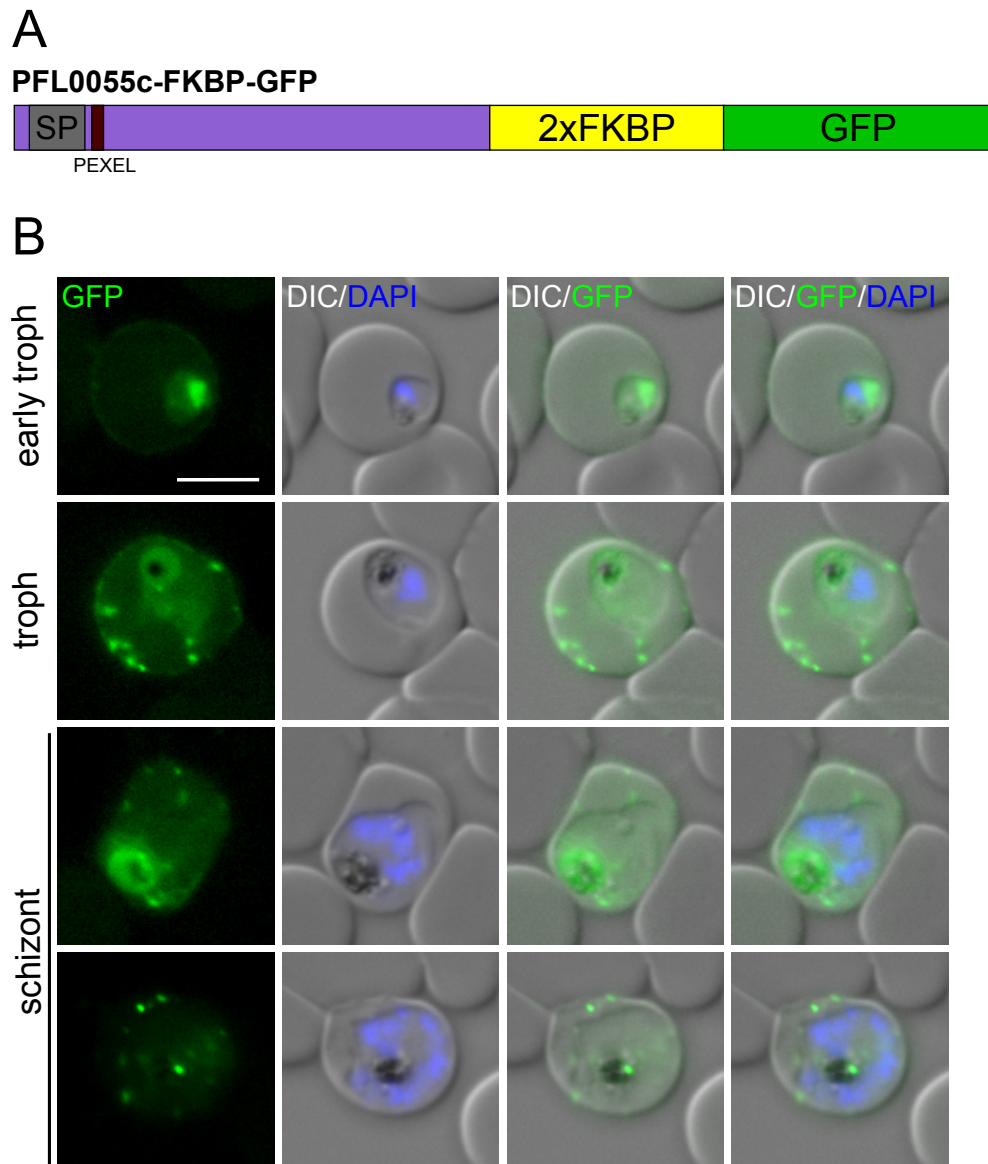
A

PFE0050w-FKBP-GFP

B

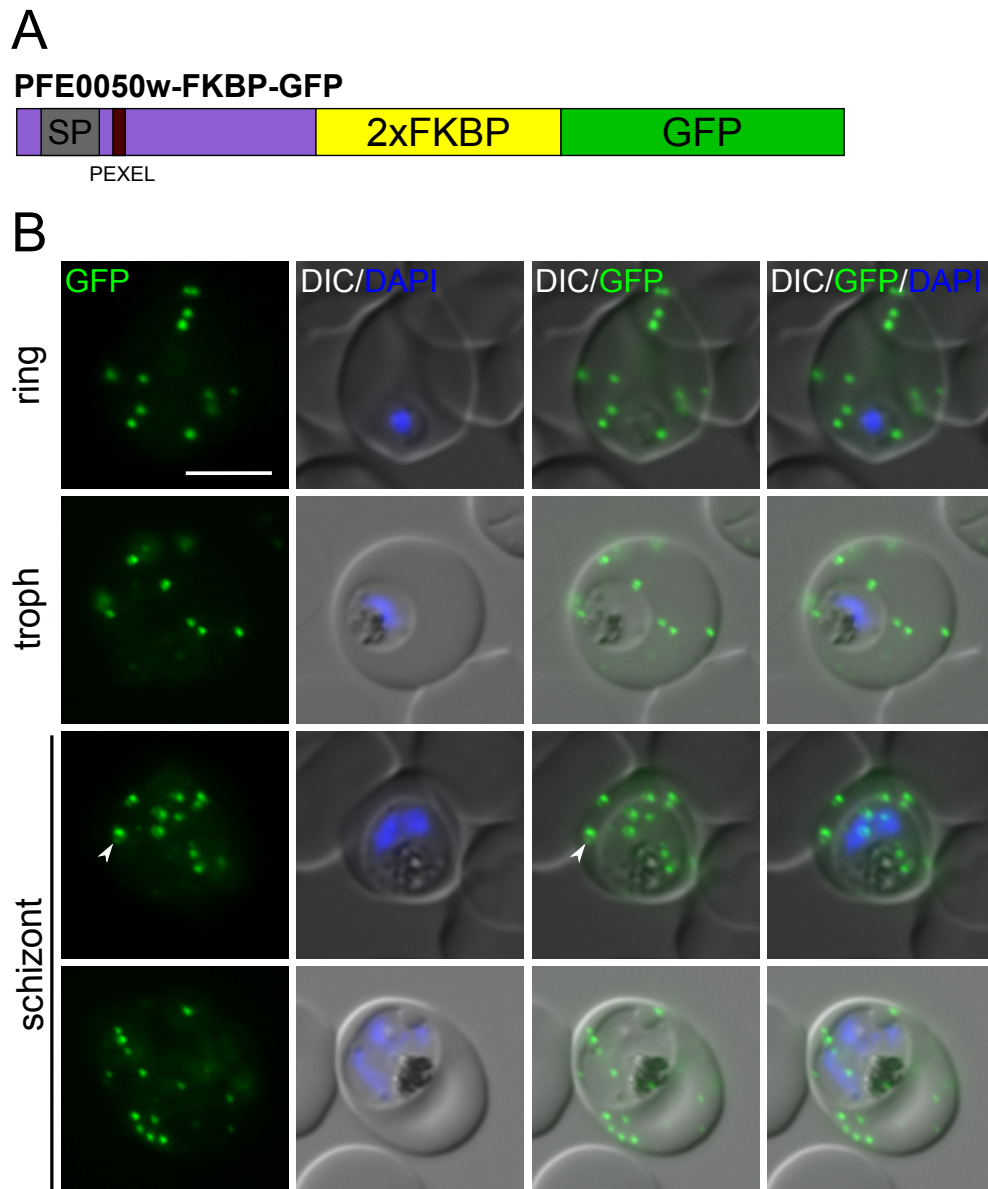**Figure 3.19.: Subcellular localization of PFE0050w-FKBP-GFP. A** Schematic showing the protein features of PFE0050w fused to 2xFKBP and GFP. (SP) signal peptide. **B** Live cell images of 3d7 parasites expressing PFE0050w-FKBP-GFP from the endogenous locus. Shown are ring, trophozoite and schizont stage parasites. Nuclei were stained with DAPI. (troph) trophozoite, (DIC) differential interference contrast. Scale bar: 5 μm.

Figure 3.20.: Subcellular localization of PFE0050w-FKBP-GFP by IFA. A IFA of acetone-fixed 3d7 parasites expressing PFE0050w-FKBP-GFP from the endogenous locus. Cells were stained with GFP-antibodies (green channel) and SBP1-antibodies (red channel). Nuclei were stained with DAPI. Scale bar: 5 μm. **B** IFA of acetone-fixed 3d7 parasites expressing PFE0050w-FKBP-GFP from the endogenous locus. Cells were stained with GFP-antibodies (green channel) and MSRP6-antibodies (red channel). Nuclei were stained with DAPI. Scale bar: 5 μm.

MAL7P1.170 MAL7P1.170 is a protein of 293 aa and contains a SP but no canonical PEXEL-motif (figure 3.21 A). The amino acid sequence RILSS is present within 20 aa downstream of the SP, resembling the RxL of the PEXEL-motif, but its functionality is unknown. MAL7P1.170 trancription levels were reported to peak in merozoites with a maximum transcription of 4244 RPKM, decreasing to 157 RPKM in late trophozoites (Le Roch et al., 2003), representing the highest transcription levels of all candidates investigated in this work (table 3.3). MAL7P1.170 is predicted to be expressed in two isoforms, differing from each other in only 2 amino acids (PlasmoDB). This difference might result in different mature N-termini, as the scores for the most likely cleavage site show a slight shift when comparing the two different isoforms (SignalP 3.0). MAL7P1.170 has no homologies to known proteins and its function and localization are unknown.

In ring stages the MAL7P1.170-FKBP-GFP fusion protein (expressed from the endogenous locus) showed a diverse localization. In some cells a single focus was present at the parasite periphery, sometimes at the tip of filopodia-like protrusions of amoeboid shaped

Figure 3.21.: Subcellular localization of MAL7P1.170-FKBP-GFP. A Schematic showing the protein features of MAL7P1.170 fused to 2xFKBP and GFP. (SP) signal peptide. **B** Live cell images of 3d7 parasites expressing MAL7P1.170-FKBP-GFP from the endogenous locus. Shown are ring, trophozoite and schizont stage parasites. Nuclei were stained with DAPI. (troph) trophozoite, (DIC) differential interference contrast. Scale bar: 5 μm.
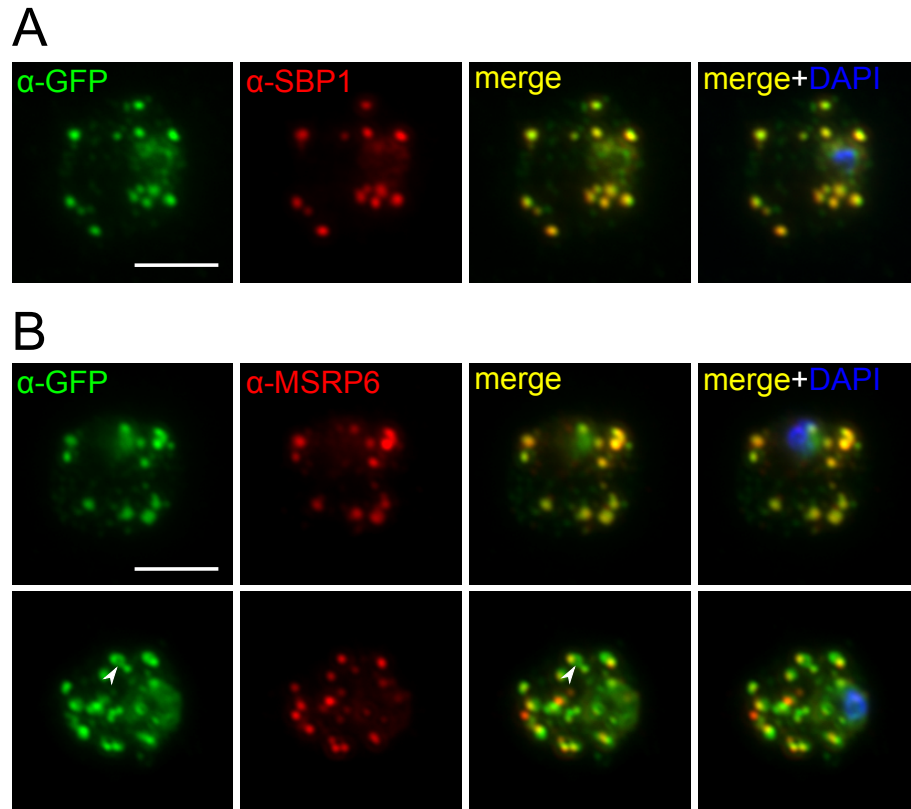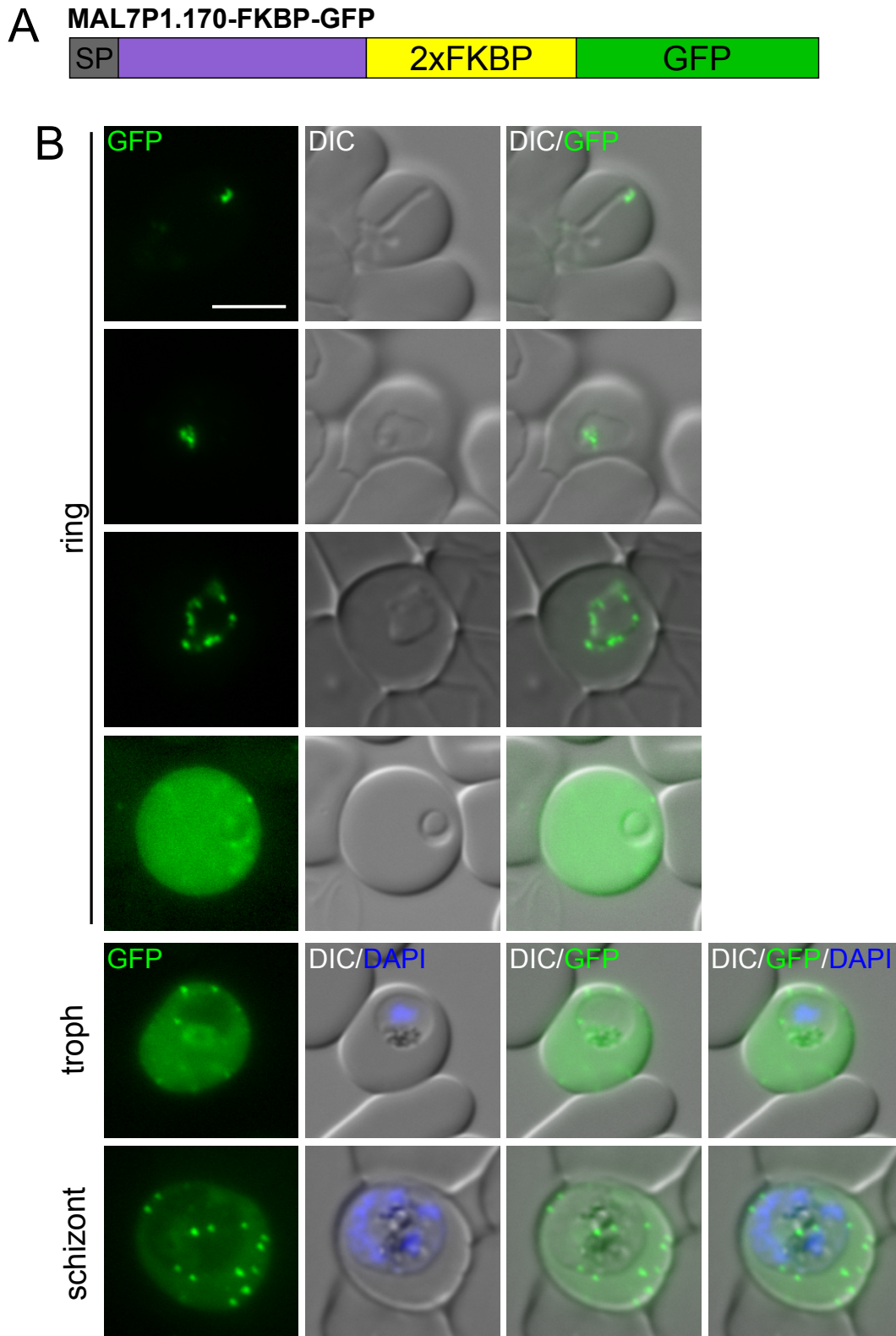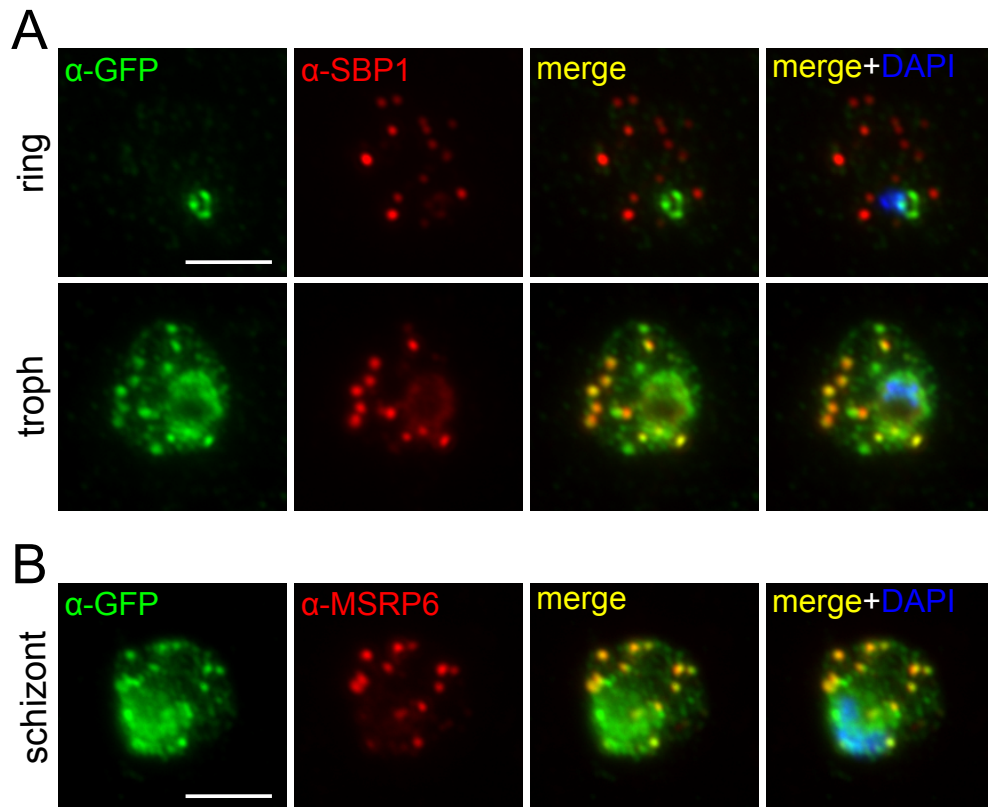
Figure 3.22.: Subcellular localization of MAL7P1.170 by IFA. A IFA of acetone-fixed 3d7 parasites expressing MAL7P1.170-FKBP-GFP from the endogenous locus. Cells were stained with GFP-antibodies (green channel) and SBP1-antibodies (red channel). Nuclei were stained with DAPI. Scale bar: 5 µm. **B** IFA of acetone fixed 3d7 parasites expressing MAL7P1.170-FKBP-GFP from the endogenous locus. Cells were stained with GFP-antibodies (green channel) and MSRP6-antibodies (red channel). Nuclei were stained with DAPI. Scale bar: 5 µm.

ring stages (figure 3.21 B, fist panel). Other cells exhibited a single spot of fluorescence at or near the cavity (figure 3.21 B, second panel), or fluorescent foci surrounding the entire parasite (figure 3.21 B, third panel). In a fraction of ring stage parasites the fusion protein was detected in the RBC cytosol, sometimes accumulating in foci (figure 3.21 B, fourth panel). In trophozoite and schizont stage parasites the protein localized to the RBC cytosol and to punctate structures within the RBC, with the soluble pool decreasing in late stages (figure 3.21 B, troph, schizont).

IFAs showed a co-localization of the MAL7P1.170 fusion protein with SBP1 in trophozoite, but not ring stages, where the protein was detected near the nucleus, resembling the localization in some of the live cells (figure 3.22 A). MAL7P1.170 co-localized with MSRP6 in trophozoite and schizont stages (figure 3.22, B). In the IFAs no soluble pool of MAL7P1.170 was detected, probably caused by the release of cytoplasmic content during acetone fixation. In summary these results show that MAL7P1.170 exhibits a differential localization in ring stage parasites, and a Maurer's cleft localization in trophozoites and

schizonts

PF11_0511 PF11_0511 is a protein of 209 aa and contains a SP and a PEXEL-motif
(figure 3.23 A). PF11_0511 was reported to be mostly transcribed from early ring to
late trophozoite stages, with a peak in early schizonts (938 RPKM) (Le Roch et al.,
2003), (table 3.3). The protein contains no conserved domains but shows homology to
two other exported *P. falciparum* proteins, PFB0926c and PFB0970c, whose functions
are also unknown (based on BLASTp analysis and PlasmoDB annotation).
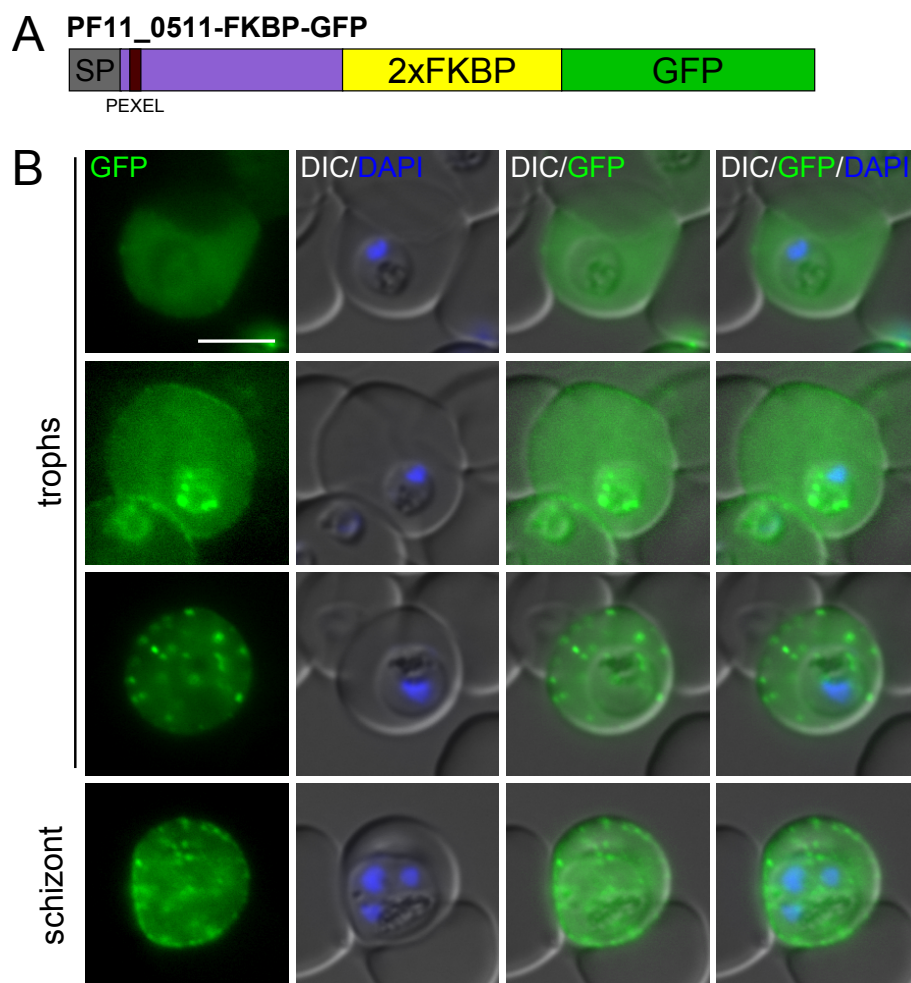
Figure 3.23.: Subcellular localization of PF11_0511-FKBP-GFP. A Schematic showing
the protein features of PF11_0511 fused to 2xFKBP and GFP. (SP) signal peptide. **B** Live cell
images of 3d7 parasites expressing PF11_0511-FKBP-GFP from the endogenous locus. Shown
are trophozoites and schizonts. Nuclei were stained with DAPI. (troph) trophozoite. **C** Live
cell images of 3d7 parasites expressing PF11_0511-FKBP-GFP from the endogenous locus and
MSRP6-mCherry episomally (*crt*-promoter). **D** Live cell images of 3d7 parasites expressing
PF11_0511-FKBP-GFP from the endogenous locus and empisomally expressed (*crt*-promoter)
MSRP6 SP+cd-mCherry. (DIC) differential interference contrast. Scale bars: 5 μm.

When endogenously expressed in 3d7 parasites the PF11_0511-FKBP-GFP fusion protein localized to the RBC cytosol with additional punctate staining within the RBC in trophozoites and schizonts. Some cells also exhibited a RBC peripheral staining, especially in young stages (figure 3.23 B). In ring stages fluorescence was hardly detectable. For PF11_0511-FKBP-GFP double transgenic cell lines co-expressing MSRP6-mCherry and MSRP6 Sp+cd-mCherry were obtained. PF11_0511-FKBP-GFP and MSRP6-mCherry co-localized in punctate structures within the RBC, demonstrating a Maurer's clefts localization for PF11_0511-FKBP-GFP. These cells usually had a seemingly reduced RBC cytosolic pool of PF11_0511-FKBP-GFP, when compared to cells expressing the GFP fusion protein alone, potentially caused by overexpression of MSRP6-mCherry (figure 3.24 A, compare to B). When co-expressed with MSRP6 SP+cd-mCherry, a construct containing only part cd of MSRP6, both proteins co-localized at the Maurer's clefts, with a fraction of both fusion proteins also present in the RBC cytosol, resembling the localization of PF11_0511-FKBP-GFP alone (figure 3.24 B). These observations were quantified by plotting the intensity profiles of the respective GFP and mCherry fluorescence using ImageJ (see appendix C). This showed that the background fluorescence was similar to the cytosolic GFP and mCherry fluorescence in the cell line co-expressing MSRP6-mCherry, indicating the lack of a cytosolic pool (figure 3.24 A). In contrast, the fluorescence intensity in the cytosol of cells co-expressing MSRP6 SP+cd-mCherry was higher than the background fluorescence, demonstrating the presence of a cytosolic pool of the fusion proteins (figure 3.24 B). The images and plots shown here are representative of all images acquired.

In IFAs PF11_0511-FKBP-GFP co-localized with both SBP1 and MSRP6, confirming the Maurer's cleft localization of this candidate (figure 3.25).

In summary, these results show that PF11_0511 localizes to the Maurer's clefts, where it co-localizes with MSRP6 and SBP1. Additionally, the protein could be detected in the RBC cytosol and in some cells in the RBC periphery. The overexpression of full length MSRP6 tagged with mCherry seemed to reduce the cytosolic pool of PF11_0511-FKBP-GFP.
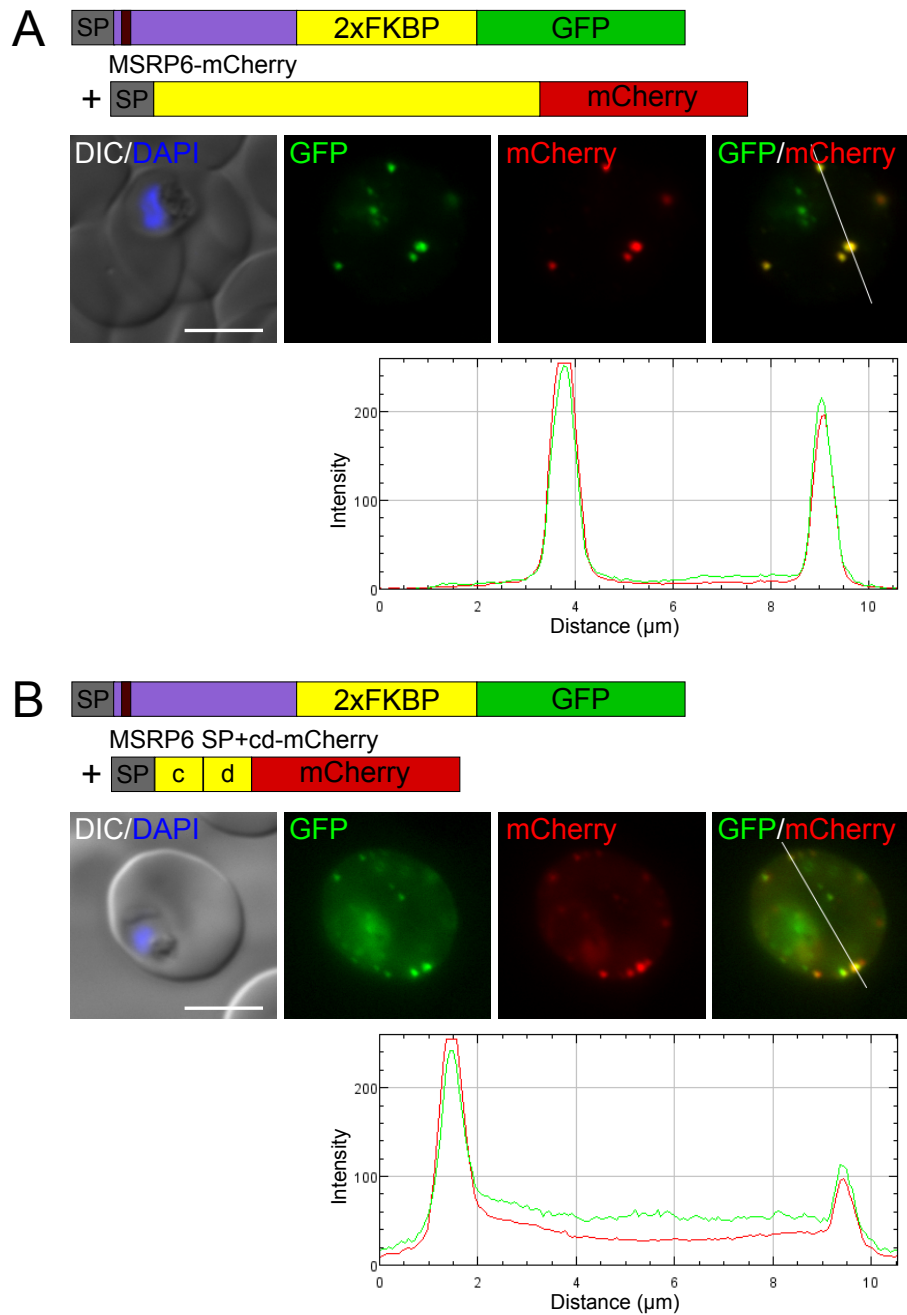
Figure 3.24.: Co-localization of PF11_0511-FKBP-GFP and mCherry tagged MSRP6 constructs. A Live cell images of 3d7 parasites expressing PF11_0511-FKBP-GFP from the endogenous locus and MSRP6-mCherry episomally (*crt*-promoter). The graphs show the intensity profiles of PF11_0511-FKBP-GFP (green line) and MSRP6-mCherry (red line) along the white line overlaying the merged image. **B** Live cell images of 3d7 parasites expressing PF11_0511-FKBP-GFP from the endogenous locus and empisomally expressed (*crt*-promoter) MSRP6 SP+cd-mCherry. The graphs show the intensity profiles of PF11_0511-FKBP-GFP (green line) and MSRP6 SP+cd-mCherry (red line) along the white line overlaying the merged image. (DIC) differential interference contrast. Scale bars: 5 μm.
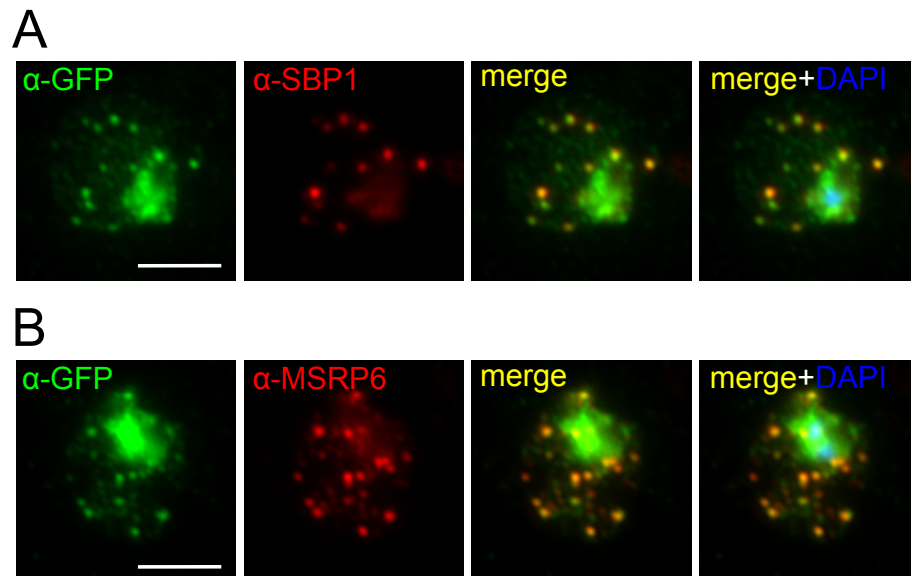
Figure 3.25.: Subcellular localization of PF11_0511 by IFA. A IFA of acetone-fixed 3d7 parasites expressing PF11_0511-FKBP-GFP from the endogenous locus. Cells were stained with GFP-antibodies (green channel) and SBP1-antibodies (red channel). Nuclei were stained with DAPI. Scale bar: 5 μm. **B** IFA of acetone-fixed 3d7 parasites expressing PF11_0511-FKBP-GFP from the endogenous locus. Cells were stained with GFP-antibodies (green channel) and MSRP6-antibodies (red channel). Nuclei were stained with DAPI. Scale bar: 5 μm.

PFI0086w   PFI0086w is a protein of 269 aa and contains a recessed SP followed by a PEXEL-motif (figure 3.26 A). No transcription data is available from Le Roch *et al.* for the corresponding gene. Transcription data from Kafsack *et al.* show that the gene has its peak transcription in trophozoites (Kafsack et al., 2012). PFI0086w contains a conserved domain of unknown function (Plasmo_dom_1) within its C-terminal part, which was found in 8 *P. falciparum* proteins (PlasmoDB). No further information on the function or localization of this protein is available.

PFI0086w-FKBP-GFP, expressed from the endogenous locus in 3d7 parasites showed a punctate localization with an additional soluble pool within the RBC in trophozoites and schizonts (figure 3.26 B). No GFP fluorescence was detected in ring stage parasites.

For PFI0086w-FKBP-GFP a double transgenic cell line co-expressing MSRP6 mCherry was obtained. PFI0086w-FKBP-GFP co-localized with MSRP6-mCherry, demonstrating that PFI0086w is localized at the Maurer's clefts (figure 3.26 C). Similarly a co-localization with MSRP6 SP+cd-mCherry was observed (figure 3.26 D). In contrast to PF11_0511-FKBP no decrease of the soluble protein pool was detected upon overexpression of MSRP6-mCherry.
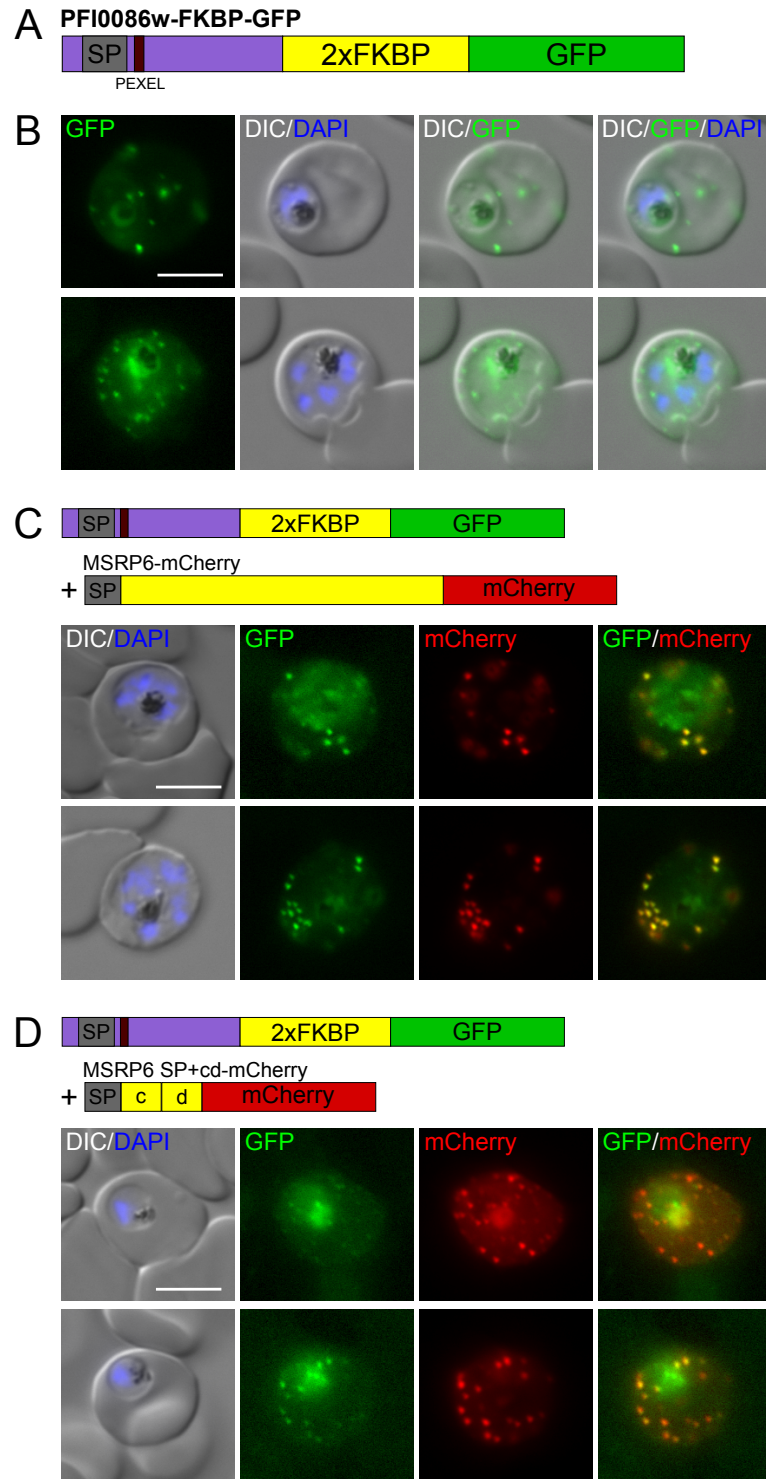
Figure 3.26.: Subcellular localization of PFI0086w-FKBP-GFP. A Schematic showing the protein features of PFI0086w fused to 2xFKBP and GFP. (SP) signal peptide .**B** Live cell images of 3d7 parasites expressing PFI0086w-FKBP-GFP from the endogenous locus. Shown are trophozoite and schizont stage parasites. Nuclei were stained with DAPI. (troph) trophozoite. **C** Live cell images of 3d7 parasites expressing PFI0086w-FKBP-GFP from the endogenous locus and episomally expressed (*crt*-promoter) MSRP6-mCherry. **D** Live cell images of 3d7 parasites expressing PFI0086w-FKBP-GFP from the endogenous locus and and episomally expressed (*crt*-promoter) MSRP6 SP+cd-mCherry. (DIC) differential interference contrast. Scale bars: 5 µm.

3.2.2.3. CoIPs show a specific interaction of several candidates with MSRP6

Ten of the 11 investigated potential MSRP6 interaction partners showed a Maurer's cleft localization and co-localized with MSRP6. For five of these proteins co-immunoprecipitation (CoIP) analyses were performed to test an interaction with MSRP6. The selected candidates were the proteins for which integration cell lines were first obtained. Due to time restrictions, CoIP experiments for the other proteins were not conducted.

For the CoIPs the GFP-tagged proteins were purified from total parasite extracts using α-GFP agarose beads and co-purification of MSRP6 was checked by Western blotting. Protein eluted from the beads was compared with total input, supernatant post-binding and the final wash and analyzed with GFP-, MSRP6- and SBP1-antibodies (figure 3.27).

The PFE0060w-FKBP-GFP fusion protein was detected with a size just below 130 kDa, which is larger than the expected size for the fusion protein (105 kDa). Similarly, the detected bands for PFE0050w-FKBP-GFP (detected: 100 kDa, calculated: 87 kDa) and MAL7P1.170-FKBP-GFP (detected: 100 kDa, calculated: 88 kDa) were larger than expected, which however is not unusual for *P. falciparum* proteins (see e.g. Hawthorne et al., 2004). Both PF11_0511-FKBP-GFP and PFI0086w-FKBP-GFP were detected at around 90 kDa and had calculated molecular weights of 82 kDa and 89 kDa, respectively.

For all candidates, the GFP signal of the fusion proteins was detected in the input, supernatant (post-binding) and eluate fractions, showing that they were captured by the α-GFP agarose beads and could be efficiently eluted (figure 3.27). MSRP6 was present in the input, supernatant (post-binding) and eluate fractions of all candidates, indicating that all candidates interacted with MSRP6 (figure 3.27). In contrast, the Maurer's clefts protein SBP1 was not detected in any of the eluate fractions (figure 3.27), which suggests that the interaction between MSRP6 and the tested candidates is specific.
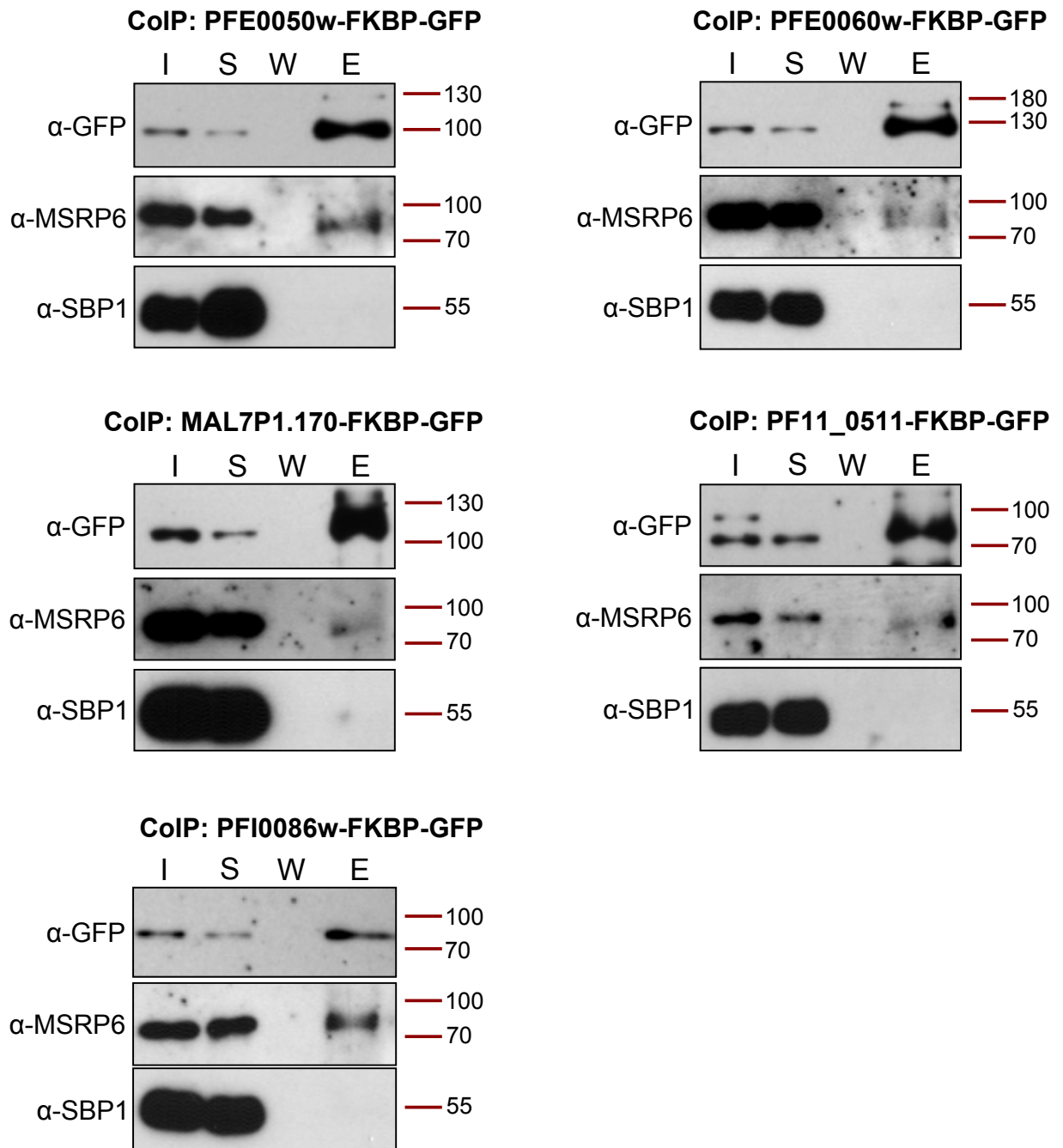
Figure 3.27.: CoIPs of five potential MSRP6 interaction candiates. CoIPs were performed using anti-GFP agarose beads. Shown are Western blots of the (I) input, (S) supernatant (post-binding), (W) final wash and (E) eluate fractions, probed with GFP-, MSRP6- and SBP1-antibodies. (kDa) kilodaltons.

4. Discussion

During asexual development *Plasmodium* parasites develop within RBCs, protecting them from the host immune system. However, this unique niche also poses challenges for the parasite. For their survival and virulence the parasites have to modify the host RBC, introducing host cell modifications that function in protein trafficking, nutrient acquisition and immune evasion (Maier et al., 2009; Desai, 2014; Maier et al., 2008; Crabb et al., 2010). The generation of these modifications requires the export of proteins beyond the parasitophorous vacuole membrane (PVM) to their final destinations, including the Maurer's clefts and RBC membrane. Most known exported proteins contain a PEXEL-motif, a five amio acid sequence ~20 amino acids downstream of a SP, that is recognized and cleaved inside the endoplasmic reticulum and marks proteins for export (Marti et al., 2004; Hiller et al., 2004; Chang et al., 2008; Boddey et al., 2010; Russo et al., 2010). PEXEL-negative exported proteins (PNEPs) do not contain a recognizable motif, although for all investigated PNEPs the N-terminus was shown to be essential for export (Haase et al., 2009; Saridaki et al., 2009; Pachlatko et al., 2010; Grüring et al., 2012; Heiber et al., 2013). Unlike PEXEL-proteins, the set of initially known PNEPs, here referred to as "classical" PNEPs, did not contain a SP, but entry into the secretory pathway was mediated by a transmembrane domain (TMD). Additionally, the TMD also played a role in export independently of its capacity for secretory pathway entry, and could not be replaced by a non-PNEP TMD (Grüring et al., 2012). Recently, other types of PNEPs were identified (referred to as "novel PNEPs"), either containing only a SP or a SP and a TMD (Heiber et al., 2013; Külzer et al., 2012). Hsp70-x is one of the novel PNEPs containing a SP, for which the 8 amino acids of the mature N-terminus were shown to mediate export, although the efficiency was rather low (Külzer et al., 2012). However, it is not known if other novel PNEPs containing a SP have a similar N-terminal export region and how PNEPs with a SP and a TMD are exported.

Once inside the host cell, proteins need to reach their final destinations. Evidence suggests that both transmembrane and soluble proteins are trafficked in a non-vesicular manner (Papakrivos et al., 2005; Grüring et al., 2011, 2012). Transmembrane proteins were detected in structures called J-dots, containing a chaperone/co-chaperone complex, which might deliver them to the Maurer's clefts (Külzer et al., 2010, 2012). For some

transmembrane proteins the Maurer's clefts are only an interstation on their way to the RBC membrane, which they probably reach via vesicles originating from the Maurer's clefts (Hanssen et al., 2008, 2010; Pachlatko et al., 2010; Cyrklaff et al., 2011). Soluble proteins can probably reach their target structures by diffusion and binding to interaction partners (Tarr et al., 2014; Proellocks et al., 2014; Spielmann and Gilberger, 2015), or by co-trafficking with interaction partners (Oberli et al., 2014).

4.1. Export requirements for novel PNEPs

In this work the novel PNEPs PF08_0004, PFL0065w, PF08_0005, PFB0115w and MSRP6 were investigated for their export requirements. PF08_0004 and PFL0065w both contain a SP and a TMD, while the other tested PNEPs only contain a SP.

4.1.1. PNEPs with a SP and TMD

Interestingly, for PF08_0004 the SP was found to be dispensable for export, although it was sufficient but not necessary to mediate entry into the secretory pathway independent of the TMD. It is puzzling that the protein contains a SP if this part of the protein is seemingly unimportant. However, apart from just mediating secretory pathway entry, signal peptides can also have influence on the timing of ER translocation by influencing SP cleavage, or have an autonomous function after cleavage and release (Hegde and Bernstein, 2006). In this regard, it would be interesting to compare the export timing and efficiency of PF08_0004 with and without a SP, preferably of the endogenously modified protein.

Similar to REX2 (Haase et al., 2009; Grüring et al., 2012), replacement of the PF08_0004 TMD with a non-PNEP TMD prevented export, demonstrating that the TMD contains export relevant information. However, replacing the PF08_0004 TMD with TMDs of other PNEPs also resulted in no export, or in slight export when the TMD flanking regions were also replaced. This indicates, that the TMD is only functional for protein export in combination with the flanking regions, potentially exhibiting a specific secondary structure or topology. The results further show, that restoring the C-terminal part of the PF08_0004 TMD after replacement with the mTRAP TMD, could re-establish a small amount of export, suggesting that the C-terminal part of the TMD is more relevant for export. To validate this hypothesis, a construct which contains a restored N-terminal TMD part would have to be expressed and export levels compared to the described construct. However, for the PNEP REX2 it was shown that the N-terminal half of the TMD is more important for export than the C-terminal half (Grüring, 2011a), which could be explained by the possible different membrane topology of PF08_0004.

Besides the SP, the only part of PF08_0004 dispensable for export was part 2, while deletion of the other parts completely blocked export. The modifications of parts 3 and 4 could have had an influence on the TMD, caused by their close proximity to this domain, and be an explanation for the observed phenotypes. However, this does not explain the abolished export in the case of the deletion of part 1, indicating that part 1 contains export information independent of the TMD, similar to other PNEPs, where the N-terminus is necessary for export. The potential role of the N-terminus of PF08_0004 is further supported by the fact that an N-terminal proline stretch inhibited export, similar to prolines contained within the N-termini of artificial reporter constructs (Ullrich, 2016). Interestingly however, membrane topology prediction indicated that the N-terminus of PF08_0004 may face the cytoplasm, contrary to REX2, where the N-terminus faces "outside" (Grüring et al., 2012). This could have consequences for the localization of the export region, which, in the case of REX2 would be present inside the ER, and implies that the export region of PF08_0004 could be localized at the C-terminus. This does however not explain the export block by N-terminal prolines and the fact that the REX2 amino acids 1-20 fused to the PF08_0004 N-terminus can promote export. These data would rather suggest that the topology prediction is incorrect (or the protein shows mixed topologies, leading to a partial export). It is also possible that mechanisms entirely different from the trafficking of conventional PNEPs contribute to the export of PF08_0004. For instance the export of PF08_0004 could require interaction partners, that mediate its export, but only recognize PF08_0004 in its properly folded full length state. In this scenario, small changes to PF08_0004 could abolish its structure and binding, hence preventing export after small changes to the sequence without actually modifying a real trafficking motif per se. Further experiments would be necessary to test the roles of the N- and C-termini in export of PF08_0004 and to evaluate potential alternative explanations for the strong export phenotypes caused by all tested modifications.

Similar to PF08_0004, the export mediating region could also not be narrowed down for PFL0065w. Any modification to this protein abolished protein export, indicating that the whole secondary structure of the protein might have to be present in an unaltered state to facilitate export. As this was similar to the situation in PF08_0004, this might be a common property of the PNEPs with a SP and a TMD. Few such proteins are known so far. Based on the data in this thesis the trafficking of these proteins seems to depend on a delicate balance of all protein domains in these proteins. The scarcity of this type of PNEP might reflect the limited sequence space and evolutionary contraints imposed by the requirement to maintain their trafficking. It should however also be noted, that for PFL0065w the SP and TMD were not tested, so it is unclear if these domains are equally important as in PF08_0004. It is also somewhat surprising that the SP in PF08_0004 is

not essential, which would suggest that these PNEPs could function if they had a domain structure resembling that of conventional PNEPs. Further data is required to understand why different PNEPs have different domain structures and how this relates to their export and function.

While folding so far was not implicated in the export of proteins in *P. falciparum*, an export motif at least in part based on folding was reported in *P. yoelii*. This semi-conserved export motif was described to span the SP in PYST proteins and the TMD in YIR proteins. This motif consisted of several conserved amino acids and secondary structure requirements (Siau et al., 2014). No similar motif has been identified in *P. falciparum*, but the study highlights the possibility that the secondary structure might play an important role in export and that export motifs might be contained within the SP or TMD. However, the SP is already cleaved during translocation into the ER, which would require exported proteins to be already recognized during this step. Plasmepsin V was reported to recognize the PEXEL-motif, before the signal peptidase cleaves off the SP (Boddey et al., 2010), indicating that exported proteins can in principle be recognized during ER translocation. All the SPs so far tested in *P. falciparum* did however not have an influence on protein export and are interchangeable with SPs from non-exported proteins. To test structural requirements for protein export, secondary structure prediction of PNEPs could be performed or the secondary structure determined experimentally, e.g. by circular dichroism (CD) spectroscopy, nuclear magnetic resonance (NMR) spectroscopy or X-ray crystallography.

PF08_0004 is highly transcribed in *P. falciparum* blood stages with a peak transcription of 2934 RPKM in merozoites (Le Roch et al., 2003). It contains a circumsporozoite-related antigen (CRA) domain, also found in the PVM-resident protein EXP1. EXP1 is a potentially essential transmembrane protein (Maier et al., 2008) present as oligomers inside the PVM (Spielmann et al., 2006) and was reported to be a glutathione-S-transferase, implicated in chloroquine resistance (Lisewski et al., 2014). In this regard it is interesting that PF08_0004 might have a dual localization in the PVM and Maurer's clefts (Heiber et al., 2013). It can, however also not be excluded that the PVM-localization is caused by the GFP-tag. The endogenous localization of this protein would have to be confirmed by specific antibodies or a smaller tag, e.g. a myc-tag, preferably introduced into the endogenous locus.

PFL0065w only has a peak transcription of 55 RPKM in blood stages and was reported to be expressed in sporozoites and in liver stages and thus named liver stage associated protein 1 (LSAP1) (Le Roch et al., 2003; Siau et al., 2008). The actual PFL0065w protein expression in blood stages would have to be tested with specific antibodies or by attempting to generate a GFP knock-in cell line, to evaluate its relevance in these stages.

For this protein, no conserved domains or sequence homologies could be identified and its function remains unknown.

4.1.2. PNEPs with a SP

The results in this thesis showed that the mature N-terminus (after SP cleavage) of PF08_0005 is both necessary and sufficient for protein export. The minimal sequence required for export could be narrowed down to the 25 N-terminal amino acids, which however could not mediate complete export of GFP. Further experiments are required to test, if incomplete export was due to the GFP tag being situated too close to the export region, or if the downstream sequence contains information contributing to export. Similarly, the N-terminal 50 amino acids (after SP cleavage) of PFB0115w were sufficient for export of this PNEP. The results from PF08_0005 implicate, that this region could also be narrowed down to a smaller region, which would require the generation of further minimal constructs. Overall, these data indicate that this presence of an N-terminal export domain is a common theme in all PNEPs (Haase et al., 2009; Saridaki et al., 2009; Pachlatko et al., 2010; Grüring et al., 2012; Heiber et al., 2013), even of PNEPs in the rodent malaria parasite *P. berghei* (De Niz et al., 2016), apart from the two cases with a SP and a TMD discussed above. While conventional PNEPs also require a fitting TMD (Saridaki et al., 2009; Grüring et al., 2012), the N-terminal domain (including the SP) in soluble PNEPs is not only necessary but also sufficient for export (this work, and Külzer et al., 2012). A comparison between the N-terminal sequences of PF08_0005, PFB0115w and Hsp70-x (Külzer et al., 2012) revealed no consensus sequence, however (alignment by ClustalΩ), implying that the secondary structure or other unknown factors might play a role.

PF08_0005 is only minimally transcribed in blood stages, with a maximum transcription value of 16 RPKM in merozoites (Le Roch et al., 2003). It was shown to be expressed on the sporozoite surface and play a role in the invasion of hepatocytes, subsequently named sporozoite invasion-associated protein 2 (SIAP2) (Siau et al., 2008). Hence, the relevance of this protein for the *P. falciparum* blood stages is unclear. To test if PF08_0005 is also expressed in blood stages specific antibodies or a knock-in cell line would be required.

PFB0115w is expressed in blood stages, demonstrated by a knock-in cell line (Reichard, 2015). The C-terminus of this protein contains a Pfg27 domain, found in proteins essential for gametocytogenesis (PlasmoDB), (Sharma et al., 2003). As a targeted gene disruption (TGD) cell line of PFB0115w (amino acids 1-414) is already existent, a potential role of this protein in gametocytogenesis could easily be tested. However, this already indicates that the protein is not essential for blood stages. The full length protein as well as the

truncated version both localized to the RBC periphery (Reichard, 2015). The minimal construct generated in this work had a RBC cytosolic localization, which indicates that the sequence responsible for the RBC peripheral localization is located between amino acids 77 and 414. The fact that the truncated protein is still bound to the RBC periphery might however indicate that this disrupted protein is still functional and nevertheless the protein could still be essential for blood stages.

Interestingly, both soluble PNEPs and the PNEP PF08_0004 are predicted to contain an apicoplast targeting sequence (transit peptide) (PlasmoAP, 4 of 5 tests positive). As these proteins do not show an apicoplast localization, this might be an indication for a relatedness between the transit peptide and the PNEP export sequence, at least in these proteins. However, PlasmoDB/PlasmoAP predicts 520 proteins to be targeted to the apicoplast, among them 46 proteins containing a PEXEL-motif and several proteins with other validated subcellular localizations, e.g. rhoptries or inner membrane complex, which indicates that either the prediction tool is inaccurate or that the targeting sequences for the recruitment to several target locations have common features recognized by the transit peptide prediction algorithm.

The N- and C-terminus of MSRP6 were found to both independently mediate export. The N-terminal export sequence could be narrowed down to amino acids 23-47 using an export reporter construct. In this regard MSRP6 is similar to the other two tested soluble PNEPs and the previously reported PNEP of this type (Külzer et al., 2012). The C-terminus (part cd) mediates both Maurer's cleft localization and export of this protein. The export might be facilitated by different mechanisms. On the one hand cd might contain a cryptic export sequence that is recognized by a part of the export machinery. This is however unlikely, as export domains usually seem to be present at the very N-terminus, and constructs containing cd at the C-terminus (lacking the N-terminal export domain) are also exported. On the other hand, export might be facilitated by an interaction of cd with another exported protein, leading to co-export of MSRP6. An important step for elucidating the export of MSRP6 cd is the identification of the interaction partner, potentially facilitating co-export, which is discussed in the next section (4.2).

4.2. Potential MSRP6 interaction candidates

In this work BioID was used to identify MSRP6 cd specific interaction partners. The use of specific controls facilitated the identification of proteins by quantitative mass spectrometry. Analysis of the significant hits revealed that almost all of these proteins are predicted to be exported, which indicates the validity of this method. For 5 of 11 chosen candidates an interaction with MSRP6 was confirmed by CoIPs. Further experiments

will be necessary to test a potential MSRP6 interaction for the remaining six candidates. Of the eleven candidates only one (PFC0070c) did not show any export, but localized to distinct foci within the parasite, although the protein contains a predicted SP and PEXEL-motif. Either one of these features is not functional, or protein export might have been be blocked by the C-terminal FKBP-GFP tag which is situtated close to the predicted TMD, potentially inhibiting correct membrane insertion into the ER membrane. This was observed previously with another PNEP with a TMD close to the proteins' C-terminus (Heiber et al., 2013). To test whether this is the case for PFC0070c, a smaller tag could be introduced (e.g. a myc tag, as previously used for such a situation (Heiber et al., 2013)) or the endogenous localization of this protein could be examined by using specific antibodies. If PFC0070c-FKBP-GFP indeed localized erroneously due to the tag, the protein could not be essential for blood stages, as otherwise the genomic integration would not have been obtained.

4.2.1. An MSRP6 protein complex at the Maurer's clefts?

The remaining ten candidates all localized to the Maurer's clefts and somewhat surprisingly for all five of these proteins that were tested an interaction with MSRP6 was confirmed. Interestingly, despite their localization at the membranous Maurer's clefts, 8 of these 10 candidates did not possess a TMD, indicating that biotinylation was specific for Maurer's clefts proteins interacting with or in close proximity of MSRP6 cd and that most of them are peripherally attached to the Maurer's clefts. In agreement with these results, previous results already indicated that MSRP6 might be present within a protein complex attached peripherally to the Maurer's clefts (Heiber et al., 2013). Recently, Rug *et al.* identified another potential protein complex at the Maurer's clefts, which includes PTP1, SBP1, and PFE0060w (referred to as PTP1-complex) (Rug et al., 2014). Interestingly, PFE0060w was also identified as an MSRP6 cd interaction partner in this work. SBP1, although not tested for its interaction with MSRP6 here, showed no interaction with any of the tested candidates, but was significantly enriched in the BioID experiments (both Rex3cd over Rex3 and Rex3cd over Stevor, with log2 ratios of 1.92/2.38 and 3.87/3.41 for Rex3cd over Rex3, and 1.15/0.35 and 1.83/1.34 for Rex3cd over Stevor). Two other members of the proposed PTP1-complex (PFE1600w and PF13_0076), identified by Rug *et al.* were not identified in the BioID experiments in this work and one (PFA0670c) was not a significantly enriched MSRP6 cd interaction hit. The partial overlap of proteins present in the PTP1-complex and the potential protein complex identified in this work (referred to as MSRP6-complex), could be explained by the high abundance of SBP1 and PFE0060w at the Maurer's clefts and subsequent unspecific co-precipitation with other Maurer's cleft proteins. Another possibility is that these proteins both interact with com-

ponents of the PTP1-complex and MSRP6-complex. A PTP1 knock-out had deleterious effects on Maurer's cleft architecture, which was attributed to aberrant actin filaments, and also negatively affected the trafficking of *Pf*EMP1 and STEVOR to the Maurer's clefts (Rug et al., 2014). Interestingly, PFE0060w, a proposed PTP1-complex member, was shown to have no effect on *Pf*EMP1 trafficking (Maier et al., 2008). In contrast, previous studies showed, that SBP1 is necessary for *Pf*EMP1 display at the RBC surface (Cooke et al., 2006) or *Pf*EMP1 trafficking beyond the PVM (Maier et al., 2007), in accordance with a role of SBP1 in the PTP1-complex. These results indicate, that either PFE0060w plays no essential role in the PTP1-complex or that it is not a part of it. However, this also highlights the importance of further experiments to confirm the presence and role of PFE0060w within the MSRP6-complex (further discussed below).

MSRP6 belongs to the family of MSP7-related proteins (MSRPs), which are found on neighboring gene loci and are probably originated from gene duplications. The family members are characterized by a SP and a MSP7-like C-terminal domain, which, in MSP7 is part of a processed fragment interacting with MSP1 on merozoite surfaces, in a complex important for RBC invasion (Kadekoppala and Holder, 2010). Hence, the C-terminal domain seems to mediate interactions with protein complexes, in line with the presence of MSRP6 in a protein complex, especially as the part mediating Maurer's cleft interaction (cd) includes a major part of the MSP7 C-terminal domain.

4.2.1.1. The potential function of the MSRP6 protein complex

MSRP6 is only expressed in trophozoite and schizont stages, when the establishment of host cell modifications is already completed (Heiber, 2011). It was proposed that MSRP6 could function in the disassembly of host cell modifications to ensure proper schizont maturation and merozoite egress. However, a knock-out of MSRP6 was shown to have no effect on parasite growth rates or invasion (Kadekoppala et al., 2010a). Also, knobs were still present in this cell line, indicating that trafficking of surface proteins is not blocked by the lack of MSRP6, although an influence on *Pf*EMP1 trafficking was not tested. A slight difference in Maurer's clefts lengths was observed in the knock-out cell line, which however was not confirmed in later experiments (unpublished and Heiber, 2011).

Other members of the MSRPs localize to the merozoite surface (see above), to the PV, or are exported to the RBC (Kadekoppala et al., 2010a; Heiber et al., 2013). Of the exported members of the MSRPs, PF13_0194 (MSRP7) and MSRP6 localize to the RBC cytosol and to Maurer's clefts, respectively, while the third possibly exported member PF13_0191 (MSRP5) may bind to the outsinde of the PVM (Heiber et al., 2013). As all of these proteins contain the MSP7 C-terminal domain, which mediates Maurer'c cleft localization in MSRP6, the interaction partners of this domain seem to be specific for

each of the MSRPs. Sequence alignments (ClustalΩ) showed that especially MSRP6 and MSRP7 share homologies in the C-terminal part and the very N-terminus, the regions here found to mediate export in MSRP6. Firstly, this indicates the presence of a similar export domain in both proteins and secondly, the small size of MSRP7 and thus lack of sequence homology to MSRP6 (besides the very N- and C-termini) indicate that there is probably no functional overlap between these proteins. In contrast, a sequence alignment of MSRP6 to MSRP5 showed similarities in an N-terminal part of the proteins containing stretches of the acidic amino acids glutamate and aspartate, indicating that both proteins might share at least some functions or interaction partners. In blood stages MSRP5 expression was not detected on the protein level (Heiber et al., 2013), although mRNA transcription was validated by RT-PCR (Kadekoppala et al., 2010a). Furthermore, the export and localization of MSRP5 has to be validated, as the observed phenotype could result from overexpression of the GFP fusion protein. Thus, the relevance of MSRP5 in blood stages remains unknown.

Identifying an MSRP6 cd specific interaction partner could help to gain more insights into the potential function of MSRP6. This work identified 5 proteins to interact with MSRP6 in CoIPs. None of these candidates shared homologies to known proteins, so no conclusions about the function of the MSRP6 complex can be drawn from them. Three of these proteins (PFE0050w, PFE0060w, MAL7P1.170) are already expressed in ring stage parasites, and thus might be involved in host cell remodeling or trafficking of virulence factors. PF11_0511 and PFI0086w could only be detected in trophozoites and schizonts, similar to MSRP6. This is notable, as only few known exported proteins show such an expression pattern. To investigate the functions of these proteins truncated versions of the endogenous genes could be generated and parasites phenotypically analyzed. Another possibility is, to use the knock-sideways strategy (Bush et al., 1994; Xu et al., 2010; Robinson and Hirst, 2013) to mislocalize the proteins from their endogenous point of action to unrelated subcellular locations. These strategies could also be used to verify the interaction with MSRP6 by visualizing MSRP6 localization upon truncation or mislocalization of potential interaction partners. However, in case MSRP6 has multiple interaction partners this could lead to false negative results, as mislocalization of one interaction partner could be compensated by another one. From the CoIPs performed in this work, it is also not possible to draw conclusions about the site of interaction in MSRP6, as proteins could interact with other parts than part cd. This could be evaluated by performing reverse CoIPs using a construct containing only part cd and this possibility is now available with some of the double transgenic cell lines generated in this work that express part cd and the FKBP-GFP-tagged interaction cancidate. In particular, cell lines co-expressing an mCherry tagged full length MSRP6 or MSRP6 SP+cd were obtained for PFI0086w

and PF11_0511. Interestingly, the detectable soluble pool of PF11_0511 decreased upon overexpression of MSRP6 but not MSRP6 SP+cd, indicating that it might be recruited to the Maurer's clefts by MSRP6, supporting the CoIP data. However, this also would suggest that vice versa MSRP6 is not recruited to the Maurer'clefts by PF11_0511 and thus would exclude this protein as the MSRP6 interaction partner mediating Maurer's clefts localization of part cd. For the MSRP6 SP+cd fusion protein a soluble pool was detected in both cell lines, thus not excluding a specific interaction of PF11_0511 with part cd. For PFI0086w no Maurer's cleft recruitment upon overexpression of MSRP6 was observed, indicating that there might not be an interaction or that the interaction is only transient.

MAL7P1.170 showed different subcellular localizations, which were partially stage specific. One possibility for the diverse localization could be explained by the presence of different isoforms. These predicted isoforms (PlasmoDB GeneIDs: PF3D7_0730800.1 and PF3D7_0730800.2) only differ in two N-terminal amino acids, but might result in different SP cleavage sites and thus mature N-termini. As this protein does not contain a PEXEL-motif these N-termini will probably not be further cleaved once inside the ER and might represent signals for the trafficking to different sub-compartments or influence the timing of export. As it is not possible to distinguish between the two isoforms on the protein level or by PCR analysis, no conclusions about the possible expression and localization of any isoforms in the knock-in cell line can be drawn. These isoforms could however be episomally expressed and their localization and trafficking compared. In ring stages MAL7P1.170 is either localized to the central cavity, distinct foci at the parasite periphery or the RBC cytosol. The cavity was proposed to have a function in lipid storage (Kruse, 2014) and together with the early expression of MAL7P1.170 this could indicate a role of this protein in establishing host cell modifications containing membranes, e.g. Maurer's clefts. In trophozoite and schizont stages MAL7P1.170 localized to the Maurer's clefts but still exhibited a significant cytosolic pool, making it an unlikely candidate for the Maurer's cleft recruitment of MSRP6. However, it could also be possible that the cytosolic pool of MAL7P1.170 interacts with other proteins blocking potential MSRP6 interaction sites, so that only the Maurer's cleft pool of MAL7P1.170 could interact with MSRP6 and thus facilitate its recruitment to the Maurer's clefts.

PFE0050w was the only confirmed MSRP6 interaction candidate besides PFE0060w exhibiting no visible RBC cytosolic localization and might thus be a valid candidate for recruiting MSRP6 to the Maurer's clefts. This could be tested by preventing the Maurer's cleft localization of PFE0050w (e.g. by truncation or mislocalization) and subsequent analysis of MSRP6 localization. However, this would only give a clear cut result if the other interaction partners did not also contribute to the Maurer's cleft binding of MSRP6.

In some cells PFE0050w showed a diffuse staining around MSRP6 foci, in addition to the co-localization, suggesting that PFE0050w partially localizes to another sub-compartment of the Maurer's clefts. The lack of MSRP6 localization in these areas indicates that if there is an interaction with PFE0050w, it could be only temporary or dependent on the environment and the presence of other interactions partners.

PFE0060w is the only confirmed MSRP6 interaction partner containing TMDs, thus it is a potential membrane anchor for the MSRP6 complex. As discussed above, the actual presence of PFE0060w within the MSRP6-complex has to be validated by further experiments, for instance by including protein truncations and performing knock-sideways.

Of the non-confirmed candidates characterized in this work, two proteins contained TMDs. PFC0070c was shown not to be exported as an endogenously expressed FKBP-GFP fusion protein, which excludes it as a potential MSRP6 interaction candidate. PF10_0024 is predominantly expressed in ring stages and does not show co-localization with MSRP6 in IFAs, which makes it an unlikely membrane anchor for the MSRP6-complex. It is interesting however that this protein possesses an unusual PEXEL-motif, that is located downstream of a TMD. It could be possible that the open reading frame is not annotated correctly and that the first TMD functions as a recessed SP, as is common for PEXEL proteins. Another explanation is that the PEXEL-motif can also be functional when it is located downstream of a TMD, which would however question the function of this TMD as it would be cleaved off inside the ER when the PEXEL is cleaved.

PF10_0018 and PF10_0020 are predicted alpha/beta hydrolases with homologies to lysophospholipases and partially co-localized with MSRP6 at Maurer's clefts. These proteins might be involved in membrane remodeling, potentially helping to disintegrate Maurer's clefts in schizont stages. Especially PF10_0020 shows a predominant intra-parasitic staining of filament-like structures. The identity of these structures was not examined in this work, but might potentially represent the apicoplast, which has a filament-like appearance in schizont stages (Waller et al., 2000). This could be tested by using apicoplast specific antibodies in IFAs.

PF10_0025 shows the highest expression of the non-validated MSRP6 interaction partners and co-localized with MSRP6. This protein was found to be essential for *Pf*EMP1 trafficking and cytoadherence (Maier et al., 2008). *Pf*EMP1 display at the RBC membrane occurs during the transition from ring stage parasites to trophozoits, possibly in a rapid event (Kriek et al., 2003). In this work expression of this protein was only detected in trophozoites and schizonts, so either small amounts of this protein are sufficient for *Pf*EMP1 trafficking or the observed phenotype in the aforementioned study could have been caused by off-target effects. Interestingly, a BLASTp search identified the presence of Ehrlichia tandem repeats, which were found on an immunodominant protein of

Ehrlichia chaffeensis. This indicates that the Ehrlichia tandem repeats cause a strong immune reaction and it could be speculated that these repeats in PF10_0025 serve an immune-modulatory role upon rupture of the RBC and release into the blood stream. However, an interaction with MSRP6 has not been tested yet. Therefore no conclusions about a function within the MSRP6-complex can be drawn.

PFL0055c showed an unusual localization, as it localized to the RBC membrane and and intra-parasitic focus, reminiscent of the golgi in early trophozoite stages. The RBC peripheral staining was lost during the intra-erythrocytic lifecycle and the protein accumulated at the Maurer's clefts. It may therefore be that the focus within the parasite represents tag-induced or physiologically retained protein that is later on exported. The presence of a MESA erythrocyte cytoskeleton-binding (MEC) domain suggests that the RBC peripheral staining is caused by an interaction with the RBC cytoskeleton. Whether the Maurer's cleft staining is caused by protein copies relocating from the RBC surface to the Maurer's clefts or by protein copies stored within the parasite, as suggested by the accumulation of intra-parasitic signal, cannot be concluded from the present results. The lack of RBC peripheral staining in schizont stages raises the question of how this localization might be regulated. It could be possible that the N-terminal MEC domain is either proteolytically cleaved off or masked in schizonts. The presence of the C-terminal DnaJ domain with Hsp70 interaction sites indicates that PFL0055c acts as a chaperone. As an interaction with MSRP6 has not been tested yet, no conclusions about PFL0055c and a possible function in the MSRP6-complex can be drawn.

As the functions of all potential MSRP6 interaction partners are unknown, the function of the MSRP6-complex remains elusive. Especially the confirmed interaction partners have no homologies to known proteins. The identity of the non-confirmed interaction partners could suggest a function in membrane remodelling, *Pf*EMP1 trafficking or immune modulation. In case the MSRP6-complex indeed plays an immune-modulatory role, *in vitro* studies will probably not be sufficient to further investigate this function. As no MSRP6 homologs were so far identified in the rodent malaria parasites (according to PlasmoDB), e.g. *P. berghei*, a model organism for *P. falciparum*, it will not be possible to test this in rodent malaria models.

4.2.1.2. The trafficking of the MSRP6-complex

The results obtained from the BioID experiments have not definitely identified the protein responsible for Maurer's cleft recruitment of MSRP6. The two most likely candidates are PFE0050w and PFE0060w, as both candidates were present among the most significant hits in both Rex3cd over Rex3 and Rex3cd over Stevor. Furthermore both do not exhibit a cytosolic pool within the RBC and are expressed during all investigated blood stages.

A cytosolic pool of a candidate would not exclude it as a MSRP6 interaction partner, however, as MSRP6 does not show a cytosolic pool, these proteins seem to be less likely to mediate Maurer's clefts recruitment of MSRP6. An important question is, at which stage of trafficking the potential MSRP6-complex is established. If the binding of cd is the reason for the export promoting activity in this domain of MSRP6 and this is responsible for the observed export phenotype of MSRP6 SP+cd, complex formation will have to take place before export beyond the PVM. For MSP1 and MSP7 it was proposed that inter-action is already established within a pre-golgi compartment, as interaction is essential for the correct trafficking to the merozoite surface (Kadekoppala and Holder, 2010). If this were a common theme in MSP7 and MSP7-like proteins, MSRP6-complex formation could also occur during early trafficking steps. However, in contrast to merozoite surface display, the export of proteins requires a translocation step across the PVM, a process that requires unfolding of the trafficked proteins. This model therefore is problematic as protein unfolding would disrupt any protein-protein interactions between MSRP6+cd and a potential escort protein established during trafficking to the PV. This leaves several options:

- Co-trafficked protein complexes are released into export competent sub-compartments of the PV, from where all proteins are exported by default and hence MSRP6+cd would not require any trafficking motifs once it was escorted to this site. This re-quires exported proteins to be sorted into export vesicles during early secretion steps as has previously been suggested as one option of how the PEXEL-motif, which is cleaved in the ER, nevertheless influences export at the PVM (Crabb et al., 2010). As a precedent for this type of trafficking, proteins containing a transit peptide, me-diating apicoplast localization were suggested to be loaded into specific apicoplast targeted vesicles inside the golgi (Heiny et al., 2014). It is therefore possible that a similar process exists for exported proteins.

- Translocon components not only recognize proteins containing export motifs but also associated proteins without export motifs themselves that are in close proximity to exported proteins containing export signals. This could also be facilitated by chaperones already interacting with exported proteins during trafficking from the ER to the PV and transferring them to the translocon.

- An alternative export pathway exists, facilitating export of unfolded proteins. This is an unlikely possibility, as all proteins tested so far, including MSRP6 require to be unfolded for export (Gehde et al., 2009; Grüring et al., 2011; Heiber et al., 2013) and all classes of exported proteins depend in their export on components of the suspected PVM translocon PTEX (Beck et al., 2014; Elsworth et al., 2014).

- The co-trafficking hypothesis is incorrect and MSRP6 SP+cd contains a cryptic

export signal recognized by the translocon (or other components of the export machinery). This possibility would suggest that the formation of protein-protein interactions during trafficking to the parasite periphery is unnecessary and could even be disadvantageous for the parasite, as resolving these interaction would consume energy. If this hypothesis were correct, cd would have two independent functions, one in mediating trafficking into the host cell and one to mediate Maurer's clefts attachment.

At present, it is unclear which of these ideas are correct, highlighting that many aspects of protein export are still unresolved and further experiments will be necessary to gain insights into these processes. Experiments to test the general possibility of a co-export are currently in progress and make use of the inducible dimerization of FKBP and FRB by a small ligand. The demonstration of a co-export would not only shed light on the specific trafficking of MSRP6 but also on protein export mechanisms in this important pathogen in general.

4.3. BioID as a tool for proteome analyses

BioID was first described as a method to identify protein-protein interaction partners and neighboring proteins (Roux et al., 2012). Using this method, the authors reproduced known interaction partners of lamin-A, a part of the nuclear envelope, but also found known members of the nuclear envelope not interacting with lamin-A (Roux et al., 2012). This indicates that BioID can be used as a tool to identify specific interaction partners of a protein of interest (POI) but also to identify proteins that localize to a specific compartment. The practical labeling radius of BioID was experimentally defined in a study using nucleoporins of the nulear pore complex as a molecular ruler and estimated to be ~10 nm. The same study also found that not all proteins within this range are labeled with the same efficiency, which is why the authors suggest that negative results should be treated with caution (Kim et al., 2014). BioID has not been used in *Plasmodium* before, but was successfully applied in the related apicomplexan parasite *Toxoplasma gondii* to identify novel members of the inner membrane complex (Chen et al., 2015).

In this work BioID identified several potential interaction partners of MSRP6 cd. The range of BirA* and the large number of significant hits suggest that not only direct and indirect interaction partners but also other proteins in close proximity were labeled by BirA*. The long incubation time of the BirA* expressing cell lines with biotin (exceeding 24 hours) applied in this work, probably contributed to the large number of significant hits, as different states of Maurer's cleft maturation were covered. The data in this work also provided a list of proteins not previously known to be Maurer's clefts associated.

In particular proteins without a TMD have several possible destinations in the host cell and the fact that most of the tested proteins of this type were found in Maurer's clefts highlights the usefulness of BirA* to obtain compartment proteomes. This indicates that BioID could also be a valuable tool to potentially describe the entire Maurer's cleft proteome.

A previously published Maurer's cleft proteome used purified infected RBC ghosts and subsequent mass spectrometry analysis to identify Maurer's cleft proteins (Vincensini et al., 2005). The study found 50 candidates of which seven previously uncharacterized proteins were chosen for further analysis. A Maurer's cleft localization was confirmed for 4 of these candidates via IFA and for a further 2 candidates by proteinase K protection assays (Vincensini et al., 2005).

To compare the results from the present work to the published Maurer's cleft proteome, all 44 significant hits relevant for Maurer's cleft proteins (Rex3cd over Stevor, Rex3cd over Rex3, Stevor over Rex3) were compared to the 50 hits found in the Vincensini *et al.* study. Ten proteins were a match for both studies, of which 3 proteins are known not to be exported. Of the remaining 7, four proteins were shown to localize to Maurer's clefts (Vincensini et al., 2005), one of which was also characterized in the present work (PFE0060w). In this work 11 proteins were analyzed for their subcellular localization and 10 of those found to localize at Maurer's clefts, indicating a false discovery rate of less that 10%. However, it should also be noted that this was a cherry picked selection and might not accurately reflect the situation for the remaining 33 hits. Furthermore it is possible that the one protein not found at the Maurer's clefts did not properly localize due to the tag (see section 4.2) and in actual fact the discovery rate in the top hits may even be higher. In line with a low false discovery rate, 33 of the 44 in total obtained significant hits are predicted or reported to be exported proteins, with 9 proteins most likely not being exported (based on reported function/localization or lack of SP/TMD) and 2 proteins containing a SP but no PEXEL-motif that potentially may represent PNEPs. Of the 50 hits identified in the Vincensini *et al.* study, only 16 were reported or annotated to be exported, including the 7 proteins that were further characterized in their study, 32 were most likely non-exported proteins (based on reported function/localization or lack of SP/TMD) and 2 proteins possessed a SP or TMD and may represent PNEPs. This comparison of both studies indicates, that for the identification of novel Maurer's clefts proteins BioID is superior to cell fractionation, as it identified more specific hits and less non-exported proteins. Hence, this method may be a valuable tool to obtain also other compartment specific or cellular structure specific proteomes in *P. falciparum* parasites.

In summary, of the 33 annotated exported proteins identified in this work, approximately one fourth (9) were shown to localize to Maurer's clefts. It is likely that testing

the subcellular localization of the remaining candidates will reveal more Maurer's clefts proteins and potential further components of the MSRP6-complex. However, 4 proteins identified by Vincensini *et al.* that localized to Maurer's clefts were not among the significant hits in this study, indicating that BioID could potentially be optimized to generate more hits. It is for instance possible that due to an inhomogeneous distribution on the Maurer's clefts it is necessary to tag other Maurer's clefts proteins to reach all subgroups of Mauer's clefts proteins using BirA*.

Recently, the generation of an improved smaller biotin ligase for BioID was reported, which shows an enhanced and more precise labeling of proximal proteins for which the range can be modulated by the use of flexible linkers (Kim et al., 2016). This improved biotin ligase could be used to generate more specific hits for the identification of specific protein-protein interactions, or using adjustable linker sequences, for proteome analyses of other compartments or protein complexes. Furthermore, it was shown that using BioID also the positions of proteins within a large complex can be determined, exploiting the limited range of the biotin ligase (Kim et al., 2014). This could be used to validate the assumed sub-compartmentalization of Maurer's clefts(Spycher et al., 2006), using bait proteins localizing to distinct parts of the organelles and may also make possible to probe into the architecture of the potential MSRP6-complex reported in this thesis and to assess its spatial relation and possible overlap with the PTP1-complex.

Bibliography

J. Achan, A. O. Talisuna, A. Erhart, A. Yeka, J. K. Tibenderana, F. N. Baliraine, P. J. Rosenthal, and U. D'Alessandro. Quinine, an old anti-malarial drug in a modern world: role in the treatment of malaria. *Malar. J.*, 10:144, 2011. [PubMed Central:PMC3121651] [DOI:10.1186/1475-2875-10-144] [PubMed:21609473].

R. Amino, S. Thiberge, B. Martin, S. Celli, S. Shorte, F. Frischknecht, and R. Menard. Quantitative imaging of Plasmodium transmission from mosquito to mammal. *Nat. Med.*, 12(2):220–224, Feb 2006. [DOI:10.1038/nm1350] [PubMed:16429144].

N. M. Anstey, B. Russell, T. W. Yeo, and R. N. Price. The pathophysiology of vivax malaria. *Trends Parasitol.*, 25(5):220–227, May 2009. [DOI:10.1016/j.pt.2009.02.003] [PubMed:19349210].

F. Ariey, B. Witkowski, C. Amaratunga, J. Beghain, A. C. Langlois, N. Khim, S. Kim, V. Duru, C. Bouchier, L. Ma, P. Lim, R. Leang, S. Duong, S. Sreng, S. Suon, C. M. Chuor, D. M. Bout, S. Menard, W. O. Rogers, B. Genton, T. Fandeur, O. Miotto, P. Ringwald, J. Le Bras, A. Berry, J. C. Barale, R. M. Fairhurst, F. Benoit-Vical, O. Mercereau-Puijalon, and D. Menard. A molecular marker of artemisinin-resistant Plasmodium falciparum malaria. *Nature*, 505(7481):50–55, Jan 2014. [DOI:10.1038/nature12876] [PubMed:24352242].

E. A. Ashley and N. J. White. The duration of Plasmodium falciparum infections. *Malar. J.*, 13:500, 2014. [PubMed Central:PMC4301960] [DOI:10.1186/1475-2875-13-500] [PubMed:25515943].

K. Baer, C. Klotz, S. H. Kappe, T. Schnieder, and U. Frevert. Release of hepatic Plasmodium yoelii merozoites into the pulmonary microvasculature. *PLoS Pathog.*, 3(11): e171, Nov 2007. [PubMed Central:PMC2065874] [DOI:10.1371/journal.ppat.0030171] [PubMed:17997605].

M. R. Baldwin, X. Li, T. Hanada, S. C. Liu, and A. H. Chishti. Merozoite surface protein 1 recognition of host glycophorin A mediates malaria parasite invasion of red blood cells. *Blood*, 125(17):2704–2711, Apr 2015. [PubMed Central:PMC4408295] [DOI:10.1182/blood-2014-11-611707] [PubMed:25778531].

N. Bano, J. D. Romano, B. Jayabalasingham, and I. Coppens. Cellular interactions of Plasmodium liver stage with its host mammalian cell. *Int. J. Parasitol.*, 37(12):1329–1341, Oct 2007. [DOI:10.1016/j.ijpara.2007.04.005] [PubMed:17537443].

C. K. Barlowe and E. A. Miller. Secretory protein biogenesis and traffic in the early secretory pathway. *Genetics*, 193(2):383–410, Feb 2013. [PubMed Central:PMC3567731] [DOI:10.1534/genetics.112.142810] [PubMed:23396477].

A. Bartoloni and L. Zammarchi. Clinical aspects of uncomplicated and severe malaria. *Mediterr J Hematol Infect Dis*, 4(1):e2012026, 2012.

J. R. Beck, V. Muralidharan, A. Oksman, and D. E. Goldberg. PTEX component HSP101 mediates export of diverse malaria effectors into host erythrocytes. *Nature*, 511 (7511):592–595, Jul 2014. [PubMed Central:PMC4130291] [DOI:10.1038/nature13574] [PubMed:25043010].

J. D. Bendtsen, H. Nielsen, G. von Heijne, and S. Brunak. Improved prediction of signal peptides: SignalP 3.0. *J. Mol. Biol.*, 340(4):783–795, Jul 2004. [DOI:10.1016/j.jmb.2004.05.028] [PubMed:15223320].

S. Bhattacharjee, R. V. Stahelin, K. D. Speicher, D. W. Speicher, and K. Haldar. Endoplasmic reticulum PI(3)P lipid binding targets malaria proteins to the host cell. *Cell*, 148(1-2):201–212, Jan 2012. [PubMed Central:PMC3268671] [DOI:10.1016/j.cell.2011.10.051] [PubMed:22265412].

M. J. Blackman and V. B. Carruthers. Recent insights into apicomplexan parasite egress provide new views to a kill. *Curr. Opin. Microbiol.*, 16(4):459–464, Aug 2013. [PubMed Central:PMC3755044] [DOI:10.1016/j.mib.2013.04.008] [PubMed:23725669].

J. A. Boddey and A. F. Cowman. Plasmodium nesting: remaking the erythrocyte from the inside out. *Annu. Rev. Microbiol.*, 67:243–269, 2013. [DOI:10.1146/annurev-micro-092412-155730] [PubMed:23808341].

J. A. Boddey, R. L. Moritz, R. J. Simpson, and A. F. Cowman. Role of the Plasmodium export element in trafficking parasite proteins to the infected erythrocyte. *Traffic*, 10(3):285–299, Mar 2009. [PubMed Central:PMC2682620] [DOI:10.1111/j.1600-0854.2008.00864.x] [PubMed:19055692].

J. A. Boddey, A. N. Hodder, S. Gunther, P. R. Gilson, H. Patsiouras, E. A. Kapp, J. A. Pearce, T. F. de Koning-Ward, R. J. Simpson, B. S. Crabb, and A. F. Cowman. An aspartyl protease directs malaria effector proteins to the host cell. *Nature*, 463 (7281):627–631, Feb 2010. [PubMed Central:PMC2818761] [DOI:10.1038/nature08728] [PubMed:20130643].

J. A. Boddey, T. G. Carvalho, A. N. Hodder, T. J. Sargeant, B. E. Sleebs, D. Marapana, S. Lopaticki, T. Nebl, and A. F. Cowman. Role of plasmepsin V in export of diverse protein families from the Plasmodium falciparum exportome. *Traffic*, 14(5):532–550, May 2013. [DOI:10.1111/tra.12053] [PubMed:23387285].

J. A. Boddey, M. T. O'Neill, S. Lopaticki, T. G. Carvalho, A. N. Hodder, T. Nebl, S. Wawra, P. van West, Z. Ebrahimzadeh, D. Richard, S. Flemming, T. Spielmann, J. Przyborski, J. J. Babon, and A. F. Cowman. Export of malaria proteins requires co-translational processing of the PEXEL motif independent of phosphatidylinositol-3-phosphate binding. *Nat Commun*, 7:10470, 2016. [PubMed Central:PMC4740378] [DOI:10.1038/ncomms10470] [PubMed:26832821].

P. J. Boersema, R. Raijmakers, S. Lemeer, S. Mohammed, and A. J. Heck. Multiplex peptide stable isotope dimethyl labeling for quantitative proteomics. *Nat Protoc*, 4(4): 484–494, 2009. [DOI:10.1038/nprot.2009.21] [PubMed:19300442].

M. J. Boyle, J. S. Richards, P. R. Gilson, W. Chai, and J. G. Beeson. Interactions with heparin-like molecules during erythrocyte invasion by Plasmodium falciparum merozoites. *Blood*, 115(22):4559–4568, Jun 2010. [DOI:10.1182/blood-2009-09-243725] [PubMed:20220119].

M. C. Bruce, P. Alano, S. Duthie, and R. Carter. Commitment of the malaria parasite Plasmodium falciparum to sexual and asexual development. *Parasitology*, 100 Pt 2: 191–200, Apr 1990. [PubMed:2189114].

K. T. Bush, B. A. Hendrickson, and S. K. Nigam. Induction of the FK506-binding protein, FKBP13, under conditions which misfold proteins in the endoplasmic reticulum. *Biochem. J.*, 303 (Pt 3):705–708, Nov 1994. [PubMed Central:PMC1137603] [PubMed:7526846].

A. S. Butterworth, T. S. Skinner-Adams, D. L. Gardiner, and K. R. Trenholme. Plasmodium falciparum gametocytes: with a view to a kill. *Parasitology*, 140(14):1718–1734, Dec 2013. [DOI:10.1017/S0031182013001236] [PubMed:23953486].

H. H. Chang, A. M. Falick, P. M. Carlton, J. W. Sedat, J. L. DeRisi, and M. A. Marletta. N-terminal processing of proteins exported by malaria parasites. *Mol. Biochem. Parasitol.*, 160(2):107–115, Aug 2008. [PubMed Central:PMC2922945] [DOI:10.1016/j.molbiopara.2008.04.011] [PubMed:18534695].

M. E. Cheetham and A. J. Caplan. Structure, function and evolution of DnaJ: conservation and adaptation of chaperone function. *Cell Stress Chaperones*, 3(1):28–36, Mar 1998. [PubMed Central:PMC312945] [PubMed:9585179].

A. L. Chen, E. W. Kim, J. Y. Toh, A. A. Vashisht, A. Q. Rashoff, C. Van, A. S. Huang, A. S. Moon, H. N. Bell, L. A. Bentolila, J. A. Wohlschlegel, and P. J. Bradley. Novel components of the Toxoplasma inner membrane complex revealed by BioID. *MBio*, 6 (1):e02357–02314, 2015. [PubMed Central:PMC4337574] [DOI:10.1128/mBio.02357-14] [PubMed:25691595].

C. Cole, J. D. Barber, and G. J. Barton. The Jpred 3 secondary structure prediction server. *Nucleic Acids Res.*, 36(Web Server issue):197–201, Jul 2008. [PubMed Central:PMC2447793] [DOI:10.1093/nar/gkn238] [PubMed:18463136].

W. E. Collins and G. M. Jeffery. Plasmodium ovale: parasite and disease. *Clin. Microbiol. Rev.*, 18(3):570–581, Jul 2005.

W. E. Collins and G. M. Jeffery. Plasmodium malariae: parasite and disease. *Clin. Microbiol. Rev.*, 20(4):579–592, Oct 2007.

B. M. Cooke, D. W. Buckingham, F. K. Glenister, K. M. Fernandez, L. H. Bannister, M. Marti, N. Mohandas, and R. L. Coppel. A Maurer's cleft-associated protein is essential for expression of the major malaria virulence antigen on the surface of infected red

blood cells. *J. Cell Biol.*, 172(6):899–908, Mar 2006. [PubMed Central:PMC2063733] [DOI:10.1083/jcb.200509122] [PubMed:16520384].

M. Cova, J. A. Rodrigues, T. K. Smith, and L. Izquierdo. Sugar activation and glycosylation in Plasmodium. *Malar. J.*, 14(1):427, 2015. [PubMed Central:PMC4628283] [DOI:10.1186/s12936-015-0949-z] [PubMed:26520586].

A. F. Cowman, D. Berry, and J. Baum. The cellular and molecular basis for malaria parasite invasion of the human red blood cell. *J. Cell Biol.*, 198(6):961–971, Sep 2012. [PubMed Central:PMC3444787] [DOI:10.1083/jcb.201206112] [PubMed:22986493].

B. S. Crabb, B. M. Cooke, J. C. Reeder, R. F. Waller, S. R. Caruana, K. M. Davern, M. E. Wickham, G. V. Brown, R. L. Coppel, and A. F. Cowman. Targeted gene disruption shows that knobs enable malaria-infected red cells to cytoadhere under physiological shear stress. *Cell*, 89(2):287–296, Apr 1997. [PubMed:9108483].

B. S. Crabb, M. Rug, T. W. Gilberger, J. K. Thompson, T. Triglia, A. G. Maier, and A. F. Cowman. Transfection of the human malaria parasite Plasmodium falciparum. *Methods Mol. Biol.*, 270:263–276, 2004. [DOI:10.1385/1-59259-793-9:263] [PubMed:15153633].

B. S. Crabb, T. F. de Koning-Ward, and P. R. Gilson. Protein export in Plasmodium parasites: from the endoplasmic reticulum to the vacuolar export machine. *Int. J. Parasitol.*, 40(5):509–513, Apr 2010. [DOI:10.1016/j.ijpara.2010.02.002] [PubMed:20170656].

L. Cui and X. Z. Su. Discovery, mechanisms of action and combination therapy of artemisinin. *Expert Rev Anti Infect Ther*, 7(8):999–1013, Oct 2009. [PubMed Central:PMC2778258] [DOI:10.1586/eri.09.68] [PubMed:19803708].

M. Cyrklaff, C. P. Sanchez, N. Kilian, C. Bisseye, J. Simpore, F. Frischknecht, and M. Lanzer. Hemoglobins S and C interfere with actin remodeling in Plasmodium falciparum-infected erythrocytes. *Science*, 334(6060):1283–1286, Dec 2011. [DOI:10.1126/science.1213775] [PubMed:22075726].

C. Daneshvar, T. M. Davis, J. Cox-Singh, M. Z. Rafa'ee, S. K. Zakaria, P. C. Divis, and B. Singh. Clinical and laboratory features of human Plasmodium knowlesi infection. *Clin. Infect. Dis.*, 49(6):852–860, Sep 2009. [PubMed Central:PMC2843824] [DOI:10.1086/605439] [PubMed:19635025].

K. W. Dantzler, D. B. Ravel, N. M. Brancucci, and M. Marti. Ensuring transmission through dynamic host environments: host-pathogen interactions in Plasmodium sexual development. *Curr. Opin. Microbiol.*, 26:17–23, Aug 2015. [PubMed Central:PMC4577303] [DOI:10.1016/j.mib.2015.03.005] [PubMed:25867628].

T. F. de Koning-Ward, P. R. Gilson, J. A. Boddey, M. Rug, B. J. Smith, A. T. Papenfuss, P. R. Sanders, R. J. Lundie, A. G. Maier, A. F. Cowman, and B. S. Crabb. A newly discovered protein export machine in malaria parasites. *Nature*, 459(7249):945–949, Jun 2009. [PubMed Central:PMC2725363] [DOI:10.1038/nature08104] [PubMed:19536257].

M. De Niz, A.-K. Ullrich, A. Heiber, A. Blancke Soares, C. Pick, R. Lyck, D. Keller, G. Kaiser, M. Prado, S. Flemming, H. del Portillo, C. Janse, V. Heussler, and T. Spielmann. The machinery underlying malaria parasite virulence is conserved between rodent and human malaria parasites. *Nature Communications*, 2016. in press.

M. Deponte, H. C. Hoppe, M. C. Lee, A. G. Maier, D. Richard, M. Rug, T. Spielmann, and J. M. Przyborski. Wherever I may roam: protein and membrane trafficking in P. falciparum-infected red blood cells. *Mol. Biochem. Parasitol.*, 186(2):95–116, Dec 2012. [DOI:10.1016/j.molbiopara.2012.09.007] [PubMed:23043991].

S. A. Desai. Why do malaria parasites increase host erythrocyte permeability? *Trends Parasitol.*, 30(3):151–159, Mar 2014. [PubMed Central:PMC3987781] [DOI:10.1016/j.pt.2014.01.003] [PubMed:24507014].

M. W. Dixon, S. Kenny, P. J. McMillan, E. Hanssen, K. R. Trenholme, D. L. Gardiner, and L. Tilley. Genetic ablation of a Maurer's cleft protein prevents assembly of the Plasmodium falciparum virulence complex. *Mol. Microbiol.*, 81(4):982–993, Aug 2011. [DOI:10.1111/j.1365-2958.2011.07740.x] [PubMed:21696460].

S. A. Dolan, L. H. Miller, and T. E. Wellems. Evidence for a switching mechanism in the invasion of erythrocytes by Plasmodium falciparum. *J. Clin. Invest.*, 86(2):618–624, Aug 1990. [PubMed Central:PMC296769] [DOI:10.1172/JCI114753] [PubMed:2200806].

A. M. Dondorp, F. Nosten, P. Yi, D. Das, A. P. Phyo, J. Tarning, K. M. Lwin, F. Ariey, W. Hanpithakpong, S. J. Lee, P. Ringwald, K. Silamut, M. Imwong, K. Chotivanich, P. Lim, T. Herdman, S. S. An, S. Yeung, P. Singhasivanon, N. P. Day, N. Lindegardh, D. Socheat, and N. J. White. Artemisinin resistance in Plasmodium falciparum malaria. *N. Engl. J. Med.*, 361(5):455–467, Jul 2009. [PubMed Central:PMC3495232] [DOI:10.1056/NEJMoa0808859] [PubMed:19641202].

B. Elsworth, K. Matthews, C. Q. Nie, M. Kalanon, S. C. Charnaud, P. R. Sanders, S. A. Chisholm, N. A. Counihan, P. J. Shaw, P. Pino, J. A. Chan, M. F. Azevedo, S. J. Rogerson, J. G. Beeson, B. S. Crabb, P. R. Gilson, and T. F. de Koning-Ward. PTEX is an essential nexus for protein export in malaria parasites. *Nature*, 511(7511):587–591, Jul 2014. [DOI:10.1038/nature13555] [PubMed:25043043].

B. Elsworth, P. R. Sanders, T. Nebl, S. Batinovic, M. Kalanon, C. Q. Nie, S. C. Charnaud, H. E. Bullen, T. F. de Koning Ward, L. Tilley, B. S. Crabb, and P. R. Gilson. Proteomic analysis reveals novel proteins associated with the Plasmodium protein exporter PTEX and a loss of complex stability upon truncation of the core PTEX component, PTEX150. *Cell. Microbiol.*, Mar 2016. [DOI:10.1111/cmi.12596] [PubMed:27019089].

A. Enayati and J. Hemingway. Malaria management: past, present, and future. *Annu. Rev. Entomol.*, 55:569–591, 2010. [DOI:10.1146/annurev-ento-112408-085423] [PubMed:19754246].

R. M. Fairhurst, G. M. Nayyar, J. G. Breman, R. Hallett, J. L. Vennerstrom, S. Duong, P. Ringwald, T. E. Wellems, C. V. Plowe, and A. M. Dondorp. Artemisinin-resistant malaria: research challenges, opportunities, and public health implications.

Am. J. Trop. Med. Hyg., 87(2):231–241, Aug 2012. [PubMed Central:PMC3414557] [DOI:10.4269/ajtmh.2012.12-0025] [PubMed:22855752].

S. Flemming. Identification of the export determinants of novel PEXEL negative exported proteins (PNEPs) in the human malaria parasite *Plasmodium falciparum*. 2011.

L. Florens, X. Liu, Y. Wang, S. Yang, O. Schwartz, M. Peglar, D. J. Carucci, J. R. Yates, and Y. Wu. Proteomics approach reveals novel proteins on the surface of malaria-infected erythrocytes. *Mol. Biochem. Parasitol.*, 135(1):1–11, May 2004. [PubMed:15287581].

M. E. Francia and B. Striepen. Cell division in apicomplexan parasites. *Nat. Rev. Microbiol.*, 12(2):125–136, Feb 2014. [DOI:10.1038/nrmicro3184] [PubMed:24384598].

V. M. Gantz, N. Jasinskiene, O. Tatarenkova, A. Fazekas, V. M. Macias, E. Bier, and A. A. James. Highly efficient Cas9-mediated gene drive for population modification of the malaria vector mosquito Anopheles stephensi. *Proc. Natl. Acad. Sci. U.S.A.*, 112(49):E6736–6743, Dec 2015. [PubMed Central:PMC4679060] [DOI:10.1073/pnas.1521077112] [PubMed:26598698].

N. Gehde, C. Hinrichs, I. Montilla, S. Charpian, K. Lingelbach, and J. M. Przyborski. Protein unfolding is an essential requirement for transport across the parasitophorous vacuolar membrane of Plasmodium falciparum. *Mol. Microbiol.*, 71(3):613–628, Feb 2009. [DOI:10.1111/j.1365-2958.2008.06552.x] [PubMed:19040635].

N. Gerald, B. Mahajan, and S. Kumar. Mitosis in the human malaria parasite Plasmodium falciparum. *Eukaryotic Cell*, 10(4):474–482, Apr 2011. [PubMed Central:PMC3127633] [DOI:10.1128/EC.00314-10] [PubMed:21317311].

D. G. Gibson, L. Young, R. Y. Chuang, J. C. Venter, C. A. Hutchison, and H. O. Smith. Enzymatic assembly of DNA molecules up to several hundred kilobases. *Nat. Methods*, 6(5):343–345, May 2009. [DOI:10.1038/nmeth.1318] [PubMed:19363495].

D. A. Gold, A. D. Kaplan, A. Lis, G. C. Bett, E. E. Rosowski, K. M. Cirelli, A. Bougdour, S. M. Sidik, J. R. Beck, S. Lourido, P. F. Egea, P. J. Bradley, M. A. Hakimi, R. L. Rasmusson, and J. P. Saeij. The Toxoplasma Dense Granule Proteins GRA17 and GRA23 Mediate the Movement of Small Molecules between the Host and the Parasitophorous Vacuole. *Cell Host Microbe*, 17(5):642–652, May 2015. [PubMed Central:PMC4435723] [DOI:10.1016/j.chom.2015.04.003] [PubMed:25974303].

D. C. Gowda and E. A. Davidson. Protein glycosylation in the malaria parasite. *Parasitol. Today (Regul. Ed.)*, 15(4):147–152, Apr 1999. [PubMed:10322336].

B. M. Greenwood, D. A. Fidock, D. E. Kyle, S. H. Kappe, P. L. Alonso, F. H. Collins, and P. E. Duffy. Malaria: progress, perils, and prospects for eradication. *J. Clin. Invest.*, 118(4):1266–1276, Apr 2008.

C. Grüring. Characterization and visualization of protein export in the human malaria parasite Plasmodium falciparum (Welch, 1897). 2011a.

C. Grüring, A. Heiber, F. Kruse, J. Ungefehr, T. W. Gilberger, and T. Spielmann. Development and host cell modifications of Plasmodium falciparum blood stages in four dimensions. *Nat Commun*, 2:165, Jan 2011. [DOI:10.1038/ncomms1169] [PubMed:21266965].

C. Grüring, A. Heiber, F. Kruse, S. Flemming, G. Franci, S. F. Colombo, E. Fasana, H. Schoeler, N. Borgese, H. G. Stunnenberg, J. M. Przyborski, T. W. Gilberger, and T. Spielmann. Uncovering common principles in protein export of malaria parasites. *Cell Host Microbe*, 12(5):717–729, Nov 2012. [DOI:10.1016/j.chom.2012.09.010] [PubMed:23159060].

P. Gueirard, J. Tavares, S. Thiberge, F. Bernex, T. Ishino, G. Milon, B. Franke-Fayard, C. J. Janse, R. Menard, and R. Amino. Development of the malaria parasite in the skin of the mammalian host. *Proc. Natl. Acad. Sci. U.S.A.*, 107(43):18640–18645, Oct 2010. [PubMed Central:PMC2972976] [DOI:10.1073/pnas.1009346107] [PubMed:20921402].

H. L. Guyatt, R. W. Snow, and D. B. Evans. Malaria epidemiology and economics: the effect of delayed immune acquisition on the cost-effectiveness of insecticide-treated bednets. *Philos. Trans. R. Soc. Lond., B, Biol. Sci.*, 354(1384):827–835, Apr 1999. [PubMed Central:PMC1692554] [DOI:10.1098/rstb.1999.0434] [PubMed:10365407].

S. Haase, S. Herrmann, C. Gruring, A. Heiber, P. W. Jansen, C. Langer, M. Treeck, A. Cabrera, C. Bruns, N. S. Struck, M. Kono, K. Engelberg, U. Ruch, H. G. Stunnenberg, T. W. Gilberger, and T. Spielmann. Sequence requirements for the export of the Plasmodium falciparum Maurer's clefts protein REX2. *Mol. Microbiol.*, 71(4): 1003–1017, Feb 2009. [DOI:10.1111/j.1365-2958.2008.06582.x] [PubMed:19170882].

A. Hammond, R. Galizi, K. Kyrou, A. Simoni, C. Siniscalchi, D. Katsanos, M. Gribble, D. Baker, E. Marois, S. Russell, A. Burt, N. Windbichler, A. Crisanti, and T. Nolan. A CRISPR-Cas9 gene drive system targeting female reproduction in the malaria mosquito vector Anopheles gambiae. *Nat. Biotechnol.*, 34(1):78–83, Jan 2016. [DOI:10.1038/nbt.3439] [PubMed:26641531].

D. Hanahan. Studies on transformation of Escherichia coli with plasmids. *J. Mol. Biol.*, 166(4):557–580, Jun 1983. [PubMed:6345791].

E. Hanssen, R. Sougrat, S. Frankland, S. Deed, N. Klonis, J. Lippincott-Schwartz, and L. Tilley. Electron tomography of the Maurer's cleft organelles of Plasmodium falciparum-infected erythrocytes reveals novel structural features. *Mol. Microbiol.*, 67 (4):703–718, Feb 2008. [DOI:10.1111/j.1365-2958.2007.06063.x] [PubMed:18067543].

E. Hanssen, P. J. McMillan, and L. Tilley. Cellular architecture of Plasmodium falciparum-infected erythrocytes. *Int. J. Parasitol.*, 40(10):1127–1135, Aug 2010. [DOI:10.1016/j.ijpara.2010.04.012] [PubMed:20478310].

K. L. Harvey, P. R. Gilson, and B. S. Crabb. A model for the progression of receptor-ligand interactions during erythrocyte invasion by Plasmodium falciparum. *Int. J. Parasitol.*, 42(6):567–573, May 2012. [DOI:10.1016/j.ijpara.2012.02.011] [PubMed:22710063].

P. L. Hawthorne, K. R. Trenholme, T. S. Skinner-Adams, T. Spielmann, K. Fischer, M. W. Dixon, M. R. Ortega, K. L. Anderson, D. J. Kemp, and D. L. Gardiner. A novel Plasmodium falciparum ring stage protein, REX, is located in Maurer's clefts. *Mol. Biochem. Parasitol.*, 136(2):181–189, Aug 2004. [PubMed:15481109].

R. S. Hegde and H. D. Bernstein. The surprising complexity of signal sequences. *Trends Biochem. Sci.*, 31(10):563–571, Oct 2006. [DOI:10.1016/j.tibs.2006.08.004] [PubMed:16919958].

A. Heiber. Identifizierung und Charakterisierung von PEXEL-negativen exportierten Proteinen in Malariaparasiten. 2011.

A. Heiber, F. Kruse, C. Pick, C. Gruring, S. Flemming, A. Oberli, H. Schoeler, S. Retzlaff, P. Mesen-Ramirez, J. A. Hiss, M. Kadekoppala, L. Hecht, A. A. Holder, T. W. Gilberger, and T. Spielmann. Identification of new PNEPs indicates a substantial non-PEXEL exportome and underpins common features in Plasmodium falciparum protein export. *PLoS Pathog.*, 9(8):e1003546, 2013. [PubMed Central:PMC3738491] [DOI:10.1371/journal.ppat.1003546] [PubMed:23950716].

S. R. Heiny, S. Pautz, M. Recker, and J. M. Przyborski. Protein Traffic to the Plasmodium falciparum apicoplast: evidence for a sorting branch point at the Golgi. *Traffic*, 15(12): 1290–1304, Dec 2014. [DOI:10.1111/tra.12226] [PubMed:25264207].

N. L. Hiller, S. Bhattacharjee, C. van Ooij, K. Liolios, T. Harrison, C. Lopez-Estrano, and K. Haldar. A host-targeting signal in virulence proteins reveals a secretome in malarial infection. *Science*, 306(5703):1934–1937, Dec 2004. [DOI:10.1126/science.1102737] [PubMed:15591203].

S. L. Hoffman, J. Vekemans, T. L. Richie, and P. E. Duffy. The March Toward Malaria Vaccines. *Am J Prev Med*, 49(6 Suppl 4):S319–333, Dec 2015. [DOI:10.1016/j.amepre.2015.09.011] [PubMed:26590432].

L. Hviid and A. T. Jensen. PfEMP1 - A Parasite Protein Family of Key Importance in Plasmodium falciparum Malaria Immunity and Pathogenesis. *Adv. Parasitol.*, 88: 51–84, Apr 2015. [DOI:10.1016/bs.apar.2015.02.004] [PubMed:25911365].

M. Kadekoppala and A. A. Holder. Merozoite surface proteins of the malaria parasite: the MSP1 complex and the MSP7 family. *Int. J. Parasitol.*, 40(10):1155–1161, Aug 2010. [DOI:10.1016/j.ijpara.2010.04.008] [PubMed:20451527].

M. Kadekoppala, S. A. Ogun, S. Howell, R. S. Gunaratne, and A. A. Holder. Systematic genetic analysis of the Plasmodium falciparum MSP7-like family reveals differences in protein expression, location, and importance in asexual growth of the blood-stage parasite. *Eukaryotic Cell*, 9(7):1064–1074, Jul 2010a. [PubMed Central:PMC2901668] [DOI:10.1128/EC.00048-10] [PubMed:20472690].

B. F. Kafsack, H. J. Painter, and M. Llinas. New Agilent platform DNA microarrays for transcriptome analysis of Plasmodium falciparum and Plasmodium berghei for the malaria research community. *Malar. J.*, 11:187, 2012. [PubMed Central:PMC3411454] [DOI:10.1186/1475-2875-11-187] [PubMed:22681930].

B. F. Kafsack, N. Rovira-Graells, T. G. Clark, C. Bancells, V. M. Crowley, S. G. Campino, A. E. Williams, L. G. Drought, D. P. Kwiatkowski, D. A. Baker, A. Cortes, and M. Llinas. A transcriptional switch underlies commitment to sexual development in malaria parasites. *Nature*, 507(7491):248–252, Mar 2014. [PubMed Central:PMC4040541] [DOI:10.1038/nature12920] [PubMed:24572369].

A. Kaushansky and S. H. Kappe. Selection and refinement: the malaria parasite's infection and exploitation of host hepatocytes. *Curr. Opin. Microbiol.*, 26:71–78, Aug 2015. [PubMed Central:PMC4577369] [DOI:10.1016/j.mib.2015.05.013] [PubMed:26102161].

A. Kaushansky, A. N. Douglass, N. Arang, V. Vigdorovich, N. Dambrauskas, H. S. Kain, L. S. Austin, D. N. Sather, and S. H. Kappe. Malaria parasites target the hepatocyte receptor EphA2 for successful host infection. *Science*, 350(6264):1089–1092, Nov 2015. [PubMed Central:PMC4783171] [DOI:10.1126/science.aad3318] [PubMed:26612952].

P. J. Keeling and J. C. Rayner. The origins of malaria: there are more things in heaven and earth. *Parasitology*, 142 Suppl 1:16–25, Feb 2015. [PubMed Central:PMC4413824] [DOI:10.1017/S0031182014000766] [PubMed:24963725].

N. Kilian, M. Dittmer, M. Cyrklaff, D. Ouermi, C. Bisseye, J. Simpore, F. Frischknecht, C. P. Sanchez, and M. Lanzer. Haemoglobin S and C affect the motion of Maurer's clefts in Plasmodium falciparum-infected erythrocytes. *Cell. Microbiol.*, 15(7):1111–1126, Jul 2013. [DOI:10.1111/cmi.12102] [PubMed:23279197].

N. Kilian, S. Srismith, M. Dittmer, D. Ouermi, C. Bisseye, J. Simpore, M. Cyrklaff, C. P. Sanchez, and M. Lanzer. Hemoglobin S and C affect protein export in Plasmodium falciparum-infected erythrocytes. *Biol Open*, 4(3):400–410, 2015. [PubMed Central:PMC4359745] [DOI:10.1242/bio.201410942] [PubMed:25701664].

G. K. Kilili and D. J. LaCount. An erythrocyte cytoskeleton-binding motif in exported Plasmodium falciparum proteins. *Eukaryotic Cell*, 10(11):1439–1447, Nov 2011. [PubMed Central:PMC3209045] [DOI:10.1128/EC.05180-11] [PubMed:21908595].

D. I. Kim, K. C. Birendra, W. Zhu, K. Motamedchaboki, V. Doye, and K. J. Roux. Probing nuclear pore complex architecture with proximity-dependent biotinylation. *Proc. Natl. Acad. Sci. U.S.A.*, 111(24):E2453–2461, Jun 2014. [PubMed Central:PMC4066523] [DOI:10.1073/pnas.1406459111] [PubMed:24927568].

D. I. Kim, S. C. Jensen, K. A. Noble, B. Kc, K. H. Roux, K. Motamedchaboki, and K. J. Roux. An improved smaller biotin ligase for BioID proximity labeling. *Mol. Biol. Cell*, 27(8):1188–1196, Apr 2016. [DOI:10.1091/mbc.E15-12-0844] [PubMed:26912792].

M. Klemba, W. Beatty, I. Gluzman, and D. E. Goldberg. Trafficking of plasmepsin II to the food vacuole of the malaria parasite Plasmodium falciparum. *J. Cell Biol.*, 164(1):47–56, Jan 2004. [PubMed Central:PMC2171955] [DOI:10.1083/jcb200307147] [PubMed:14709539].

M. Kono, D. Heincke, L. Wilcke, T. W. Wong, C. Bruns, S. Herrmann, T. Spielmann, and T. W. Gilberger. Pellicle formation in the malaria parasite. *J. Cell. Sci.*,

129(4):673–680, Feb 2016. [PubMed Central:PMC4760376] [DOI:10.1242/jcs.181230] [PubMed:26763910].

N. Kriek, L. Tilley, P. Horrocks, R. Pinches, B. C. Elford, D. J. Ferguson, K. Lingelbach, and C. I. Newbold. Characterization of the pathway for transport of the cytoadherence-mediating protein, PfEMP1, to the host cell surface in malaria parasite-infected erythrocytes. *Mol. Microbiol.*, 50(4):1215–1227, Nov 2003. [PubMed:14622410].

M. Krugliak, J. Zhang, and H. Ginsburg. Intraerythrocytic Plasmodium falciparum utilizes only a fraction of the amino acids derived from the digestion of host cell cytosol for the biosynthesis of its proteins. *Mol. Biochem. Parasitol.*, 119(2):249–256, Feb 2002. [PubMed:11814576].

F. Kruse. xxxxxxxx. 2014. Dissertation.

S. Külzer, M. Rug, K. Brinkmann, P. Cannon, A. Cowman, K. Lingelbach, G. L. Blatch, A. G. Maier, and J. M. Przyborski. Parasite-encoded Hsp40 proteins define novel mobile structures in the cytosol of the P. falciparum-infected erythrocyte. *Cell. Microbiol.*, 12(10):1398–1420, Oct 2010. [DOI:10.1111/j.1462-5822.2010.01477.x] [PubMed:20482550].

S. Külzer, S. Charnaud, T. Dagan, J. Riedel, P. Mandal, E. R. Pesce, G. L. Blatch, B. S. Crabb, P. R. Gilson, and J. M. Przyborski. Plasmodium falciparum-encoded exported hsp70/hsp40 chaperone/co-chaperone complexes within the host erythrocyte. *Cell. Microbiol.*, 14(11):1784–1795, Nov 2012. [DOI:10.1111/j.1462-5822.2012.01840.x] [PubMed:22925632].

U. K. Laemmli. Cleavage of structural proteins during the assembly of the head of bacteriophage T4. *Nature*, 227(5259):680–685, Aug 1970. [PubMed:5432063].

S. A. Lauer, P. K. Rathod, N. Ghori, and K. Haldar. A membrane network for nutrient import in red cells infected with the malaria parasite. *Science*, 276(5315):1122–1125, May 1997. [PubMed:9148808].

K. G. Le Roch, Y. Zhou, P. L. Blair, M. Grainger, J. K. Moch, J. D. Haynes, P. De La Vega, A. A. Holder, S. Batalov, D. J. Carucci, and E. A. Winzeler. Discovery of gene function by expression profiling of the malaria parasite life cycle. *Science*, 301(5639):1503–1508, Sep 2003. [DOI:10.1126/science.1087025] [PubMed:12893887].

M. C. Lee, P. A. Moura, E. A. Miller, and D. A. Fidock. Plasmodium falciparum Sec24 marks transitional ER that exports a model cargo via a diacidic motif. *Mol. Microbiol.*, 68(6):1535–1546, Jun 2008. [PubMed Central:PMC2676333] [DOI:10.1111/j.1365-2958.2008.06250.x] [PubMed:18410493].

A. M. Lisewski, J. P. Quiros, C. L. Ng, A. K. Adikesavan, K. Miura, N. Putluri, R. T. Eastman, D. Scanfeld, S. J. Regenbogen, L. Altenhofen, M. Llinas, A. Sreekumar, C. Long, D. A. Fidock, and O. Lichtarge. Supergenomic network compression and the discovery of EXP1 as a glutathione transferase inhibited by artesunate. *Cell*, 158(4): 916–928, Aug 2014. [PubMed Central:PMC4167585] [DOI:10.1016/j.cell.2014.07.011] [PubMed:25126794].

A. G. Maier, M. Rug, M. T. O'Neill, J. G. Beeson, M. Marti, J. Reeder, and A. F. Cowman. Skeleton-binding protein 1 functions at the parasitophorous vacuole membrane to traffic PfEMP1 to the Plasmodium falciparum-infected erythrocyte surface. *Blood*, 109(3): 1289–1297, Feb 2007. [PubMed Central:PMC1785152] [DOI:10.1182/blood-2006-08-043364] [PubMed:17023587].

A. G. Maier, M. Rug, M. T. O'Neill, M. Brown, S. Chakravorty, T. Szestak, J. Chesson, Y. Wu, K. Hughes, R. L. Coppel, C. Newbold, J. G. Beeson, A. Craig, B. S. Crabb, and A. F. Cowman. Exported proteins required for virulence and rigidity of Plasmodium falciparum-infected human erythrocytes. *Cell*, 134(1):48–61, Jul 2008. [PubMed Central:PMC2568870] [DOI:10.1016/j.cell.2008.04.051] [PubMed:18614010].

A. G. Maier, B. M. Cooke, A. F. Cowman, and L. Tilley. Malaria parasite proteins that remodel the host erythrocyte. *Nat. Rev. Microbiol.*, 7(5):341–354, May 2009. [DOI:10.1038/nrmicro2110] [PubMed:19369950].

P. Y. Mantel, A. N. Hoang, I. Goldowitz, D. Potashnikova, B. Hamza, I. Vorobjev, I. Ghiran, M. Toner, D. Irimia, A. R. Ivanov, N. Barteneva, and M. Marti. Malaria-infected erythrocyte-derived microvesicles mediate cellular communication within the parasite population and with the host immune system. *Cell Host Microbe*, 13(5): 521–534, May 2013. [PubMed Central:PMC3687518] [DOI:10.1016/j.chom.2013.04.009] [PubMed:23684304].

M. Marti, R. T. Good, M. Rug, E. Knuepfer, and A. F. Cowman. Targeting malaria virulence and remodeling proteins to the host erythrocyte. *Science*, 306(5703):1930–1933, Dec 2004. [DOI:10.1126/science.1102452] [PubMed:15591202].

K. Matthews, M. Kalanon, S. A. Chisholm, A. Sturm, C. D. Goodman, M. W. Dixon, P. R. Sanders, T. Nebl, F. Fraser, S. Haase, G. I. McFadden, P. R. Gilson, B. S. Crabb, and T. F. de Koning-Ward. The Plasmodium translocon of exported proteins (PTEX) component thioredoxin-2 is important for maintaining normal blood-stage growth. *Mol. Microbiol.*, 89(6):1167–1186, Sep 2013. [DOI:10.1111/mmi.12334] [PubMed:23869529].

K. Matuschewski. Getting infectious: formation and maturation of Plasmodium sporozoites in the Anopheles vector. *Cell. Microbiol.*, 8(10):1547–1556, Oct 2006. [DOI:10.1111/j.1462-5822.2006.00778.x] [PubMed:16984410].

J. M. Matz, A. Ingmundson, J. Costa Nunes, W. Stenzel, K. Matuschewski, and T. W. Kooij. In Vivo Function of PTEX88 in Malaria Parasite Sequestration and Virulence. *Eukaryotic Cell*, 14(6):528–534, Jun 2015. [PubMed Central:PMC4452575] [DOI:10.1128/EC.00276-14] [PubMed:25820521].

G. Maurer. Die Malaria pernicosa. *Centralblatt für Bakteriologie. Parasitenkunde und Infektionskrankheiten*, 32:695–719, 1902.

A. Mbengue, N. Audiger, E. Vialla, J. F. Dubremetz, and C. Braun-Breton. Novel Plasmodium falciparum Maurer's clefts protein families implicated in the release of infectious merozoites. *Mol. Microbiol.*, 88(2):425–442, Apr 2013. [DOI:10.1111/mmi.12193] [PubMed:23517413].

A. Mbengue, S. Bhattacharjee, T. Pandharkar, H. Liu, G. Estiu, R. V. Stahelin, S. S. Rizk, D. L. Njimoh, Y. Ryan, K. Chotivanich, C. Nguon, M. Ghorbal, J. J. Lopez-Rubio, M. Pfrender, S. Emrich, N. Mohandas, A. M. Dondorp, O. Wiest, and K. Haldar. A molecular mechanism of artemisinin resistance in Plasmodium falciparum malaria. *Nature*, 520(7549):683–687, Apr 2015. [PubMed Central:PMC4417027] [DOI:10.1038/nature14412] [PubMed:25874676].

P. J. McMillan, C. Millet, S. Batinovic, M. Maiorca, E. Hanssen, S. Kenny, R. A. Muhle, M. Melcher, D. A. Fidock, J. D. Smith, M. W. Dixon, and L. Tilley. Spatial and temporal mapping of the PfEMP1 export pathway in Plasmodium falciparum. *Cell. Microbiol.*, 15(8):1401–1418, Aug 2013. [PubMed Central:PMC3711974] [DOI:10.1111/cmi.12125] [PubMed:23421990].

P. Mesén-Ramírez, F. Reinsch, A. Blancke Soares, B. Bergmann, A. Ullrich, T. Tenzer, and T. Spielmann. Stable translocation intermediates jam global protein export in Plasmodium falciparum parasites and link the PTEX component EXP2 with translocation activity. *PLOS Pathogens*, 2016. accepted article.

D. A. Milner, R. O. Whitten, S. Kamiza, R. Carr, G. Liomba, C. Dzamalala, K. B. Seydel, M. E. Molyneux, and T. E. Taylor. The systemic pathology of cerebral malaria in African children. *Front Cell Infect Microbiol*, 4:104, 2014. [PubMed Central:PMC4139913] [DOI:10.3389/fcimb.2014.00104] [PubMed:25191643].

D. A. Milner, J. J. Lee, C. Frantzreb, R. O. Whitten, S. Kamiza, R. A. Carr, A. Pradham, R. E. Factor, K. Playforth, G. Liomba, C. Dzamalala, K. B. Seydel, M. E. Molyneux, and T. E. Taylor. Quantitative Assessment of Multiorgan Sequestration of Parasites in Fatal Pediatric Cerebral Malaria. *J. Infect. Dis.*, 212(8):1317–1321, Oct 2015. [PubMed Central:PMC4577044] [DOI:10.1093/infdis/jiv205] [PubMed:25852120].

A. Moreno and C. Joyner. Malaria vaccine clinical trials: what's on the horizon. *Curr. Opin. Immunol.*, 35:98–106, Aug 2015. [PubMed Central:PMC4553069] [DOI:10.1016/j.coi.2015.06.008] [PubMed:26172291].

D. A. Moreno-Perez, J. A. Ruiz, and M. A. Patarroyo. Reticulocytes: Plasmodium vivax target cells. *Biol. Cell*, 105(6):251–260, Jun 2013. [DOI:10.1111/boc.201200093] [PubMed:23458497].

I. B. Müller and J. E. Hyde. Antimalarial drugs: modes of action and mechanisms of parasite resistance. *Future Microbiol*, 5(12):1857–1873, Dec 2010. [DOI:10.2217/fmb.10.136] [PubMed:21155666].

E. Mundwiler-Pachlatko and H. P. Beck. Maurer's clefts, the enigma of Plasmodium falciparum. *Proc. Natl. Acad. Sci. U.S.A.*, 110(50):19987–19994, Dec 2013. [PubMed Central:PMC3864307] [DOI:10.1073/pnas.1309247110] [PubMed:24284172].

M. Niang, A. K. Bei, K. G. Madnani, S. Pelly, S. Dankwa, U. Kanjee, K. Gunalan, A. Amaladoss, K. P. Yeo, N. S. Bob, B. Malleret, M. T. Duraisingh, and P. R. Preiser. STEVOR is a Plasmodium falciparum erythrocyte binding protein that mediates merozoite invasion and rosetting. *Cell Host Microbe*, 16(1):81–93, Jul 2014. [PubMed Central:PMC4382205] [DOI:10.1016/j.chom.2014.06.004] [PubMed:25011110].

D. Nikolaeva, S. J. Draper, and S. Biswas. Toward the development of effective transmission-blocking vaccines for malaria. *Expert Rev Vaccines*, 14(5):653–680, May 2015. [DOI:10.1586/14760584.2015.993383] [PubMed:25597923].

S. K. Nilsson, L. M. Childs, C. Buckee, and M. Marti. Targeting Human Transmission Biology for Malaria Elimination. *PLoS Pathog.*, 11(6):e1004871, Jun 2015. [PubMed Central:PMC4472755] [DOI:10.1371/journal.ppat.1004871] [PubMed:26086192].

M. S. Oakley, N. Gerald, T. F. McCutchan, L. Aravind, and S. Kumar. Clinical and molecular aspects of malaria fever. *Trends Parasitol.*, 27(10):442–449, Oct 2011. [DOI:10.1016/j.pt.2011.06.004] [PubMed:21795115].

A. A. Obala, J. N. Mangeni, A. Platt, D. Aswa, L. Abel, J. Namae, and W. Prud-homme O'Meara. What Is Threatening the Effectiveness of Insecticide-Treated Bed-nets? A Case-Control Study of Environmental, Behavioral, and Physical Factors As-sociated with Prevention Failure. *PLoS ONE*, 10(7):e0132778, 2015. [PubMed Cen-tral:PMC4501815] [DOI:10.1371/journal.pone.0132778] [PubMed:26171962].

A. Oberli, L. M. Slater, E. Cutts, F. Brand, E. Mundwiler-Pachlatko, S. Rusch, M. F. Masik, M. C. Erat, H. P. Beck, and I. Vakonakis. A Plasmodium falciparum PHIST protein binds the virulence factor PfEMP1 and comigrates to knobs on the host cell surface. *FASEB J.*, 28(10):4420–4433, Oct 2014. [PubMed Central:PMC4202109] [DOI:10.1096/fj.14-256057] [PubMed:24983468].

A. Oberli, L. Zurbrugg, S. Rusch, F. Brand, M. E. Butler, J. L. Day, E. E. Cutts, T. Lavst-sen, I. Vakonakis, and H. P. Beck. Plasmodium falciparum PHIST Proteins Contribute to Cytoadherence and Anchor PfEMP1 to the Host Cell Cytoskeleton. *Cell. Microbiol.*, Feb 2016. [DOI:10.1111/cmi.12583] [PubMed:26916885].

A. Ouattara and M. B. Laurens. Vaccines against malaria. *Clin. Infect. Dis.*, 60 (6):930–936, Mar 2015. [PubMed Central:PMC4357819] [DOI:10.1093/cid/ciu954] [PubMed:25452593].

E. Pachlatko, S. Rusch, A. Muller, A. Hemphill, L. Tilley, E. Hanssen, and H. P. Beck. MAHRP2, an exported protein of Plasmodium falciparum, is an essential component of Maurer's cleft tethers. *Mol. Microbiol.*, 77(5):1136–1152, Sep 2010. [DOI:10.1111/j.1365-2958.2010.07278.x] [PubMed:20624222].

J. Papakrivos, C. I. Newbold, and K. Lingelbach. A potential novel mechanism for the insertion of a membrane protein revealed by a biochemical analysis of the Plasmodium falciparum cytoadherence molecule PfEMP-1. *Mol. Microbiol.*, 55(4):1272–1284, Feb 2005. [DOI:10.1111/j.1365-2958.2004.04468.x] [PubMed:15686570].

L. A. Parish, D. W. Mai, M. L. Jones, E. L. Kitson, and J. C. Rayner. A member of the Plasmodium falciparum PHIST family binds to the erythrocyte cytoskeleton component band 4.1. *Malar. J.*, 12:160, 2013. [PubMed Central:PMC3658886] [DOI:10.1186/1475-2875-12-160] [PubMed:23663475].

E. Pennisi. SCIENCE AND SOCIETY. Gene drive turns mosquitoes into malaria fighters. *Science*, 350(6264):1014, Nov 2015. [DOI:10.1126/science.350.6264.1014] [PubMed:26612928].

B. Pluess, F. C. Tanser, C. Lengeler, and B. L. Sharp. Indoor residual spraying for preventing malaria. *Cochrane Database Syst Rev*, (4):CD006657, 2010. [DOI:10.1002/14651858.CD006657.pub2] [PubMed:20393950].

N. I. Proellocks, S. Herrmann, D. W. Buckingham, E. Hanssen, E. K. Hodges, B. Elsworth, B. J. Morahan, R. L. Coppel, and B. M. Cooke. A lysine-rich membrane-associated PHISTb protein involved in alteration of the cytoadhesive properties of Plasmodium falciparum-infected red blood cells. *FASEB J.*, 28(7):3103–3113, Jul 2014. [DOI:10.1096/fj.14-250399] [PubMed:24706359].

T. A. Rapoport. Protein translocation across the eukaryotic endoplasmic reticulum and bacterial plasma membranes. *Nature*, 450(7170):663–669, Nov 2007. [DOI:10.1038/nature06384] [PubMed:18046402].

N. Regev-Rudzki, D. W. Wilson, T. G. Carvalho, X. Sisquella, B. M. Coleman, M. Rug, D. Bursac, F. Angrisano, M. Gee, A. F. Hill, J. Baum, and A. F. Cowman. Cell-cell communication between malaria-infected red blood cells via exosome-like vesicles. *Cell*, 153(5):1120–1133, May 2013. [DOI:10.1016/j.cell.2013.04.029] [PubMed:23683579].

N. Reichard. A screen to characterize unknown proteins in the human malaria parasite *Plasmodium falciparum*. Juli 2015.

V. Risco-Castillo, S. Topcu, C. Marinach, G. Manzoni, A. E. Bigorgne, S. Briquet, X. Baudin, M. Lebrun, J. F. Dubremetz, and O. Silvie. Malaria Sporozoites Traverse Host Cells within Transient Vacuoles. *Cell Host Microbe*, 18(5):593–603, Nov 2015. [DOI:10.1016/j.chom.2015.10.006] [PubMed:26607162].

M. S. Robinson and J. Hirst. Rapid inactivation of proteins by knocksideways. *Curr Protoc Cell Biol*, 61:1–7, 2013. [DOI:10.1002/0471143030.cb1520s61] [PubMed:24510805].

M. Rottmann, C. McNamara, B. K. Yeung, M. C. Lee, B. Zou, B. Russell, P. Seitz, D. M. Plouffe, N. V. Dharia, J. Tan, S. B. Cohen, K. R. Spencer, G. E. Gonzalez-Paez, S. B. Lakshminarayana, A. Goh, R. Suwanarusk, T. Jegla, E. K. Schmitt, H. P. Beck, R. Brun, F. Nosten, L. Renia, V. Dartois, T. H. Keller, D. A. Fidock, E. A. Winzeler, and T. T. Diagana. Spiroindolones, a potent compound class for the treatment of malaria. *Science*, 329(5996):1175–1180, Sep 2010. [PubMed Central:PMC3050001] [DOI:10.1126/science.1193225] [PubMed:20813948].

K. J. Roux, D. I. Kim, M. Raida, and B. Burke. A promiscuous biotin ligase fusion protein identifies proximal and interacting proteins in mammalian cells. *J. Cell Biol.*, 196 (6):801–810, Mar 2012. [PubMed Central:PMC3308701] [DOI:10.1083/jcb.201112098] [PubMed:22412018].

M. Rug, M. Cyrklaff, A. Mikkonen, L. Lemgruber, S. Kuelzer, C. P. Sanchez, J. Thompson, E. Hanssen, M. O'Neill, C. Langer, M. Lanzer, F. Frischknecht, A. G. Maier, and A. F. Cowman. Export of virulence proteins by malaria-infected erythrocytes involves

remodeling of host actin cytoskeleton. *Blood*, 124(23):3459–3468, Nov 2014. [PubMed Central:PMC4246041] [DOI:10.1182/blood-2014-06-583054] [PubMed:25139348].

I. Russo, S. Babbitt, V. Muralidharan, T. Butler, A. Oksman, and D. E. Goldberg. Plasmepsin V licenses Plasmodium proteins for export into the host erythrocyte. *Nature*, 463 (7281):632–636, Feb 2010. [PubMed Central:PMC2826791] [DOI:10.1038/nature08726] [PubMed:20130644].

J. Sachs and P. Malaney. The economic and social burden of malaria. *Nature*, 415(6872): 680–685, Feb 2002.

R. K. Saiki, D. H. Gelfand, S. Stoffel, S. J. Scharf, R. Higuchi, G. T. Horn, K. B. Mullis, and H. A. Erlich. Primer-directed enzymatic amplification of DNA with a thermostable DNA polymerase. *Science*, 239(4839):487–491, Jan 1988. [PubMed:2448875].

S. Sanyal, S. Egee, G. Bouyer, S. Perrot, I. Safeukui, E. Bischoff, P. Buffet, K. W. Deitsch, O. Mercereau-Puijalon, P. H. David, T. J. Templeton, and C. Lavazec. Plasmodium falciparum STEVOR proteins impact erythrocyte mechanical properties. *Blood*, 119(2): 1–8, Jan 2012. [PubMed Central:PMC3257022] [DOI:10.1182/blood-2011-08-370734] [PubMed:22106347].

T. J. Sargeant, M. Marti, E. Caler, J. M. Carlton, K. Simpson, T. P. Speed, and A. F. Cowman. Lineage-specific expansion of proteins exported to erythrocytes in malaria parasites. *Genome Biol.*, 7(2):R12, 2006. [PubMed Central:PMC1431722] [DOI:10.1186/gb-2006-7-2-r12] [PubMed:16507167].

T. Saridaki, K. S. Frohlich, C. Braun-Breton, and M. Lanzer. Export of PfSBP1 to the Plasmodium falciparum Maurer's clefts. *Traffic*, 10(2):137–152, Feb 2009. [DOI:10.1111/j.1600-0854.2008.00860.x] [PubMed:19054387].

K. N. Schoeler. Analyse der Export-vermittelnden Domʹanen verschiedener PEXEL-negativer exportierter Proteine im menschlichen Malariaerreger *Plasmodium falciparum*. Oktober 2012.

L. Schofield, M. C. Hewitt, K. Evans, M. A. Siomos, and P. H. Seeberger. Synthetic GPI as a candidate anti-toxic vaccine in a model of malaria. *Nature*, 418(6899):785–789, Aug 2002. [DOI:10.1038/nature00937] [PubMed:12181569].

J. Schulze, M. Kwiatkowski, J. Borner, H. Schluter, I. Bruchhaus, T. Burmester, T. Spielmann, and C. Pick. The Plasmodium falciparum exportome contains non-canonical PEXEL/HT proteins. *Mol. Microbiol.*, 97(2):301–314, Jul 2015. [DOI:10.1111/mmi.13024] [PubMed:25850860].

R. A. Seder, L. J. Chang, M. E. Enama, K. L. Zephir, U. N. Sarwar, I. J. Gordon, L. A. Holman, E. R. James, P. F. Billingsley, A. Gunasekera, A. Richman, S. Chakravarty, A. Manoj, S. Velmurugan, M. Li, A. J. Ruben, T. Li, A. G. Eappen, R. E. Stafford, S. H. Plummer, C. S. Hendel, L. Novik, P. J. Costner, F. H. Mendoza, J. G. Saunders, M. C. Nason, J. H. Richardson, J. Murphy, S. A. Davidson, T. L. Richie, M. Sedegah, A. Sutamihardja, G. A. Fahle, K. E. Lyke, M. B. Laurens, M. Roederer, K. Tewari, J. E. Epstein, B. K. Sim, J. E. Ledgerwood, B. S. Graham, S. L. Hoffman, C. DiGiovanni,

P. Williams, N. Luongo, J. Mitchell, M. B. Florez, B. Larkin, N. Berkowitz, B. Wilson, T. Clarke, O. Vasilenko, G. Yamshchikov, S. Sitar, L. Stanford, I. Pittman, R. T. Bailer, J. Casazza, H. Decederfelt, J. Starling, E. C. Williams, A. Lau, S. Antonara, J. Brocious, M. Kemp, J. Inglese, P. Dranchak, E. N. Abot, S. Reyes, H. Ganeshan, M. Belmonte, J. Huang, A. Belmonte, J. Komisar, Y. Abebe, Y. Getachew, A. Patil, S. Matheny, K. Nelson, J. Overby, V. Pich, Y. Wen, R. Fan, E. Fomumbod, A. Awe, C. Chakiath, M. King, M. S. Orozco, T. Murshedkar, D. Padilla, B. Jiang, L. Gao, N. Kc, R. Xu, M. Adams, C. Plowe, H. Loblein, P. Z. Renehan, M. Kunchai, and L. Diep. Protection against malaria by intravenous immunization with a nonreplicating sporozoite vaccine. *Science*, 341(6152):1359–1365, Sep 2013. [DOI:10.1126/science.1241800] [PubMed:23929949].

A. Sharma, I. Sharma, D. Kogkasuriyachai, and N. Kumar. Structure of a gametocyte protein essential for sexual development in Plasmodium falciparum. *Nat. Struct. Biol.*, 10(3):197–203, Mar 2003. [DOI:10.1038/nsb899] [PubMed:12577051].

A. Siau, O. Silvie, J. F. Franetich, S. Yalaoui, C. Marinach, L. Hannoun, G. J. van Gemert, A. J. Luty, E. Bischoff, P. H. David, G. Snounou, C. Vaquero, P. Froissard, and D. Mazier. Temperature shift and host cell contact up-regulate sporozoite expression of Plasmodium falciparum genes involved in hepatocyte infection. *PLoS Pathog.*, 4(8): e1000121, 2008. [PubMed Central:PMC2488394] [DOI:10.1371/journal.ppat.1000121] [PubMed:18688281].

A. Siau, X. Huang, X. Y. Yam, N. S. Bob, H. Sun, J. C. Rajapakse, L. Renia, and P. R. Preiser. Identification of a new export signal in Plasmodium yoelii: identification of a new exportome. *Cell. Microbiol.*, 16(5):673–686, May 2014. [DOI:10.1111/cmi.12293] [PubMed:24636637].

A. Sinha, K. R. Hughes, K. K. Modrzynska, T. D. Otto, C. Pfander, N. J. Dickens, A. A. Religa, E. Bushell, A. L. Graham, R. Cameron, B. F. Kafsack, A. E. Williams, M. Llinas, M. Berriman, O. Billker, and A. P. Waters. A cascade of DNA-binding proteins for sexual commitment and development in Plasmodium. *Nature*, 507(7491):253–257, Mar 2014. [PubMed Central:PMC4105895] [DOI:10.1038/nature12970] [PubMed:24572359].

M. E. Sinka, M. J. Bangs, S. Manguin, M. Coetzee, C. M. Mbogo, J. Hemingway, A. P. Patil, W. H. Temperley, P. W. Gething, C. W. Kabaria, R. M. Okara, T. Van Boeckel, H. C. Godfray, R. E. Harbach, and S. I. Hay. The dominant Anopheles vectors of human malaria in Africa, Europe and the Middle East: occurrence data, distribution maps and bionomic prÃ©cis. *Parasit Vectors*, 3:117, 2010. [PubMed Central:PMC3016360] [DOI:10.1186/1756-3305-3-117] [PubMed:21129198].

M. E. Sinka, M. J. Bangs, S. Manguin, T. Chareonviriyaphap, A. P. Patil, W. H. Temperley, P. W. Gething, I. R. Elyazar, C. W. Kabaria, R. E. Harbach, and S. I. Hay. The dominant Anopheles vectors of human malaria in the Asia-Pacific region: occurrence data, distribution maps and bionomic prÃ©cis. *Parasit Vectors*, 4:89, 2011. [PubMed Central:PMC3127851] [DOI:10.1186/1756-3305-4-89] [PubMed:21612587].

T. Spielmann and T. W. Gilberger. Protein export in malaria parasites: do multiple export motifs add up to multiple export pathways? *Trends Parasitol.*, 26(1):6–10, Jan 2010. [DOI:10.1016/j.pt.2009.10.001] [PubMed:19879191].

T. Spielmann and T. W. Gilberger. Critical Steps in Protein Export of Plasmodium falciparum Blood Stages. *Trends Parasitol.*, 31(10):514–525, Oct 2015. [DOI:10.1016/j.pt.2015.06.010] [PubMed:26433254].

T. Spielmann, D. L. Gardiner, H. P. Beck, K. R. Trenholme, and D. J. Kemp. Organization of ETRAMPs and EXP-1 at the parasite-host cell interface of malaria parasites. *Mol. Microbiol.*, 59(3):779–794, Feb 2006. [DOI:10.1111/j.1365-2958.2005.04983.x] [PubMed:16420351].

C. Spycher, M. Rug, N. Klonis, D. J. Ferguson, A. F. Cowman, H. P. Beck, and L. Tilley. Genesis of and trafficking to the Maurer's clefts of Plasmodium falciparum-infected erythrocytes. *Mol. Cell. Biol.*, 26(11):4074–4085, Jun 2006. [PubMed Central:PMC1489082] [DOI:10.1128/MCB.00095-06] [PubMed:16705161].

C. Spycher, M. Rug, E. Pachlatko, E. Hanssen, D. Ferguson, A. F. Cowman, L. Tilley, and H. P. Beck. The Maurer's cleft protein MAHRP1 is essential for trafficking of PfEMP1 to the surface of Plasmodium falciparum-infected erythrocytes. *Mol. Microbiol.*, 68(5): 1300–1314, Jun 2008. [DOI:10.1111/j.1365-2958.2008.06235.x] [PubMed:18410498].

J. Storm and A. G. Craig. Pathogenesis of cerebral malaria–inflammation and cytoadherence. *Front Cell Infect Microbiol*, 4:100, 2014. [PubMed Central:PMC4114466] [DOI:10.3389/fcimb.2014.00100] [PubMed:25120958].

N. S. Struck, S. de Souza Dias, C. Langer, M. Marti, J. A. Pearce, A. F. Cowman, and T. W. Gilberger. Re-defining the Golgi complex in Plasmodium falciparum using the novel Golgi marker PfGRASP. *J. Cell. Sci.*, 118(Pt 23):5603–5613, Dec 2005. [DOI:10.1242/jcs.02673] [PubMed:16306223].

N. S. Struck, S. Herrmann, I. Schmuck-Barkmann, S. de Souza Dias, S. Haase, A. L. Cabrera, M. Treeck, C. Bruns, C. Langer, A. F. Cowman, M. Marti, T. Spielmann, and T. W. Gilberger. Spatial dissection of the cis- and trans-Golgi compartments in the malaria parasite Plasmodium falciparum. *Mol. Microbiol.*, 67(6):1320–1330, Mar 2008. [DOI:10.1111/j.1365-2958.2008.06125.x] [PubMed:18284574].

A. Sturm, R. Amino, C. van de Sand, T. Regen, S. Retzlaff, A. Rennenberg, A. Krueger, J. M. Pollok, R. Menard, and V. T. Heussler. Manipulation of host hepatocytes by the malaria parasite for delivery into liver sinusoids. *Science*, 313(5791):1287–1290, Sep 2006. [DOI:10.1126/science.1129720] [PubMed:16888102].

S. J. Tarr, A. Cryar, K. Thalassinos, K. Haldar, and A. R. Osborne. The C-terminal portion of the cleaved HT motif is necessary and sufficient to mediate export of proteins from the malaria parasite into its host cell. *Mol. Microbiol.*, 87(4):835–850, Feb 2013. [PubMed Central:PMC3567231] [DOI:10.1111/mmi.12133] [PubMed:23279267].

S. J. Tarr, R. W. Moon, I. Hardege, and A. R. Osborne. A conserved domain targets exported PHISTb family proteins to the periphery of Plasmodium infected erythrocytes. *Mol. Biochem. Parasitol.*, 196(1):29–40, Aug 2014. [PubMed Central:PMC4165601] [DOI:10.1016/j.molbiopara.2014.07.011] [PubMed:25106850].

V. Turusov, V. Rakitsky, and L. Tomatis. Dichlorodiphenyltrichloroethane (DDT): ubiquity, persistence, and risks. *Environ. Health Perspect.*, 110(2):125–128, Feb 2002. [PubMed Central:PMC1240724] [PubMed:11836138].

R. Tuteja. Unraveling the components of protein translocation pathway in human malaria parasite Plasmodium falciparum. *Arch. Biochem. Biophys.*, 467(2):249–260, Nov 2007. [DOI:10.1016/j.abb.2007.08.031] [PubMed:17919451].

A.-K. Ullrich. Sequence requirements for the export of PEXEL-negative exported proteins (PNEPs) in the human malaria parasite *Plasmodium falciparum*. Apr 2016.

A. J. Umbers, E. H. Aitken, and S. J. Rogerson. Malaria in pregnancy: small babies, big problem. *Trends Parasitol.*, 27(4):168–175, Apr 2011.

A. M. Vaughan, S. A. Mikolajczak, E. M. Wilson, M. Grompe, A. Kaushansky, N. Camargo, J. Bial, A. Ploss, and S. H. Kappe. Complete Plasmodium falciparum liver-stage development in liver-chimeric mice. *J. Clin. Invest.*, 122(10):3618–3628, Oct 2012. [PubMed Central:PMC3461911] [DOI:10.1172/JCI62684] [PubMed:22996664].

L. Vincensini, S. Richert, T. Blisnick, A. Van Dorsselaer, E. Leize-Wagner, T. Rabilloud, and C. Braun Breton. Proteomic analysis identifies novel proteins of the Maurer's clefts, a secretory compartment delivering Plasmodium falciparum proteins to the surface of its host cell. *Mol. Cell Proteomics*, 4(4):582–593, Apr 2005. [DOI:10.1074/mcp.M400176-MCP200] [PubMed:15671043].

G. von Heijne. Membrane protein structure prediction. Hydrophobicity analysis and the positive-inside rule. *J. Mol. Biol.*, 225(2):487–494, May 1992. [PubMed:1593632].

R. F. Waller, M. B. Reed, A. F. Cowman, and G. I. McFadden. Protein trafficking to the plastid of Plasmodium falciparum is via the secretory pathway. *EMBO J.*, 19(8): 1794–1802, Apr 2000. [PubMed Central:PMC302007] [DOI:10.1093/emboj/19.8.1794] [PubMed:10775264].

J. Wang, C. J. Zhang, W. N. Chia, C. C. Loh, Z. Li, Y. M. Lee, Y. He, L. X. Yuan, T. K. Lim, M. Liu, C. X. Liew, Y. Q. Lee, J. Zhang, N. Lu, C. T. Lim, Z. C. Hua, B. Liu, H. M. Shen, K. S. Tan, and Q. Lin. Haem-activated promiscuous targeting of artemisinin in Plasmodium falciparum. *Nat Commun*, 6:10111, 2015. [PubMed Central:PMC4703832] [DOI:10.1038/ncomms10111] [PubMed:26694030].

S. C. Wassmer, T. E. Taylor, P. K. Rathod, S. K. Mishra, S. Mohanty, M. Arevalo-Herrera, M. T. Duraisingh, and J. D. Smith. Investigating the Pathogenesis of Severe Malaria: A Multidisciplinary and Cross-Geographical Approach. *Am. J. Trop. Med. Hyg.*, 93(3 Suppl):42–56, Sep 2015. [PubMed Central:PMC4574273] [DOI:10.4269/ajtmh.14-0841] [PubMed:26259939].

G. E. Weiss, P. R. Gilson, T. Taechalertpaisarn, W. H. Tham, N. W. de Jong, K. L. Harvey, F. J. Fowkes, P. N. Barlow, J. C. Rayner, G. J. Wright, A. F. Cowman, and B. S. Crabb. Revealing the sequence and resulting cellular morphology of receptor-ligand interactions during Plasmodium falciparum invasion of erythrocytes. *PLoS Pathog.*, 11(2):e1004670, Feb 2015. [PubMed Central:PMC4344246] [DOI:10.1371/journal.ppat.1004670] [PubMed:25723550].

G. E. Weiss, B. S. Crabb, and P. R. Gilson. Overlaying Molecular and Temporal Aspects of Malaria Parasite Invasion. *Trends Parasitol.*, Jan 2016. [DOI:10.1016/j.pt.2015.12.007] [PubMed:26778295].

T. N. Wells, R. Hooft van Huijsduijnen, and W. C. Van Voorhis. Malaria medicines: a glass half full? *Nat Rev Drug Discov*, 14(6):424–442, Jun 2015. [DOI:10.1038/nrd4573] [PubMed:26000721].

N. J. White, G. D. Turner, N. P. Day, and A. M. Dondorp. Lethal malaria: Marchiafava and Bignami were right. *J. Infect. Dis.*, 208(2):192–198, Jul 2013. [PubMed Central:PMC3685223] [DOI:10.1093/infdis/jit116] [PubMed:23585685].

C. Wongsrichanalai, A. L. Pickard, W. H. Wernsdorfer, and S. R. Meshnick. Epidemiology of drug-resistant malaria. *Lancet Infect Dis*, 2(4):209–218, Apr 2002. [PubMed:11937421].

World Health Organization. World Malaria Report. 2015.

World Health Organization. Malaria vaccine: WHO position paper-January 2016. *Wkly. Epidemiol. Rec.*, 91(4):33–51, Jan 2016. [PubMed:26829826].

T. Xu, C. A. Johnson, J. E. Gestwicki, and A. Kumar. Conditionally controlling nuclear trafficking in yeast by chemical-induced protein dimerization. *Nat Protoc*, 5(11):1831–1843, Nov 2010. [DOI:10.1038/nprot.2010.141] [PubMed:21030958].

Appendix A.

Primers

Name	5'-3' sequence
PF08_0004-d1_F	CTGATTTTTATTGATTCAGCAAAAGGAGTAAATC ACCCTATTAAAAAAGAAG
KpnI-PF08_0004_F	GATAggtaccATGAAGAATAAACTTTCTACATTATT TTTTATTACAATTTTTCTTATTCTGATTTTTATT GATTCAGCAAAAGG
PF08_0004-AvrII_R	GCGCcctaggAAGCATCCATACGCGGTTAC
Pf08_0004-d2_F	CAATATAACAAATAAGCCAACTGAAGACGAATCC CGTGTTATGCTC
PF08_0004-d2overlap_R	TTCAGTTGGCTTATTTGTTATATTGCC
PF08_0004-d3_F	GAGCGTAGGTAAAGGTGATCACAAAAAACATAA AAAATATAAATCTATAACTG
PF08_0004-d3overlap_R	GTGATCACCTTTACCTACGCTC
PF08_0004-d4myc-AvrII_R	CATAcctaggCAAATCTTCTTCACTTATTAATTTTT GtaaatcttcttcgcttatgagtttttgttcATATAATAATGATCC AATATTACGC
PF08_0004d1scr-d2 overlap_F	AATAAAACAGGAGAATGGAGTTTTAATAATTTTA GAAGAAAGCAACAAGAAAACCAATAGGAGATA CAGAAGTAAATCACCCTATTAAAAAAGAAG
KpnI-PF08_0004SP-d1scroverlap_F	GCATggtaccATGAAGAATAAACTTTCTACATTATT TTTTATTACAATTTTTCTTATTCTGATTTTTATT GATTCAGCAAAAGGAAATAAAACAGGAGAATGG AGTTTTA
PF08_0004 d2overlap-d3scr_R	TAACATTATATAATTTACTAATTTTTCATCTTCT TTACTTAATTCTAATTGATCTACTCTATTTCTGT GATCACCTTTACCTACGCTC
PF08_0004d3 scroverlap-TM_F	GAAAAATTAGTAAATTATATAATGTTAAAAAAAC ATAAAAAATATAAATCTATAACTG

PF08_0004-d1+2-linker-AvrII_R	ATATcctaggaccggcaccggctcctgcaccagcaccggctcctgcaccagc GTTTTCACCTTCTTTTTTAATAGGG
PF08_0004-overlap-Rex2TMflanksN_R	cctgtacataataaaagaaatataacgtacaaaaataatacttgtggtaaacac tcGCGGACTATATTTAATTCATTATC
PF08_0004-overlap-Rex2TMflanksN_R	cgttatatttcttttattatgtacaggaattttatgcataataagaataagctta aaaaaTTAAATCAAAAAAGTAACCGCGTATGGATG CTTcctaggATAG
Rex2TMflanksC-PF08_0004C-term-AvrII_R	CTATcctaggAAGCATCCATACGCGGTTACTTTTTT GATTTAAttttttaagcttattcttattatgcataaaaattcctgtacataat aaaagaaatataacg
PF08_0004-Rex2TM-Overlap_R	cataaaaattcctgtacataataaaagaaatataacgtacaaaaataatacGC GGACTATATTTAATTCATTATC
Rex2TM-overlap-PF08_0004-AvrII_R	CTTAcctaggAAGCATCCATACGCGGTTACTTTTTT GATTTAAcataaaaattcctgtacataataaaag
PF08_0004overlap+Rex2 TMflanks	cataaaaattcctgtacataataaaagaaatataacgtacaaaaataatacttg tggtaaacactCGCGGACTATATTTAATTCATTATC
PF08_0004flanksoverlap-Rex2TM_R	cataaaaattcctgtacataataaaagaaatataacgtacaaaaataatacTT TATATTTTTTATGTTTTTTGCGGAC
Rex2TM-overlap-PF08_0004flanks-AvrII_R	atatcctaggAAGCATCCATACGCGGTTACTTTTTTGA TTTAATCTGGTAACGGTATCcataaaaattcctgtacataata aaag
PF08_0004-mTRAP TM_R	cgtaagaaatagaaagttatacttcctcccaagagtacaagagtagctacacca ctagcaatatataaTTTATATTTTTTATGTTTTTTGCGG AC
PF08_0004-mTRAP TMoverlap-AvrIIcorr_R	GCTGcctaggAAGCATCCATACGCGGTTACTTTTTT GATTTAATCTGGTAACGGTATCacgtaagaaatagaaagtt atacttcc
PF08_0004-scr mTRAP_R	ATTTGGGTTATATATCTTATCATTTATATGATCT TCTACATCTGTTTCTTCTCTATGCTTGTTTATGT TTTTATATTTTTTATGTTTTTTGCGGAC
PF08_0004-mTRAPoverlap-AvrII_R	GCTGcctaggAAGCATCCATACGCGGTTACTTTTTT GATTTAATCTGGTAACGGTATCATTTGGGTTATA TATCTTATCATT
SERA7SP-FP08_0004 overlap_F	CAAATGTAATAGTAGGACAAGAAAAGCCTCCTCC TGATAGTACTGTTGGTGCAGATGAAAGAAAGAA TTTCTGGAAATC

KpnI_SERA7SP overlap_F	GTTAggtaccATGGTATATCGCTTATTTATTATTTT AGTATTGTATGTTATCTGTTGTACAAATGTAATA GTAGGACAAGAAAAGC
pArl1-KpnI-PF08_0004d1_G_F	TATTTCTTACATATAACTCGACCCGGGATGGTAC CATGGATGAAAGAAAGAATTTCTGGAAATCGAG
PF08_0004d4-AvrII-GFP_G_R	actccagtgaaaagttcttctcctttactcctaggAAGCATCCATACG CGGTTACTTTTTTGATTTAATC
pArl1-KpnI-Rex2 1-20-PF08_0004_G_F	TTTCTTACATATAACTCGACCCGGGATGGTACCA TGAAAATGTATTTAGCTGAAATTTTTAGTTCTGG TAAAGAGTCTTTGTTATCTTTAAAGGATGAAAGA AAGAATTTCTGGAAATCG
PF08_0004-AvrII-GFP_G_R	actccagtgaaaagttcttctcctttactcctaggAAGCATCCATACG CGGTTACTTTTTTGATTTAATCTGGTAACGGTAT C
pArl1-KpnI-PF08_0004SP_G_F	TATTTCTTACATATAACTCGACCCGGGATGGTAC CATGAAGAATAAACTTTCTACATTATTTTTTATT AC
mTRAP-N-PF08_0004-overlap_R	TACTTTTTTGATTTAATCTGGTAACGGTATCATA TAATAATGATCCAATATTACGCAATAACATgagtac aagagtagctacaccactagcaatatataa
PF08_0004N-PFL0065wTM-PF08_0004C_R	TTTAATCTGGTAACGGTATCTATTCTGATACCCC ATAAGGAACTAAGAGAGAGTAAGATACTAGCAC ATACAGCTGATAAAATAATTAATTTATATTTTTT ATGTTTTTTGCGGAC
PFL0065w-Nscrambled_F	TATGAATTTAGAGTAGATGAAAATACAAATCCAT TATTAGATAAACCAAAAGAAATAGTAACAATATA TAGTAACACAAAAACTCAGTTAAT
KpnI-PFL0065w-SP-N-scrambledoverlap_F	CAGCggtaccATGAAAACCATAATAATAGTAACCCT TTTCATTTTAATTTTAAATACAATTATTATAAAT CCATGTACTTGTTATGAATTTAGAGTAGATGAAA ATAC
PFL0065w-Cscrambled-AvrII_R	GCTGcctaggATCATCTATATTATTTAATTTTTCAA ATAAACTTTCTAAATTCATTACATAATATGCATC TTCTTTTTTATTCATTTCATGATTATAATG
PFL0065w-N1scr-N2 overlap_F	TATGAATTTAGAGTAGATGAAAATACAAATCCAT ATGAAACCCTCAAAGAAAATGTCAAAATTCG
PFL0065w-N1overl-N2scr_F	GTCCCTAATACACTGCCTATTGAATATTTCGATT TATTAGATAAACCAAAAGAAATAGTAACAATATA TAGTAACACAAAAACTCAGTTAAT

PFL0065w SP-d1 overlap_F	TATAggtaccATGAAAACCATAATAATAGTAACCCT TTTCATTTTAATTTTAAATACAATTATTATAAAT CCATGTACTTGTGTCCCTAATACACTGCCTATTG
PFL0065w-N1scr-AvrII_R	TATAcctaggTTCTACCATATAAAAATCTGCATCTT TTAAACTTTCTAAATTCATTACATAATATGCATC TTCTTTTTTATTCATTTCATGATTATAATG
PFL0065w-N2scr-AvrII_R	TATAcctaggATCATCTATATTATTTAATTTTTCAA ATAATAGATCGCTATTTAATTCATAATTATTAAT TTC
PFL65w-avr-rv	CAGCCCTAGGTTCTACCATATAAAAATCTGCATC
PF08_0005-AvrII_R	GCGCcctaggTTGTATTTTTTTAGATATCATAGC
PF08_0005-d1_F	AATTTTTATAAATTCCTGCCATCTAAATAATGAA AATGAAATAAATACCTTC
KpnI-PF08_0005_F	GATCggtaccATGAACATGTACGTAATCTATTACTA CTTTTTAATTTTAATTTTTATAAATTCCTGCCAT C
PF08_0005-d3-AvrII_R	GATCcctaggAAAAACCTTTGTGTGTTTTTTTTTAT ATGGTCCG
PF08_0005-d2-overlap_R	CATAATTTCTTGTCATTTTAAAATTTTCATGATG AATAGTATTGTTATTTTG
PF08_0005-d2_F	GAAAATTTTAAAATGACAAGAAATTATGACG
PF08_0005d1a-overlap_F	AATTTTTATAAATTCCTGCCATCTAAATAATAGT AATAATAATAATACAAATG
PF08_0005d1b_F	TCTCCTTCTTCTACTATGATAGACC
PF08_0005d1b-overlap_R	GGTCTATCATAGTAGAAGAAGGAGATTTTTTTAA TGTATTCGTTCTTGTG
PF08_0005d1c-overlap_R	GGTATTTATTTCATTTTCATTATTGGGGTGGTCT ATGTTAGTTGATC
PF08_0005d1c_F	AATAATGAAAATGAAATAAATACC
PF08_0005-parta+b-linkerAG-AvrII_R	ATATcctaggaccggcaccggctcctgcaccagcaccggctcctgcaccagc GGGGTGGTCTATGTTAGTTGATCTTG
PF08_0005-d1a-linker-AvrII_R	ATATcctaggaccggcaccggctcctgcaccagcaccggctcctgcaccagc TTTTTTTAATGTATTCGTTCTTGTG
pArl1-KpnI-PFB0115wSP_G_F	TATTTCTTACATATAACTCGACCCGGGATGGTAC CATGTTAAAGAAATATATTATATTAATATATATC GGTG

PFB0115wd1-L-AvrII-GFP_G_R	actccagtgaaaagttcttctcctttactcctaggTGAACCTCCTGATCCATTTTTTGTTTCTTTATTTATATCTTTATTTTCTTGTG
NheI-MSRP6 partc_F	TACTGCTAGCCTACCTCAATATGAAGAATC
MSRP6 partd-linker-AvrII_R	ATTACCTAGGTGAACCTCCTGATCCTAATTTCGTGGGATTTAAAGCTAAG
KpnI-MSRP6 SP overlap part c_F	GGTACCATGAAAAGCAAAAAATAATATGTTCATCTTGCTTATTTTTAATATTTTTAAGTGTAATATTTTGTCTACCTCAATATGAAGAATCTAATAAAAC
KpnI-MSRP6_F	TAATGGTACCATGAAAAGCAAAAAATAATATGTTCATCTTGC
MSRP6-part2a-linker-AvrII_R	ATATCCTAGGTGAACCTCCTGATCCTTTCATATTTCGTAATTCATTTTCTATATC
KpnI-MSRP6 24-47-mTRAP-overlap_F	TATAggtaccATGAGTGAACCAGATACAAATTCATTTGATGAAAATGTAAAGAAGAATGAAGTTTTTAATGCCTTAAATGAACATTTATCTGCATTATATGAACATATGAATAC
mTRAP1-26scr-mTRAPoverlap_F	ACAGGAGATCAAGCAGATAGTAATAAAGAACCACATAATGCATATTTACATATGGAACAAACACATCAAAGTGAACATCACTTTGAAGATTACAGTAAAGT
KpnI-MSRP624-47-mTRAPscr overlap_F	TATAggtaccATGAGTGAACCAGATACAAATTCATTTGATGAAAATGTAAAGAAGAATGAAGTTTTTAATGCCTTAAATGAACATTTAACAGGAGATCAAGCAGATAGTAATA
KpnI-Rex3trunc_F	GCGCGGTACCATGCAAACCCGTAAATATAATA
Rex3trunc-PstI_R	CATGCTGCAGTGCTTCTATATGTGATGACT
PstI-Partcd_F	CGCACTGCAGCTACCTCAATATGAAGAATC
Partcd-PstI_R	CGCGCTGCAGTAATTTCGTGGGATTTAAAGC
NheI-linker-BirA_F	GATAGCTAGCTCAGGATCTGGTAGTGGATCAGGTTCTGGAAGTGGTTCTGGAAGTATGAAAGATAATACAGTACCATTAAAAT
BirA-Stop-XhoI_R	CATGCTCGAGTTAACCTTTTTCAGCTGATCTTAATG
Stevor1-260-AvrII_R	CATCCCTAGGTGCACCTATAGCAGCACCTGTAGC

KpnI-Stevor-overlapintron_F	CTATggtaccATGAAGATGTATTACCTTAAAATGTTATTGTTTAACTTTTTAATAAATGTTTTAGTATTACCACATTATGAAAATTATCAAAATAACCATTATAAC
pArl1-NotI-TAA-PFE0050w_G_F	acgccaagctatttaggtgacactatagaatactcgcggccgcTAAcccttacattaatttcttagAACGTATCATCC
PFE0050w-AvrII-linkeroverl_G_R	GCAGCAGCAGATCTTGATCTCAATCCTGAcctaggTTTATTTGATTCTTGTTCGTTACGTAGTG
pArl1-NotI-TAA-PFE0060w_G_F	acgccaagctatttaggtgacactatagaatactcgcggccgcTAACAAATCAACATAACTATAAAGAAGGTCCC
PFE0060w-AvrII-linkeroverl_G_R	GCAGCAGCAGATCTTGATCTCAATCCTGAcctaggAGTTAGTAATAAATTATGAAGACCTAATG
pArl1-NotI-TAA-PFI0086w_G_F	acgccaagctatttaggtgacactatagaatactcgcggccgcTAAttattagCATAACACCAATAAATATTGC
PFI0086w-AvrII-linkeroverl_G_R	GCAGCAGCAGATCTTGATCTCAATCCTGAcctaggTTTAACACCGTAAAGATCTTTTTTATCTTCTGTTATG
pArl1-NotI-TAA-PF11_0511_G_F	acgccaagctatttaggtgacactatagaatactcgcggccgcTAAATCTTTACGAACTTCAAAATATTATCCATAG
PF11_0511-AvrII-linkeroverl_G_R	GCAGCAGCAGATCTTGATCTCAATCCTGAcctaggCATGTAGGGAAATATAGTGTATAAAAAC
pArl1-NotI-TAA-MAL7P1.170_G_F	acgccaagctatttaggtgacactatagaatactcgcggccgcTAAGGAGTTCTTTCCAAGAGTTATGATATG
MAL7P1.170-AvrII-linkeroverl_G_R	GCAGCAGCAGATCTTGATCTCAATCCTGAcctaggAAATTTTTTTTTTTTCCTCTCAATGTAGAAGTACCAGC
pArl1-NotI-TAA-PFC0070c_G_F	acgccaagctatttaggtgacactatagaatactcgcggccgcTAACAAAGTTTGTGGTATAAATTCCAAGAACC
PFC0070c-AvrII-linkeroverl_G_R	GCAGCAGCAGATCTTGATCTCAATCCTGAcctaggTGGATTTGACATCATTTGACTAAATTTA
pArl1-NotI-TAA-PF10_0024_G_F	acgccaagctatttaggtgacactatagaatactcgcggccgcTAAGAACCAATTTTCGGATTTGATGTCATG
PF10_0024-AvrII-linkeroverl_G_R	GCAGCAGCAGATCTTGATCTCAATCCTGAcctaggATCTATATTTAAGAATCGACATATTC
pArl1-NotI-TAA-PF10_0025_G_F	acgccaagctatttaggtgacactatagaatactcgcggccgcTAACATAGTGAAACTTCATCACATCAAGG

PF10_0025-AvrII-linkeroverl_G_R	GCAGCAGCAGATCTTGATCTCAATCCTGAcctaggACGTTTACATTCTAAAAATACATTTACC
pArl1-NotI-TAA-PF10_0018_G_F	acgccaagctatttaggtgacactatagaatactcgcggccgcTAAAGTTGGATTGAAAAATTAAATGAGAATGG
PF10_0018-AvrII-linkeroverl_G_R	GCAGCAGCAGATCTTGATCTCAATCCTGAcctaggTACAAATATATTATTTATCCAGTCAG
pArl1-NotI-TAA-PF10_0020_G_F	acgccaagctatttaggtgacactatagaatactcgcggccgcTAAGGTTTATCAGATGGGTTCAAAGATGAACG
PF10_0020-AvrII-linkeroverl_G_R	GCAGCAGCAGATCTTGATCTCAATCCTGAcctaggTGGATATATATTATTAAGCCAATTAAC
pArl1-NotI-TAA-PFL0055c_G_F	acgccaagctatttaggtgacactatagaatactcgcggccgcTAAATCATAGTGTTAATGCAGTATCACCCG
PFL0055c-AvrII-linkeroverl_G_R	GCAGCAGCAGATCTTGATCTCAATCCTGAcctaggCATATTATAAGCTCTTGCCTTTTCC
CRT-XhoI-MSRP6SPoverl_G_F	CATTTATTATTTTGTTTTTTTTAATTTCTTACATATAActcgagATGAAAAGCAAAAAAATAATATGTTCATC
MSRP6cd-SpeI-linkeroverl_G_R	ctggattatcatatggataacttgtactagtTAATTTCGTGGGATTTAAAGCTAAGTCC
PFE0050w-Int-check_F	CATATGGATTTTAAAGAGTGCAAAGCATg
PFE0050w-Int-check_R	Cgataattgcaaaagaaatatatgc
PFE0060w-Int-check_F	gAGGTCATATCCCAAATCTGGCC
PFE0060w-Int-check_R	cacgaatatatagaacaacaaaaatggg
PFI0086w-Int-check_F	ACGATTCTATTACAGGTGTACC
PFI0086w-Int-check_R	cataaacatatatataattcataatagtttatatag
PF11_0511-Int-Check_F	acatatttacaaaacattttgttaaaac
PF11_0511-Int-Check_R	caattatgaataattcctttagtattttcgc
Mal7P1.170-Int-check_F	GCTGCTACTTTTCAATGTTC
Mal7P1.170-Int-check_R	ggcttttcaaaattacaacaaaacattaaatatg
PFC0070c-Intcheck_F	CTTTATGTCACCATGGAATTAC
PFC0070c-Intcheck_R	ctatatattttccttgtaataaaccc
PF10_0024-Intcheck_F	GAGAATTGTGGTGGTCTAAGATA
PF10_0024-Intcheck_R	cattattaaattttatttattcataac

PF10_0025-Intcheck_F	GATACAGGTGATATTAAGAAAGAAG
PF10_0025-Intcheck_R	gttaataataaaaaagtatgaattaaaac
PF10_0018-Intcheck_F	GAACATTGTAATTGTGGTAAGAGAACC
PF10_0018-Intcheck_R	gtacatatatttatagacatacacatac
PF10_0020-Intcheck_F	GCTGGATACAAAAATTTAACGATAATC
PF10_0020-Intcheck_R	tttatagcggaatgaaatatc
PFL0055c-Intcheck_F	CCCAATAGATACTAGAATGTCAGAAAG
PFL0055c-Intcheck_R	catattattcgttttggtttttatttgag
pArl55 sense	ggaattgtgagcggataacaatttcacacagg
GFP42 rev	CATCACCATCTAATTCAACAAG

Table A.1.: Primers used for the amplification of DNA sequences

Candidate	5'PCR (bp)		3'PCR (bp)		vector PCR (bp)	
	Int.	3d7	Int.	3d7	Int.	3d7
PFE0050w	1684	–	–	1097	942	–
PFE0060w	1981	–	–	1234	982	–
PFI0086w	1774	–	–	1006	768	–
PF11_0511	1629	–	–	874	932	–
MAL7P1.170	1854	–	–	1120	1011	–
PFC0070c	1590	–	–	797	758	–
PF10_0024	1911	–	–	1122	1178	–
PF10_0025	2154	–	–	1408	1441	–
PF10_0018	1974	–	–	1189	1245	–
PF10_0020	1934	–	–	1188	1221	–
PFL0055c	2263	–	–	1473	1272	–

Table A.2.: Expected sizes for diagnostic PCRs on *P. falciparum* genomic DNA This table shows the expected sizes in basepairs (bp) of the PCR products of diagnostic PCRs on genomic DNA from transgenic knock-in cell lines (Int.) and 3d7 controls(3d7), in case of correct integration into the parasite genome.

Appendix B.

Mass spectrometry results

The following table lists gene IDs, log2 ratios, peptide counts and sequence coverage of proteins enriched in cd over Stevor and cd over Rex3 down to a log2 ratio of 0.5 (for duplicate A), for both experiment 1 and experiment 2.

Experiment 1

Majority protein IDs	LOG2 Ratio H/L normalized Set_A_Rex3cd_OVER_Stevor	LOG2 Ratio H/L normalized Set_B_LS_Stevor_OVER_Rex3cd	Peptide counts (all)	Peptide counts (unique)	Sequence coverage [%]	Unique sequence coverage [%]
PF3D7_1400600	4,16	2,60	NaN	NaN	10,6	8,2
PF3D7_0220000	2,60	3,58	14	14	11,1	11,1
PF3D7_0501200	1,62	2,02	26	26	62,3	62,3
PF3D7_0730800.1	1,49	1,96	NaN	NaN	26,6	26,6
PF3D7_0501300	1,15	0,35	3	3	12,8	12,8
PF3D7_1002000	1,13	1,46	12	12	29,2	29,2
PF3D7_0301400	1,13	NaN	4	4	13,6	13,6
PF3D7_0104200	0,96	0,91	5	5	12,9	12,9
PF3D7_0830500	0,95	1,36	19	19	31,1	31,1
PF3D7_1204300	0,95	-0,07	1	1	10,6	10,6
PF3D7_1149000	0,87	1,13	130	130	26	26
PF3D7_0202000	0,87	1,45	8	8	11,9	11,9
PF3D7_1353000	0,84	1,14	11	11	14,9	14,9
PF3D7_1201100	0,82	0,80	8	8	10,6	10,6
PF3D7_0903500	0,82	0,78	15	15	14,3	14,3
PF3D7_1252700	0,81	0,91	1	1	2,2	2,2
PF3D7_0702400	0,79	NaN	3	3	18,7	18,7
PF3D7_1002100	0,79	0,24	5	5	23,8	23,8
PF3D7_1370300	0,78	2,19	4	4	16,5	16,5
PF3D7_0113900	0,72	NaN	2	2	11,5	11,5
PF3D7_1426200	0,69	-0,93	4	4	8,5	8,5
PF3D7_1353200	0,69	-1,19	3	3	15,3	15,3
PF3D7_1001400	0,65	0,21	14	14	18,6	18,6
PF3D7_0301600	0,64	0,21	2	2	3,6	3,6
PF3D7_1334500	0,64	1,01	34	34	48,5	48,5
PF3D7_1252500	0,59	0,73	1	1	3,8	3,8
PF3D7_1016300	0,59	0,08	NaN	NaN	78,4	78,4
PF3D7_0501000	0,57	0,99	2	2	9,6	9,6
PF3D7_1149400	0,54	2,03	4	4	20,6	20,6
PF3D7_1016400	0,54	0,04	12	12	20,9	20,9
PF3D7_1201000	0,51	0,54	1	1	2,1	2,1
PF3D7_0731100	0,50	0,10	4	4	6,4	6,4

Majority protein IDs	LOG2 Ratio H/L normalized Set_A_Rex3cd_OVER_Rex3	LOG2 Ratio H/L normalized Set_B_LS_Rex3_OVER_Rex3cd				
PF3D7_0501200	4,39	3,45	26	26	62,3	62,3
PF3D7_0936800	4,09	NaN	5	5	9,9	9,9
PF3D7_1002000	3,59	2,69	12	12	29,2	29,2

PF3D7_1370300	3,15	2,13	4	4	16,5	16,5
PF3D7_0301400	3,08 NaN		4	4	13,6	13,6
PF3D7_0830500	2,90	3,14	19	19	31,1	31,1
PF3D7_1002100	2,86	2,74	5	5	23,8	23,8
PF3D7_0501000	2,61	2,60	2	2	9,6	9,6
PF3D7_1001400	2,36	1,65	14	14	18,6	18,6
PF3D7_0901800	2,29	1,20	4	4	17,1	17,1
PF3D7_0935900	2,25	1,13	32	32	62,3	62,3
PF3D7_1149400	2,25	2,45	4	4	20,6	20,6
PF3D7_1334500	2,04	1,57	34	34	48,5	48,5
PF3D7_0501300	1,92	2,38	3	3	12,8	12,8
PF3D7_1016400	1,85	1,29	12	12	20,9	20,9
PF3D7_1353000	1,76	1,45	11	11	14,9	14,9
PF3D7_1001600	1,73	1,51	21	21	23,2	23,2
PF3D7_0113900	1,72 NaN		2	2	11,5	11,5
PF3D7_0935600	1,58	1,98	1	1	3,1	3,1
PF3D7_0104200	1,45	1,87	5	5	12,9	12,9
PF3D7_1252700	1,39	1,72	1	1	2,2	2,2
PF3D7_0611800	1,35	1,34	5	5	2,1	2,1
PF3D7_0220000	1,33	0,85	14	14	11,1	11,1
PF3D7_1205800	1,29	0,74	2	2	1,3	1,3
PF3D7_1001700	1,27	0,82	2	2	9,4	9,4
PF3D7_0817300	1,27	-0,17	2	2	1,2	1,2
PF3D7_1353200	1,26	-2,16	3	3	15,3	15,3
PF3D7_1201100	1,24	1,81	8	8	10,6	10,6
PF3D7_0301700	1,11	2,36	4	4	12,9	12,9
PF3D7_0705500	1,08	1,70	9	9	3,2	3,2
PF3D7_1149000	1,06	1,28	130	130	26	26
PF3D7_1120100	1,03	1,43	15	15	66,4	66,4
PF3D7_1252500	0,98	1,22	1	1	3,8	3,8
PF3D7_0324600						
PF3D7_0101800						
PF3D7_0732000						
PF3D7_1372800	0,88	0,42	NaN	NaN	18,6	7
PF3D7_0903500	0,87	0,99	15	15	14,3	14,3
PF3D7_1014600	0,86	0,64	17	17	7,6	7,6
PF3D7_1454000	0,81 NaN		1	1	1,4	1,4
PF3D7_0702300	0,81	0,35	2	2	3,2	3,2
PF3D7_1204300	0,80	0,47	1	1	10,6	10,6
PF3D7_0702400	0,76 NaN		3	3	18,7	18,7
PF3D7_1409600	0,75	0,94	2	2	3,1	3,1
PF3D7_1477500	0,72	0,94	4	4	10,4	10,4
PF3D7_0702500	0,71	0,83	7	7	30	30
PF3D7_1445700	0,70	-0,40	1	1	4	4
PF3D7_1401200	0,65	0,08	2	2	7,6	7,6
PF3D7_1253000	0,65	0,19	2	2	4,3	4,3
PF3D7_0922100	0,61	-0,60	1	1	1,1	1,1
PF3D7_0301600	0,60	1,09	2	2	3,6	3,6
PF3D7_1478100	0,54	-0,40	1	1	4	4
PF3D7_0730800	0,54	0,83	NaN	NaN	26,6	26,6

PF3D7_0532400	0,52	0,00	10	10	28,6	28,6
PF3D7_1211400	0,50	-0,29	9	9	41,4	41,4

Experiment 2

	LOG2 Ratio H/L normalized Set_A_Rex3cd_OVER_Stevor	LOG2 Ratio H/L normalized Set_B_LS_Stevor_OVER_Rex3cd				
PF3D7_0220000	4,24	4,11	12	12	9,4	9,4
PF3D7_0501200	2,39	2,47	24	24	61,5	61,5
PF3D7_0301400	2,38	1,74	3	3	12,8	12,8
PF3D7_1002000	2,37	NaN	11	11	32,2	32,2
PF3D7_0730800.1	2,33	2,29	4	4	21,5	21,5
PF3D7_0501000	2,23	2,05	5	5	22,3	22,3
PF3D7_0830500	2,15	2,16	22	22	29,2	29,2
PF3D7_1149400	1,96	1,30	5	5	25,8	25,8
PF3D7_1400600	1,86	NaN	3	2	7,6	5,2
PF3D7_0501300	1,83	1,34	4	4	15,4	15,4
PF3D7_1149000	1,79	1,88	121	121	25,9	25,9
PF3D7_1002100	1,56	1,68	5	5	23,8	23,8
PF3D7_0702400	1,51	1,53	2	2	13,8	13,8
PF3D7_0702300	1,48	NaN	2	2	2,9	2,9
PF3D7_0935900	1,43	1,54	23	23	46,1	46,1
PF3D7_1123500	1,40	1,61	12	12	11,9	11,9
PF3D7_1201000	1,37	1,25	2	2	4,7	4,7
PF3D7_0213100	1,33	-0,52	2	2	7,3	7,3
PF3D7_1353000	1,32	1,54	9	9	14,4	14,4
PF3D7_1016400	1,31	1,25	12	12	22,8	22,8
PF3D7_1353200	1,25	1,19	3	3	21,9	21,9
PF3D7_0917900	1,25	1,11	45	45	58,9	58,9
PF3D7_1334500	1,24	1,30	32	32	43,6	43,6
PF3D7_1016300	1,17	1,15	31	31	77,2	77,2
PF3D7_1001400	1,16	1,04	18	18	21,2	21,2
PF3D7_0301700	1,09	1,39	4	4	12,9	12,9
PF3D7_1201100	1,09	1,15	7	7	8,9	8,9
PF3D7_1320000	1,08	1,64	6	6	6,1	6,1
PF3D7_1001900	1,07	NaN	1	1	4,7	4,7
PF3D7_0817900	1,07	0,08	1	1	14,1	14,1
PF3D7_1414300	0,98	0,77	4	4	16,9	16,9
PF3D7_1445700	0,88	0,62	1	1	4	4
PF3D7_0731100	0,81	0,81	2	2	4	4
PF3D7_1124900	0,80	0,83	3	3	17,7	17,7
PF3D7_0212100	0,74	0,88	13	13	8,8	8,8
PF3D7_0935600	0,70	0,94	1	1	3,1	3,1
PF3D7_0210100.1	0,70	0,54	3	3	27,1	27,1
PF3D7_1205800	0,69	0,48	2	2	1,2	1,2
PF3D7_0716300	0,67	0,79	2	2	4,2	4,2

PF3D7_0821700	0,64	0,05	2	2	15,1	15,1
PF3D7_1253000	0,64	0,54	3	3	6,6	6,6
PF3D7_0702500	0,63	0,68	7	7	32,8	32,8
PF3D7_0732200						
PF3D7_1200500	0,62	0,21	2	1	5,7	3,3
PF3D7_0104200	0,57	1,19	5	5	14,8	14,8
PF3D7_1338200	0,57	0,05	7	7	38	38
PF3D7_1470100	0,56	0,04	1	1	0,5	0,5
PF3D7_1473700	0,56	-0,14	2	2	1	1
PF3D7_0516900	0,56	0,29	8	8	29,6	29,6
PF3D7_1136500	0,56	-0,32	4	4	13,6	13,6
PF3D7_1253400						
PF3D7_1372400	0,53	0,28	9	9	13,8	13,8
PF3D7_0801800	0,53	-0,35	2	2	2,5	2,5
PF3D7_1353100	0,52	0,75	2	2	8,4	8,4
PF3D7_0719600	0,52	-0,07	3	3	19,7	19,7
PF3D7_0625400	0,51	0,67	2	2	5,1	5,1
PF3D7_0831700	0,51	0,60	22	17	36,1	27,7
PF3D7_1109900	0,51	0,42	3	3	34,8	34,8

	LOG2 Ratio H/L normalized SetA_cd_OVER_Rex3	LOG2 Ratio H/L normalized SetB_LS_Rex3_OVER_cd				
PF3D7_0501200	4,59	4,40	24	24	61,5	61,5
PF3D7_0830500	4,34	4,02	22	22	29,2	29,2
PF3D7_0501000	4,10	3,47	5	5	22,3	22,3
PF3D7_1002000	4,00	NaN	11	11	32,2	32,2
PF3D7_1002100	3,91	3,45	5	5	23,8	23,8
PF3D7_0501300	3,87	3,41	4	4	15,4	15,4
PF3D7_0301400	3,75	2,86	3	3	12,8	12,8
PF3D7_0301700	3,04	2,57	4	4	12,9	12,9
PF3D7_1334500	3,03	2,31	32	32	43,6	43,6
PF3D7_1016400	2,88	2,45	12	12	22,8	22,8
PF3D7_1409600	2,74	NaN	1	1	1,7	1,7
PF3D7_1001400	2,71	2,04	18	18	21,2	21,2
PF3D7_1149000	2,70	2,17	121	121	25,9	25,9
PF3D7_1201100	2,56	2,12	7	7	8,9	8,9
PF3D7_0935900	2,56	2,02	23	23	46,1	46,1
PF3D7_1001900	2,52	NaN	1	1	4,7	4,7
PF3D7_1353000	2,43	1,79	9	9	14,4	14,4
PF3D7_0935600	2,42	1,89	1	1	3,1	3,1
PF3D7_1001600	2,41	2,14	21	21	29,2	29,2
PF3D7_1149400	2,35	1,92	5	5	25,8	25,8
PF3D7_0702500	2,24	1,52	7	7	32,8	32,8
PF3D7_0702400	2,08	2,40	2	2	13,8	13,8
PF3D7_0702300	2,04	NaN	2	2	2,9	2,9
PF3D7_0220000	1,87	1,53	12	12	9,4	9,4

PF3D7_1414300	1,82	1,08	4	4	16,9	16,9
PF3D7_1253400						
PF3D7_1372400	1,78	1,50	9	9	13,8	13,8
PF3D7_0104200	1,76	1,90	5	5	14,8	14,8
PF3D7_0402400	1,73	1,27	5	5	23,2	23,2
PF3D7_1353200	1,71	1,45	3	3	21,9	21,9
PF3D7_0831700	1,66	1,18	22	17	36,1	27,7
PF3D7_1253000	1,60	0,62	3	3	6,6	6,6
PF3D7_0716300	1,53	2,04	2	2	4,2	4,2
PF3D7_0317600	1,53	1,13	10	10	56,5	56,5
PF3D7_0730800	1,52	1,17	4	4	21,5	21,5
PF3D7_1229400	1,27	0,39	4	4	34,5	34,5
PF3D7_1001000	1,22	1,24	4	4	19	19
PF3D7_1320000	1,22	0,93	6	6	6,1	6,1
PF3D7_1123500	1,20	0,93	12	12	11,9	11,9
PF3D7_1444800	1,12	0,85	12	12	41,5	41,5
PF3D7_0917900	1,12	0,54	45	45	58,9	58,9
PF3D7_0503400	1,12	0,62	3	3	28,7	28,7
PF3D7_1027800	1,11	0,79	12	12	36,3	36,3
PF3D7_0731600	1,08	0,75	9	9	13,3	13,3
PF3D7_1317800	1,07	0,48	2	2	11,7	11,7
PF3D7_0826700	1,06	0,55	10	10	40,6	40,6
PF3D7_1353100	1,01	1,22	2	2	8,4	8,4
PF3D7_0705700	1,01	0,72	2	2	33,3	33,3
PF3D7_0532400	1,00	0,38	10	10	28,8	28,8
PF3D7_0516900	1,00	0,79	8	8	29,6	29,6
PF3D7_0308500	0,99	0,65	3	3	28,6	28,6
PF3D7_1010600	0,98	0,68	1	1	5,4	5,4
PF3D7_1130100	0,98	0,14	5	5	41,4	41,4
PF3D7_0719600	0,94	0,37	3	3	19,7	19,7
PF3D7_1465900	0,91	0,58	10	10	47,1	47,1
PF3D7_1460700	0,91	0,53	9	9	50,7	50,7
PF3D7_0310400	0,90	0,72	1	1	1,2	1,2
PF3D7_0915400	0,90	0,63	3	3	2,6	2,6
PF3D7_0731100	0,89	0,27	2	2	4	4
PF3D7_1345700	0,88	0,92	10	10	22,9	22,9
PF3D7_1417800	0,84	-0,50	2	2	3,6	3,6
PF3D7_1105400	0,84	0,42	10	10	44,4	44,4
PF3D7_0211800	0,83	0,43	7	7	13,8	13,8
PF3D7_1242700	0,83	0,31	5	5	36,5	36,5
PF3D7_1323100	0,82	0,23	2	2	8,9	8,9
PF3D7_1302800	0,81	0,49	7	7	29,9	29,9
PF3D7_1441200	0,81	-0,10	4	4	25,3	25,3
PF3D7_0801800	0,81	0,37	2	2	2,5	2,5
PF3D7_0306300	0,81	0,71	3	3	26,1	26,1
PF3D7_1142600	0,81	0,37	4	4	25	25
PF3D7_0415900	0,80	0,39	8	8	32,7	32,7
PF3D7_1108700	0,80	0,88	10	10	21,7	21,7
PF3D7_1447000	0,80	0,28	6	6	25	25
PF3D7_1019400	0,80	0,29	4	4	54,6	54,6

PF3D7_1437900	0,79	0,51	2	2	5,7	5,7
PF3D7_1408600	0,78	0,12	7	7	41,3	41,3
PF3D7_1144000	0,78	0,56	3	3	32,9	32,9
PF3D7_1317100	0,78	0,64	4	4	5,7	5,7
PF3D7_1132200	0,78	0,73	5	5	9	9
PF3D7_0312800	0,77	0,07	2	2	14,3	14,3
PF3D7_1457200	0,76	0,32	3	3	30,8	30,8
PF3D7_0818200	0,75	0,32	8	7	33,2	30,2
PF3D7_0212300	0,75 NaN		2	2	5,9	5,9
PF3D7_0306800	0,74	0,22	6	6	15,4	15,4
PF3D7_1454400	0,74	0,45	7	7	10,3	10,3
PF3D7_0617800	0,73	0,41	2	1	24,2	17,4
PF3D7_0922200	0,73	0,46	14	14	44,3	44,3
PF3D7_1358800	0,73	0,16	6	6	41,1	41,1
PF3D7_0608800	0,73	0,46	15	15	41,3	41,3
PF3D7_0821400	0,73	0,01	2	2	16,9	16,9
PF3D7_1351400	0,71	0,25	5	5	28,1	28,1
PF3D7_1222300	0,70	0,23	45	45	51,6	51,6
PF3D7_1120100	0,70	0,54	17	17	57,2	57,2
PF3D7_0520000	0,69	0,08	6	6	34,4	34,4
PF3D7_1460300	0,68	0,05	2	2	13,4	13,4
PF3D7_1320800	0,68	-0,13	18	18	37,1	37,1
PF3D7_0507100	0,67	0,46	17	17	42,1	42,1
PF3D7_0708400	0,67	0,18	24	24	33,4	33,4
PF3D7_1311800	0,66	0,80	10	10	11,1	11,1
PF3D7_1108400	0,66	0,25	2	2	7,5	7,5
PF3D7_1004000	0,65	0,40	5	5	26,7	26,7
PF3D7_0614500	0,64	0,27	5	5	24,2	24,2
PF3D7_0507700	0,64 NaN		1	1	2,6	2,6
PF3D7_1343000	0,64	0,58	12	12	50	50
PF3D7_1424100	0,63	0,34	11	11	39,8	39,8
PF3D7_0813900	0,63	0,19	7	7	41,7	41,7
PF3D7_1338300	0,63	0,42	8	8	17	17
PF3D7_1405600	0,62 NaN		2	2	6,3	6,3
PF3D7_1420400	0,62	0,23	1	1	1,2	1,2
PF3D7_0624000	0,61	0,21	3	3	8,7	8,7
PF3D7_0209800	0,61	0,40	7	7	23	23
PF3D7_0516200	0,61	0,25	8	8	51,7	51,7
PF3D7_1003500	0,61	-0,01	3	3	25,4	25,4
PF3D7_0627500	0,61	0,46	3	3	12,7	12,7
PF3D7_1129000	0,60	0,51	3	3	11,5	11,5
PF3D7_0818900	0,59	0,23	33	28	45,8	36,8
PF3D7_1142500	0,59	0,16	4	4	37	37
PF3D7_1034900	0,58	-0,11	4	4	6,4	6,4
PF3D7_1341200	0,58	0,24	3	3	21,2	21,2
PF3D7_1338200	0,57	0,00	7	7	38	38
PF3D7_0402000	0,57	0,00	6	6	14,5	14,5
PF3D7_0309600	0,57	0,33	1	1	21,4	21,4
PF3D7_1220900	0,57	0,25	2	2	10,2	10,2
PF3D7_1308200	0,57	0,28	8	8	3,7	3,7

PF3D7_0618300	0,56	0,04	8	8	42,6	42,6
PF3D7_0812400	0,56	0,35	4	4	9,2	9,2
PF3D7_0422400	0,56	0,09	7	7	35,3	35,3
PF3D7_0608700	0,56	-0,45	4	4	6,6	6,6
PF3D7_1431700	0,55	0,20	4	4	21,8	21,8
PF3D7_1357800	0,55	0,12	2	2	5,7	5,7
PF3D7_1311900	0,55	0,13	4	4	9,5	9,5
PF3D7_1136500	0,55	0,40	4	4	13,6	13,6
PF3D7_1324900	0,54	0,38	5	5	15,5	15,5
PF3D7_1026800	0,53	0,65	5	5	32,7	32,7
PF3D7_0813300	0,53	0,31	3	3	10,8	10,8
PF3D7_0322900	0,53	0,03	17	17	54,6	54,6
PF3D7_1008700	0,53	0,07	8	6	22,2	16,2
PF3D7_1134000	0,51	0,05	5	5	8,7	8,7
PF3D7_1341300	0,51	0,09	2	2	5,3	5,3
PF3D7_1446200	0,51	0,42	4	4	6,3	6,3
PF3D7_1309100	0,51	0,04	6	6	29	29
PF3D7_0324600						
PF3D7_0101800						
PF3D7_0732000						
PF3D7_1372800						
PF3D7_0222800	0,51	-0,01	7	2	18,6	7

Appendix C.

ImageJ

This macro was used for generating the intensity profiles in figure 3.24.

```
ylabel = "Intensity";
if (bitDepth!=24)
   exit("RGB image required");
setKeyDown("none");
setRGBWeights(1,0,0); r=getProfile();
setRGBWeights(0,1,0); g=getProfile();
setRGBWeights(0,0,1); b=getProfile();
getVoxelSize(vw, vh, vd, unit);
x = newArray(r.length);
for (i=0; i<x.length; i++)
   x[i] = i*vw;
Plot.create("RGB Profiles","Distance ("+unit+")", ylabel);
ymax = getMax(r,g,b)+5;
//if (ymax>255) ymax=255;
Plot.setLimits(0, (r.length-1)*vw, 0, ymax);
Plot.setColor("red");
Plot.add("line", x, r);
Plot.setColor("green");
Plot.add("line", x, g);
Plot.setColor("blue");
Plot.add("line", x, b);
Plot.update();

function getMax(a,b,c) {
    max=a[0];
   for (i=0; i<a.length; i++) {
      max = maxOf(max,a[i]);
      max = maxOf(max,b[i]);
      max = maxOf(max,c[i]);
   }
   return max;
}
```

Publications

Stable translocation intermediates jam global protein export in *Plasmodium falciparum* parasites and link the PTEX component EXP2 with translocation activity
Paolo Mesén-Ramírez, Ferdinand Reinsch, **Alexandra Blancke Soares**, Bärbel Bergmann, Ann-Katrin Ullrich, Stefan Tenzer, and Tobias Spielmann
2016 PLOS Pathogens (accepted)

The machinery underlying malaria parasite virulence is conserved between rodent and human malaria parasites
Mariana De Niz, Ann-Katrin Ullrich, Arlett Heiber, **Alexandra Blancke Soares**, Christian Pick, Ruth Lyck, Derya Keller, Gesine Kaiser, Monica Prado, Sven Flemming, Hernando del Portillo, Chris Janse, Volker Heussler, and Tobias Spielmann
2016 Nature Communications (accepted)

Identity of a *Plasmodium* lactate/H$^+$ symporter structurally unrelated to human transporters
Binghua Wu, Janis Rambow, Sinja Bock, Julia Holm-Bertelsen, Marie Wiechert, **Alexandra Blancke Soares**, Tobias Spielmann and Eric Beitz
Nature Communications 6, Article number: 6284, doi:10.1038/ncomms7284, Published 11 February 2015

Danksagung